UNIVERSITY OF CALIFORNIA
RIVERSIDE

Secondary Organic Aerosol Formation From Radical-Initiated Reactions of Alkenes: Development of Mechanisms

A Dissertation submitted in partial satisfaction
of the requirements for the degree of

Doctor of Philosophy

in

Chemistry

by

Aiko Matsunaga

August 2009

Dissertation Committee:

Dr. Paul. J. Ziemann, Chairperson
Dr. Jingsong Zhang
Dr. Roger Atkinson

The Dissertation of Aiko Matsunaga is approved:

_____

_____

_____

Committee Chairperson

University of California, Riverside

ACKNOWLEDGEMENTS

First of all, I would like to thank my advisor Dr. Paul. J. Ziemann for five years of guidance of my research. He introduced me the world of aerosol science and the nature of research. I greatly appreciate many valuable discussions and suggestions. I also would like to thank Dr. Roger Atkinson and Dr. Janet Arey for helpful discussions.

The colleagues in Air Pollution Research Center enriched my graduate school life. Discussions we made and sharing the experiences helped me in many ways in the research. I also would like to thank the technical support staffs for helping me about the instruments and the environmental chamber.

I cannot forget about my family. Without having their supports and love, I would not be able to complete all the works required for Doctor of Philosophy.

Chapter 2 was reprinted with permission from *Journal of Physical Chemistry A*, volume 113, Aiko Matsunaga and Paul J. Ziemann, Yields of β-Hydroxynitrates and Dihydroxynitrates in Aerosol Formed from OH Radical-Initiated Reactions of Linear

Alkenes in the Presence of NO, pp 599-606, 2009, from American Chemical Society Publications. Copyright 2009 American Chemical Society. The coauthor Paul J. Ziemann listed in that publication directed and supervised the research which forms the basis for this dissertation.

Chapter 3 was reprinted from *Atmospheric Environment*, volume 43, Aiko Matsunaga, Kenneth S. Docherty, Yong B. Lim, and Paul J. Ziemann, Composition and Yields of Secondary Organic Aerosol Formed from OH Radical-Initiated Reactions of Linear Alkenes in the Presence of NO_x: Modeling and Measurements, pp 1349-1357, 2009, with permission from Elsevier. The coauthors, Kenneth S. Docherty conducted preliminary experiments (but no data was used in the publication), Yong B. Lim provided yields of the products in H-abstraction pathway, and Paul J. Ziemann directed and supervised the research which forms the basis for this dissertation.

Chapter 4 and 5 are currently in preparation as journal publications. The expected coauthor Paul J. Ziemann directed and supervised the researches which form the basis for this dissertation.

Chapter 6 was reprinted with permission from *Journal of Physical Chemistry A*, volume 109, Huiming Gong, Aiko Matsunaga, and Paul J. Ziemann, pp 4312-4324, 2005, from American Chemical Society Publications. Copyright 2005 American Chemical Society. The coauthors, Huiming Gong conducted the experiments involving linear terminal and internal alkenes reactions with NO_3 radicals, and Paul. J. Ziemann directed and supervised the research which forms the basis for this dissertation.

ABSTRACT OF THE DISSERTATION

Secondary Organic Aerosol Formation From Radical-Initiated Reactions of Alkenes: Development of Mechanisms

by

Aiko Matsunaga

Doctor of Philosophy, Graduate Program in Chemistry
University of California, Riverside, August 2009
Dr. Paul J. Ziemann, Chairperson

The products and mechanisms of secondary organic aerosol (SOA) formation from reactions of 1-alkenes, internal alkenes, and 2-methyl-1-alkenes with OH radicals in the presence of NO_x were investigated in an environmental chamber and the results used to develop quantitative models for SOA formation. Aerosol chemical composition was analyzed using a thermal desorption particle beam mass spectrometer (TDPBMS), and multifunctional organic nitrate products were quantified using a high–performance liquid chromatograph with UV-vis detector and identified using the TDPBMS and ^{1}H NMR. The major products observed in reactions of linear alkenes were β-hydroxynitrates, dihydroxynitrates, cyclic hemiacetals, dihydrofurans, and dimers formed from

dihydroxycarbonyls. Trihydroxynitrates and trihydroxycarbonyls were observed in reactions of 2-methyl-1-alkenes, in addition to the products listed above. Dimers were not observed, apparently because electron donation by the additional methyl group (compared to linear 1-alkenes) reduces the driving force for hemiacetal formation. The measured yields of β-hydroxynitrates, dihydroxynitrates, and trihydroxynitrates were used to calculate relative ratios of 1.0:1.9:4.3 for forming primary, secondary, and tertiary β-hydroxyalkyl radicals by OH radical addition to the C=C double bond, and branching ratios of 0.12, 0.15, and 0.25 for forming β-hydroxynitrates from reactions of primary, secondary, and tertiary β-hydroxyperoxy radicals with NO. The trends are consistent with expected relative stabilities of β-hydroxyalkyl radicals and β-hydroxyperoxy radical-NO complexes. It should be possible to use these values to estimate product yields from similar reactions of other alkenes. Comparison of measured and model-calculated SOA yields showed that in some cases the models provide accurate predictions of SOA yields, but that uncertainties in gas- and particle-phase chemistry and gas-particle partitioning can lead to significant discrepancies. More limited environmental chamber studies were also carried out on SOA formation from reactions of linear alkenes with NO_3 radicals. The major products were β-hydroxynitrates, β-carbonylnitrates, dihydroxynitrates, and

hydroxy- and oxo- dinitrooxytetrahydrofurans, which had not been observed previously. It was observed that isomerization of δ-hydroxycarbonyls to cyclic hemiacetals, followed by dehydration to highly reactive dihydrofurans that can be further oxidized, can be important sources of SOA from reactions of alkenes with OH and NO_3 radicals.

TABLE OF CONTENTS

Appendix C: Supporting Information for Chapter 4

Appendix D: Supporting Information for Chapter 5

Appendix E: Supporting Information for Chapter 6

LIST OF FIGURES

LIST OF TABLES

Chapter 1

Introduction

1.1 Structure of the Atmosphere

The atmosphere of the Earth can be separated into several layers as shown in Figure 1.1. Starting from the ground, the layers are called the troposphere, stratosphere, mesosphere, and thermosphere (not shown in the figure). Between these layers are transition zones called the tropopause, stratopause, and mesopause (not shown in the figure). As Figure 1.1 shows, the pressure decreases exponentially with altitude according to the equation

$$p(z) = p_0 e^{-z/H} \qquad (1.1)$$

where p(z) is the pressure at the altitude z km, p_0 is the pressure at altitude 0 km, and H is the scale height, which is 7.4 km for the mean tropospheric temperature of 253 K (Seinfeld and Pandis, 2006). The troposphere and stratosphere are the regions where most atmospheric chemical reactions occur.

The troposphere extends from ground level to the tropopause (~ 15 km), and is a region where air masses mix well vertically. The temperature decreases 9.7 K km^{-1} for dry air (Seinfeld and Pandis, 2006), but more slowly at higher relative humidity. In the

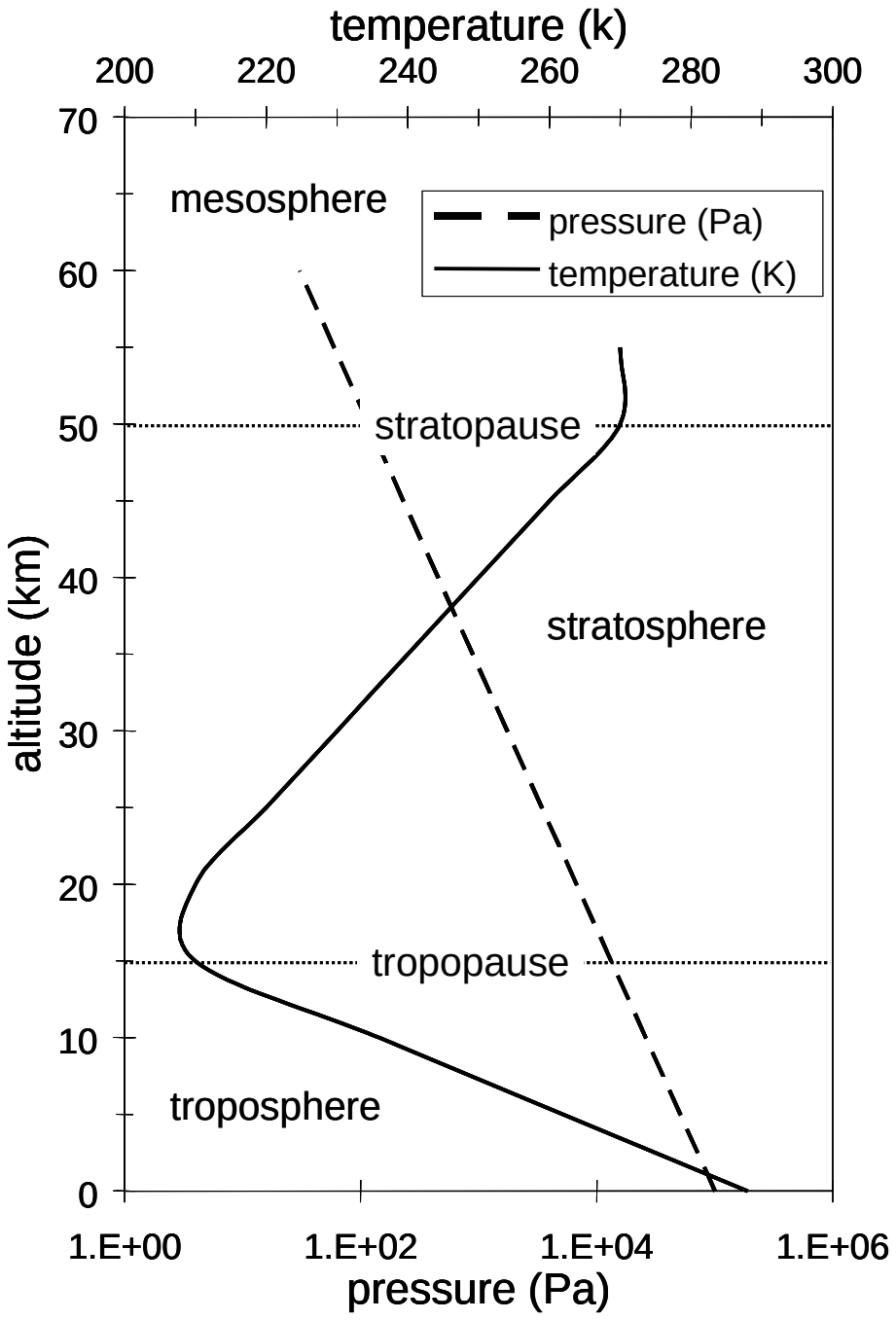

Figure 1.1 Layers of the atmosphere with dependence of and typical temperature (K) and pressure (Pa) on altitude.

troposphere, the planetary boundary layer extends to ~1 km from the ground, and then the free troposphere extends upwards to the tropopause. The planetary boundary layer is where most emissions of pollutants occurs, so its composition and properties vary dramatically over the course of a day. Conversely, the free troposphere responds more slowly to activities at the ground level. The troposphere is the major region of the atmosphere for chemical reactions of compounds that do not require radiation with wavelengths < 290 nm to initiate their reactions.

In contrast to the troposphere, the stratosphere is characterized by a positive temperature gradient. In the region shown in Figure 1.1, the temperature increases from ~210 K at the tropopause (~ 15 km) to the stratopause (~ 50 km). This is also the region where the ozone layer is observed, formed by the so-called Chapman reactions (Finlayson-Pitts and Pitts, 2000), which involve the photolysis of O_2 and ozone by absorption of wavelengths < 290 nm. Absorption of this energetic radiation also photolyzes compounds that are largely unreactive in the troposphere, such as CFCs. Most chemicals decompose within the troposphere or stratosphere.

1.2 Atmospheric Aerosols

A suspension of particles in air is called an aerosol. Aerosol particles are an important category of air pollutants because of their impacts on human health (Englert, 2004), visibility (Finlayson-Pitts and Pitts, 2000), and global climate (Kanakidou et al., 2005). Aerosols impact global climate directly by cooling and warming the atmosphere by scattering and absorbing radiation, and indirectly by acting as nuclei for cloud droplets (Ramanathan et al., 2001). The magnitudes of the impacts depend on the size and composition of the particles. The effects of size are well known and will be described below, but composition effects are still active research topics (Song et al., 2007; Petters et al., 2006).

Atmospheric aerosols can be divided into two categories based on their sizes: particles with diameters > 2.5 μm are called coarse particles, and particles with diameters < 2.5 μm are called fine particles. Coarse particles are generated by mechanical processes such as wind and are directly emitted into the atmosphere from a source. These include, for example, soil dust and sea salt. Fine particles can be divided into three major modes. Two of the modes were discovered by Whitby and co-workers (Willeke and Whitby, 1975; Whitby and Sverdrup, 1980), and another mode was added later as instruments

became capable of measuring smaller particle (Finlayson-Pitts and Pitts, 2000). Accumulation mode particles, which have diameters of 0.08 – 2.5 μm, are mainly formed by coagulation of smaller particles and by gas-to-particle conversion of volatile compounds. Particles in this mode are the most efficient at degrading visibility by scattering light (Seinfeld and Pandis, 2006), because of the similarity in particle diameters and the wavelengths of visible light. They are also the greatest concern for causing health problems (Kappos et al., 2004), because their low deposition velocitites allow them to penetrate deeply into the lungs. This same property causes them to normally have the longest particle lifetimes in the atmosphere, and thus to be a significant component of the free troposphere (Seinfeld and Pandis, 2006). Aerosols in the planetary boundary layer reflect more the local sources and geography. Aitken mode particles, which have diameters of 0.01 – 0.08 μm, are mainly formed by the condensation of hot vapor from combustion, whereas nucleation mode particles, which are those with diameters less than 0.01 μm, are formed by homogeneous nucleation of low volatility products of the atmospheric oxidation of volatile compounds. These particles grow into the Aitken and accumulation modes by coagulation and condensation of gases. Recently, a subset of the fine particles, called ultrafine particles, has been defined as those with

diameters ≤ 0.1 μm. This is because of studies indicating that these small particles may be especially effective at causing health effects.

Atmospheric organic aerosols (OA) can be classified on the basis of how they are introduced to the atmosphere. The major categories are primary and secondary. Primary organic aerosol (POA) is directly emitted into the atmosphere; with soot being the most important example. On the other hand, secondary organic aerosol (SOA) is formed in the atmosphere when volatile organic compounds (VOCs) are oxidized to condensable products. As functional groups are added to the VOCs, vapor pressures decrease, and the products may either nucleate to form new particles or condense onto pre-existing particles as shown in Figure 1.2. When VOCs are initially oxidized, but the first-generation products are still too volatile to condense, they can be oxidized further to second- and higher-generation products. In the atmosphere, multi-generation products may be very important contributors to SOA formation, based on measured oxygen-to-carbon ratios that are close to 1 (Sun et al., 2009). When a compound condenses onto a particle, it can be absorbed into the particle if the particle is liquid or remain at the surface. Heterogeneous reactions with oxidants may lead to the addition of functional groups or molecular fragmentation; in the latter case, the compound may

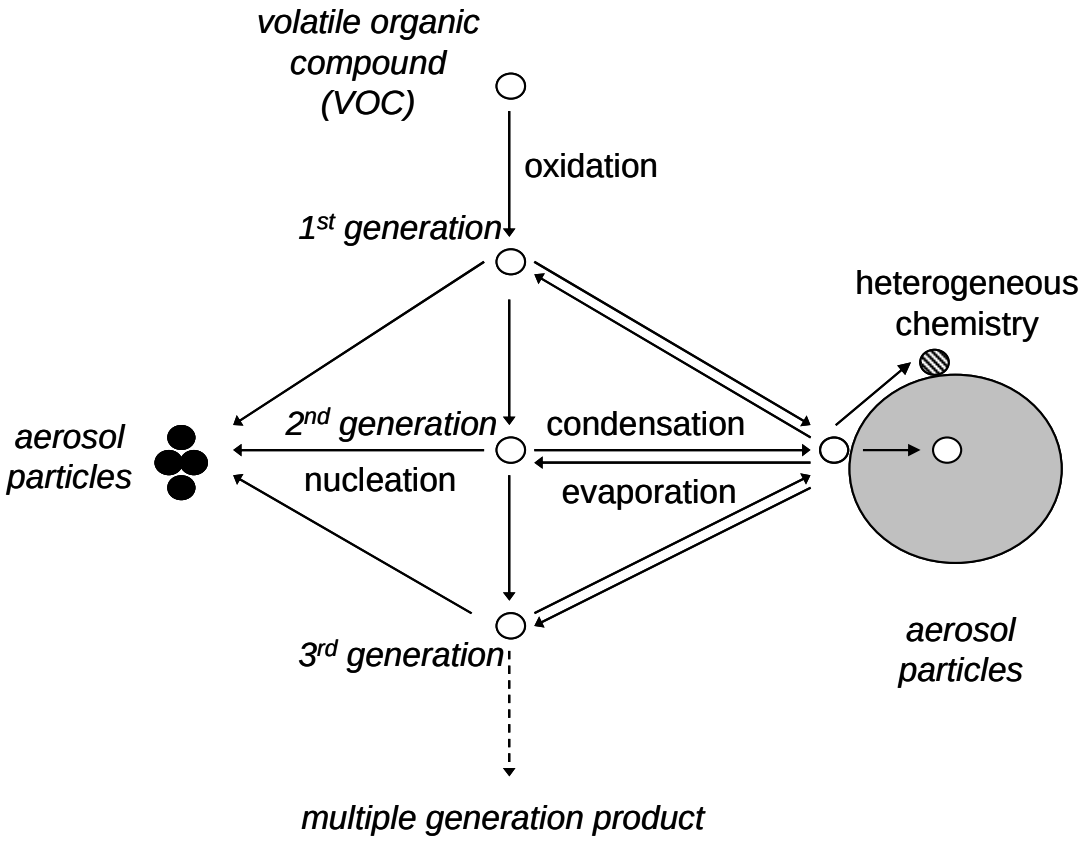

Figure 1.2 A schematic diagram of SOA formation.

evaporate from the surface if its vapor pressure becomes sufficiently high. Organic compounds present in particles can also react with each other to form lower volatility oligomers.

A classic example of SOA formation is the photochemical smog found in Los Angeles, where VOCs emitted mainly from vehicles and industrial operations react with NO_x in the presence of sunlight (Finlayson-Pitts and Pitts, 2000), and some of the VOCs are oxidized and converted to particles by gas-to-particle conversion. For recent measurements, Docherty et al. (2008) reported that SOA fraction in total OA is 70-90% at the peak with the minimum value of ~45% in Riverside, California based on the measurements in a field campaign, Study of Organic Aerosols in Riverside, in 2005. For the northern hemisphere, the fraction of oxygenated OA, which is mainly SOA, in total OA in urban, urban downwind, and rural/remote sites are 64%, 83%, and 95%, respectively (Zhang et al., 2007).

Because of the environmental and health impacts of aerosols, atmospheric aerosol particles are one of the most important components in air quality and climate models. In order to model SOA formation, information on emissions of VOCs, reaction mechanisms, meteorology, and transport are needed. Unfortunately, current models

underestimate atmospheric SOA concentrations by up to an order of magnitude or more (Johnson et al., 2006; Henze et al., 2008; de Gouw et al., 2005; Heald et al., 2006; Volkamer et al., 2006), so more studies are clearly necessary for better predictions. The laboratory studies presented in this thesis provide information about the chemistry of SOA formation from reactions of a major class of organic compounds, the alkenes. The information obtained is valuable for developing detailed models of SOA chemistry, as was done here, and also for providing clues about the relationships between parent hydrocarbon structure and SOA formation mechanisms. Such insight is necessary for condensing detailed laboratory-scale models into simpler versions that are appropriate for broad classes of VOCs, and which can be applied at the local, regional, or global scale.

1.3 Radical-Initiated Reactions of Alkenes

Approximately 90% of global hydrocarbon emissions come from biogenic sources (Guenther et al., 1995). As shown in Figure 1.3, the estimated major contributions are ~44% from isoprene, ~11% from monoterpenes, ~23% from other reactive VOCs such as sesquiterpenes and oxidized VOCs, and the remainder from non-reactive hydrocarbons. The majority of the alkenes, which are dominated in

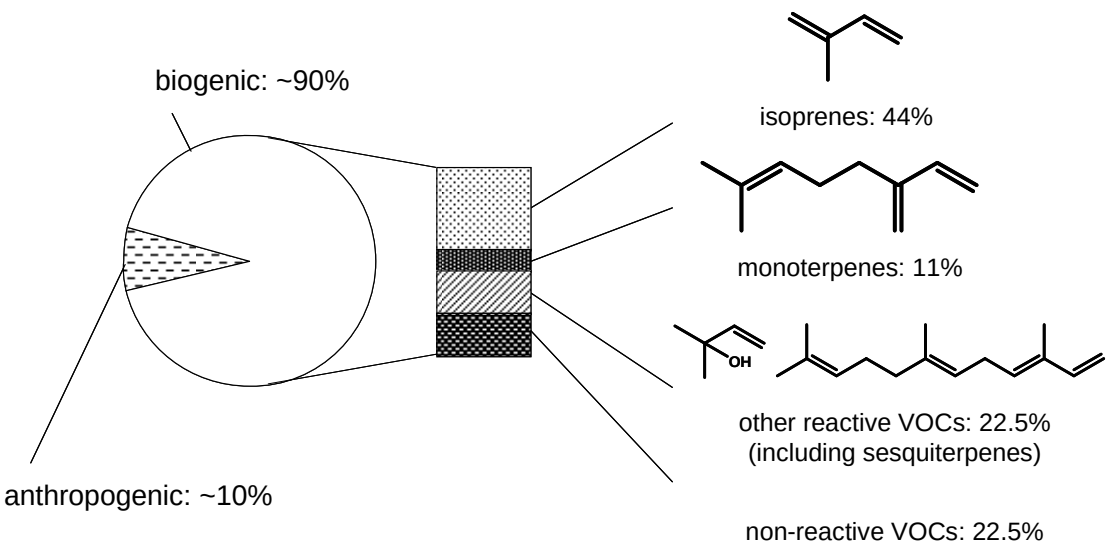

Figure 1.3 A pie chart of the ratios of anthropogenic and biogenic hydrocarbons in global hydrocarbon emission. The bar graph is showing the ratios of each class of the compounds in the biogenic hydrocarbon emission.

abundance by isoprene and monoterpenes, have multiple C=C double bonds. In the atmosphere, biogenic VOCs react primarily with O_3, OH radicals, and NO_3 radicals. For alkenes, reactions are usually initiated by addition of the oxidant to a C=C double bond, as shown in Figure 1.4, although for OH radicals H-atom abstraction can also be important. A detailed discussion of H-atom abstraction pathways can be found elsewhere (Atkinson and Arey, 2003; Lim and Ziemann, 2009). Addition of an OH or NO_3 radical forms an alkyl radical (more specifically, β-hydroxy and β-nitrooxy alkyl radicals for OH and NO_3 radical reactions, respectively), which in air immediately reacts with O_2 to form a peroxy radical, whereas addition of O_3 forms a primary ozonide. A detailed discussion of O_3 reaction mechanisms can be found elsewhere (Atkinson and Arey, 2003; Docherty et al., 2005), and is omitted here because the studies in this thesis focused on reactions of alkenes with OH and NO_3 radicals. Peroxy radicals react with NO, NO_2, HO_2, or RO_2 depending on the conditions of the reaction. Reaction with NO or RO_2 forms an alkoxy radical, which can decompose or react with O_2 to form carbonyls, or isomerize. The branching ratio for each pathway depends on the structure of the alkoxy radical (Atkinson, 2007). If the alkoxy radicals isomerizes, an alkyl radical is formed. The subsequent reactions are then the same as those described above for alkyl radicals. The alkoxy radical

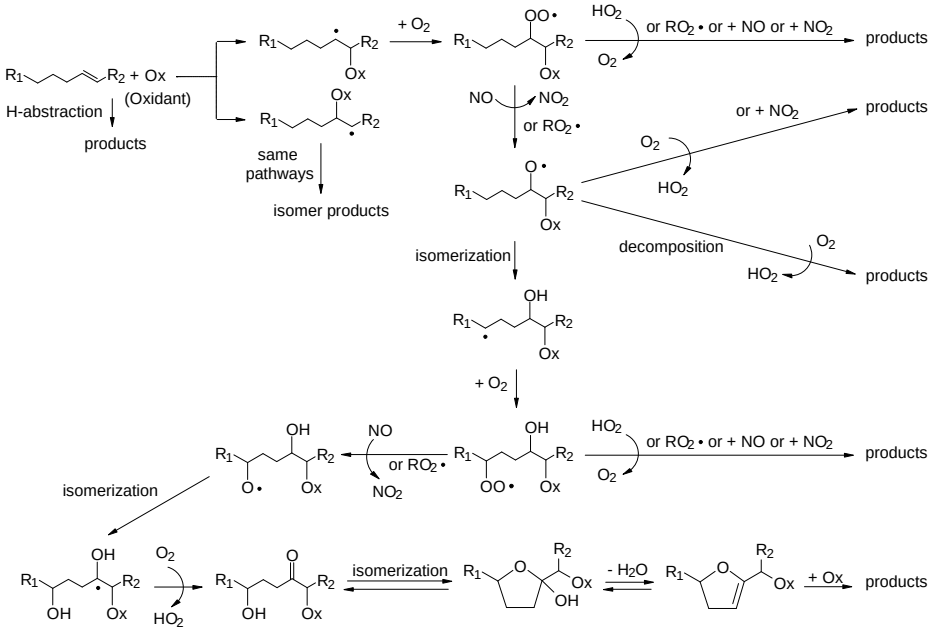

Figure 1.4 A general mechanism of the OH or NO_3 radical-initiated reaction of alkenes. R_1 and R_2 can potentially be any functional group.

formed by isomerization has a hydroxy group located 3 carbon atoms away, and this enhances the reverse isomerization rate such that abstraction of an H atom at the α position relative to the hydroxy group dominates (Atkinson, 2007). Reaction with O_2 then forms 1,4-hydroxycarbonyls, which can isomerize in the particle phase or on chamber walls to form cyclic hemiacetals. Cyclic hemiacetals dehydrate to form dihydrofurans. This pathway has been observed in previous laboratory studies (Martin et al., 2002; Cavalli et al., 2000). As shown in Figure 1.4, the dihydrofurans formed by dehydration have another C=C double bond to which an oxidant can add on to initiate another reaction. For alkenes that only one double bond, this new double bond is therefore a key to forming more highly oxized, lower volatility, second-generation products that may form SOA.

1.4 Gas-to-Particle Partitioning

Once a reaction product is formed, as for example by the mechanism described above, it can partition into a particle if its vapor pressure has been sufficiently reduced relative to that of the parent VOC. This is called gas-to-particle partitioning, and is an important process in gas-to-particle conversion and SOA formation. Based on the vapor

pressure of a compound and its environment, equilibrium is established between the compound in the gas and particle phases as

$$A_g + PM \leftrightarrow A_p \qquad (1.I)$$

where A_g represents compound A in the gas phase, and A_p represents compound A in the particle phase. PM represents the particulate matter into which compound A partitions.

Equilibrium gas-particle partitioning of a compound can be calculated by using the theory introduced by Pankow (1994b). As written by Tobias et al. (2000), the equation for the particle / (particle + gas) ratio, G, is

$$G = [1 + A_i / F_{i,\,om}]^{-1}$$

$$= [1 + MW_{om} 10^6 \zeta_i P_{L,\,i}^{\,0} / 760RTf_{om}TSP]^{-1} \qquad (1.2)$$

where A_i (ng m^{-3}) is the concentration of the compound *i* in gas phase, $F_{i,\,om}$ (ng m^{-3}) is the concentration of compound *i* in the organic material phase associated with suspended particles, MW_{om} (g mol^{-1}) is the mean molecular weight of the absorbing organic material, ζ_i is the activity coefficient of compound *i* in the organic material phase, $P^0_{L,\,i}$ (torr) is the (sub-cooled) vapor pressure of pure compound *i* as a liquid, R is the ideal gas constant (8.206×10^{-5} m^3 atm mol^{-1} K^{-1}), T (K) is the temperature, f_{om} is the mass fraction of TSP that is the absorbing organic material phase, and TSP (μg m^{-3}) is the concentration of total

suspended particulate matter. The value of G as a function of log of vapor pressure in torr when TSP = 1000 μg m^{-3}, MW_{om} = 300 g mol^{-1}, T = 298 K, ζ_i = 1 (assumed an ideal solution), and f_{om} = 1, is shown in Figure 1.5. Under this condition, compounds with vapor pressure < 10^{-6} torr are in the particle phase, compounds with vapor pressure > 10^{-6} torr start to partition into the gas phase, and compounds with vapor pressure > 10^{-2} torr are > 99 % in the gas phase. As shown in equation 1.2, G will increase or the curve in Figure 1.5 will shift to the right when TSP increases. As Figure 1.5 also shows, G will increase as the vapor pressure becomes smaller. As a general rule, for a homologous series of compounds, vapor pressure decreases as carbon number increases. For an example, 1-octene has a higher vapor pressure than 1-tetradecene. Also, when functional groups are added to a compound the vapor pressure decreases. When using this theory with a chemical reaction mechanism to model experimental SOA data, as was done in the studies presented here, equation 1.2 needs to be solved iteratively because TSP changes over time (Colville and Griffin, 2004).

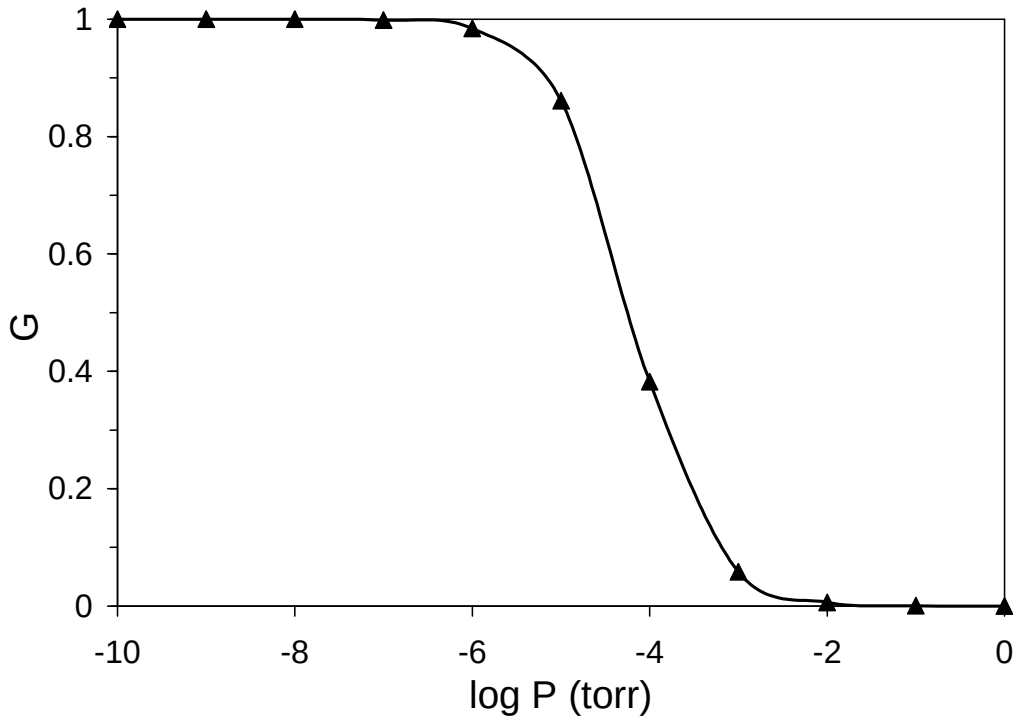

Figure 1.5 The value of G as a function of log of vapor pressure (torr) when TSP = 1000 μg m^{-3}, MW_{om} = 300 g mol^{-1}, T = 298 K, ζ_i = 1 (assumed an ideal solution), and f_{om} = 1 in Equation 1.2.

1.5 Objective and Overview of the Dissertation

The objective of my dissertation research was to investigate the products and mechanisms of SOA formation from the OH and NO_3 radical-initiated reactions of alkenes. The research included experimental studies of the products of reactions of gas-phase and particle-phase alkenes, analytical method development, chemical mechanism development, and SOA modeling. A summary of each thesis chapter is given below.

In Chapters 2 and 3, studies of the OH radical-initiated reactions of linear alkenes in the presence of NO_x are discussed. Aerosol products were analyzed in real time using the TDPBMS and off-line with the TPTD technique. Particle-phase hydroxynitrates were identified by coupling a TDPBMS to a high-performance liquid chromatograph (HPLC) via a Collison atomizer and quantified from UV absorbance. The structures of hydroxynitrate products were also determined by ^{1}H NMR spectroscopy. Gas chromatography with flame ionization detection (GC-FID) was used to quantify the amount of alkene reacted, and combined HPLC analyses of hydroxynitrates and with scanning mobility particle sizer (SMPS) measurements of aerosol mass to calculate hydroxynitrate and SOA yields. Chapter 2 primarily focuses on the yields of β-hydroxynitrates and dihydroxynitrates and the determination of branching ratios for the

pathways leading to their formation. The effects of the structure of the β–hydroxyperoxy radical, which is the precursor of the β-hydroxynitrates, and the presence of water vapor and NH_3, on the branching ratios for the formation of β-hydroxynitrate are also discussed. Chapter 3 focuses on the identification of SOA products other than hydroxynitrates, in particular cyclic hemiacetals, dihydrofurans, and dimers formed from dihydroxycarbonyls, and the development of a model to estimate the composition and yields of gas-phase and SOA products from the reaction. The model is developed based on measured product yields, kinetics data (Kwok and Atkinson, 1995; Aschmann and Atkinson, 2008; Nishino et al., 2009; Atkinson, 2007), and estimated vapor pressures. Since the SOA products formed from dihydroxycarbonyls were not quantifiable with our methods, SOA model simulations were performed assuming two extreme cases: equilibrium gas-particle portioning of dihydroxycarbonyls and non-volatile dihydroxycarbonyls (e.g., through dimer formation). Comparing model results with measured SOA yields provided information on model performance and the extent to which particle-phase reactions might influence SOA model results.

In Chapters 4 and 5, studies of the OH-radical initiated reactions of 2-methyl-1-alkenes in the presence of NO_x are discussed. The experimental and modeling methods

were similar to those described in Chapters 2 and 3. In these reactions, trihydroxynitrates were observed in addition to β-hydroxynitrates and dihydroxynitrates, and no dihydroxycarbonyls dimers were observed. Chapter 4 focuses on the determination of branching ratios for the formation of the various hydroxynitrate products and gas-phase ketones. By combining data with those described in Chapter 2 for the reactions of linear alkenes, branching ratios for the formation of β-hydroxynitrates from primary, secondary, and tertiary β-hydroxyperoxy radicals were calculated. The effect of having water vapor and NH_3 in the system was also determined. Chapter 5 focuses on the development of a model to estimate the yields and the composition of the gas-phase and SOA products. The model is more complete than the one developed in Chapter 3 for the OH-radical initiated reactions of linear alkenes, because we were able to quantify most of the SOA products and the absence of particle-phase reactions simplified the chemistry.

In Chapter 6, studies of NO_3 radical-initiated reactions of alkenes are discussed. The reactions were carried out in an environmental chamber, and the SOA products were analyzed in real time by using a thermal desorption particle beam mass spectrometer (TDPBMS) (Tobias et al., 2000). The technique called temperature-programmed thermal desorption (TPTD) (Tobias and Ziemann, 1999) was used for off-line qualitative and

quantitative analysis of the SOA products. Briefly, the mass spectra of aerosol compounds that can be separated based on their desorption temperatures are obtained by using TPTD analysis. A mass yield of a product can be calculated by using a thermal desorption profile of total ion signal from TPTD analysis, because total ion signal is proportional to organic mass (Crable and Coggeshall, 1958). Also, a vapor pressure can be estimated from the compound desorption temperature (Chattopadhyay et al., 2001). A mechanism for the reactions was developed based on previous studies of gas-phase NO_3 radical-initiated reactions with alkenes (Jay and Stieglitz, 1989; Barnes et al., 1990; Skov et al., 1992; Wängberg, 1993; Kwok et al., 1996; Tuazon et al., 1999) and the products identified in this study. A key part of the proposed mechanism, which is the isomerization of δ-hydroxycarbonyls to form cyclic hemiacetals, which then dehydrate and react further with NO_3 radicals, was confirmed by comparing SOA yields from the reactions of 3,5,5-trimethyl-1-hexene and 2-methyl-1-octene. The ratios of the yields of first-generation and second-generation products were also estimated.

1.6 References

Aschmann, S. M. and Atkinson, R., 2008. Rate Constants for the Gas-Phase Reactions of OH Radicals with E-7-Tetradecene, 2-Methyl-1-Tridecene, and the C_7-C_{14} 1-Alkenes at 295 ± 1 K. *Phys. Chem. Chem. Phys.*, *10*, 4159-4164.

Atkinson, R., 2007. Rate Constants for the Atmospheric Reactions of Alkoxy Radicals: An Updated Estimation Method. *Atmos. Environ.*, *41*, 8468-8485.

Atkinson R. and Arey J., 2003. Atmospheric Degradation of Volatile Organic Compounds. *Chem. Rev.*, *103*, 4605-4638.

Barnes, I., Bastian, V., Becker, K. H., Tong, Z., 1990. Kinetics and Products of the Reactions of NO_3 with Monoalkenes, Dialkenes, and Monoterpenes. *J. Phys. Chem.*, *94*, 2413–2419.

Cavalli, F., Barnes, I., Becker, K. H., 2000. FT-IR Kinetic and Product Study f the OH Radical-Initiated Oxidation of 1-pentanol. *Environ. Sci. Technol.*, *34*, 4111–4116.

Chattopadhyay, S., Tobias, H. J., Ziemann, P. J., 2001. A Method for Measuring Vapor Pressures of Low-Volatility Organic Aerosol Compounds Using a Thermal Desorption Particle Beam Mass Spectrometer. *Anal. Chem.*, *73*, 3797-3803.

Colville, C. J. and Griffin, R. J., 2004. The Roles of Individual Oxidants in Secondary Organic Aerosol Formation from Δ^3-Carene: 2. Soa Formation and Oxidant Contribution. *Atmos. Environ.*, *38*, 4013-4023.

Crable, G. F. and Coggeshall, N. D., 1958. Application of Total Ionization Principles to Mass Spectrometric Analysis. *Anal. Chem.*, *30*, 310-313.

de Gouw, J. A., Middlebrook, A. M., Warneke, C., Goldan, P. D., Kuster, W. C., Roberts, J. M., Fehsenfeld, F. C., Worsnop, D. R., Canagaratna, M. R., Pszenny, A. A. P., Keene, W. C., Marchewka, M., Bertman, S. B., Bates, T. S., 2005. Budget of Organic Carbon in a

Polluted Atmosphere: Results from the New England Air Quality Study in 2002. *J. Geophys. Res.*, *110*, doi:10.1029/2004JD005623.

Docherty, K. S., Wu, W.; Lim, Y. B., Ziemann, P. J., 2005. Contributions of Organic Peroxides to Secondary Aerosol Formed from Reactions of Monoterpenes with O_3. *Environ. Sci. Technol.*, *39*, 4049-4059.

Docherty, K. S., Stone, E. A., Ulbrich, I. M., DeCarlo, P. F., Snyder, D. C., Schauer, J. J., Peltier, R. E., Weber, R. J., Murphy, S. M., Seinfeld, J. H., Grover, B. D., Eatough, D. J., Jimenez, J. L., 2008. Apportionment of Primary and Secondary Organic Aerosols in Southern California during the 2005 Study of Organic Aerosols in Riverside (SOAR-1). *Environ. Sci. Technol.*, *42*, 7655-7662.

Englert, N., 2004. Fine Particles and Human Health – a Review of Epidemiological Studies. *Toxicol. Lett.*, *149*, 235-242.

Finlayson-Pitts, B. J. and Pitts, J. N., Jr., 2000. Chemistry of the Upper and Lower Atmosphere. Academic Press, San Diego.

Grieshop, A. P., Donahue, N. M., Robinson, A. L., 2009. Laboratory Investigation of Photochemical Oxidation of Organic Aerosol from Wood Fires 1: Measurement and Simulation of Organic Aerosol Evolution. *Atmos. Chem. Phys.*, *9*, 1263-1277.

Guenther, A., Hewitt, C. N., Erickson, D., Fall, R., Geron, C., Graedel, T., Harley, P., Klinger, L., Lerdau, M., McKay, W. A., Pierce, T., Scholes, B., Steinbrecher, R., Tallamraju, R., Taylor, J., Zimmermann, P., 1995. A Global Model of Natural Volatile Organic Compound Emissions. *J. Geophys. Res.*, *100*, 8873-8892.

Heald, C. L., Jacob, D. J., Turquenty, S., Hudman R. C., Weber, R. J., Sullivan, A. P., Peltier, R. E., Atlas, E. L., de Gorw, J. A., Warneke, C., Holloway, J. S., Neuman, J. A., Flocke, F. M., Seinfeld, J. H., 2006. Concentrations and Sources of Organic Carbon Aerosols in the Free Troposphere over North America. *J. Geophys. Res.*, *111*, doi:10.1029/2006JD007705.

Henze, D. K., Seinfeld, J. H., Ng, N. L., Kroll, J. H., Fu, T. –M., Jacob, D. J., Heald, C. L., 2008. Global Modeling of Secondary Organic Aerosol Formation from Aromatic Hydrocarbons: High- vs. Low-Yield Pathways. *Atmos. Chem. Phys., 8*, 2405-2421.

Jay, K. and Stieglitz, L., 1989. The Gas Phase Addition of NO_x to Olefins. *Chemosphere, 19*, 1939–1950.

Johnson, D., Utembe, S. R., Jenkin, M. E., 2006. Simulating the Detailed Chemical Composition of Secondary Organic Aerosol Formed on a Regional Scale During the TORCH 2003 Campaign in the Southern UK. *Atmos. Chem. Phys., 6*, 419-431.

Kanakidou, M. et al. (21 co-authors), 2005. Organic Aerosol and Global Climate Modelling: A Review. *Atmos. Chem. Phys., 5*, 1053-1123.

Kappos, A. D., Bruckmann, P., Eikmann, T., Englert, N., Heinrich, U., Höppe, P., Koch, E., Krause, G. H. M., Kreyling, W. G., Rauchfuss, K., Rombout, P., Schulz-Klemp, V., Thiel, W. R., Wichmann., H. –E., 2004. Health Effects of Particles in Ambient Air. *Int. J. Hyg. Environ. Health, 207*, 399-407.

Kwok, E. S. C. and Atkinson. R., 1995. Estimation of Hydroxyl Radical Reaction Rate Constants for Gas-Phase Organic Compounds Using a Structure-Reactivity Relationship: An Update. *Atmos. Environ., 29*, 1685-1695.

Kwok, E. S. C., Aschmann, S. M., Arey, J., Atkinson, R., 1996a. Product Formation from the Reaction of the NO_3 Radical with Isoprene and Rate Constants for the Reactions of Methacrolein and Methyl Vinyl Ketone with the NO_3 Radical. *Int. J. Chem. Kinet., 28*, 925–934.

Lim, Y. B. and Ziemann, P. J., 2009. Chemistry of Secondary Organic Aerosol Formation from OH Radical-Initiated Reactions of Linear, Branched, and Cyclic Alkanes in the Presence of NO_x. *Aerosol Sci. Technol., 43*, 604-619.

Martin, P., Tuazon, E. C., Aschmann, S. M., Arey, J., Atkinson, R., 2002. Formation and Atmospheric Reactions of 4,5-Dihydro-2-Methylfuran. *J. Phys. Chem. A, 106*, 11492–11501.

Molina, M. J., Ivanov, A. V., Trakhtenberg, S., Molina, L. T., 2004. Atmospheric Evolution of Organic Aerosol. *Geophys. Res. Lett.*, *31*, L22104, doi:10.1029/2004GL020910.

Nishino, N., Arey, J., Atkinson, R., 2009. Rate Constants for the Gas-Phase Reactions of OH Radicals with a Series of C_6-C_{14} Alkenes at 299 ± 2 K. *J. Phys. Chem. A, 113*, 852-857.

Pankow, J. F., 1994a. An Absorption Model of Gas/Particle Partitioning of Organic Compounds in the Atmosphere. *Atmos. Environ.*, *28*, 185-188.

Pankow, J. F., 1994b. An Absorption Model of the Gas/Aerosol Partitioning Involved in the Formation of Secondary Organic Aerosol. *Atmos. Environ.*, *28*, 189-193.

Petters, M. D., Prenni, A. J., Kreidenweis, S. M., DeMott, P. J., Matsunaga, A., Lim, Y. B., Ziemann, P. J., 2006. Chemical Aging and the Hydrophobic-to-Hydrophilic Conversion of Carbonaceous Aerosol. *Geophys. Res. Lett.*, *33*, L24806, doi:10.1029/2006GL027249.

Ramanathan, V., Crutzen, P. J., Kiehl, J. T., Rosenfeld, D., 2001. Aerosols, Climate, and the Hydrological Cycle. *Science*, *294*, 2119-2124.

Seinfeld, J. H. and Pandis, S. N., 2006. Atmospheric Chemistry and Physics. 2nd ed. John Wiley & Sons, New Jersey.

Skov, H., Hjorth, J., Lohse, C., Jensen, N. R., Restelli, G., 1992. Products and Mechanism of the Reactions of the Nitrate Radical (NO_3) with Isoprene, 1,3-Butadiene and 2,3-Dimethyl-1,3-Butadiene in Air. *Atmos. Environ.*, *26A*, 2771–2783.

Song, C., Zaveri, R. A., Alexander, M. L., Thornton, J. A., Madronich, S., Ortega, J. V., Zelenyuk, A., Yu, X. –Y., Laskin, A., Maughan, D. A., 2007. Effect of Hydrophobic Primary Organic Aerosols on Secondary Organic Aerosol Formation from Ozonolysis of α-Pinene. *Geophys. Res. Lett.*, *34*, L20803, doi:10.1029/2007GL030720.

Sun, Y., Zhang, Q., Macdonald, A. M., Hayden, K., Li, S. M., Liggio, J., Liu, P. S. K., Anlauf, K. G., Leaitch, W. R., Steffen, A., Cubison, M., Worsnop, D. R., van Donkelaar, A., Martin, R. V., 2009. Size-Resolved Aerosol Chemistry on Whistler Mountain, Canada with a High-Resolution Aerosol Mass Spectrometer During INTEX-B. *Atmos. Chem. Phys.*, *9*, 3095-3111.

Tobias, H. J. and Ziemann, P. J., 1999. Compound Identification in Organic Aerosols Using Temperature-Programmed Thermal Desorption Particle Beam Mass Spectrometry. *Anal. Chem.*, *71*, 3428–3435.

Tobias, H. J., Kooiman, P. M., Docherty, K. S., Ziemann, P. J., 2000. Real-Time Chemical Analysis of Organic Aerosols Using a Thermal Desorption Particle Beam Mass Spectrometer. *Aerosol Sci. Technol.*, *33*, 170-190.

Tuazon, E. C., Alvarado, A., Aschmann, S. M., Atkinson, R., Arey, J., 1999. Products of the Gas-Phase Reactions of 1,3-Butadiene with OH and NO_3 Radicals. *Environ. Sci. Technol.*, *33*, 3586–3595.

Volkamer, R., Jimenez, J. L., San Martini, F., Dzepina, K., Zhang, Q., Salacedo, D., Molina, L. T., Worsnop, D. R., Molina, M. J., 2006. Secondary Organic Aerosol Formation from Anthropogenic Air Pollution: Rapid and Higher than Expected. *Geophys. Res. Lett.*, *33*, doi:10.1029/2006GL026899.

Wängberg, I., 1993. Mechanism and Products of the Reactions of NO_3 with Cycloalkenes. *J. Atmos. Chem.*, *17*, 229–247.

Willeke, K. and Whitby K. T., 1975. Atmospheric Aerosols: Size Distribution Interpretation. *J. Air Pollut. Control Assoc.*, *25*, 529-534.

Zhang, Q. et al. (35 co-authors), 2007. Ubiquity and Dominance of Oxygenated Species in Organic Aerosols in Anthrogenically-Influenced Northern Hemisphere Midlatitudes. *Geophys. Res. Lett.*, *34*, L13801, doi:10.1029/2007GL029979.

Ziemann, P. J., 2005. Aerosol Products, Mechanisms, and Kinetics of Heterogeneous Reactions of Ozone with Oleic Acid in Pure and Mixed Particles. *Faraday Discuss.*, *130*, 469-490.

Chapter 2

Yields of β-Hydroxynitrates and Dihydroxynitrates in Aerosol Formed from OH Radical-Initiated Reactions of Linear Alkenes in the Presence of NO_x

2.1 Abstract

Yields of β-hydroxynitrates and dihydroxynitrates in aerosol formed from OH radical-initiated reactions of linear C_8-C_{17} 1-alkenes and C_{14}-C_{17} internal alkenes in the presence of NO_x were measured using a thermal desorption particle beam mass spectrometer coupled to a HPLC with UV-Vis detector for identification and quantification. For 1-alkenes, total yields of β-hydroxynitrates normalized for OH radical addition to the C=C double bond increased with carbon number, primarily because of enhanced gas-to-particle partitioning, to a plateau of 0.140 ± 0.009 in the C_{14}-C_{17} range, with 1-hydroxy:2-hydroxy isomer fractions of 0.7:0.3. When combined with yields measured by O'Brien et al. (1998) for reactions of smaller alkenes, the results for both 1-alkenes and internal alkenes indicate that the branching ratios for the formation of β-hydroxynitrates from the reactions of NO with β-hydroxyperoxy radicals (averaged over both isomers) increase from 0.009 for C_2 up to 0.13-0.15 for C_{14} and larger, and are

approximately half the values determined by Arey et al. (2001) for the corresponding alkyl peroxy radicals. The range of branching ratios may be higher for individual isomers, but this could not be determined. It is estimated that for 1-alkenes, approximately 60-70% of OH radical addition occurred at the terminal carbon atom. Average yields of dihydroxynitrates normalized for OH radical addition were 0.039 ± 0.006 and 0.006 ± 0.002 for 1-alkenes and internal alkenes, with differences reflecting enhanced decomposition of β-hydroxyalkoxy radicals formed from internal alkenes. The addition of NH_3 reduced yields significantly, apparently by altering hydrogen bonding between hydroxy and peroxy groups in hydroxyperoxy radical-NO complexes, whereas adding H_2O had no obvious effect.

2.2 Introduction

Alkenes are a major component of the ~1150 Tg of non-methane volatile organic compounds (NMVOCs) emitted annually to the atmosphere (Guenther et al., 1995). Most come from biogenic emissions estimated to be approximately 44% isoprene, 11% monoterpenes, and 1% sesquiterpenes and ~10 times greater than global anthropogenic emissions (Guenther et al., 1995; Griffin et al, 1999). In urban areas, alkenes constitute ~10% of NMVOCs (Calvert et al., 2000). In the atmosphere, alkenes react with OH radicals, NO_3 radicals, and O_3. The kinetics, products, and mechanisms of these reactions have been studied (Calvert et al., 2000; Atkinson, 1997; Atkinson and Arey, 2003), with results indicating that reactions with OH radicals are the largest atmospheric loss process and lead to the formation of a variety of oxygenated products. Products containing multiple functional groups may condense to form secondary organic aerosol (SOA) and so are of special interest because of the effects of aerosol particles on global climate and human health (Andreae and Crutzen, 1997; Englert, 2004). For example, the formation of SOA from OH radical-initiated reactions of isoprene, monoterpenes, and sesquiterpenes has received considerable attention (Surratt et al., 2006; Lee et al., 2006; Jaoui and

Kamens, 2003a; Jaoui and Kamens, 2003b) because of the large contribution of terpene photooxidation products to global SOA (Griffin et al., 1999).

The products of OH radical-initiated reactions of alkenes depend on the concentration of NO_x, which influences the reactions of organic peroxy radical intermediates. In polluted areas, where NO_x concentrations are high, they react primarily with NO, leading to the formation of carbonyls, β-hydroxcarbonyls, dihydroxycarbonyls, β-hydroxynitrates, and dihydroxynitrates (Calvert et al., 2000; Atkinson, 1997; Atkinson, 2003). Analyses of the latter two products have focused on the gas phase, primarily because of analytical challenges. β-Hydroxynitrates up to C_6 have been measured in the atmosphere (O'Brien et al., 1995; O'Brien et al., 1997; Werner et al., 1999; Fisher et al., 2000) and up to C_{10} in the laboratory (O'Brien et al., 1998; Tuazon et al., 1998; Chen et al., 1998; Spengnether et al., 2002; Noziére et al., 1999; Aschmann et al., 1998; Aschmann et al., 2002). In the most comprehensive laboratory study to date, O'Brien et al. (1998) measured yields of β-hydroxynitrates from reactions of a series of C_2-C_6 linear alkenes. Yields increased with carbon number from 0.009 to 0.055 and were approximately half those of alkyl nitrates formed from reactions of the corresponding alkanes. Since measurements and modeling indicate that the yields of alkyl nitrates reach

a plateau value of ~0.3 at ~C_{15}(Arey et al., 2001; Zhang et al., 2004), these results suggest that yields of β-hydroxynitrates might be as high as ~0.15 for large alkenes. This would be consistent with the yield of 0.18 measured by Nozière et al. (1999) via FTIR analysis of the total (gas + particle phase) organic nitrate products of the reaction of α-pinene, a C_{10} cyclic alkene. To our knowledge, the only identifications of dihydroxynitrates are those of Aschmann et al. (1998; 2002) for the gas-phase products of the reactions of α-pinene and β-pinene.

Because of the absence of data on the formation of large, low volatility β-hydroxynitrates and dihydroxynitrates, which could contribute to atmospheric SOA, we recently measured the yields of these compounds in SOA formed from OH radical-initiated reactions of a series of C_8-C_{17} 1-alkenes and C_{14}-C_{17} internal alkenes in the presence of NO_x. Analyses were carried out by coupling a thermal desorption particle beam mass spectrometer to a high-performance liquid chromatograph (HPLC) with UV-Vis detector (Ziemann, 2005), allowing identification and quantification of nitrate-containing products. The results provide new quantitative data as well as insights into the effects of carbon number, the position of the C=C double bond, and also H_2O and NH_3, on the yields of these compounds and the branching ratios of pathways that lead to their

formation. In a study presented elsewhere (Matsunaga et al., 2009), these results were used with data obtained by us and from the literature on other products, and from reaction rate constants calculated using structure-reactivity methods, to develop and evaluate a quantitative chemical mechanism and model of SOA formation from these reactions.

2.3 Experimental Section

Chemicals. The following chemicals, with purities (when available) and suppliers, were used: 1-octene (99%), 1-nonene (96%), 1-decene (96%), 1-undecene (97%), 1-dodecene (95%), 1-tridecene (99%), 1-tetradecene (96%), 1-pentadecene (98%), 1-hexadecene (99.8%), 1-heptadecene (≥97%), 2-ethylhexyl nitrate (97%), chloroform-d (99.8 atom % D), and dioctyl sebacate (90%) [Sigma-Aldrich], 7-pentadecene (0.25 *cis*: 0.75 *trans*) and 8-heptadecene (0.25 *cis*: 0.75 *trans*) [ChemSampCo], 7-tetradecene (0.30 *cis*: 0.70 *trans*) [TCI], and NO and NH_3 [Matheson Gas]. The *cis*:*trans* fractions were determined by ^{1}H NMR using a Bruker Avance 600 MHz instrument. Methyl nitrite was synthesized (Taylor et al., 1980) and stored in liquid nitrogen.

Environmental Chamber Method. Reactions of C_8-C_{17} 1-alkenes, 7-tetradecene, 7-pentadecene, and 8-heptadecene with OH radicals in the presence of NO_x

were performed in a 5900 L PTFE environmental chamber at ~25^{o}C and atmospheric pressure. The chamber was filled with clean, dry air (<5 ppbv hydrocarbons, <1% RH) and has blacklights covering two walls. Dioctyl sebacate (DOS) particles from an evaporation-condensation apparatus were flushed into the chamber to achieve a seed particle concentration of ~200-400 μg m^{-3}. An alkene, methyl nitrite, and NO were then added to achieve concentrations of 1 (0.5 and 0.3 for 1-heptadecene and 8-heptadecene), 5, and 5 ppmv. NO suppresses O_3 and NO_3 radical formation. Reactions were also performed with 1-tetradecene at 50% RH and with 20 ppmv NH_3 in dry air.

Reactions were initiated by turning on the blacklights to form OH radicals by methyl nitrite photolysis (Atkinson et al., 1981). After 6 min the blacklights were turned off. Typically, ~40-50% of the alkene reacted, NO decreased by 1-2 ppmv, NO_x stayed approximately constant, and SOA formed within a minute. The average OH radical concentration estimated from the amount of alkene reacted and its OH radical rate constant (Aschmann and Atkinson, 2008) was ~3 x 10^{7} cm^{-3}.

Particle and Gas Analysis. A thermal desorption particle beam mass spectrometer (TDPBMS) was used to analyze particle composition in real-time (Tobias et al., 2000) and by temperature-programmed thermal desorption (TPTD) (Tobias and

Ziemann, 1999). Aerosol was sampled into an aerodynamic lens to form a particle beam that impacted on a polymer-coated metal vaporizer rod (Chattopadhyay and Ziemann, 2005). For real-time analysis, the rod was resistively heated to 160°C. Particles vaporized upon impact and the vapor was ionized by 70 eV electrons and analyzed in a quadrupole mass spectrometer. For TPTD analysis, the rod was cooled to -40°C and particles were collected for 30 min. The rod was allowed to warm to -5°C and then heated to 200°C using a 2°C min^{-1} ramp to desorb and separate compounds by volatility prior to mass analysis.

After a reaction, replicate particle samples were collected for 2 h on Millipore filters (1.0 μm pore size, Fluoropore FALP, 47 mm) at flow rates of ~15 L min^{-1}. In side-by-side tests these filters performed as well as those with 0.45 μm pore size, but had a smaller pressure drop and so less effect on sample flow rates during collection. Filters were extracted immediately or stored at –20^{o}C. Filters were extracted twice in 4 mL of ethyl acetate at room temperature for >10 min. Extracts were combined, dried with N_2, and dissolved in 50 μL of ethyl acetate. Tests using different solvents, sonication, multiple extractions, and filter spiking indicated recovery efficiencies were 90-100%.

Extracts were analyzed using an Agilent 1100 Series HPLC coupled to a UV-Vis diode array detector for quantification and the TDPBMS for identification. A 10 µL sample was separated on a 250 x 4.6 mm Zorbax 5 µm XDB-C18 column at room temperature and a flow rate of 1 mL min^{-1} using a water/acetonitrile gradient elution method: 50% acetonitrile for 10 min increasing to 100% over 50 min. Absorbance was measured at 210 nm, where the molar absorptivity of alkyl nitrates is ≥20 times that of alcohols, ketones, carboxylic acids, or alkenes (Docherty and Ziemann, 2006). The flow then entered a Collison atomizer to form an aerosol, passed through charcoal diffusion dryers to remove solvent vapor, and the dried particles entered the TDPBMS for real-time analysis (Ziemann, 2005). Selected compounds associated with chromatographic peaks were collected, dried, and dissolved in $CDCl_3$ for ^1H NMR analysis using a Varian Inova 400 MHz instrument.

Standard curves used for quantification were prepared using *β*-hydroxynitrates and dihydroxynitrates purified from the SOA extract from the 1-tetradecene reaction. The extract was fractionated using HPLC and mixtures of *β*-hydroxynitrate isomers and dihydroxynitrate isomers were collected separately after their UV-Vis peaks were detected. Samples were dried under vacuum, weighed in a microbalance, and dissolved in

ethyl acetate to create primary standards. Sample purity was verified by HPLC analysis. The calibration curve for β-hydroxynitrates was prepared using the mixture of C_{14} β-hydroxynitrate isomers. The calibration curve for dihydroxynitrates was prepared using 2-ethylhexyl nitrate as a secondary standard because the dihydroxynitrate isomer sample was too small to prepare a dilution series. The molar absorptivities of the dihydroxynitrate and β-hydroxynitrate standards relative to 2-ethylhexyl nitrate were 0.963 and 0.786. The β-hydroxy group affects nitrate UV absorption whereas more distant groups do not (Shriner et al., 1964). The molar yield of an organic nitrate in particles was calculated as (moles of compound on filter/sampled air volume)(aerosol mass concentration after reaction/average aerosol mass concentration during sampling)/(moles of alkene reacted per volume of air). The second term accounts for wall losses during sampling and was calculated from scanning mobility particle sizer (SMPS) measurements. Yields of β-hydroxynitrates and dihydroxynitrates measured in replicate experiments were within ±10% of the value.

Aerosol volume concentrations were measured using a SMPS (Wang and Flagan, 1990) comprised of a long differential mobility analyzer, ^{210}Po bipolar charger, TSI Model 310 CPC, and software from the McMurry group at the University of Minnesota.

Number and volume concentrations were within ±10% of those measured with a TSI 3936L72 SMPS system. SOA volume concentrations were calculated from the difference between seed and SOA + seed aerosol volume concentrations, without corrections for chamber wall losses since they were negligible for these 6 min experiments. SOA mass concentrations, M_{SOA}, were calculated by multiplying SOA volume concentrations by a particle density of 1.13 g cm^{-3}. This value was determined from a dried SOA filter extract from a 1-tetradecene reaction with no seed aerosol: a microliter syringe was weighed, a measured volume of liquid SOA was drawn into the syringe, and then it was re-weighed. Organic aerosol mass concentrations measured with the SMPS were within ±20% of those determined by weighing dried filter extracts.

Alkenes were collected on Tenax TA and analyzed by gas chromatography with flame ionization detector (GC-FID) (Docherty et al., 2005). Concentrations measured for replicate samples taken at 30 min intervals both before and after reaction agreed to within ±5%, so no corrections were made for wall losses.

2.4 Results and Discussion

Reaction Mechanism. The mechanism of OH radical-initiated reactions of linear alkenes in the presence of NO_x (Atkinson and Arey, 2003) is shown in Figure 2.1, where R_1 represents an alkyl group and R_2 represents an H-atom for 1-alkenes and an alkyl group for internal alkenes. Branching ratios are defined as $\alpha_i = r_i/\sum r_i$, where r_i is the rate a species reacts by pathway i and the sum is over all pathways by which the species reacts. The sum of the branching ratios for a species is 1. The branching ratios quantified here are $\alpha_{C=C}$ and α_1-α_6. Note that α_4 and α_6 are associated with the portion of the mechanism labeled "same pathways" in Figure 2.1, and correspond to α_3 and α_5. The reaction is initiated by addition of an OH radical to the C=C double bond or by H-atom abstraction, with branching ratios $\alpha_{C=C}$ and 1-$\alpha_{C=C}$. Products of H-atom abstraction should be similar to those formed from reactions of alkanes (Arey et al., 2001; Atkinson and Arey, 2003; Lim and Ziemann, 2005). We focus here on OH radical addition, which dominates for C_8-C_{17} alkenes, although H-atom abstraction is significant. This pathway forms two isomeric β-hydroxyalkyl radicals (one for a symmetrical alkene) with branching ratios α_1 and α_2 ($\alpha_1 + \alpha_2 = \alpha_{C=C}$). The β-hydroxyalkyl radicals react with O_2 to form β-hydroxyperoxy radicals that react with NO, forming β-hydroxynitrates [**P1**, **P2**]

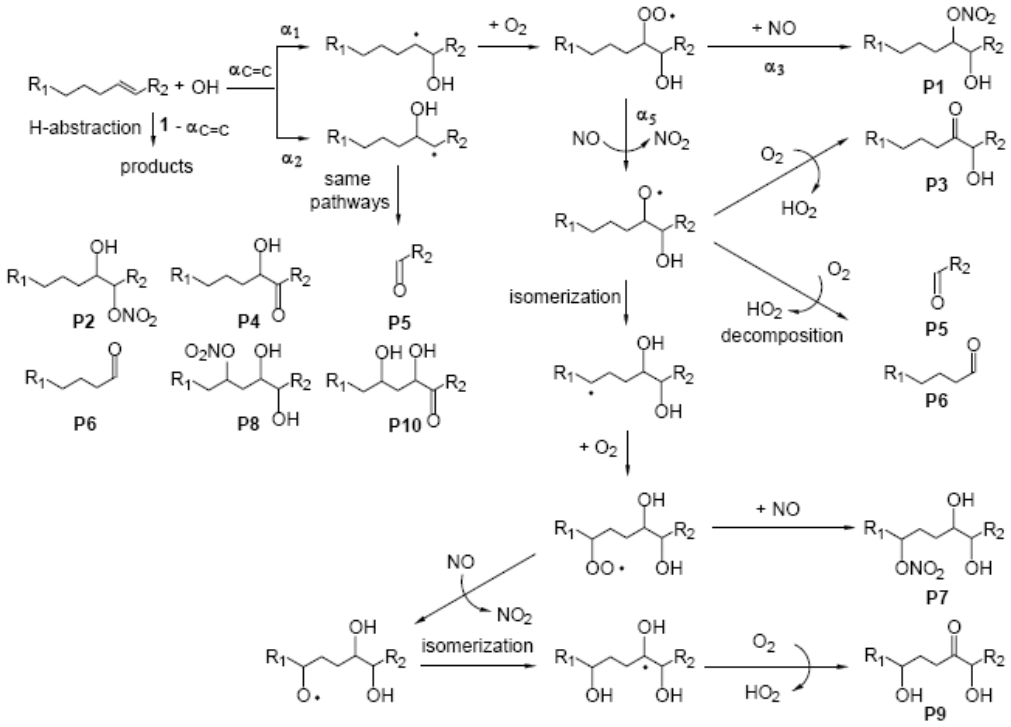

Figure 2.1 Mechanism of the OH radical-initiated reaction of linear alkenes in the presence of NO_x.

with branching ratios α_3 and α_4 or β-hydroxyalkoxy radicals with branching ratios α_5 = 1-α_3 and α_6 = 1-α_4. The β-hydroxyalkoxy radicals can react with O_2, decompose, or isomerize. Reaction with O_2 forms β-hydroxycarbonyls [**P3**, **P4**], but is unimportant for C_n>5 (Atkinson, 2007). Decomposition followed by reaction with O_2 creates two aldehydes [**P5**, **P6**] (the same for both β-hydroxyalkoxy isomers) that are too volatile to form SOA. Isomerization through a six-membered ring followed by reaction with O_2 forms dihydroxyperoxy radicals that react similarly to β-hydroxyperoxy radicals. The products are dihydroxynitrates [**P7**, **P8**] and dihydroxyalkoxy radicals that isomerize and react with O_2 to form dihydroxycarbonyls [**P9**, **P10**]. As is shown elsewhere (Matsunaga et al., 2009), dihydroxycarbonyls present in particles can isomerize to cyclic hemiacetals that can dehydrate to dihydrofurans, or they can form dimers.

SOA Product Identification. Real-time mass spectra of SOA formed from the reaction of 1-tetradecene are shown in Figure 2.2A. Peaks at *m/z* 179, 197, and 199 are characteristic of β-hydroxynitrates and dihydroxynitrates, as verified below. Thermal desorption profiles are shown in Figure 2.2B. Total ion (TI) signal is proportional to organic mass (Crable and Coggeshall, 1958) and *m/z* 46 identifies organic nitrates. The overlap of TI and *m/z* 46 profiles at low temperature suggests the most volatile products

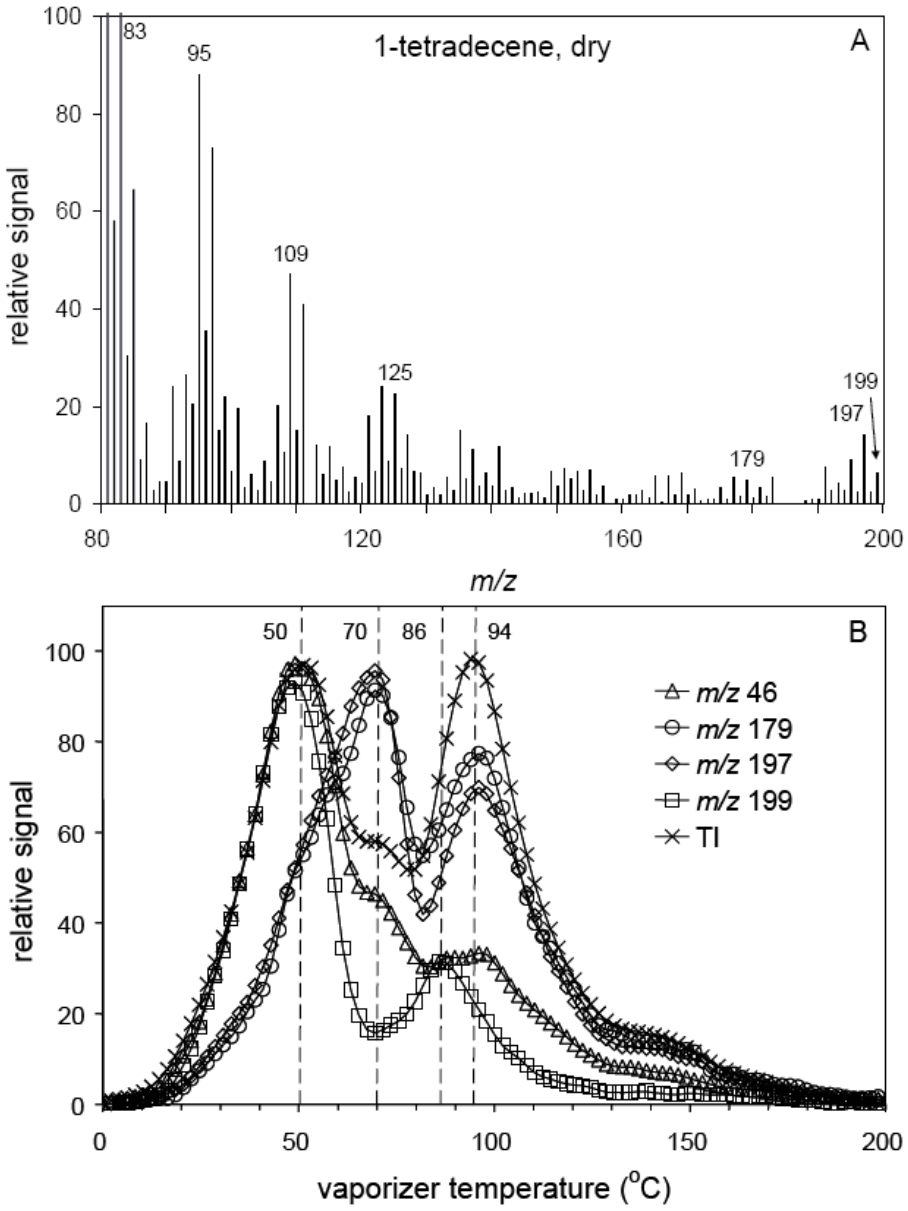

Figure 2.2 (A) Real-time TDPBMS mass spectra and (B) thermal desorption profiles for SOA formed from the OH radical-initiated reaction of 1-tetradecene in dry air in the presence of NO_x. Thermal desorption profiles were smoothed and normalized to peak values.

are organic nitrates, consistent with the expectation that aldehydes are too volatile to form SOA. The most volatile organic nitrates are β-hydroxynitrates, assigned to the peak at 50^{o}C. Dihydroxynitrates are assigned to the peak at 70^{o}C.

This assignment is consistent with results of HPLC analysis shown in Figures 2.3 and 2.4. Structures of β-hydroxynitrates and dihydroxynitrates are designated using the following notation: (1) hydroxy and nitrooxy groups are designated H and N; (2) the location of a group on the alkyl chain is designated by a number placed before the letter; and (3) the length of the alkyl chain is designated by a number following the letter C. For example, 1,2-dihydroxy-4-nitrooxytetradecane is designated 1,2H4NC_{14}.

The predominant fragmentation channel for compounds having adjacent functional groups, as do the β-hydroxynitrates and dihydroxynitrates, is scission of the C-C bond between the two groups. For 1N2HC_{14}, 7H8NC_{14}, 7H8NC_{15}, 7N8HC_{15}, 8H9NC_{17}, and 8N9HC_{17}, this leads to peaks at *m/z* 199, 115, 115, 129, 129, 143 from $RCHOH^{+}$ ions, and neutral aldehyde and NO_2 co-products. For small carbon chains, $RCHOH^{+}$ ions can lose H_2O, as occurs for all these ions except *m/z* 199. For 7H8NC_{14}, 7H8NC_{15}, 7N8HC_{15}, 8H9NC_{17}, and 8N9HC_{17} this gives ions at *m/z* 97, 97, 111, 111, and 125. This is observed in mass spectra of 1,2-dihydroxytetradecane and 7-hydroxytetradecane, which have peaks

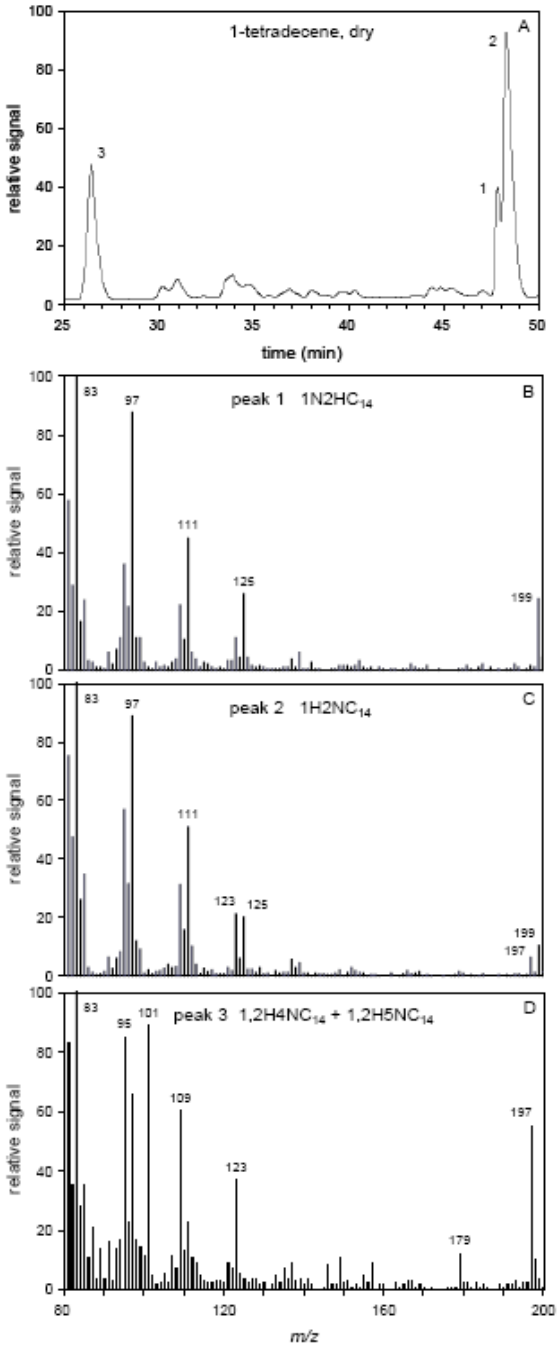

Figure 2.3 (A) HPLC-UV chromatogram and HPLC-TDPBMS mass spectra of (B and C) β-hydroxynitrate isomers and (D) dihydroxynitrates formed from the OH radical-initiated reaction of 1-tetradecene in dry air in the presence of NO_x.

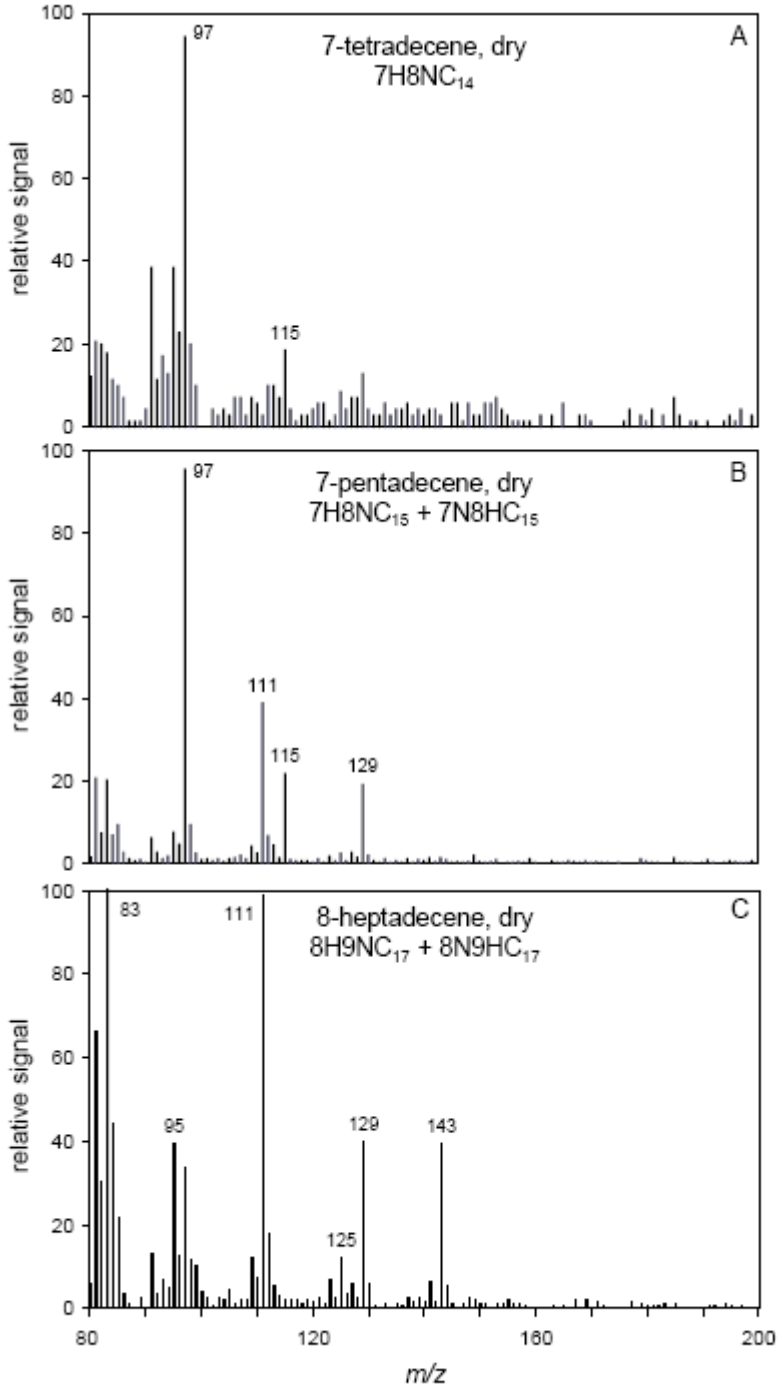

Figure 2.4 HPLC-TDPBMS mass spectra of β-hydroxynitrates formed from the OH radical-initiated reactions of (A) 7-tetradecene, (B) 7-pentadecene, and (C) 8-heptadecene in dry air in the presence of NO_x.

at *m/z* 199 and *m/z* 129, 115, 111, and 97, respectively (Gong et al., 2005). For the 1,2H4NC$_{14}$ and 1,2H5NC$_{14}$ dihydroxynitrates, scission forms an unstable *m/z* 260 ion that loses HNO_3 or $HNO_3 + H_2O$ to form *m/z* 197 and 179 ions. For 1H2NC$_{14}$, scission forms RCO^+ at *m/z* 197 and $CH_3OH + NO_2$. These product assignments are consistent with results of ^{1}H NMR analyses of β-hydroxynitrates and dihydroxynitrates formed from the 1-tetradecene reaction presented in Appendix Table A.2.

β-Hydroxynitrate Yields. Measured molar yields (moles of product formed/moles of alkene reacted) of β-hydroxynitrates are presented in Figure 2.5 and Appendix Table A.1. Losses by secondary reactions with OH radicals were estimated at ≤5% using a model that accounted for decreased reactivity in particles and so were neglected. Yields of both β-hydroxynitrate isomers are reported for reactions of 1-alkenes, but total yields are reported for internal alkenes because isomers could not be resolved. Also presented are yields normalized for the fraction of the OH radical reaction that occurred by addition to the C=C double bond, $\alpha_{C=C} = k_{add}/(k_{add} + k_{abs})$, where k_{add} and k_{abs} are the rate constants for OH radical addition and H-atom abstraction, respectively, with their sum being equal to the total rate constant. Values of $\alpha_{C=C}$ were calculated using equations for k_{abs} (Kwok and Atkinson, 1995) and k_{add} (Nishino et al., 2009) developed

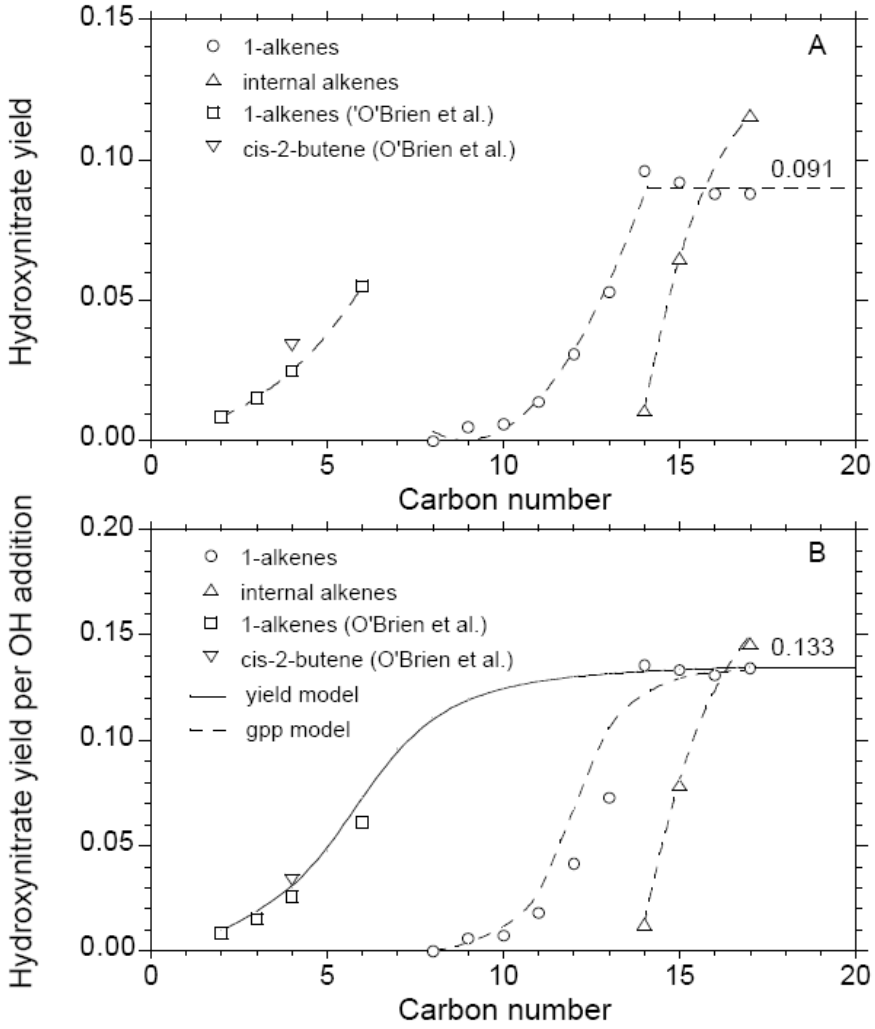

Figure 2.5 Molar yields of β-hydroxynitrates formed fro the OH radical-initiated reaction of linear alkenes in dry air in the presence of NO_x (A) without and (B) with normalization for the fraction of the OH radical reaction that occurred by addition to the double bond. In panel A, the dashed curves were drawn to aid the eye. In panel B, the solid line (yield model) is a scaled version of an equation from Arey et al. (2001) for secondary alkyl nitrate yields, the dashed curve through the yields for 1-alkenes (gpp model) is calculated using gas-particle partitioning theory, and the dashed curve through the yields for internal alkenes was drawn to aid the eye.

by Atkinson and co-workers from measured rate constant data. For 1-alkenes, k_{abs} = 2.47 + 1.4 x (CN-5) and k_{add} = 28 + 9 x [1-exp(-0.35 x (CN-3))], where CN is the carbon number and k values are in units of 10^{-12} cm^3 $molecule^{-1}$ s^{-1}. For *cis* and *trans* internal alkenes, k_{abs} = 4.93 + 1.4 x (CN-8), k_{add}(*cis*) = 56.4, and k_{add}(*trans*) = 64, and were used with the measured fractions of *cis* and *trans* isomers to calculate weighted values of $\alpha_{C=C}$. In general, $\alpha_{C=C}$ increases with increased alkyl group substitution at the C=C double bond and decreases with increasing carbon number.

Total β-hydroxynitrate yields measured for reactions of 1-alkenes and internal alkenes without and with normalization for OH addition are shown in Figure 2.5. Normalization reduces scatter caused by differences in the relative reactivity of the C=C double bond. Yields increase with carbon number and for 1-alkenes reach a plateau at C_{14}-C_{17}, where the average OH addition-normalized yield is 0.133 ± 0.002. Stated uncertainties here and throughout the text are one standard deviation. Yields for internal alkenes may reach a plateau at about C_{17}, where the OH addition-normalized yield is 0.150, but this could not be verified because C_{16} or C_{18} internal alkenes were not available for experiments. Also shown in Figure 2.5 are total yields of β-hydroxynitrates formed from reactions of C_2-C_4 and C_6 1-alkenes and *cis*-2-butene, measured using gas

chromatography (O'Brien et al., 1998). Note that C_2-C_6 β-hydroxynitrates are gas phase products, whereas C_8-C_{17} β-hydroxynitrates could be in the gas and/or particle phases. Yields reported here are for particulate C_8-C_{17} β-hydroxynitrates and can be affected by gas-particle partitioning.

The solid curve in Figure 2.5B was calculated using a scaled version of an equation developed by Arey et al. (2001) from measurements of yields of C_2-C_8 secondary alkyl nitrates formed from reactions of *n*-alkanes with OH radicals in the presence of NO_x. Results of computational studies (Zhang et al., 2004) are consistent with the form of this equation. They predict alkyl nitrate yields increase with carbon number to a plateau at ~C_{15} because the internal energy generated by formation of the alkyl peroxy radical-NO intermediate is distributed among more vibrational modes, increasing stability and thereby nitrate formation. The scaling factor used for the curve in Figure 2.5B was 0.455, chosen to reduce the yield calculated for a C_{15} β-hydroxynitrate from 0.292, the value for a C_{15} secondary alkyl nitrate, to 0.133, the average total OH addition-normalized β-hydroxynitrate yield at the plateau. Previous studies of $C_n \leq 8$ alkenes noted that β-hydroxynitrate yields are about half those of alkyl nitrates (O'Brien et al., 1998; Atkinson et al., 1995). Quantum chemical calculations indicate yields are

lower for β-hydroxynitrates because hydrogen bonding between hydroxy and peroxy groups weakens the O-O bond in the β-hydroxyperoxy radical-NO intermediate, enhancing formation of a β-hydroxyalkoxy radical and NO_2 (O'Brien et al., 1998).

Comparison of measured and modeled β-hydroxynitrate yields (Figure 2.5) indicates the increase in measured yields with increasing carbon number is primarily due to enhanced gas-to-particle partitioning. This conclusion is also consistent with yields that have been corrected for gas-particle partitioning, shown by the dashed curve in Figure 2.5B. Values were calculated by multiplying the plateau value of 0.133 by the fraction of each β-hydroxynitrate estimated to be in the particle phase using gas-particle partitioning theory (Pankow, 1994) and β-hydroxynitrate vapor pressures assumed to be the same as those of 1,2-dialkynitrates (Fischer and Ballschmiter, 1998). Yields measured for reactions of internal alkenes are shifted to higher carbon numbers because functional groups located away from the ends of a molecule have less effect on vapor pressure. The shift in the two curves is ~2-3 carbon numbers, which suggests that the yield measured for the C_{17} internal alkene should, like the corresponding C_{14} or C_{15} 1-alkenes, be close to a plateau. The OH addition-normalized yields measured for the β-hydroxynitrate isomers, $1H2NC_n$ and $1N2HC_n$, formed from reactions of 1-alkenes are shown in Figure 2.6 with

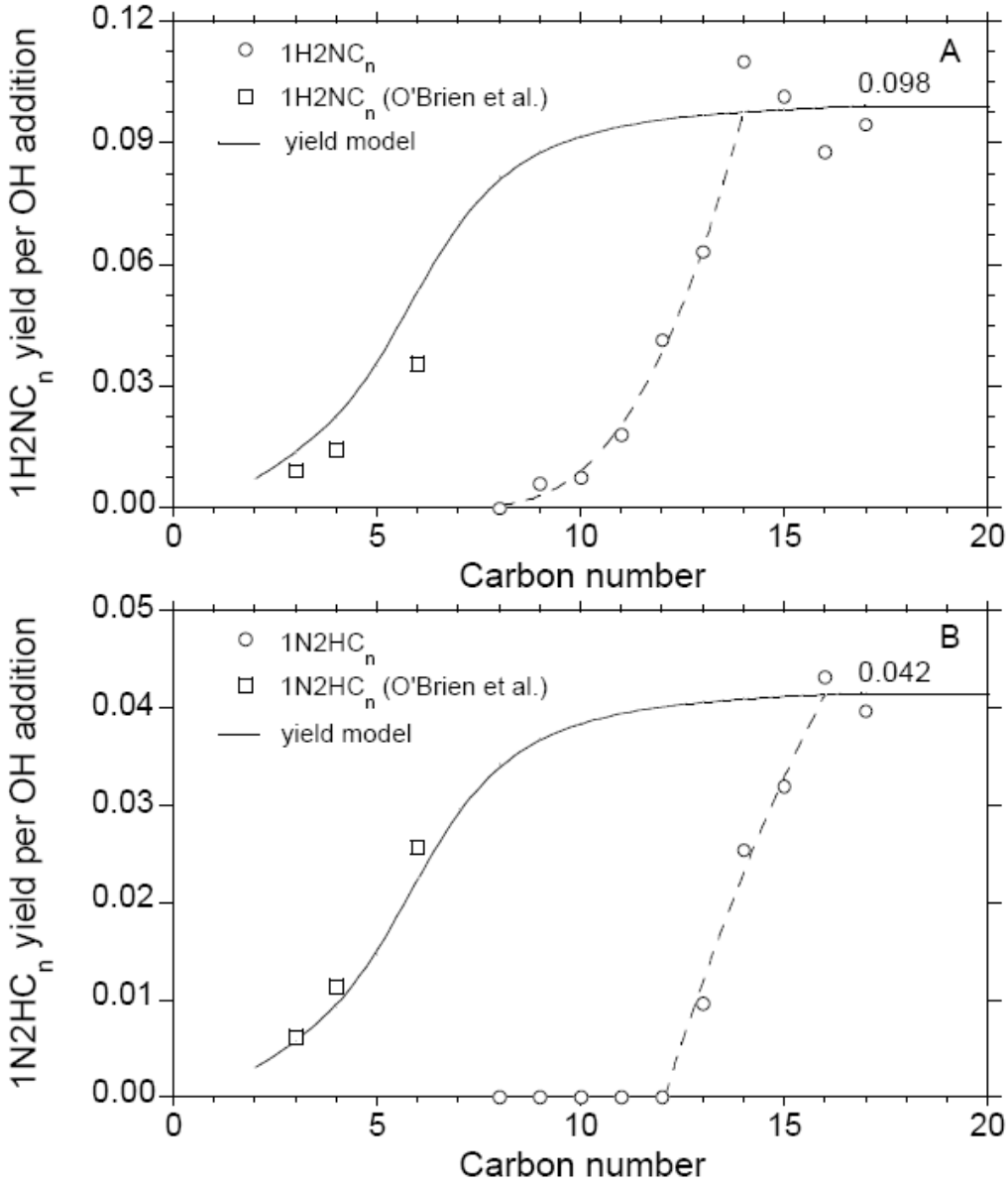

Figure 2.6 Molar yields of *β*-hydroxynitrate isomers formed from the OH radical-initiated reaction of 1-alkenes in the presence of NO_x, with normalization for the fraction of the OH radical reaction that occurred by addition to the double bond. The solid curves (yield model) are scaled versions of an equation from Arey et al. (2001) for secondary alkyl nitrate yields, and the dashed curves were drawn to aid the eye.

model curves adjusted to match average plateau values at C_{15}. Yields are much larger for $1H2NC_n$ than $1N2HC_n$ isomers; a $1H2NC_n$ isomer was first detected at C_9 and a $1N2HC_n$ isomer at C_{13}. Yields increase with increasing carbon number reaching plateaus at C_{14} for $1H2NC_n$ isomers and C_{16} for $1N2HC_n$ isomers. Average OH addition-normalized yields for $1H2NC_n$ and $1N2HC_n$ isomers are 0.098 ± 0.009 and 0.042 ± 0.002 within the C_{14}-C_{17} and C_{16}-C_{17} plateau regions, corresponding to fractions of 0.70 and 0.30 of the total yield of 0.140 ± 0.009. Fractions measured for C_3, C_4, and C_6 1-alkenes were 0.59 and 0.41 (O'Brien et al., 1998). The value of 0.140 does not include yields for the $1N2HC_{14}$ and $1N2HC_{15}$ isomers, which are impacted by gas-particle partitioning, and so is more accurate than the value of 0.133 obtained from the total OH addition-normalized yields (Figure 2.5B).

Branching Ratios. From Figure 2.1 and the discussion above, it can be seen that the OH addition-normalized yields of the $1H2NC_n$ [**P1**] and $1N2HC_n$ [**P2**] isomers are equal to $Y_{P1}/\alpha_{C=C} = (\alpha_1/\alpha_{C=C})(\alpha_3)$ and $Y_{P2}/\alpha_{C=C} = (\alpha_2/\alpha_{C=C})(\alpha_4)$, where Y is the measured yield. The fraction of OH radical addition reactions that occur at the first and second carbon atoms, $\alpha_1/\alpha_{C=C}$ and $\alpha_2/\alpha_{C=C}$, can therefore be calculated from our reported OH-normalized yields, if the branching ratios for the formation of these compounds from the

reactions of NO with 1-hydroxy-2-peroxy radicals, α_3, and 1-peroxy-2-hydroxy radicals, α_4, are known. Here, we estimate these values using two plausible sets of values for α_3 and α_4 and isomer yield data for $C_n \geq 16$, where gas-particle partitioning is not important.

In the first case, we assume that $\alpha_3 = \alpha_4$. Since $(\alpha_1/\alpha_{C=C}) + (\alpha_2/\alpha_{C=C}) = 1$, then $\alpha_3 = \alpha_4 = 0.14$, the sum of the OH addition-normalized isomer yields, and $(\alpha_1/\alpha_{C=C}) = 0.098/0.14 = 0.70$ and $(\alpha_2/\alpha_{C=C}) = 0.042/0.14 = 0.30$. These values agree well with values of 0.65 and 0.35 measured by Cvetanovic for 1-propene (1976). For the internal alkenes studied here, OH radical addition should not depend on the alkyl groups attached to the double-bonded carbon atoms, so that $(\alpha_1/\alpha_{C=C}) = (\alpha_2/\alpha_{C=C}) = 0.5$ and $\alpha_3 = \alpha_4 = 0.15$, the sum of OH addition-normalized yields measured for the reaction of 8-heptadecene. In this case, then, the branching ratios for the formation of β-hydroxynitrates from reactions of NO with β-hydroxyperoxy radicals appear to be similar for 1-alkenes and internal alkenes at their plateaus (assuming for reasons discussed above that the value for 8-heptadecene is close to the plateau) and ~0.13-0.15.

In the second case, we assume that $\alpha_3/\alpha_4 = 1.5$, the ratio measured recently by Cassanelli et al. (2007) for the formation of alkyl nitrates from reactions of NO with pentyl peroxy radical isomers. These results indicate that the branching ratio for 1-

hydroxy-2-peroxy radicals, α_3, could be ~1.5 times the value for 1-peroxy-2-hydroxy radicals, α_4, although β-hydroxyperoxy radicals may not necessarily behave the same as alkyl peroxy radicals, due to the presence of the hydroxy group. Combining the equations $\alpha_3/\alpha_4 = 1.5$, $Y_{P1}/\alpha_{C=C} = 0.098 = (\alpha_1/\alpha_{C=C})(\alpha_3)$, $Y_{P2}/\alpha_{C=C} = 0.042 = (\alpha_2/\alpha_{C=C})(\alpha_4)$, and $(\alpha_1/\alpha_{C=C}) + (\alpha_2/\alpha_{C=C}) = 1$ then gives for reactions of 1-alkenes, $\alpha_1/\alpha_{C=C} = 0.62$ $\alpha_2/\alpha_{C=C} = 0.38$, $\alpha_3 = 0.16$, and $\alpha_4 = 0.11$. The value of α_3 for reactions of internal alkenes should therefore be ~0.16 in this case. The agreement between these values and those noted above for 1-propene (Cvetanovic, 1976) and 8-heptadecene is again good, indicating that both sets of branching ratios are consistent with the experimental results and that it is not possible to identify differences in the branching ratios for nitrate formation from reactions of NO with primary and secondary peroxy groups in β-hydroxyperoxy radicals. It is worth noting that values of $\alpha_3/\alpha_4 \sim 2$ have been suggested (Atkinson et al., 1982), although the measurements were less precise than those of Cassanelli et al. (2007). The resulting branching ratios are, $\alpha_1/\alpha_{C=C} = 0.54$ $\alpha_2/\alpha_{C=C} = 0.46$, $\alpha_3 = 0.18$, and $\alpha_4 = 0.09$, which do not agree as well with the measurements.

Dihydroxynitrate Yields. Total yields of dihydroxynitrates in particles are given in Appendix Table A.1; the isomers could not be resolved. Unlike β-hydroxynitrate yields,

dihydroxynitrate yields are independent of carbon number. This is probably because the additional hydroxy group leads to almost complete gas-to-particle partitioning. Yields without and with normalization for OH addition were 0.029 ± 0.005 and 0.039 ± 0.006 for the C_{10}-C_{17} 1-alkenes and 0.005 ± 0.002 and 0.006 ± 0.002 for the internal alkenes. The lower yields for internal alkenes reflect the higher rates of decomposition relative to isomerization for the β-hydroxyalkoxy radicals (Atkinson, 2007).

Effects of Humidity and Ammonia on β-Hydroxynitrate and Dihydroxynitrate Yields. As mentioned above, it is thought that the lower branching ratios for nitrate formation from reactions of NO with β-hydroxyperoxy radicals compared to alkyl peroxy radicals is due to hydrogen bonding between hydroxy and peroxy groups (O'Brien et al., 1998). This effect was further investigated here by comparing yields of β-hydroxynitrates and dihydroxynitrates formed from reactions of 1-tetradecene in dry air with those formed at 50% RH and in dry air with 20 ppmv of NH_3. H_2O and NH_3 are both capable of hydrogen bonding and so could affect yields.

Results are given in Table 2.1. They show that H_2O did not affect the yields of β-hydroxynitrates, but may have reduced those of dihydroxynitrates (the difference is within uncertainties). The absence of an effect is consistent with results of computations

Table 2.1 Effects of Experimental Conditions on Molar Yields of β-Hydroxynitrates and Dihydroxynitrates Formed from OH Radical-Initiated Reactions of 1-Tetradecene in the Presence of NO_x.

condition[a]	$1H2NC_{14}$	$1N2HC_{14}$	dihydroxynitrates[b]
Dry	0.078	0.018	0.033
H_2O	0.082	0.018	0.023
NH_3	0.018	0.004	0.010

[a]Dry = <1% RH; H_2O = 50% RH; NH_3 = 20 ppmv NH_3.

[b]Dihydroxynitrate isomers are $1,2H4NC_{14}$ and $1,2H5NC_{14}$.

that predict that at 300K and 50% RH ~1% of β-hydroxyperoxy radicals exist as complexes with H_2O (Clark et al., 2008). The additional hydroxy group in dihydroxyperoxy radicals might enhance complex formation with H_2O sufficiently to reduce the yields. Conversely, NH_3 had a large impact on yields, reducing those of β-hydroxynitrates and dihydroxynitrates by ~70-80%. The greater effect of NH_3 probably results from stronger hydrogen bonding weakening the O-O bond. According to calculations (Clark et al., 2008), $\log K_{eq}$ for forming complexes of H_2O with various peroxy radicals at 300K is a linear function of the binding energy of the complex, BE (kcal mol^{-1}), with slope ~0.5. If this relationship holds in general, then the fraction of β-hydroxyperoxy radicals present as complexes, F, with a species C is approximately given by eq. 2.1 with [C] in ppmv.

$$\log F = (0.5 \times BE) + \log[C] - 9.5 \qquad (2.1)$$

This equation is used here to estimate the minimum binding energy for a β-hydroxyperoxy radical-NH_3 complex. From our results, the minimum value of F at 20 ppmv NH_3 is ~0.75 if the branching ratio for β-hydroxynitrate formation from the reaction of NO with a complex is zero. Otherwise, F and BE are higher. Substituting these values into eq. 2.1 gives BE ~16 kcal mol^{-1}, compared to ~6.4 kcal mol^{-1} for the

H_2O complex. In the atmosphere, NH_3 concentrations can range from tens of ppbv in polluted air to tens of pptv in clean air (Finlayson-Pitts and Pitts, 2000). Under these conditions, calculated binding energies of ~22-28 kcal mol^{-1}, which are unlikely, are required to achieve a similar fraction of complexes, suggesting ammonia does not effect these reactions.

2.5 Conclusions

The results presented here represent the first measurements to date of the yields of β-hydroxynitrates and dihydroxynitrates in SOA, in this case formed from OH radical-initiated reactions of linear alkenes in the presence of NO_x. The yields depend on the structure of the parent alkene, which influences a number of important aspects of the reaction mechanism. These include the rates at which OH radicals abstract H atoms and add to the C=C double bond, the C atom to which the OH radical adds, branching ratios for the reactions of organic peroxy radicals with NO, and rates of decomposition and isomerization of alkoxy radicals, as well as gas-particle partitioning of products. The yields can also be impacted by the presence of species such as NH_3, which can form hydrogen bonds with organic peroxy radicals. Reactions were carried out with C_8-C_{17}

alkenes in order to form at least some products that were sufficiently large that gas-to-particle partitioning was essentially complete (and therefore yields measured in aerosol were the same as total yields) and that reaction branching ratios did not depend on carbon number. For 1-alkenes, a plateau was reached at C_{14}-C_{17} for the yields of β-hydroxynitrates normalized for OH radical addition to the C=C double bond, corresponding to branching ratios for their formation from reactions of NO with β-hydroxyperoxy radicals (averaged over both isomers) of 0.13-0.15. A similar value was obtained for internal alkenes, but with less data. A simple model developed previously (Arey et al., 2001) to describe the carbon number dependence of this branching ratio for reactions of alkyl peroxy radicals with NO also works well for these reactions after scaling by a factor of 0.455 to match the plateau value. The lower branching ratios for β-hydroxyperoxy radicals apparently result from hydrogen bonding between the hydroxy and peroxy groups. This branching ratio equation can be used with structure-reactivity calculations (Kwok and Atkinson, 1995; Nishino et al., 2009) of OH radical addition and abstraction to estimate yields of β-hydroxynitrates from the reactions of alkenes. For example, for C_{10} monoterpenes and C_{15} sesquiterpenes, major atmospheric alkene emissions whose OH radical reactions are dominated by addition, β-hydroxynitrate yields

should be close to 0.14, consistent with a total organic nitrate yield of 0.18 measured for the α-pinene reaction (Noziére et al., 1999).

Yields of dihydroxynitrates were highly dependent on the structure of the parent alkene, most likely because of differences in rates of decomposition of β-hydroxyalkoxy radicals, and possibly branching ratios for the reactions of dihydroxyperoxy radicals with NO. Partitioning to the aerosol phase appeared to be complete over the C_{10}-C_{17} carbon number range where analysis was possible, reflecting the lower volatility of these compounds compared to β-hydroxynitrates. As is shown elsewhere (Matsunaga et al., 2009), the dihydroxynitrate yields measured here can be used with the β-hydroxynitrate yields, carbonyl yields from the literature, and structure-reactivity calculations for OH radical reactions and β-hydroxyalkoxy radical isomerization and decomposition to develop a quantitative chemical mechanism and model of SOA formation from these reactions.

It is also worth emphasizing that the yields reported here were measured by coupling a TDPBMS to a HPLC with UV-Vis detector via an atomizer. For these experiments, it was therefore possible to analyze SOA in three different ways with the TDPBMS: in real-time, by temperature-programmed thermal desorption, and following

HPLC separation. Products were therefore separated according to their temporal behavior during formation, volatility, and solvent-column interactions. All of this information can aid in product identification, which is difficult in SOA studies because of the general lack of authentic standards of potential products. Here, authentic standards were synthesized by HPLC purification of SOA samples, followed by ^{1}H NMR analysis to verify their identity. The use of the same particle mass spectrometer for all analyses also has the advantage that it is easier to identify possible artifacts that can occur during off-line analysis, since the mass spectra can be directly compared. We have recently used this approach with a high-resolution time-of-flight Aerodyne aerosol mass spectrometer (AMS), which further enhances analytical capabilities by providing elemental analysis, to aid in the creation of a database of multifunctional organic nitrate mass spectra. Given the variety of particle mass spectrometers currently in use, this may be an approach for others to consider.

2.6 References

Andreae, M. O. and Crutzen, P. J., 1997. Atmospheric Aerosols: Biogeochemical Sources and Role in Atmospheric Chemistry. *Science, 276,* 1052-1058.

Arey, J., Aschmann, S. M., Kwok, E. S. C., Atkinson, R., 2001. Alkyl Nitrate, Hydorxyalkyl Nitrate, and Hydroxycarbonyl Formation from the NO_x-Air Photooxidations of C_5-C_8 *n*-Alkanes. *J. Phys. Chem. A, 105,* 1020-1027.

Aschmann, S. M. and Atkinson, R., 2008. Rate Constants for the Gas-Phase Reactions of OH Radicals with *E*-7-Tetradecene, 2-Methyl-1-Tridecene and the C_7-C_{14} 1-Alkenes at 295 ± 1 K. *Phys. Chem. Chem. Phys., 10,* 4159-4164.

Aschmann, S. M., Reissell, A., Atkinson, R., Arey, J., 1998. Products of the Gas Phase Reactions of the OH Radical with α- and β-Pinene in the Presence of NO. *J. Geophys. Res., 103,* 25553-25561.

Aschmann, S. M., Atkinson, R., Arey, J., 2002. Products of Reaction of OH Radicals with α-Pinene. *J. Geophys. Res., 107,* doi:10.1029/2001JD001098.

Atkinson, R., 1997. Gas-Phase Tropospheric Chemistry of Volatile Organic Compounds: 1. Alkanes and Alkenes. *J. Phys. Chem. Ref. Data, 26,* 215-290.

Atkinson, R., 2007. Rate Constants for the Atmospheric Reactions of Alkoxy Radicals: An Updated Estimation Method. *Atmos. Environ., 41,* 8468-8485.

Atkinson, R. and Arey, J., 2003. Atmospheric Degradation of Volatile Organic Compounds. *Chem. Rev., 103,* 4605-4638.

Atkinson, R., Carter, W. P. L., Winer, A. M., Pitts, J. N., Jr., 1981. An Experimental Protocol for the Determination of OH Radical Rate Constants with Organics Using Methyl Nitirite Photolysis as an OH Radical Source. *Air Pollut. Control Assoc., 31,* 1090-1092.

Atkinson, R., Aschmann, S. M., Carter, W. P. L., Winer, A. M., Pitts, J. N., Jr., 1982. Alkyl Nitrate Formation from the Nitrogen Oxide (NO_x)-Air Photooxidations of C_2-C_8 *n*-Alkanes. *J. Phys. Chem.*, *86*, 4563-4569.

Atkinson, R., Tuazon, E. C., Aschmann, S. M., 1995. Products of the Gas-Phase Reactions of a Series of 1-Alkenes and 1-Methylcyclohexene with the OH Radical in the Presence of NO. *Environ. Sci. Technol.*, *29*, 1674-1680.

Calvert, J.G., Atkinson, R., Kerr, J.A., Madronich, S., Moortgat, G.K., Wallington, T.J., Yarwood, G., 2000. The Mechanisms of Atmospheric Oxidation of the Alkenes. Oxford University Press, New York.

Cassanelli, P., Fox, D. J., Cox, R. A., 2007. Temperature Dependence of Pentyl Nitrate Formation from the Reactions of Pentyl Peroxy Radicals with NO. *Phys. Chem. Chem. Phys.*, *9*, 4332-4337.

Chattopadhyay, S. and Ziemann, P. J., 2005. Vapor Pressures of Substituted and Unsubstituted Monocarboxylic and Dicarboxylic Acids Measured Using an Improved Thermal Desorption Particle Beam Mass Spectrometry Method. *Aerosol Sci. Technol.*, *39*, 1085-1100.

Chen, X., Hulbert, D., Shepson, P. B., 1998. Measurement of the Organic Nitrate Yield from OH Reaction with Isoprene. *J. Geophys. Res.*, *103*, 25563-25568.

Clark, J., English, A. M., Hansen, J. C., Francisco, J. S., 2008. Computational Study on the Existence of Organic Peroxy Radical-water Complexes ($RO_2 \cdot H_2O$). *J. Phys. Chem. A*, *112*, 1587-1595.

Crable, G.F. and Coggeshall, N.D., 1958. Application of Total Ionization Principles to Mass Spectrometric Analysis. *Anal. Chem.*, *30*, 310-313.

Cvetanovic, R. J., 1976. unpublished report presented at the 12th International Symposium on Free Radicals, Laguna Beach, CA. Cited in: Calvert, J.G., Atkinson, R., Kerr, J.A., Madronich, S., Moortgat, G.K., Wallington, T.J., Yarwood, G., 2000. The

Mechanisms of Atmospheric Oxidation of the Alkenes. Oxford University Press, New York.

Docherty, K. S. and Ziemann, P. J., 2006. Reaction of Oleic Acid Particles with NO_3 Radicals: Products, Mechanism, and Implications for Radical-Initiated Organic Aerosol Oxidation. *J. Phys. Chem. A, 110*, 3567-3577.

Docherty, K. S., Wu, W.; Lim, Y. B., Ziemann, P. J., 2005. Contributions of Organic Peroxides to Secondary Aerosol Formed from Reactions of Monoterpenes with O_3. *Environ. Sci. Technol., 39*, 4049-4059.

Englert, N., 2004. Fine Particles and Human Health – a Review of Epidemiological Studies. *Toxicol. Lett., 149*, 235-242.

Finlayson-Pitts, B. J. and Pitts, J. N., Jr., 2000. Chemistry of the Upper and Lower Atmosphere. Academic Press, San Diego.

Fischer, R. G. and Ballschmiter, K., 1998. Prediction of the Environmental Distribution of Alkyl Dinitrates – Chromatographic Determination of Vapor Pressure p^0, Water Solubility S_{H2O}, Gas-Water Partition Coefficient K_{GW} (Henry's Law Constant) and Octanol-Water Partition Coefficient K_{OW}. *Fresenius J. Anal. Chem., 360*, 769-776.

Fisher, R. G., Kastler, J., Ballschmiter, K., 2000. Levels and Pattern of Alkyl Nitrates, Multifunctional Alkyl Nitrates, and Halocarbons in the Air over the Atlantic Ocean. *J. Geophys. Res., 105*, 14473-14494.

Gong, H., Matsunaga, A., Ziemann, P. J., 2005. Products and Mechanism of Secondary Organic Aerosol Formation from Reactions of Linear Alkenes with NO_3 Radicals. *J. Phys. Chem. A, 109*, 4312-4324.

Griffin, R. J., Cocker, D. R., III, Seinfeld, J. H., Dabdub, D., 1999. Estimate of Global Atmospheric Organic Aerosol from Oxidation of Biogenic Hydrocarbons. *Geophys. Res. Lett., 17*, 2721-2724.

Guenther, A., Hewitt, C. N., Erickson, D., Fall, R., Geron, C., Graedel, T., Harley, P., Klinger, L., Lerdau, M., McKay, W. A., Pierce, T., Scholes, B., Steinbrecher, R., Tallamraju, R., Taylor, J., Zimmermann, P., 1995. A Global Model of Natural Volatile Organic Compound Emissions. *J. Geophys. Res.*, *100*, 8873-8892.

Jaoui, M. and Kamens, R. M., 2003a. Gaseous and Particulate Oxidation Products Analysis of a Mixuture of α-Pinene + β-Pinene/O_3/Air in the Absence of Light and α-Pinene + β-Pinene/NO_x/Air in the Presence of Natural Sunlight. *J. Atmos. Chem.*, *44*, 259-297.

Jaoui, M. and Kamens, R. M., 2003b. Gas and Particulate Products Distribution from the Photooxidation of α-Humulene in the Presence of NO_x, Natural Atmospheric Air and Sunlight. *J. Atmos. Chem.*, *46*, 29-54.

Kwok, E. S. C. and Atkinson. R., 1995. Estimation of Hydroxyl Radical Reaction Rate Constants for Gas-Phase Organic Compounds Using a Structure-Reactivity Relationship: An Update. *Atmos. Environ.*, *29*, 1685-1695.

Lee, A., Goldstein, A. H., Kroll, J. H., Ng, N. L., Varutbangkul, V., Flagan, R. C., Seinfeld, J. H., 2006. Gas-Phase Products and Secondary Aerosol Yields from the Photooxidation of 16 Different Terpenes. *J. Geophys. Res.*, *111*, doi:10.1029/2006JD007050.

Lim, Y. B. and Ziemann, P. J., 2005. Products and Mechanism of Secondary Organic Aerosol Formation from Reactions of *n*-Alkanes with OH Radicals in the Presence of NO_x. *Environ. Sci. Technol.*, *39*, 9229-9236.

Matsunaga, A., Docherty, K. S., Lim, Y. B., Ziemann, P. J., 2009. Composition and Yields of Secondary Organic Aerosol Formed from OH Radical-Initiated Reactions of Linear Alkenes in the Presence of NO_x: Modeling and Measurements. *Atmos. Environ.*, *43*, 1349-1357.

Nishino, N., Arey, J., Atkinson, R., 2009. Rate Constants for the Gas-Phase Reactions of OH Radicals with a Series of C_6-C_{14} Alkenes at 299 ± 2 K. *J. Phys. Chem. A, 113*, 852-857.

Nozière, B., Barnes, I., Becker, K.-H., 1999. Product Study and Mechanisms of the Reactions of α-Pinene and of Pinonaldehyde with OH Radicals. *J. Geophys. Res.*, *104*, 23645-23656.

O'Brien, J. M., Shepson, P. B., Muthuramu, K., Hao, C., Niki, H., Hastie, D. R., Taylor, R., Roussel, P. B., 1995. Measurements of Alkyl and Multifunctional Organic Nitrates at a Rural Site in Ontario. *J. Geophys. Res.*, *100*, 22795-22804.

O'Brien, J. M., Shepson, P. B., Wu, Q., Biesenthal, T., Bottenheim, J. W., Wiebe, H. A., Anlauf, K. G., Brickwell, P., 1997. Production and Distribution of Organic Nitrates, and Their Relationship to Carbonyl Compounds in an Urban Environment. *Atmos. Environ.*, *31*, 2059-2069.

O'Brien, J. M., Czuba, E., Hastie, D. R., Francisco, J. S., Shepson, P. B., 1998. Determination of the Hydroxy Nitrate Yields from the Reaction of C_2-C_6 Alkenes with OH in the Presence of NO. *J. Phys. Chem. A, 102*, 8903-8908.

Pankow, J. F., 1994. An Absorption Model of the Gas/Aerosol Partitioning Involved in the Formation of Secondary Organic Aerosol. *Atmos. Environ.*, *28*, 189-193.

Shriner, R. L., Fuson, R. C., Curtin, D. Y., 1964. The Systematic Identification of Organic Compounds. John Wiley & Sons, Inc.: New York.

Spengnether, M., Demerjian, K. L., Donahue, N. M., Anderson, J. G., 2002. Product Analysis of the OH Oxidation of Isoprene and 1,3-Butandiene in the Presence of NO. *J. Geophys. Res.*, *107*, doi:10.1029/2001JD000716.

Surratt, J.D., Murphy, S.M., Kroll, J.H., Ng, N.L., Hildebrandt, L., Sorooshian, A., Szmigielski, R., Vermeylen, R., Maenhaut, W., Claeys, M., Flagan, R.C., Seinfeld, J.H.,

2006. Chemical Composition of Secondary Organic Aerosol Formed from the Photooxidation of Isoprene. *J. Phys. Chem. A, 110*, 9665-9690.

Taylor, W. D., Allston, T. D., Moscato, M. J., Fazekas, G. B., Kozlowski, R., Takacs, G. A., 1980. Atmospheric Photodissociation Lifetimes for Nitromethane, Methyl Nitrite, and Methyl Nitrate. *Int. J. Chem. Kinet., 12*, 231-240.

Tobias, H. J. and Ziemann, P. J., 1999. Compound Identification in Organic Aerosols Using Temperature-Programmed Thermal Desorption Particle Beam Mass Spectrometry. *Anal. Chem., 71*, 3428-3435.

Tobias, H. J., Kooiman, P. M., Docherty, K. S., Ziemann, P. J., 2000. Real-Time Chemical Analysis of Organic Aerosols Using a Thermal Desorption Particle Beam Mass Spectrometer. *Aerosol Sci. Technol., 33*, 170-190.

Tuazon, E. C., Aschmann, S. M., Arey, J., Atkinson, R., 1998. Products of the Gas-Phase Reactions of a Series of Methyl-Substituted Ethenes with the OH Radical. *Environ. Sci. Technol., 32*, 2106-2112.

Wang, S. C. and Flagan, R. C., 1990. Scanning Electrical Mobility Spectrometer. *Aerosol Sci. Technol., 13*, 230-240.

Werner, G., Kastler, J., Looser, R., Ballschmiter, K., 1999. Organic Nitrates of Isoprene as Atmospheric Trace Compounds. *Angnew. Chem. Int. Ed., 38*, 1634-1637.

Zhang, J., Dransfield, T., Donahue, N. M., 2004. On the Mechanism for Nitrate Formation via the Peroxy Radical + NO Reaction. *J. Phys. Chem. A, 108*, 9082-9095.

Ziemann, P. J., 2005. Aerosol Products, Mechanisms, and Kinetics of Heterogeneous Reactions of Ozone with Oleic Acid in Pure and Mixed Particles. *Faraday Discuss., 130*, 469-490.

Chapter 3

Composition and Yields of Secondary Organic Aerosol Formed from Radical-Initiated Reactions of Linear Alkenes in the Presence of NO_x: Modeling and Measurements

3.1 Abstract

The products and mechanism of secondary organic aerosol (SOA) formation from the OH radical-initiated reactions of linear alkenes in the presence of NO_x were investigated in an environmental chamber. The SOA consisted primarily of products formed through reactions initiated by OH radical addition to the C=C double bond, including β-hydroxynitrates and dihydroxynitrates, as well as cyclic hemiacetals, dihydrofurans, and dimers formed from particle-phase reactions of dihydroxycarbonyls. 1,4-Hydroxynitrates formed through reactions initiated by H-atom abstraction also appeared to contribute. Product yields and OH radical and alkoxy radical rate constants taken from the literature or calculated using structure-reactivity methods were used to develop a quantitative chemical mechanism for these reactions. SOA yields were then calculated using this mechanism with gas-particle partitioning theory and estimated

product vapor pressures for comparison with measured values. Calculated and measured SOA yields agreed very well at high carbon numbers when semi-volatile products were primarily in the particle phase, but diverged with decreasing carbon number to a degree that depended on the model treatment of dihydroxycarbonyls, which appeared to undergo reversible reactions in the particle phase. The results indicate that the chemical mechanism developed here provides an accurate representation of the gas-phase chemistry, but the utility of the SOA model depends on the partitioning regime. The results also demonstrate some of the advantages of studying simple aerosol-forming reactions in which the majority of products can be identified and quantified, in this case leading to insights into both gas- and particle-phase chemistry.

3.2. Introduction

One purpose of experimental studies of aerosols is to provide data for developing detailed models of the physical and chemical processes controlling atmospheric aerosol properties such as chemical composition, size distribution, light scattering and absorption, hygroscopicity, and cloud condensation nucleating activity. These models in turn are incorporated in simplified form into local, regional, and global scale models, which can be used to understand collective effects and to develop strategies for minimizing the impacts of human activities on air quality, visibility, climate, and human and ecosystem health (Seinfeld and Pandis, 1998). A major challenge is the development of models of secondary organic aerosol (SOA) formation, a complex process in which gas- and particle-phase reactions involving organic compounds and oxidants lead to an array of products that can partition to particles (Kroll and Seinfeld, 2008). In most models, these processes are treated using simple empirical parameterizations (Kanakidou et al., 2005). In a few cases, however, detailed mechanisms of gas-phase chemical reactions have been combined with gas-particle partitioning, emissions, and meteorology to predict the chemical composition and mass of atmospheric SOA (Johnson et al., 2006). Unfortunately, current models tend to under-predict

atmospheric SOA mass concentrations (deGouw et al., 2005; Heald et al., 2005; Johnson et al., 2006; Volkamer et al., 2006) probably for a variety of reasons. For example, discrepancies have been attributed to problems with laboratory SOA yield measurements (Presto and Donahue, 2006; Kroll et al., 2007), and to an absence in models of possible sources of SOA such as heterogeneous chemistry (Johnson et al., 2006), first-generation products of anthropogenic VOC oxidation (Volkamer et al., 2006), semi-volatile emissions (Robinson et al., 2007), higher-generation reaction products (Donahue et al., 2006), and cloud processing (Altieri et al., 2006).

In general, models predict that global SOA is derived primarily from the oxidation of biogenic alkenes, in particular linear, branched, and cyclic terpenes consisting of isoprene (C_5H_8), monoterpenes ($C_{10}H_{16}$), and sesquiterpenes ($C_{15}H_{24}$) (Kanakidou et al., 2005). Recent field studies (Weber et al., 2007) also indicate terpene oxidation is responsible for a large fraction of SOA in urban areas. In spite of the importance of these reactions and the considerable effort expended investigating gas- and particle-phase products, the chemical mechanisms are poorly understood (Atkinson and Arey, 2003; Kroll and Seinfeld, 2008). Recently, we investigated SOA products formed from OH radical-initiated reactions of simple linear alkenes in the presence of NO_x,

conditions representative of a polluted atmosphere. Such studies provide insights into products and mechanisms of more complex alkene reactions. Major β-hydroxynitrate and dihydroxynitrate SOA products were identified and quantified and used to determine some of the branching ratios for reaction pathways leading to their formation (Matsunaga and Ziemann, 2008). Here, those results were used with additional SOA composition information obtained in that study but not previously reported, along with product data from the literature and structure-reactivity calculations of rate constants to develop a quantitative chemical mechanism for reactions of linear 1-alkenes and internal alkenes. This mechanism was then used to model the formation of SOA and the results were compared with measured SOA yields.

3.3. Experimental

Chemicals. The C_8-C_{17} linear 1-alkenes, 7-tetradecene, 7-pentadecene, 8-heptadecene, dioctyl sebacate, and NO were obtained from commercial suppliers (Matsunaga and Ziemann, 2008). Methyl nitrite was synthesized (Taylor et al., 1980) and stored in liquid nitrogen until used, and O_3 was generated using a Welsbach T-408 O_3 generator.

Environmental Chamber Method. Alkenes were reacted with OH radicals in the presence of NO_x in a 5900 L PTFE environmental chamber filled with clean, dry air (<5 ppbv hydrocarbons, <1% RH) at ~25^{o}C and atmospheric pressure. The reaction mixture was ~200-400 µg m^{-3} of dioctyl sebacate (DOS) seed particles added from an evaporation-condensation source and 1 (0.5 and 0.3 for 1- and 8-heptadecene), 5, and 5 ppmv of alkene, methyl nitrite, and NO. Reactions were initiated by turning on blacklights to form OH radicals by methyl nitrite photolysis (Atkinson et al., 1981). The average OH radical concentration for 6 min of reaction was ~3 x 10^7 cm^{-3}, determined from the 40-50% of alkene that reacted and reaction rate constants (Aschmann and Atkinson, 2008a).

Particle and Gas Analysis. A thermal desorption particle beam mass spectrometer (TDPBMS) was used to analyze particle composition in real-time (Tobias et al., 2000) and by temperature-programmed thermal desorption (TPTD) (Tobias and Ziemann, 1999). Air was sampled into the TDPBMS and particles were formed into a beam and impacted on a polymer-coated metal vaporizer (Chattopadhyay and Ziemann, 2005). For real-time analysis, the vaporizer was resistively heated to 160°C and particles evaporated on impact. Vapor was ionized by 70 eV electrons and analyzed in a

quadrupole mass spectrometer. For TPTD analysis, the vaporizer was cooled to -40°C, particles were collected for 30 min, and the vaporizer was allowed to warm to -5°C and was then heated to 200°C using a 2°C min^{-1} ramp to desorb and separate compounds by volatility prior to mass analysis.

SOA mass concentration, M_{SOA}, was calculated as the difference in aerosol volume concentrations of seed and SOA + seed measured using a scanning mobility particle sizer (SMPS) (Wang and Flagan, 1990), multiplied by a SOA density of 1.13 g cm^{-3} measured using a microliter syringe, a microbalance, and a dried filter extract of liquid SOA formed in the reaction of 1-tetradecene. Alkenes were collected on Tenax TA solid adsorbent before and after reaction and analyzed by GC-FID (Docherty et al., 2005) to determine the mass of alkene reacted, ΔM_{alkene}. SOA yields were calculated as $Y_{SOA} = M_{SOA}/\Delta M_{alkene}$ (Odum et al., 1996).

3.4. Development of a chemical mechanism and model of SOA formation

Reaction Mechanism. The mechanism of OH radical-initiated reactions of linear alkenes in the presence of NO_x is shown in Figure 3.1., where R_1 represents an alkyl group and R_2 represents an H-atom in 1-alkenes and an alkyl group in internal

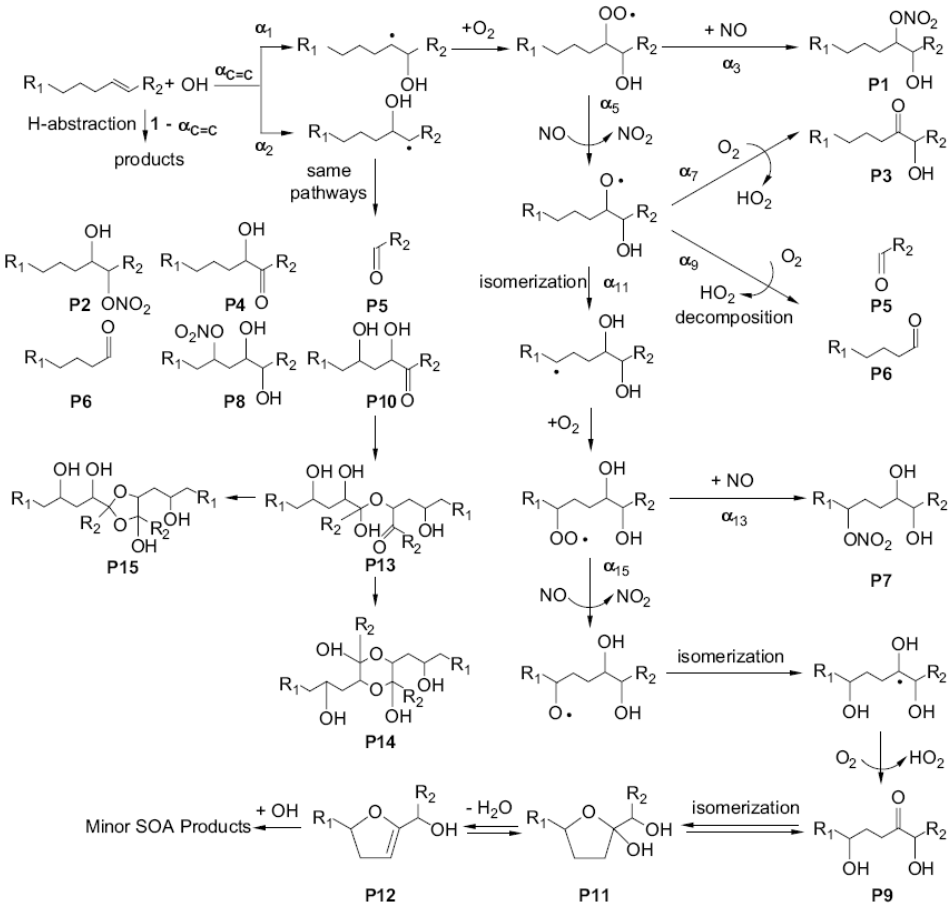

Figure 3.1 Mechanism of the OH radical-initiated reaction of linear alkenes in the presence of NO_x. R_1 represents an alkyl group and R_2 represents an H-atom in 1-alkenes and an alkyl group in internal alkenes.

alkenes. Detailed discussions of the pathways leading to products **P1**-**P10** can be found in Atkinson and Arey (2003). The reaction is initiated primarily by addition of an OH radical to the C=C double bond, although H-atom abstraction is significant. Addition forms two β-hydroxyalkyl radical isomers, which react with O_2 to form β-hydroxyperoxy radicals that react with NO, forming β-hydroxynitrates [**P1**, **P2**] or β-hydroxyalkoxy radicals. The β-hydroxyalkoxy radicals can react with O_2, decompose, or isomerize. Reaction with O_2 forms β-hydroxycarbonyls [**P3**, **P4**], but is not important for the large alkenes of interest here (Atkinson, 2007). Decomposition followed by reaction with O_2 forms two aldehydes [**P5**, **P6**] (and a small fraction of other products that are not shown, such as 1,4-hydroxycarbonyls and 1,4-hydroxynitrates; Aschmann and Atkinson, in preparation), and isomerization followed by reaction with O_2 forms dihydroxyperoxy radicals that react similarly to β-hydroxyperoxy radicals. The products are dihydroxynitrates [**P7**, **P8**] and dihydroxyalkoxy radicals that isomerize and react with O_2 to form dihydroxycarbonyls [**P9**, **P10**]. Dihydroxycarbonyls [**P9**, **P10**] can isomerize to cyclic hemiacetals [**P11**] that can dehydrate to dihydrofurans [**P12**], or they can form dimers [**P13**-**P15**]. On the basis of other studies (Holt et al., 2005; Gong et al., 2005; Lim and Ziemann, 2005; Kern and Spiteller, 1996) and results presented below,

dihydroxyketones [**P9**] probably form mostly cyclic hemiacetals [**P11**] and dihydrofurans [**P12**] and dihydroxyaldehydes [**P10**] form mostly dimers [**P13-P15**].

Branching Ratios and Product Yields. The branching ratios shown in Figure 3.1 are defined as $\alpha_i = r_i/\sum r_i$, where r_i is the rate a species reacts by pathway i and the sum is over all pathways by which the species reacts. The sum of branching ratios for a species is 1. Note that α_4, α_6, α_8, α_{10}, α_{12}, α_{14}, and α_{16} are associated with the portion of the mechanism labeled "same pathways" and correspond to α_3, α_5, α_7, α_9, α_{11}, α_{13}, and α_{15}, respectively. Values used in the model are given in Table 3.1, and the methods by which they were calculated described in Appendix B. The values are consistent with experimental data (Matsunaga and Ziemann, 2008; Aschmann and Atkinson, in preparation) and with rate constants for OH radical (Kwok and Atkinson, 1995; Ashmann and Atkinson, 2008; Nishino et al., 2009) and alkoxy radical reactions (Atkinson, 2007). Molar yields normalized for OH radical addition [(moles of product/moles of alkene reacted)/ $\alpha_{C=C}$], which are equal to the product of the branching ratios along the pathway leading to the reaction product divided by $\alpha_{C=C}$, were calculated using branching ratios in Table 3.1 and are given in Table 3.2 along with molar yields of 1,4-hydroxynitrates

Table 3.1 Branching ratios used for modeling SOA formation from OH radical-initiated reactions of linear alkenes in dry air in the presence of NO_x.

branching ratio	1-alkenes	internal alkenes
$\alpha_{C=C}$[a]	$\alpha_{C=C}$	$\alpha_{C=C}$
a_1	0.70 x $\alpha_{C=C}$	0.50 x $\alpha_{C=C}$
a_2	0.30 x $\alpha_{C=C}$	0.50 x $\alpha_{C=C}$
a_3, a_4	0.14	0.15
a_5, a_6	0.86	0.85
a_7, a_8	0.00	0.00
a_9	0.51	0.67
a_{10}	0.34	0.67
a_{11}	0.49	0.33
a_{12}	0.66	0.33
a_{13}, a_{14}	0.08	0.02
a_{15}, a_{16}	0.92	0.98

[a] $\alpha_{C=C} = k_{add}/(k_{add} + k_{abs})$. For 1-alkenes, $k_{abs} = 2.47 + 1.4 \times (CN-5)$ and $k_{add} = 28 + 9 \times [1-\exp(-0.35 \times (CN-3))]$. For *cis* and *trans* internal alkenes, $k_{abs} = 4.93 + 1.4 \times (CN-8)$, $k_{add}(cis) = 56.4$, and $k_{add}(trans) = 64$. CN is the alkene carbon number. See Appendix B for additional details.

Table 3.2 Normalized molar yields of products used to model SOA formation from OH radical addition and H-atom abstraction reactions of linear alkenes in dry air in the presence of NO_x.

product	normalized molar yield[a]	
	1-alkenes	internal alkenes
OH radical addition		
β-hydroxynitrates		
P1	0.098	0.075
P2	0.042	0.075
P1 + P2	0.140	0.150
β-hydroxycarbonyls		
P3	0.000	0.000
P4	0.000	0.000
carbonyls		
P5	0.395	0.570
P6	0.395	0.570
P5 + P6		1.140
dihydroxynitrates		
P7	0.024	0.003
P8	0.014	0.003
P7 + P8	0.038	0.006
dihydroxycarbonyls		
P9	0.271	0.137
P10	0.157	0.137
P9 + P10	0.428	0.274
H-atom abstraction		
1,4-hydroxynitrates	0.1	0.1

[a]Normalized molar yields (OH radical addition) = (moles of product/moles of alkene reacted)/$\alpha_{C=C}$. Normalized molar yield (H-atom abstraction) = (moles of product/moles of alkene reacted)/(1 - $\alpha_{C=C}$). Values of $\alpha_{C=C}$ calculated using equations in Table 3.1.

normalized for H-atom abstraction [(moles of product/moles of alkene reacted)/(1 - $\alpha_{C=C}$)].

H-atom Abstraction and Secondary Reactions. First-generation products formed through H-atom abstraction pathways and second-generation products formed through reactions of first-generation products with OH radicals have the potential to form SOA, but the reaction mechanisms are complex and the product contributions difficult to quantify (Lim and Ziemann, 2005). For simplicity, in a first set of calculations it was assumed that the only contribution of H-atom abstraction pathways to SOA formation was from 1,4-hydroxynitrates, and that the formation of SOA products from secondary reactions with OH radicals was negligible. The 1,4-hydroxynitrates were assumed to be formed with an H-atom abstraction-normalized molar yield of 0.1 estimated from measured yields (Lim and Ziemann, 2005; Reisen et al., 2005) and consistent with values recently determined by us for C_{13}-C_{17} *n*-alkanes. The major first generation products of H-atom abstraction should be alkyl nitrates, 1,4-hydroxycarbonyls, and 1,4-hydroxynitrates, as observed in similar reactions of *n*-alkanes (Lim and Ziemann, 2005; Reisen et al., 2005). As shown below, thermal desorption profiles showed no alkyl nitrates or 1,4-hydroxycarbonyls, which would be easily detected since they would

desorb before β-hydroxynitrates. Most likely, alkyl nitrates were too volatile to form SOA, and 1,4-hydroxycarbonyls were absent because they isomerized to cyclic hemiacetals that dehydrated to volatile dihydrofurans (they are more volatile than **P12** in Figure 3.1 because they do not have the hydroxy group) (Holt et al., 2005; Lim and Ziemann, 2005). The dihydrofurans may have then reacted with OH radicals, but would mostly form volatile carbonylesters (Martin et al., 2002).

In a second set of calculations, upper limits to the possible contributions of secondary reaction products to SOA yields were estimated using a kinetic model written in FACSIMILE that included gas-phase reactions of alkenes and first-generation products with OH radicals, and gas-particle partitioning. The rate constants for H-atom abstraction and OH radical addition reactions for alkenes were calculated using the equations of Nishino et al. (2009) given in Supporting Information, and rate constants for H-atom abstraction from saturated products were calculated using the structure-reactivity method of Kwok and Atkinson (1995). An equation for the time-dependent OH radical concentration was obtained from multiple measurements of alkene concentrations made during an experiment with 1-tetradecene. Gas-particle partitioning was calculated as described below using measured aerosol mass concentrations. Yields of products formed

by H-atom abstraction followed by OH radical addition were calculated by assuming all H-atom abstraction products (alkyl nitrates, 1,4-hydroxycarbonyls, and 1,4-hydroxynitrates) stayed in the gas phase during the entire reaction, thereby overestimating to some extent the formation of secondary reaction products. Yields of products formed by OH radical addition followed by H-atom abstraction were calculated by assuming that during the reaction all OH-addition products (β-hydroxynitrates, dihydroxynitrates, and dihydroxycarbonyls) other than carbonyls underwent gas-particle partitioning to the same extent as β-hydroxynitrates, and that in the particle phase they did not react with OH radicals. Since the actual vapor pressures of these compounds are the same or less than β-hydroxynitrates, these calculations also overestimate the formation of secondary reaction products. Because carbonyls are volatile fragmentation products and generally react with OH radicals to form even smaller carbonyls (Atkinson and Arey, 2003), it was assumed that their reactions did not to contribute to SOA formation. Calculated molar yields of products were converted to mass yields using ratios of the molecular weights of product and alkene, and these mass yields were then used as a upper limit estimate of the contribution of these reactions to the SOA yields.

Gas-Particle Partitioning. The equilibrium gas-particle partitioning of products was calculated using the theory of Pankow (1994), which assumes that particulate organic matter (POM) is a single, liquid organic phase. This assumption seems valid since dried filter extracts were clear liquids and when seed particle concentrations were increased from ~200 to ~1000 μg m^{-3} in 7-tetradecene experiments the SOA yield of β-hydroxynitrates was ~4 times larger, indicating enhanced gas-to-particle partitioning. Partitioning coefficients were calculated from compound vapor pressures, activity coefficients, and mean molecular weights of POM and used with organic aerosol mass concentration, M_O (M_{SOA} + M_{seed}), to calculate the fraction of each compound in the particle phase. Activity coefficients were assumed to be unity (Seinfeld et al., 2001) and the mean molecular weight of POM was assumed to be that of β-hydroxynitrates. Product vapor pressures were estimated from measured partitioning of β-hydroxynitrates and group contribution calculations described in Appendix Figure B.1 and Table B.1.

SOA Yield Calculations. For each alkene, the total (gas + particle) mass concentration of each product was calculated by multiplying the molar yield in Table 2 by $\alpha_{C=C}$ for OH radical addition and 1-$\alpha_{C=C}$ for H-atom abstraction, the ratio of the molecular weights of product and alkene, and ΔM_{alkene}. Product mass concentrations,

partitioning coefficients, and seed particle mass concentration were then used to calculate SOA yield (Colville and Griffin, 2004). In one case, it was assumed that dihydroxycarbonyls [**P9**, **P10**] existed entirely in the particle phase as non-volatile cyclic hemiacetals [**P11**], dihydrofurans [**P12**], and dimers [**P13**-**P15**] rather than in gas-particle partitioning equilibrium.

3.5 Results and discussion

Measured SOA Products. Thermal desorption profiles and real-time mass spectra of SOA formed from reactions of 1-tetradecene and 7-tetradecene are shown in Figure 3.2. In Figure 3.2A, total ion (TI) signal is proportional to organic mass (Crable and Coggeshall, 1958), so profiles represent distributions of SOA mass with respect to volatility. For both reactions, there are peaks at 40-50^{o}C and 70-80^{o}C. For 1-tetradecene, a large peak is also observed at 90-100^{o}C, whereas for 7-tetradecene only a tail appears in this temperature range. The first two peaks are from β-hydroxynitrates [**P1**, **P2**] and dihydroxynitrates [**P7**, **P8**]; their mass spectra after HPLC separation, desorption profiles of characteristic ions, fragmentation pathways, and yields are discussed elsewhere (Matsunaga and Ziemann, 2008). Those formed from reactions of 1-tetradecene and 7-

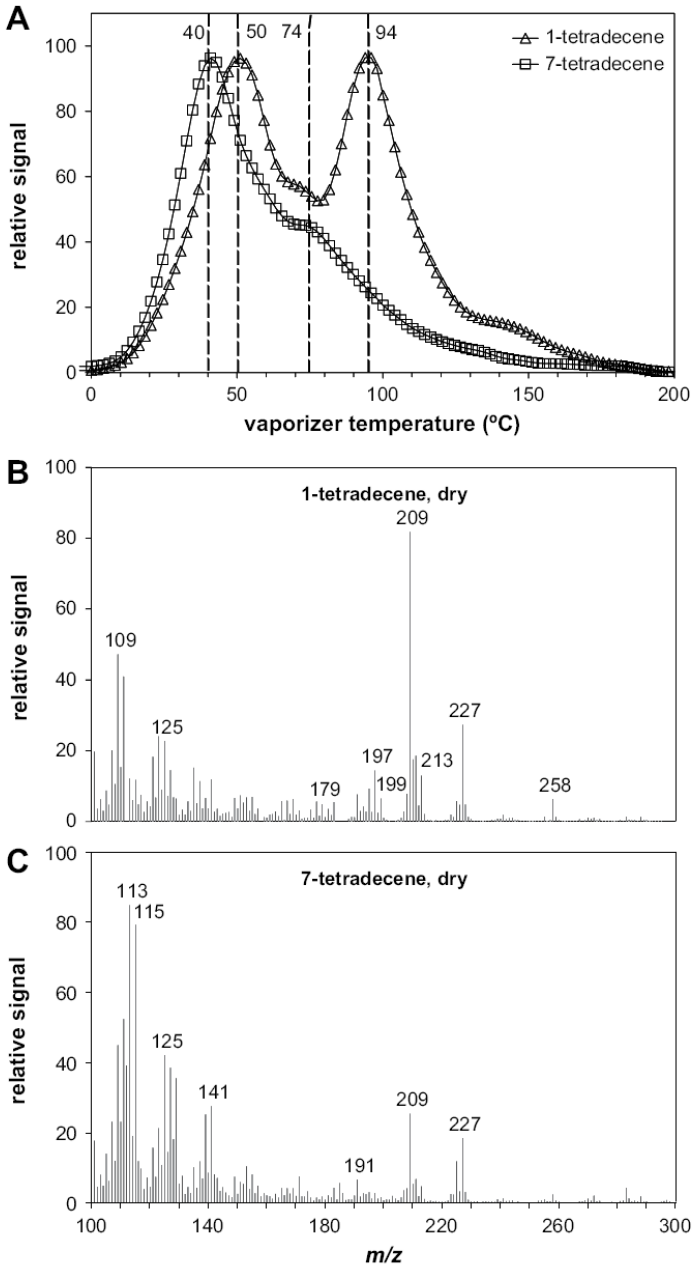

Figure 3.2 (A) Total ion (*m/z* 50-500) thermal desorption profiles and (B,C) real-time mass spectra of SOA formed from the OH radical-initiated reactions of 1-tetradecene and 7-tetradecene in dry air in the presence of NO_x. In Figure 3.2A, signals from DOS seed particles were removed by multiplying the *m/z* 185 profiles (due to overwhelmingly to DOS) by the ratio of (total ion)/(*m/z* 185) signals measured for DOS seed particles in real-time, and then subtracting. Thermal desorption profiles were smoothed and normalized to peak values.

tetradecene have characteristic peaks at *m/z* 179, 197, and 199, and at *m/z* 97 and 115, respectively.

Peaks at *m/z* 227 and 209 in Figures 3.2B, 3.2C are characteristic of cyclic hemiacetals [**P11**] and dihydrofurans [**P12**], the ions being formed by loss of OH fromthe molecular ion (Gong et al., 2005; Lim and Ziemann, 2005). These compounds have low vapor pressures, as indicated by thermal desorption profiles shown in Figure 3.3A. The cyclic hemiacetal desorbed after the dihydrofuran because the extra hydroxy group lowers its vapor pressure. These profiles overlap with a large peak at 90-100^{o}C in the TI profile in Figure 3.2A, indicating the compounds may contribute significant SOA mass. This product assignment is supported by results shown in Figure 3.3B. In this experiment, 20 ppmv of O_3 was added to the chamber 4 hr after the lights were turned off. SOA *m/z* 209 signal disappeared immediately due to reaction of the dihydrofuran double bond with O_3. The *m/z* 227 signal decayed with a lifetime of ~5-10 min, consistent with measured rates of dehydration of cyclic hemiacetals (Holt et al., 2005). The slower decay of *m/z* 185 signal, mostly from DOS seed particles, is consistent with H-atom abstraction by NO_3 radicals (Docherty and Ziemann, 2006) formed from reaction of O_3 with NO_2.

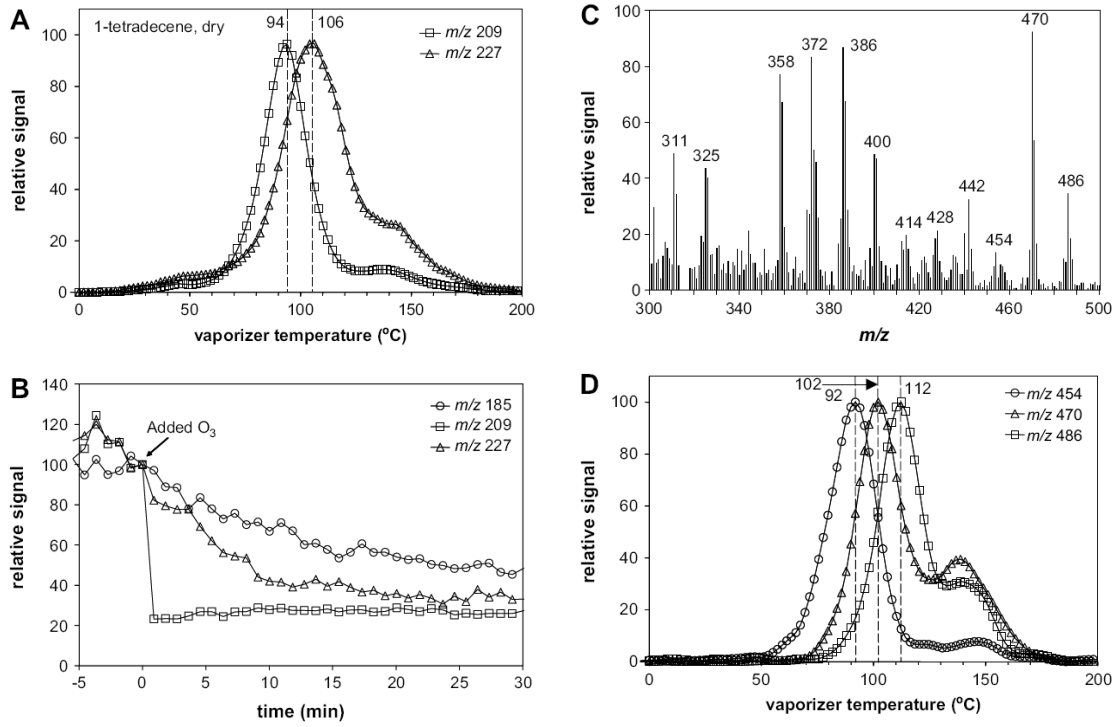

Figure 3.3 Mass spectral analyses of SOA formed from OH radical-initiated reactions of 1-tetradecene in dry air in the presence of NO_x. (A) Thermal desorption profiles of ions characteristic of cyclic hemiacetals (*m/z* 227) and dihydrofurans (*m/z* 209), (B) real-time signals of these ions after adding O_3 to the chamber containing SOA, (C) real-time mass spectra for *m/z* 300-500, and (D) thermal desorption profiles of ions characteristic of dimers. A, C, and D were obtained without added O_3. Thermal desorption profiles were smoothed and normalized to peak values, and signals in B were normalized to values and 0 min.

The *m/z* 300-500 region of the real-time mass spectrum from the reaction of 1-tetradecene is shown in Figure 3.3C. These peaks extend beyond masses of potential products of secondary reactions with OH radicals. For example, addition of three hydroxy groups and two nitrooxy groups gives a product with molecular weight 368. Instead, these peaks are probably associated with oligomeric species formed by particle-phase reactions. Trends observed in mass spectra for reactions of 1-undecene, 1-dodecene, and 1-tridecene (Figure 3.4), and 1-tetradecene (Figure 3.3C) support this idea. The mass spectra exhibit two patterns. Peaks at *m/z* 316, 330, 344, and 358 for the reaction of 1-undecene are shifted by *m/z* 14, 28, and 42 in mass spectra from reactions of 1-dodecene, 1-tridecene, and 1-tetradecene. This is expected for products of reactions of a homologous series of compounds with successive molecular weights increasing by 14 units. A different pattern is observed at higher masses, however. Peaks at *m/z* 370, 386, and 402 for the reaction of 1-undecene are shifted by *m/z* 28, 56, and 84 in mass spectra from reactions of 1-dodecene, 1-tridecene, and 1-tetradecene. This pattern is consistent with the formation of dimers [**P13**-**P15**], where an increase of 14 units in monomer mass increases dimer mass by 28 units.

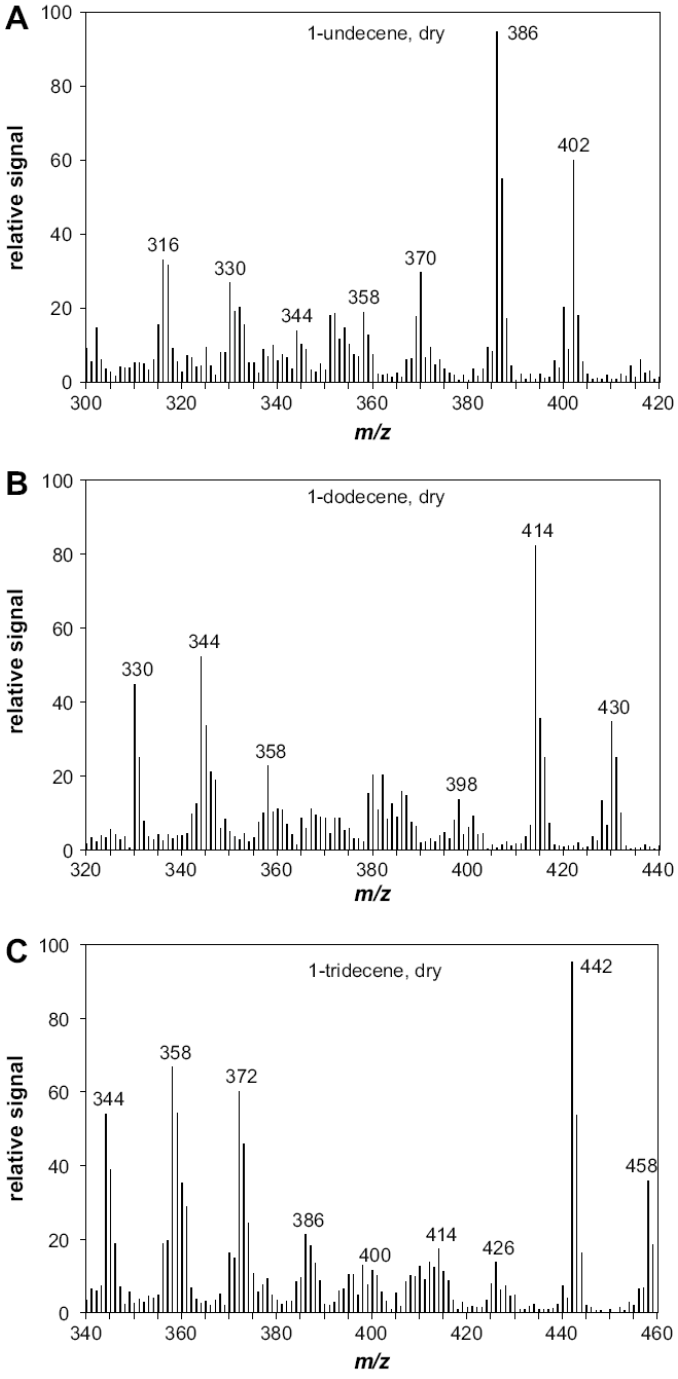

Figure 3.4 Real-time mass spectra characteristic of dimers in SOA formed from the OH radical-initiated reactions of (A) 1-undecene, (B) 1-dodecene, and (C) 1-tridecene in dry air in the presence of NO_x.

For these reactions, the most likely monomers are dihydroxyaldehydes [**P10**]. These compounds are major gas-phase products from reactions of C_4-C_8 1-alkenes (Kwok et al., 1996), and synthetic organic chemistry studies showed α-hydroxyaldehydes such as these are unstable and rapidly form dimers (Kern and Spiteller, 1996). Dimers formed from products of the reaction of 1-tetradecene would have molecular weight 488. Peaks at *m/z* 454, 470, and 486 would correspond to $(M-34)^+$, $(M-18)^+$, and $(M-2)^+$ ions formed by loss of H_2O_2, H_2O, and H_2 from a dimer (or dimer isomers) of mass M, which is reasonable. Desorption profiles of these ions have peaks at 92, 102, and 112^{o}C, as shown in Figure 3.3D, indicating three dimers with different volatilities. If all are dihydroxyaldehyde dimers, then three possible isomer **s**tructures are shown in Figure 3.1. Product **P13** is a linear hemiacetal and products **P14** and **P15** are cyclic hemiacetals. The latter two structures were proposed for dimers formed from synthesized α-hydroxyaldehydes (Kern and Spiteller, 1996). In the experiment described above in which O_3 was added to the chamber 4 hr after the lights were off, *m/z* 470 and 486 signals decayed in a few minutes (the *m/z* 454 initial signal was too small to monitor). This indicated the compounds are saturated but can dehydrate to dihydrofurans, as expected for products **P14** and **P15**. Because desorption profiles of dimer ions overlap with the

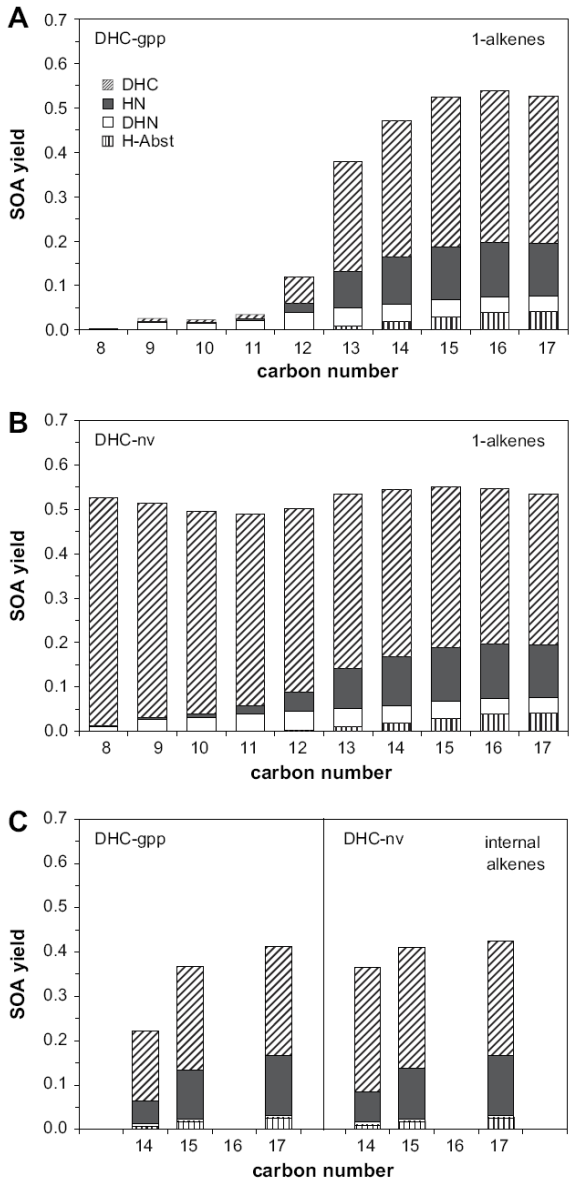

Figure 3.5 Calculated yields of SOA products formed from OH radical-initiated reactions of 1-alknenes and internal alkenes in dry air in the presence of NO_x. Figures show results for dihydroxycarbonyls (DHC), β-hydroxynitrates (HN), and dihydroxynitrates (DHN) formed by OH radical addition pathways, and 1,4-hydroxynitrates formed by the H-atom abstraction (HAA) pathway. The models assumed that secondary reaction products did not contribute to SOA mass and that dihydroxycarbonyls were either (gpp) in gas-particle partitioning equilibrium or (nv) entirely in the particle phase as non-volatile cyclic hemiacetals, dihydrofurans, or dimers.

large peak at 90-100^{o}C in the TI profile in Figure 3.2A, these compounds may contribute significant SOA mass. Mass spectra showed no evidence for dimer formation from reactions of internal alkenes, probably because the dihydroxycarbonyl products are dihydroxyketones, which have less of a tendency than dihydroxyaldehydes to form hemiacetals and cyclic dimers.

SOA Composition and Yields: Model Results and Measurements. Yields of SOA products calculated using the model described above, without estimates for contributions from secondary reaction products, are shown in Figure 3.5 and Appendix Tables B.3 and B.4. The difference between Figures 3.5A and 3.5B and the two halves of Figure 3.5C is the model treatment of dihydroxycarbonyls. For results labeled DHC-gpp it was assumed that dihydroxycarbonyls are in gas-particle partitioning equilibrium, whereas for results labeled DHC-nv it was assumed they form non-volatile cyclic hemiacetals, dihydrofurans, and dimers that are entirely in the particle phase. For 1-alkenes $\geq C_{15}$, differences in composition calculated with the two models are small because in both cases dihydroxycarbonyls are almost entirely in the particle phase. Calculated yields of individual products in SOA averaged over this carbon number range were 0.337 (DHC-gpp) and 0.350 (DHC-nv) for dihydroxycarbonyls, 0.121 for β-

hydroxynitrates, 0.036 for dihydroxynitrates, and 0.037 for 1,4-hydroxynitrates. The average total yields for SOA products of 0.530 (DHC-gpp) and 0.544 (DHC-nv) agree very well with the average measured SOA yield of 0.518. Note that the measured SOA yields were not used in the development of the model, so this is a comparison of the model output with independent measurements. Dihydroxycarbonyls were calculated to contribute ~65% of SOA mass, consistent with the total ion profile shown in Fig. 2A for the 1-tetradecene reaction where roughly half of the area is contributed by the peak at 94^{o}C. As the carbon number decreased from C_{15} to C_{8}, SOA composition changed due to gas-particle partitioning, with compounds being preferentially lost to the gas phase in the order of vapor pressures: 1,4-hydroxynitrates > β-hydroxynitrates ~ dihydroxycarbonyls (DHC-gpp) > dihydroxynitrates > dihydroxycarbonyls (DHC-nv). The differences in composition predicted by the two models also increased dramatically because dihydroxycarbonyls had the largest total (gas + particle) yields of all potential SOA-forming products and, depending on the model, could be predominantly in either the gas or particle phases. For the C_{15} and C_{17} internal alkenes, differences in calculated composition due to the treatment of dihydroxycarbonyls were small. Calculated average yields of individual products in SOA were 0.240 (DHC-gpp) and 0.265 (DHC-nv) for

dihydroxycarbonyls, 0.124 for β-hydroxynitrates, 0.006 for dihydroxynitrates, and 0.021 for 1,4-hydroxynitrates. The average total SOA yields of 0.390 (DHC-gpp) and 0.418 (DHC-nv) agree very well with the measured value of 0.405 for C_{17}. As the carbon number decreased from C_{15} to C_{14}, SOA composition changed as it did for reactions of 1-alkenes, but with greater loss of compounds to the gas phase because of their higher vapor pressures.

SOA yields calculated without and with upper limit estimates for the contributions from secondary reaction products are compared with measured values over the entire carbon number range in Figures 3.6A and 3.6B, respectively, and are also given in Appendix Tables B.2-B.4. Results shown in Figure 3.6A indicate that for 1-alkenes the DHC-nv and DHC-gpp models work very well down to about C_{12} and C_{13}, respectively. Below these carbon numbers, the DHC-nv model over-predicts SOA yields by an amount that increases with decreasing carbon number, whereas the DHC-gpp model under-predicts SOA yields by an amount that decreases with decreasing carbon number. Results shown in Figure 3.6A also indicate that for internal alkenes the DHC-nv and DHC-gpp models both work very well at C_{17} (and presumably at higher carbon numbers), but that for smaller carbon numbers they significantly over-predict SOA yields. This is due

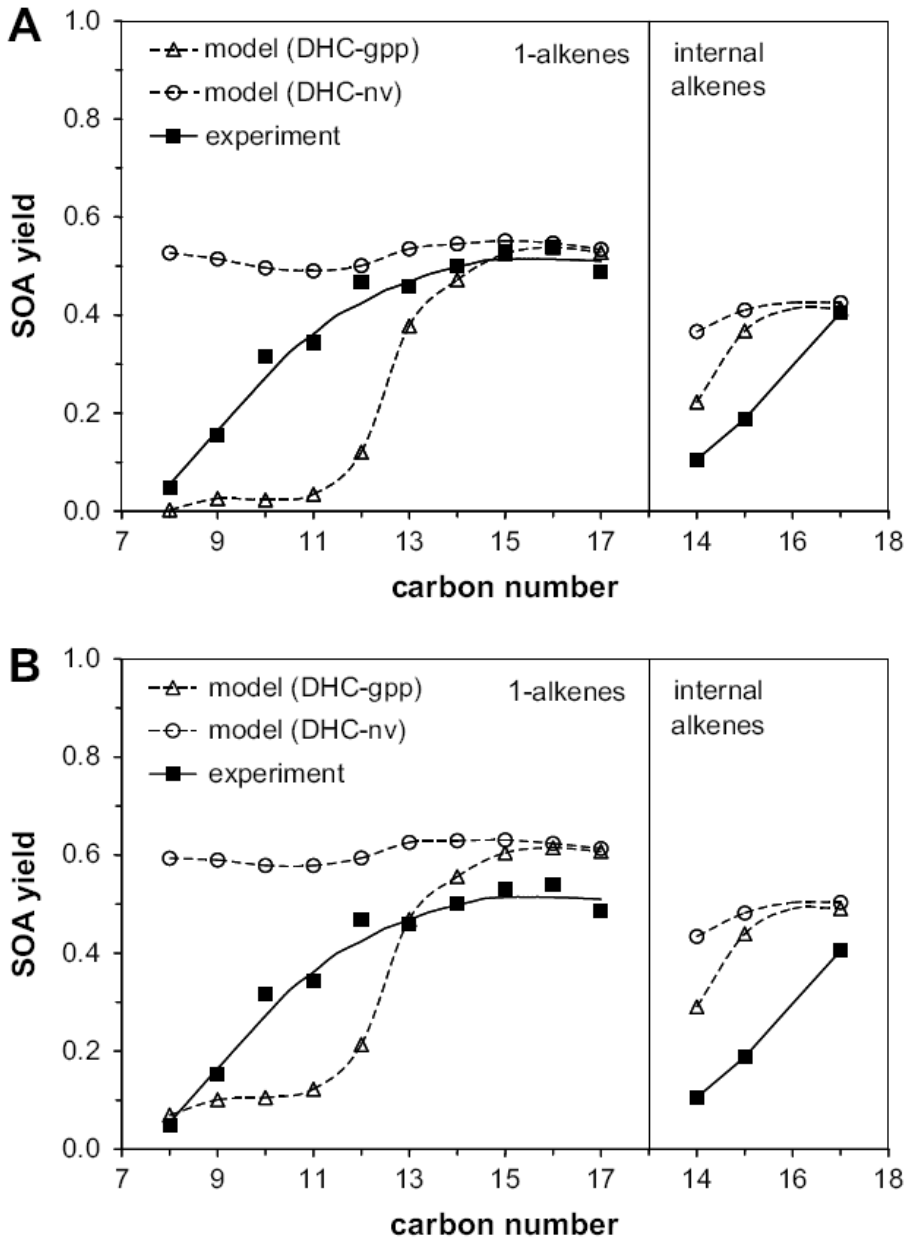

Figure 3.6 Calculated and measured yields of SOA formed from OH radical-initiated reactions of 1-alkenes and internal alkenes in dry air in the presence of NO_x. The models assumed that secondary reaction products (A) did not or (B) did contribute to SOA mass and that dihydroxycarbonyls were either (gpp) in gas-particle partitioning equilibrium or (nv) entirely in the particle phase as non-volatile cyclic hemiacetals, dihydrofurans, or dimers.

primarily to excess contributions from dihydroxycarbonyls, which in Figure 3.2A are shown to comprise only a small fraction of the SOA mass for the 7-tetradecene reaction. A plausible explanation for this excess is that the vapor pressures used in the model for dihydroxycarbonyls formed from reactions of internal alkenes are too low by a factor of ~3, which is equivalent to a decrease of ~1 carbon number. If the vapor pressures used in the DHC-gpp model were increased by this amount, then the model curve shown in Figure 3.6A would be shifted to the right by ~1 carbon number, and the agreement with measured yields would be quite good.

As expected, and as is shown in Figure 3.6B, including secondary reaction products in the models increases the calculated SOA yields. Above C_{13}, the DHC-gpp and DHC-nv models both over-predict SOA yields. Below C_{13}, the DHC-nv model over-predictions are larger and the DHC-gpp model under-predictions are smaller. The best region to compare these models is probably above C_{13}, since all the products are entirely in the particle phase and uncertainties due to gas-particle partitioning are therefore minimized. Results for that region suggest that secondary reaction products do not contribute significantly to SOA mass, since adding them to the model worsens the agreement between the calculated and measured SOA yields.

The observation that SOA yields measured for the reactions of 1-alkenes < C_{13} are between those calculated using the DHC-gpp and DHC-nv models indicates that the formation of cyclic hemiacetals, dihydrofurans, and dimers from dihydroxcarbonyls is reversible. Mass spectra show peaks due to cyclic hemiacetals, dihydrofurans, and dimers formed from dihydroxcarbonyls at least as small as C_9, indicating that these reactions occur for the smallest compounds studied. If the reactions were irreversible, they should lead to complete gas-to-particle partitioning of dihydroxycarbonyls and therefore SOA yields similar to those calculated using the DHC-nv model. Conversely, reversible reactions should lead to some fraction of dihydroxycarbonyls existing in the gas phase in equilibrium with the non-volatile products, and SOA yields between those calculated using the two models, as observed here. These reversible reactions cannot be incorporated into the model is a rigorous way, since there are insufficient data to constrain the particle-phase equilibria between dihydroxycarbonyls and their various reaction products. Nonetheless, if, for example, one assumes that particle-phase reactions of dihydroxycarbonyls form only dimers, then this reaction can be added to the model and the equilibrium constant, $K\ (m^3\ \mu g^{-1}) = [dimer]_p/[dihydroxycarbonyl]_p^2$, can be estimated by fitting to measured SOA yields. When this was done, a value of ~5 gave a

good fit (not shown). While this is not a chemically meaningful quantity, such an approach might be sufficiently accurate for some modeling purposes.

3.6 Conclusions

The very good agreement between calculated and measured SOA yields for reactions of large alkenes in which gas-to-particle partitioning of dihydroxycarbonyl, β-hydroxynitrate, dihydroxynitrate, and 1,4-hydroxynitrate products is essentially complete, indicates that the chemical mechanism developed here using measured product yields and structure-reactivity methods provides an accurate representation of the gas-phase chemistry. The model should therefore be useful in this partitioning regime. The divergence between model predictions (whether assuming gas-particle partitioning equilibrium or complete gas-to-particle partitioning of dihydroxycarbonyls) and measured SOA yields for smaller alkenes is problematic, however, and clearly demonstrates the challenges to be faced in incorporating particle-phase chemistry into this and other SOA models. Fortunately, for this system the gas-phase reaction products are sufficiently well known and few in number that the particle-phase reactants and products can be identified. In particular, dihydroxycarbonyls are shown to undergo a

number of reversible, particle-phase reactions to form lower volatility products. It appears that those containing a 1,4-hydroxyketone unit form cyclic hemiacetals and dihydrofurans, whereas those containing a β-hydroxyaldehyde unit form hemiacetal dimers. Previous studies of similar OH radical-initiated reactions of alkanes (Lim and Ziemann, 2005) and of reactions of alkenes with NO_3 radicals (Gong et al., 2005) have also observed the formation of cyclic hemiacetals, while studies of alkene ozonolysis have observed that hydroperoxides can undergo intramolecular or intermolecular reactions with aldehydes to form cyclic (Ziemann, 2003) and linear peroxyhemiacetals (Tobias and Ziemann, 2000).

Accurate modeling of even the simple set of reactions identified here will require substantially more information on particle-phase kinetics and the effects of environmental variables, such as relative humidity and particle acidity, on the chemistry. For example, it was observed (though not shown here) that SOA formation was insensitive to changes in relative humidity but that adding ammonia reduced the formation of cyclic hemiacetals, dihydrofurans, and dimers, apparently by neutralizing nitric acid (formed by the OH + NO_2 reaction) that catalyzes the particle-phase reactions. Although acquiring such detailed information will be a challenge, it may be difficult to develop chemically

speciated SOA models that can be applied to the laboratory or atmosphere with confidence without a much greater understanding of these types of reactions. The current state of models for reactions of terpenes (Jenkin 2004) and aromatics (Johnson et al., 2004), in which SOA is known to contain significant amounts of oligomers (Tolocka et al., 2004; Docherty et al., 2005; Kalberer et al., 2004), is that the vapor pressures of gas-phase reaction products must be reduced by a few orders of magnitude below their calculated values in order to mimic the effects of particle-phase reactions on volatility and achieve good agreement with measured SOA yields.

3.7 References

Altieri, K.E., Carlton, A.G., Lim, H.-J., Turpin, B.J., Seitzinger, S.P., 2006. Evidence for Oligomer Formation in Clouds: Reactions of Isoprene Oxidation Products. *Environ. Sci. Technol.*, 40, 4956-4960.

Aschmann, S. M. and Atkinson, R., 2008. Rate Constants for the Gas-Phase Reactions of OH Radicals with E-7-Tetradecene, 2-Methyl-1-Tridecene, and the C_7-C_{14} 1-Alkenes at 295 ± 1 K. *Phys. Chem. Chem. Phys.*, *10*, 4159-4164.

Aschmann, S. M. and Atkinson, R. Products and Mechanism of the OH Radical-Initiated Reactions of 1-Octene and 7-Tetradecene in the Presence of NO. *Environ. Sci. Technol.*, in preparation.

Atkinson, R., 2007. Rate Constants for the Atmospheric Reactions of Alkoxy Radicals: An Updated Estimation Method. *Atmos. Environ.*, *41*, 8468-8485.

Atkinson, R. and Arey, J., 2003. Gas-Phase Tropospheric Chemistry of Biogenic Volatile Organic Compounds: A Review. *Atmos. Environ.*, *37*, Suppl. 2, S197-S219.

Atkinson, R., Carter, W. P. L., Winer, A. M., Pitts, J. N., Jr., 1981. An Experimental Protocol for the Determination of OH Radical Rate Constants with Organics Using Methyl Nitrite Photolysis as an OH Radical Source. *Air Pollut. Control Assoc.*, *31*, 1090-1092.

Atkinson, R., Tuazon, E. C., Ashmann, S. M., 1995. Products of the Gas-Phase Reactions of a Series of 1-Alkenes and 1-Methylcyclohexene with the OH Radical in the Presence of NO. *Environ. Sci. Technol.*, *29*, 1674-1680.

Cassanelli, P., Fox, D. J., Cox, R. A., 2007. Temperature Dependence of Pentyl Nitrate Formation from the Reaction of Pentyl Peroxy Radicals with NO. *Phys. Chem. Chem. Phys.*, *9*, 4332-4337.

Chattopadhyay, S. and Ziemann, P. J., 2005. Vapor Pressures of Substituted and Unsubstituted Monocarboxylic and Dicarboxylic Acids Measured Using an Improved Thermal Desorption Particle Beam Mass Spectrometry Method. *Aerosol Sci. Technol., 39*, 1085-1100.

Colville, C. J. and Griffin, R. J., 2004. The Roles of Individual Oxidants in Secondary Organic Aerosol Formation from Δ^3-Carene: 2. Soa Formation and Oxidant Contribution. *Atmos. Environ., 38*, 4013-4023.

Crable, G.F. and Coggeshall, N.D., 1958. Application of Total Ionization Principles to Mass Spectrometric Analysis. *Anal. Chem., 30*, 310-313.

de Gouw, J. A., Middlebrook, A. M., Warneke, C., Goldan, P. D., Kuster, W. C., Roberts, J. M., Fehsenfeld, F. C., Worsnop, D. R., Canagaratna, M. R., Pszenny, A. A. P., Keene, W. C., Marchewka, M., Bertman, S. B., Bates, T. S., 2005. Budget of Organic Carbon in a Polluted Atmosphere: Results from the New England Air Quality Study in 2002. *J. Geophys. Res., 110*, doi:10.1029/2004JD005623.

Docherty, K. S. and Ziemann, P. J., 2006. Reaction of Oleic Acid Particles with NO_3 Radicals: Products, Mechanism, and Implications for Radical-Initiated Organic Aerosol Oxidation. *J. Phys. Chem. A, 110*, 3567-3577.

Docherty, K. S., Wu, W., Lim, Y. B., Ziemann, P. J., 2005. Contributions of Organic Peroxides to Secondary Aerosol Formed from Reactions of Monoterpenes with O_3. *Environ. Sci. Technol., 39*, 4049-4059.

Donahue, N. M., Robinson, A. L., Stanier, C. O., Pandis, S. N., 2006. Coupled Partitioning, Dilution, and Chemical Aging of Semivolatile Organics. *Environ. Sci. Technol., 40*, 2635-2643.

Gong, H., Matsunaga, A., Ziemann, P. J., 2005. Products and Mechanism of Secondary Organic Aerosol Formation from Reactions of Linear Alkenes with NO_3 Radicals. *J. Phys. Chem. A, 109*, 4312-4324.

Heald, C. L., Jacob, D. L., Park, R. J., Russell, L. M., Huebert, B. J., Seinfeld, J. H., Liao, H., Weber, R. J., 2005. A Large Organic Aerosol Source in the Free Troposphere Missing from Current Models. *Geophys. Res. Lett.*, *32*, doi: 10.1029/2005GL023831.

Holt, T., Atkinson, R., Arey, J., 2005. Effect of Water Vapor Concentration on the Conversion of a Series of 1,4-Hydroxycabonyls to Dihydrofurans. *J. Photochem. Photobiol. A: Chem.*, *176*, 231-237.

Jenkin, M. E., 2004. Modeling the Formation and Composition of Secondary Organic Aerosol from α- and β-Pinene Ozonolysis Using MCM v3. *Atmos. Chem. Phys.*, *4*, 1741-1757.

Johnson, D., Jenkin, M. E., Wirtz, K., Martin-Reviejo, M., 2004. Simulating the Formation of Secondary Organic Aerosol from the Photooxidation of Toluene. *Environ. Chem.*, *4*, 150-165.

Johnson, D., Utembe, S. R., Jenkin, M. E., 2006. Simulating the Detailed Chemical Composition of Secondary Organic Aerosol Formed on a Regional Scale During the TORCH 2003 Campaign in the Southern UK. *Atmos. Chem. Phys.*, *6*, 419-431.

Kalberer, M., Paulsen, D., Sax, M., Steinbacher, M., Dommen, J., Prevot, A. S. H., Fisseha, R., Weingartner, E., Frankevich, V., Zenobi, R., Baltensperger, U., 2004. Identification of Polymers as Major Components of Atmospheric Organic Aerosols. *Science*, *303*, 1659-1662.

Kanakidou, M. et al. (21 co-authors), 2005. Organic Aerosol and Global Climate Modelling: A Review. *Atmos. Chem. Phys.*, *5*, 1053-1123.

Kern, W. and Spiteller, G., 1996. Synthesis and Properties of Naturally Occurring α-Hydroxyaldehydes. *Tetrahedron*, *12*, 4347-4362.

Kroll, J. H., Chan, A. W. H., Ng, N. L., Flagan, R. C., Seinfeld, J. H., 2007. Reactions of Semivolatile Organics and Their Effects on Secondary Organic Aerosol Formation. *Environ. Sci. Technol.*, *41*, 3545-3550.

Kroll, J. H. and Seinfeld, J. H., 2008. Chemistry of Secondary Organic Aerosol: Formation and Evolution of Low-Volatility Organics in the Atmosphere. *Atmos. Environ.*, *42*, 3593-3624.

Kwok E. S. C. and Atkinson, R. J., 1995. Estimation of Hydroxyl Radical Reaction Rate Constants for Gas-Phase Organic Compounds Using a Structure-Reactivity Relationship: An Update. *Atmos. Environ.*, *29*, 1685-1695.

Kwok, E. S. C., Atkinson, R., Arey, J., 1996. Isomerization of β-Hydroxyalkoxy Radicals Formed from the OH Radical-Initiated Reaction of C_4-C_8 1-Alkenes. *Environ. Sci. Technol.*, *30*, 1048-1052.

Lim, Y. B. and Ziemann, P. J., 2005 Products and Mechanism of Secondary Organic Aerosol Formation from Reactions of *n*-Alkanes with OH Radicals in the Presence of NO_x. *Environ. Sci. Technol.*, *39*, 9229-9236.

Martin, P., Tuazon, E. C., Aschmann, S. M., Arey, J., Atkinson, R., 2002. Formation and Atmospheric Reactions of 4,5-Dihydro-2-Methylfuran. *J. Phys. Chem. A*, *106*, 11492–11501.

Matsunaga, A. and Ziemann, P. J., 2009. Yields of β-Hydroxynitrates and Dihydroxynitrates in Aerosol Formed from the OH Radical-Initiated Reactions of Linear Alkenes in the Presence of NO_x. *J. Phys. Chem. A*, *113*, 599-606.

Nishino, N., Arey, J., Atkinson, R., 2009. Rate Constants for the Gas-Phase Reactions of OH Radicals with a Series of C_6-C_{14} Alkenes at 299 ± 2 K. *J. Phys. Chem. A*, *113*, 852-857.

O'Brien, J. M., Czuba, E., Hastie, D. R., Francisco, J. S., Shepson, P. B., 1998. Determination of the Hydroxy Nitrate Yields from the Reaction of C2-C6 Alkenes with OH in the Presence of NO. *J. Phys. Chem. A*, *102*, 8903-8908.

Odum, J. R., Hoffmann, T., Bowman, F., Collins, D., Flagan, R. C., Seinfeld, J. H., 1996. Gas/Particle Partitioning and Secondary Organic Aerosol Yields. *Environ. Sci. Technol.*, *30*, 2580-2585.

Pankow, J. F., 1994. An Absorption Model of the Gas/Aerosol Partitioning Involved in the Formation of Secondary Organic Aerosol. *Atmos. Environ.*, *28*, 189-193.

Presto, A. A. and Donahue, N. M., 2006. Investigation of α-Pinene + Ozone Secondary Organic Aerosol Formation at Low Total Aerosol Mass. *Environ. Sci. Technol.*, *40*, 3536-3543.

Reisen, F., Ashmann, S. M., Atkinson, R., Arey. J., 2005. 1,4-Hydroxycarbonyl Products of the OH Radical Initiated Reactions of C5-C8 Alkanes in the Presence of NO. *Environ. Sci. Technol.*, *39*, 4447-4453.

Robinson, A. L., Donahue, N. M., Shrivastava, M. K., Weitkamp, E. A., Sage, A. M., Grieshop, A. P., Lane, T. E., Pierce, J. R., Pandis, S. N., 2007. Rethinking Organic Aerosols: Semivolatile Emissions and Photochemical Aging. *Science*, *315*, 1259-1262.

Seinfeld, J. H. and Pandis, S. N., 1998. Atmospheric Chemistry and Physics. John Wiley & Sons, New York.

Seinfeld, J. H., Erdakos, G. B., Asher, W. E., Pankow, J. F., 2001. Modeling the Formation of Secondary Organic Aerosol (SOA). 2. The Predicted Effects of Relative Humidity on Aerosol Formation in the α-Pinene-, β-Pinene-, Sabinene-, Δ^3-Carene-, and Cyclohexene-Ozone Systems. *Environ. Sci. Technol.*, *35*, 1806-1817.

Taylor, W. D., Allston, T. D., Moscato, M. J., Fazekas, G. B., Kozlowski, R., Takacs, G. A., 1980. Atmospheric Photodissociation Lifetimes for Nitromethane, Methyl Nitrite, and Methyl Nitrate. *Int. J. Chem. Kinet.*, *12*, 231-240.

Tobias, H. J. and Ziemann, P. J., 1999. Compound Identification in Organic Aerosols Using Temperature-Programmed Thermal Desorption Particle Beam Mass Spectrometry. *Anal. Chem., 71,* 3428-3435.

Tobias, H. J. and Ziemann, P. J., 2000. Thermal Desorption Mass Spectrometric Analysis of Organic Aerosol Formed from Reactions of 1-Tetradecene and O_3 in the Presence of Alcohols and Carboxylic Acids. *Environ. Sci. Technol., 34,* 2105-2115.

Tobias, H. J., Kooiman, P. M., Docherty, K. S., Ziemann, P. J., 2000. Real-Time Chemical Analysis of Organic Aerosols Using a Thermal Desorption Particle Beam Mass Spectrometer. *Aerosol Sci. Technol., 33,* 170-190.

Tolocka, M. P., Jang, M., Ginter, J., Cox, F., Kamens, R., Johnston, M., 2004. Formation of Oligomers in Secondary Organic Aerosol. *Environ. Sci. Technol., 38,* 1428-1434.

Volkamer, R., Jimenez, J. L., San Martini, F., Dzepina, K., Zhang, Q., Salacedo, D., Molina, L. T., Worsnop, D. R., Molina, M. J., 2006. Secondary Organic Aerosol Formation from Anthropogenic Air Pollution: Rapid and Higher than Expected. *Geophys. Res. Lett., 33,* doi:10.1029/2006GL026899.

Wang, S. C. and Flagan, R. C., 1990. Scanning Electrical Mobility Spectrometer. *Aerosol Sci. Technol., 13,* 230-240.

Weber, R. J., Sullivan, A. P., Peltier, R. E., Russell, A., Yan, B., Zheng, M., de Gouw, J., Warneke, C., Brock, C., Holloway, J. S., Atlas, E. L., Edgerton, E., 2007. A Study of Secondary Organic Aerosol Formation in the Anthropogenic-Influenced Southeastern United States. *J. Geophys. Res., 112,* doi:10.1029/2007JD008408.

Ziemann, P. J., 2003. Formation of Alkoxyhydroperoxy Aldehydes and Cyclic Peroxyhemiacetals from Reactions of Cyclic Alkenes with O_3 in the Presence of Alcohols. *J. Phys. Chem. A, 107,* 2048-2060.

Chapter 4

Yields of β-Hydroxynitrates, Dihydroxynitrates, and Trihydroxynitrates in Aerosol Formed from OH Radical-Initiated Reactions of 2-Methyl-1-Alkenes in the Presence of NO_x

4.1 Abstract

Yields of β-hydroxynitrates, dihydroxynitrates, and trihydroxynitrates formed from OH radical-initiated reactions of C_9-C_{15} 2-methyl-1-alkenes in the presence of NO_x were measured using a thermal desorption particle beam mass spectrometer coupled to a high-performance liquid chromatograph (HPLC) with UV-vis detector for identification and quantification. When normalized for OH radical addition to the C=C double bond, yields of β-hydroxynitrates and dihydroxynitrates increased with carbon number primarily due to enhanced gas-to-particle partitioning to plateaus at C_{14} or C_{15} of 0.225 ± 0.007 and 0.055 ± 0.006 respectively. The ratio of 1-hydroxy/2-hydroxy β-hydroxynitrate isomers was 0.90:0.10. Average of C_{14} and C_{15} OH addition-normalized trihydroxynitrate yields were 0.042 ± 0.006. Calculations performed by combining yield measurements from this and a previous study of similar reactions of linear 1-alkenes and linear internal

alkenes (Matsunaga and Ziemann, 2009) indicate that the relative ratios for forming primary, secondary, and tertiary β-hydroxyalkyl radicals by OH radical addition to the double bond are 1.0:1.9:4.3, and the branching ratios for forming β-hydroxynitrates from reactions of primary, secondary, and tertiary β-hydroxyperoxy radicals with NO are 0.12, 0.15, and 0.25. The effects of H_2O vapor and NH_3 on yields were also explored

4.2 Introduction

Hydrocarbons are emitted from both anthropogenic and biogenic sources. Approximately 90 % of global emissions are biogenic hydrocarbons, with a large fraction of these being alkenes including isoprene and monoterpenes (Guenther et al., 1995). Alkenes are oxidized in the atmosphere through reactions initiated by O_3, OH radicals, and NO_3 radicals, with reactions with OH radicals being the major daytime sink. As a result of these reactions, a large variety of oxygenated products are formed (Atkinson and Arey, 2003a; Calvert et al., 2000), some of which may have sufficiently low vapor pressures because of the addition of functional groups, to condense onto particles and form secondary organic aerosol (SOA) (Kroll and Seinfeld, 2008). SOA is known to comprise a large fraction of the mass of atmospheric fine particles (Zhang et al., 2007), and to have important impacts on human health (Englert, 2004), visibility (Finlayson-Pitts and Pitts, 2000), and global climate (Andreae and Crutzen, 1997), but significant uncertainties still exist regarding its sources (DeGouw and Jimenez, 2009). Modeling studies indicate that the products of isoprene and monoterpene reactions are the major contributors to SOA mass on a global scale (Kanakidou et al., 2005) and that in urban areas, products of aromatic reactions are also thought to be important (perhaps dominant),

including those formed from reactions of first-generation, unsaturated ring-opened products (Johnson et al., 2004).

The basic steps (involving alkyl, peroxy, and alkoxy radicals) in the reactions by which alkenes are oxidized in the atmosphere are reasonably well understood (Atkinson and Arey, 2003a); however, few reaction products have been identified and even fewer quantified. This in understandable, since the mechanisms are complex and the products are many. In an effort to address this lack of fundamental knowledge on reaction mechanisms, we recently carried out a detailed study of the products and mechanism SOA formation from the OH radical-initiated reactions of linear alkenes in the presence of NO_x (Matsunaga and Ziemann, 2009; Matsunaga et al., 2009). The reactions are sufficiently "simple" that we were able to identify nearly all the particle-phase products, and to quantify hydroxynitrates and dihydroxynitrates. Using these results and some additional information from the literature, we were then able to develop a quantitative reaction mechanism and a model for SOA formation (Matsunaga et al., 2009). Recently, we extended these studies to similar reactions of 2-methyl-1-alkenes. To our knowledge, only the gas-phase products of the reaction of 2-methyl-1-propene have been measured (Tuazon et al., 1998). As is shown below, the presence of a methyl group on the C=C

double bond alters the reaction mechanism and products in interesting and important ways. The results should help in understanding the chemistry of some of the most abundant compounds in the atmosphere, since isoprene and the monoterpenes α- and β-pinene, as well as sesquiterpenes and others, have this subunit in their structure.

4.3 Experimental Section

Chemicals. The following chemicals, with purities (when available) and suppliers, were used: 2-methyl-1-nonene (97%), 2-methyl-1-undecene (97%), 2-ethylhexyl nitrate (97%), chloroform-d (99.8 atom % D), 2-nonanone (99+%), and 2-octanone (98%) [Sigma-Aldrich], 2-methyl-1-octene (97%), 2-methyl-1-tridecene (99%), and 2-methyl-1-tetradecene (97%) [ChemSampCo], 2-methyl-1-decene (97%) and 2-methyl-1-dodecene (>97%) [Rieke Metals], dioctyl sebacate (≥97%) [Fluka], and NO [Matheson Tri Gas]. All chemicals were used without further purification. O_3 was generated using a Welsbach T-408 O_3 generator.

Environmental Chamber Method. Reactions of 2-methyl-1-alkenes with OH radicals in the presence of NO_x were conducted in a ~5900 L PTFE environmental chamber at room temperature (~25 °C) and atmospheric pressure. The chamber, which

has blacklights covering two walls, was filled with clean, dry air (< 5 ppbv hydrocarbons, < 1% RH, < 50 ppbv NO_x, < 10 ppbv O_3) from an Aadco clean air system. In a typical experiment, ~200 μg m^{-3} dioctyl sebacate seed particles generated by an evaporation-condensation apparatus were added to the chamber, 1 ppmv of alkene was evaporated from a glass bulb using gentle heating and flushed into the chamber in a clean air stream, and 5 ppmv each of methyl nitrite and NO were added. NO was added to the chamber to suppress O_3 and NO_3 radical formation. For 2-methyl-1-tetradecene, reactions were also performed at 50%RH and with 20 ppmv NH_3 in dry air.

The reactions were initiated by turning on the blacklights, which generates OH radicals by photolyzing methyl nitrite (Atkinson et al., 1981). The chamber was irradiated for 6 min, during which time 40-50% of the alkene reacted, NO decreased by 1-2 ppmv, and NO_x stayed approximately constant. SOA formed within 1 min of turning on the blacklights. The average OH radical concentration estimated from the amounts of alkenes reacted and OH radical rate constants (Nishino et al., 2009) was ~3 x 10^7 cm^{-3}. O_3 was measured using a Dasibi model 1003-AH O_3 monitor and NO and NO_x were measured using a Thermo Environmental Instruments Inc. 42C NO-NO_2-NO_x analyzer.

Particle Mass Spectrometric Analysis. A thermal desorption particle beam mass spectrometer (TDPBMS) was used to analyze particle composition in real-time (Tobias et al., 2000) and by temperature-programmed thermal desorption (TPTD) (Tobias and Ziemann, 1999). Aerosols were sampled from the chamber through an aerodynamic lens (Liu et al., 1995a; Liu et al., 1995b), and the resulting beam impacted in a V-shaped notch in the tip of a gold-coated copper vaporizer rod coated with a nonstick polymer (Chattopadhyay and Ziemann, 2005). For real-time analyses, the rod was resistively heated to 160 °C. Particles were vaporized upon impact, and the vapor was ionized by 70 eV electrons and analyzed in an ABB Extrel MEXM 500 quadrupole mass spectrometer. For TPTD analysis, the vaporizer rod was cooled to -40 °C and particles were sampled for 30 min. The rod was allowed to warm to -5 °C and then heated to 200 °C with a computer controlled linear temperature ramp of 2 °C min^{-1}. Compounds desorbed from the vaporizer according to their volatilities, allowing separation of components for mass spectral analysis. The mass spectrometer was typically scanned from *m/z* 40-500 in 30 s.

Aerosol Size Distribution and Alkene Analysis. Alkene concentrations were measured before and after reaction by using gas chromatography with flame ionization detection (GC-FID) to analyze samples collected on Tenax TA solid adsorbent

(Docherty et al., 2005). Analyses of replicate samples taken at 30 min intervals agreed within ±5% both before and after reaction, and the FID signals from alkenes collected before reaction were within ±5% of values expected for a 1 ppmv chamber concentration (based on solution calibration curves), so no wall loss corrections were necessary. Particle size distributions were measured every 2 min during reactions and filter sampling with a scanning mobility particle sizer (SMPS) (Wang and Flagan, 1990). The SMPS consists of a ^{210}Po bipolar charger, a long differential mobility analyzer similar design to the TSI model 3934, a TSI Model 3010 Condensation Particle Counter, and a scanning/inversion program developed by the McMurry group at the University of Minnesota for use with Labview software. A microliter syringe and balance were used to measure a density of 1.1 g cm^{-3}for the dried SOA filter extract from a reaction of 2-methyl-1-tridecene without seed aerosol. Aerosol mass yields [aerosol formed (μg m^{-3})/alkene reacted (μg m^{-3})] were calculated using the aerosol volume concentration calculated from SMPS data, the measured SOA density, and the mass of reacted alkene calculated from GC-FID data.

Hydroxynitrate Analysis. After each reaction, filter samples were collected for 2 h on Millipore filters (1.0 μm pore size, Fluoropore FALP, 47 mm, without pretreatment) at ~15 L min^{-1}. The collection efficiency of these filters was determined to be the same as

0.45 μm pore size filters, but had the advantage of a smaller pressure drop. This was helpful, since the sampling flow rate was controlled by a calibrated critical orifice located between the filter holder and a vacuum pump, and corrections for the reduction in flow that occurred as the filter accumulated sample were minimized (< 5-10%) by using the 1.0 μm pore size filters. Filter samples were extracted immediately or stored at -20 °C, and stored samples were extracted within 1week of collection because it was determined that all hydroxynitrates were stable for at least this period of time. Samples extracted after 1 month showed losses of β-hydroxynitrates (but not the other hydroxnitrates) due to decomposition. . Filters were extracted twice with 4 mL of ethyl acetate at room temperature for >10 min, the extracts were combined, dried with N_2, and, depending on the aerosol mass collected, re-dissolved in 30-50 μL ethyl acetate. Tests carried out using different solvents, sonication, multiple extractions, and filter spiking indicated recovery rates were 90-100%.

Extracts were analyzed using an Agilent 1100 Series HPLC coupled to a UV-Vis diode array detector at 210 nm, a wavelength at which nitrate absorbs strongly (Docherty and Ziemann, 2006). The HPLC contained a 250 x 4.6 mm Zorbax 5 μm XDB-C18 column that operated at room temperature. The HPLC method employed gradient elution

using water and acetonitrile, with the contribution of acetonitrile to the mobile phase maintained at 50% for 10 min and then increasing linearly to 100% in 50 min. The flow rate was 1 mL min^{-1} and the sample injection volume was 10 μL. Hydroxynitrates were quantified using three calibration curves prepared using a mixture of either β-hydroxynitrate isomers, dihydroxynitrate isomers, or trihydroxynitrate isomers formed from a 2-methyl-1-tridecene reaction. The purified mixtures of each class of hydroxynitrate used to prepare the curves were obtained by collecting aliquots of the appropriate mixture after it had passed through the UV-Vis detector. Purities of the standards were verified by HPLC analysis. The molar yield of organic nitrate in particles was calculated as (moles of compound collected on filter/volume of air sampled)(aerosol mass concentration after reaction/average aerosol mass concentration during filter sampling)/(moles of alkene reacted per volume of air). The term containing aerosol mass concentrations is to collect for the wall loss of aerosols during filter sampling, and the aerosol mass concentrations were measured with an SMPS.The molar absorptivities of the β-hydroxynitrate, dihydroxynitrate, and trihydroxynitrate standards relative to 2-ethylhexyl nitrate were 0.412, 0.964, and 0.608, respectively. The values measured previously for β-hydroxynitrates and dihydroxynitrates (no trihydroxynitrates were

observed) formed from the reaction of 1-tetradecene were 0.786 and 0.963 (Matsunaga and Ziemann, 2009). It is worth noting that these data exhibit some interesting trends that can be explained by hydroxgen bonding, which is known to affect UV absorption (Pavia et al., 2001). The lower molar absorptivities of hydroxynitrates compared to alkyl nitrates indicates that hydrogen bonding with hydroxy groups reduces absorption by the nitrooxy group. The effect is smallest for dihydroxynitrates (0.963 and 0.964), apparently because the hydroxy groups are on adjacent carbon atoms and so preferentially bond to each other. The effect is larger for trihydroxynitrates (0.608), since the third hydroxy group is located three carbon atoms away from the other hydroxy groups and so is relatively free to bond to the nitrooxy group. The largest effect is observed for β-hydroxynitrates in which the nitrooxy group is on a tertiary carbon atom adjacent to the carbon atom on which the hydroxy group is located (0.412), and the effect is reduced when the nitrooxy group is instead on a secondary carbon atom (0.786).

Hydroxynitrates were identified from particle mass spectra obtained by coupling the HPLC to the TDPBMS via a Collison atomizer. Effluent from the HPLC column was atomized, the solvent was removed as the drops passed through activated charcoal and silica gel diffusion dryers, and the remaining hydroxynitrate particles were analyzed in

the TDPBMS. Identifications were verified by ^{1}H NMR analysis of purified samples using a Varian Inova 500 MHz instrument.

4.4 Results and Discussion

Reaction Mechanism. The mechanism of the reaction of 2-methyl-1-alkenes with OH radicals in the presence of NO_x is developed based on previous studies of OH-radical initiated reactions of alkenes in the presence of NO_x (Atkinson and Arey, 2003b; Matsunaga and Ziemann, 2009; Matsunaga et al., 2009) and is shown in Figure 4.1, where R represents an alkyl group. In Figure 4.1, α_i is the branching ratio for the reaction of a specie by pathway *i*, defined as $\alpha_i = r_i/\Sigma r_i$, where r_i is the reaction rate for pathway *i* and the sum is over all pathways for the specie and equal to 1. The focus here is on quantifying branching ratios $\alpha_{C=C}$ and α_1-α_6, so only these are discussed below; the others are discussed in Chapter 5. The reaction is initiated either by addition of an OH radical to the C=C double bond ($\alpha_{C=C}$) or abstraction of a H atom (1-$\alpha_{C=C}$).The reactions that follow H-atom abstraction are the same as those that occur in OH-radical initiated reactions of alkanes, and are described elsewhere (Atkinson and Arey, 2003a; Lim and

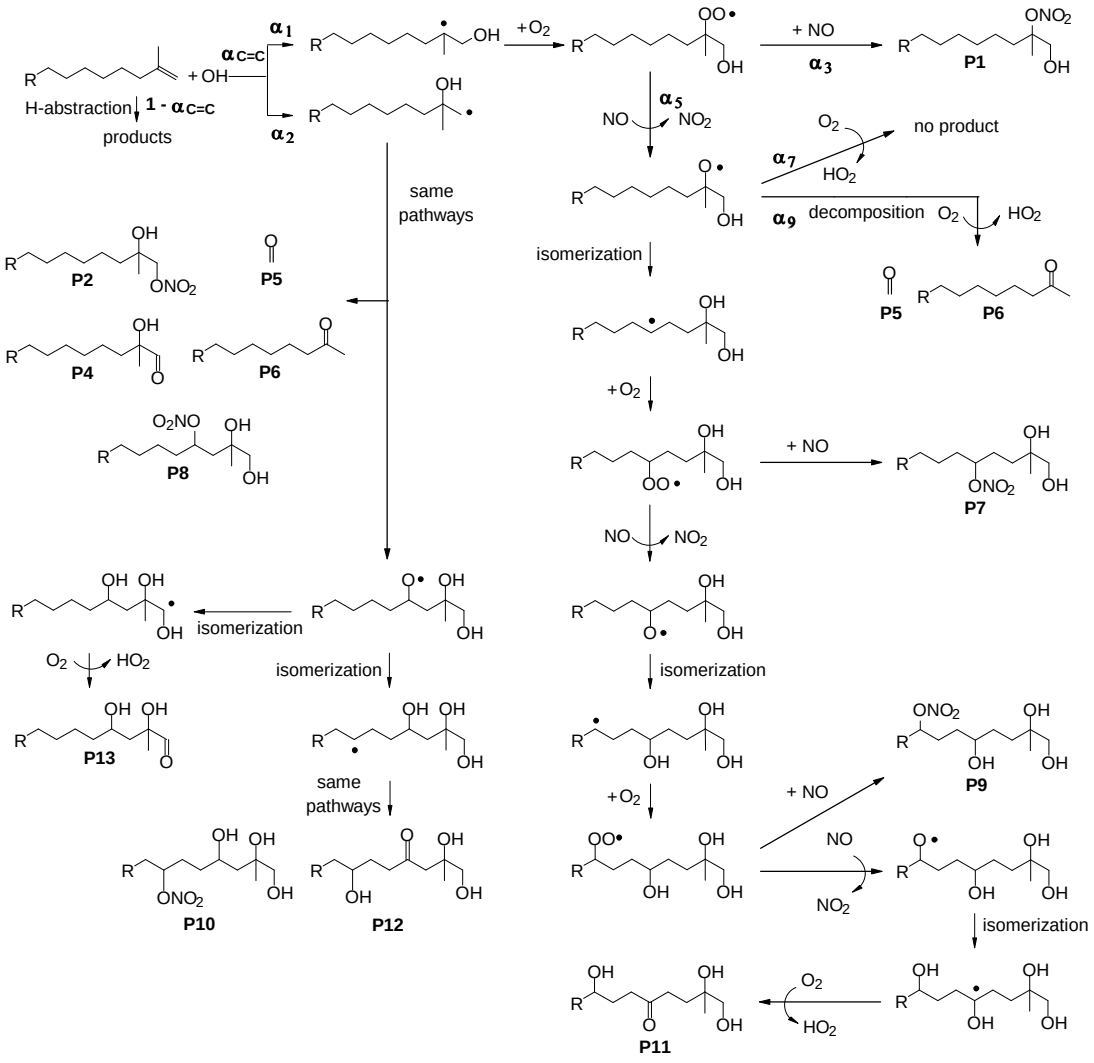

Figure 4.1 Mechanism of the OH radical-initiated reaction of 2-methyl-1-alkenes in the presence of NO_x.

Ziemann, 2009). For the OH radical addition pathway, addition can occur at either carbon of the C=C double bond to form a pair of β-hydroxyalkyl radical isomers. The branching ratios for addition to the first and second carbon atoms are α_1 and α_2, with $\alpha_1 + \alpha_2 = \alpha_{C=C}$. The β-hydroxyalkyl radicals react with O_2 to form β-hydroxyperoxy radicals that then react with NO to form β-hydroxynitrates [P1, P2] with branching ratios α_3 and α_4, or β-hydroxyalkoxy radicals with branching ratios α_5 and α_6. Note that $\alpha_3 + \alpha_5 = 1$ and $\alpha_4 + \alpha_6 = 1$, and that α_4 and α_6 (not shown in Figure 4.1) correspond to α_3 and α_5 except they are associated with reactions of 2-hydroxy isomers instead of 1-hydroxy isomers. The term "same pathways" that appears in Figure 4.1 is associated with species derived from reactions of 2-hydroxyalkyl radicals (left-hand side of Figure 4.1), and is meant to refer the reader to the corresponding species derived from reactions of 1-hydroxy isomers (right-hand side of Figure 4.1) for detailed mechanisms.

The β-hydroxyalkoxy radicals react with O_2, decompose, or isomerize through a 6-member ring transition state. Reaction of the 2-hydroxyalkoxy radical with O_2 forms a α–hydroxycarbonyl [P4], but this pathway is not accessible to the 1-hydroxyalkoxy radical because there is no H atom available on the second carbon atom for abstraction by O_2. Decomposition followed by reaction with O_2 forms formaldehyde [P5] and a ketone

[P6], and isomerization followed by reaction with O_2 forms dihydroxyperoxy radicals that then react (similar to the β-hydroxyperoxy radicals) with NO to form either dihydroxynitrates or dihydroxyalkoxy radicals.

The dihydroxyalkoxy radicals can isomerize in two different ways. Those derived from reactions of 2-hydroxyalkoxy radicals primarily undergo a rapid "reverse" isomerization in which the alkoxy group abstracts an H atom from the terminal carbon atom, and then reaction with O_2 forms a dihydroxycarbonyl [P13] (Atkinson, 2007). A very minor isomerization pathway involves abstraction of an H-atom from a CH_2 group further along the carbon chain followed by reaction with O_2 to form trihydroxyperoxy radicals, which then react by pathways similar to those described above for dihydroxyperoxy radicals to form trihydroxynitrates [P10] and trihydroxycarbonyls [P12]. In the case of dihydroxyalkoxy radicals derived from reactions of 1-hydroxyalkoxy radicals, reverse isomerization cannot occur because there is no H atom for abstraction on the second carbon atom. Isomerization therefore continues along the carbon chain, leading to the formation of trihydroxynitrates [P9] and trihydroxycarbonyls [P11].

SOA Product Identification. The TDPBMS real-time mass spectrum and thermal desorption profiles of selected single ions of the aerosol products formed from

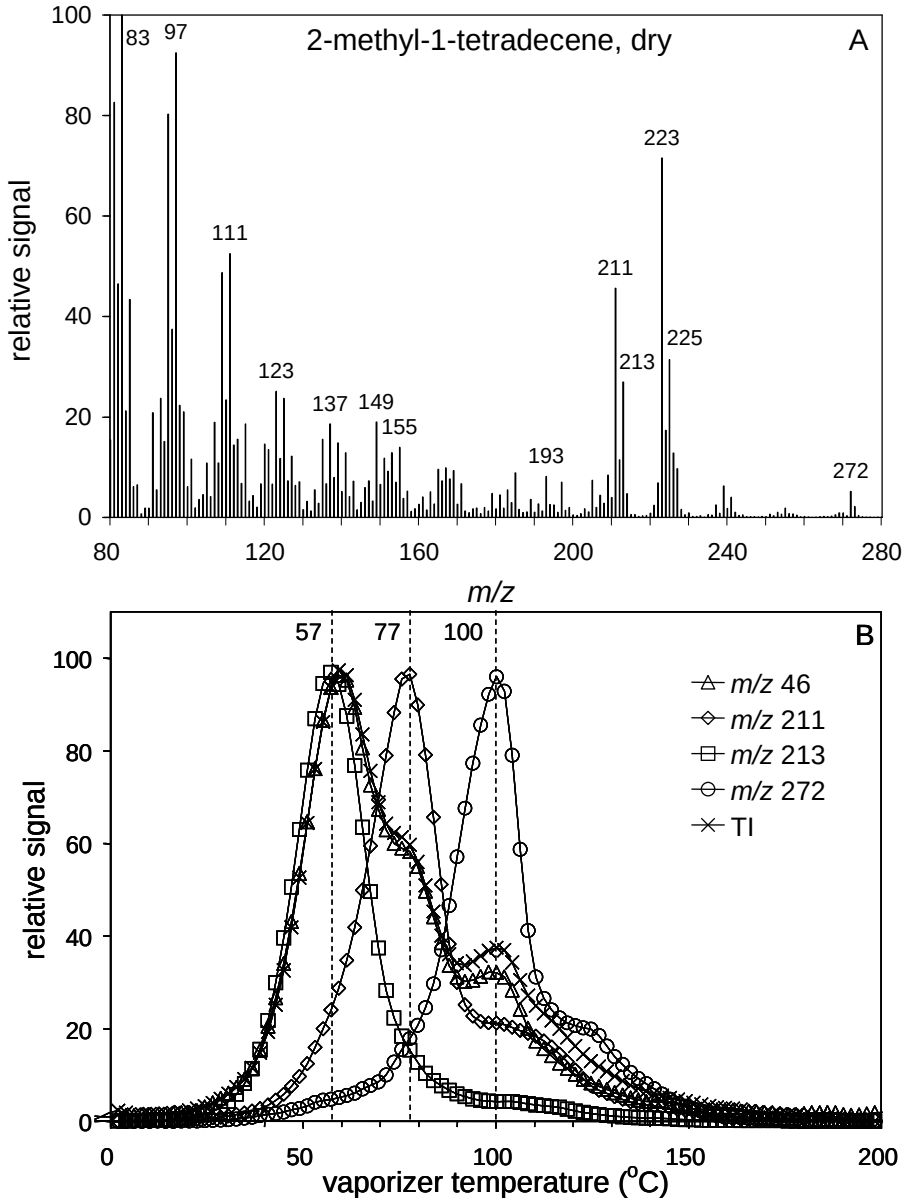

Figure 4.2 (A) Real-time TDPBMS mass spectra and (B) thermal desorption profiles for SOA formed from the OH radical-initiated reaction of 2-methyl-1-tetradecene in dry air in the presence of NO_x. Thermal desorption profiles were smoothed and normalized to peak values.

the OH radical-initiated reaction of 2-methyl-1-tetradecene in the presence of NO_x are shown in Figure 4.2. Desorption profiles are normalized to the maximum values. The desorption temperature of a compound is related to the compound vapor pressure, and in general, compounds with lower vapor pressures have higher desorption temperatures. The total ion (TI) signal is approximately proportional to aerosol mass (Crable and Coggeshall, 1958), so the relative intensities of peaks in a TI profile are indicative of the relative abundance of the aerosol compounds associated with those peaks. In Figure 4.2, the TI profile has three major peaks or shoulders at approximately 57, 77, and 100 °C, indicating the presence of at least (since some compounds may have similar desorption temperatures) three major SOA products. These peaks overlap with peaks in the *m/z* 46 profile, which is due to NO_2^+ and is characteristic of organic nitrates. The absence of non-nitrate compounds more volatile than the three organic nitrates is consistent with the expectation that formaldehyde [P5] and ketones [P6] are too volatile to be in particles. The large high mass peaks observed at *m/z* 213, *m/z* 211, and *m/z* 272 in the real-time mass spectrum are associated with the compounds that desorb at 57, 77, and 100 °C, respectively, and are assigned to β-hydroxynitrates, dihydroxynitrates, and trihydroxynitrates. This assignment is consistent with the three nitrate products expected

for this reaction (Figure 4.1), whose vapor pressures progressively decrease due to the presence of one, two, and three hydroxy groups.

This assignment also agrees with the results of HPLC-TDPBMS analysis shown in Figure 4.3. For convenience, the following notation will be used here for the structures of β-hydroxynitrates, dihydroxynitrates, and trihydroxynitrates. In the notation, hydroxy and nitrooxy groups are designated H and N, the location of a group on a carbon chain is designated by a number before a letter, and the number of carbons in the chain plus the methyl group are indicated by a subscript number following the letter C. For example, 1,2-dihydroxy-4-nitrooxy-2-methyltetradecane is designated $1,2H4NC_{15}$. The chromatogram shown in Figure 4.3A was taken under reverse phase conditions, so polar compounds have earlier retention times. The three peaks are assigned in order of increasing retention time and decreasing polarity as (1) trihydroxynitrates, (2) dihydroxynitrates, and (3) β-hydroxynitrates. The structures of the compounds were verified by ^{1}H NMR analysis; the chemical shifts are presented in Appendix Table C.2. The small, partially resolved peak at the front of peak 3 in Figure 4.3A indicates that one isomer dominates in β-hydroxynitrates. On the basis of ^{1}H NMR analysis the major isomer was determined to be $1H2NC_{15}$, and from the ratio of the chromatographic peak

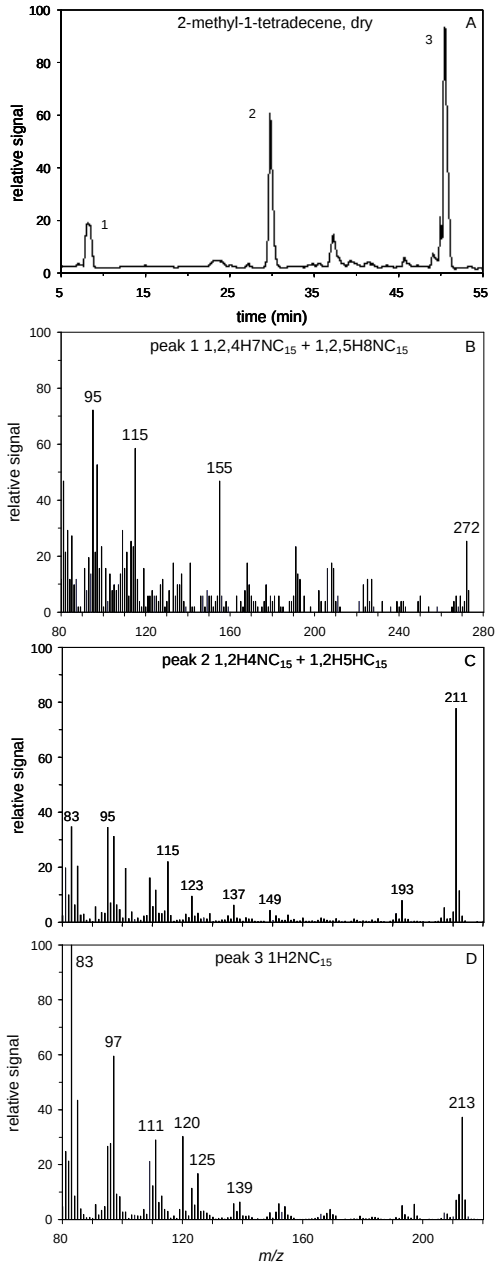

Figure 4.3 (A) HPLC-UV chromatogram and HPLC-TDPBMS mass spectra of (B) trihydroxynitrates, (C) dihydroxynitrates, and (D) *β*-hydroxynitrates formed from the OH radical-initiated reaction of 2-methyl-1-tetradecene in dry air in the presence of NO_x.

areas the relative amounts of the $1H2NC_{15}$ and $1N2HC_{15}$ isomers was determined to be 90:10.

The mass spectra shown in Figure 4.3B and 4.3C are the mass spectra of the mixtures of the isomers of trihydroxynitrate and dihydroxynitrate, respectively. Figure 4.3D is the mass spectrum of the mixture of the isomers of β-hydroxynitrate, but the major peaks in Figure 4.3D should represent the mass spectrum of the major isomer, $1H2NC_{15}$. The spectra verify the assertion made above that *m/z* 213, *m/z* 211, and *m/z* 272 in Figure 4.2A are characteristic of β-hydroxynitrates, dihydroxynitrates, and trihydroxynitrates. The other major peaks, *m/z* 223 and *m/z* 225, are assigned to non-nitrate organic compounds and are discussed in Chapter 5. The major fragmentation channel for compounds having two adjacent functional groups is scission of the C-C bond between the two groups (Matsunaga and Ziemann, 2009; Gong et al., 2005). The major ions observed for the dihydroxynitrates and trihydroxynitrates can be explained as being formed through this fragmentation channel. The molecular weight of the dihydroxynitrates is 305, and *m/z* 211 is likely a $[M-(31+63)]^+$ ion formed by losing CH_2OH and HNO_3, and the *m/z* 193 ion is then formed by the additional loss of H_2O. . The molecular weight of trihydroxynitrates is 321, and *m/z* 272 is likely a$[M-(31+18)]^+$

ion formed by losing CH_2OH and H_2O. The molecular weight of the β-hydroxynitrates is 289, and fragmentation of $1H2N2MC_{13}$ gives the *m/z* 213 ion which is likely a $[M-(30 + 46)]^+$ ion formed by losing CH_2O and NO_2. Transfer of an H atom from the CH_2OH scission product to the ion forms more stable products: a $CH_3(CH_2)_{11}C(CH_3)=OH^+$ ion and formaldehyde (McLafferty and Tureček, 1993).

β-Hydroxynitrate Yields. The molar yields (moles of product formed per mole of alkene reacted) of β-hydroxynitrates are presented in Appendix Table C.1. Losses of β-hydroxynitrates due to secondary reactions with OH radicals were neglected because the estimated losses using a model that accounted for decreased reactivity in particles were ≤ 5%. The Table contains yields without and with normalization for the fraction of OH-radical addition that occurs by addition to the C=C double bond, $\alpha_{C=C} = k_{add} / (k_{add} + k_{abs})$, where k_{abs} and k_{add} are the rate constants for H-atom abstraction and OHradical addition, respectively. Values of k_{abs} (Kwok and Atkinson, 1995) and k_{add} (Nishino et al., 2009) were calculated using equations developed by Atkinson and co-workers from measured rate constant data for 2-methyl-1-alkenes: $k_{abs} = 2.6 + 1.4 \times (C_n-6)$ and $k_{add} = 51 + 16 \times [1-\exp(-0.35 \times (C_n-3))]$, where C_n is the alkene carbon number and the units of k_{add} and k_{abs} are 10^{-12} cm^3 $molecule^{-1}$ s^{-1}. Values of k_{add} and k_{abs} increase with increasing C_n, but

because for the C_9-C_{15} alkenes k_{abs} increases more than k_{add}, $\alpha_{C=C}$ decreases from 0.91 at C_9 to 0.81 at C_{15}. As a result, OH addition-normalized yields are ~10-20% higher than those that have not been normalized. Also, values of $\alpha_{C=C}$ are larger for 2-methyl-1-alkenes compared to the corresponding 1-alkenes (Matsunaga and Ziemann, 2009), indicating that the presence of a methyl group on the C=C double bond increases $\alpha_{C=C}$. The molar yields of the individual β-hydroxynitrate isomers in the particle phase, without and with normalization for OH radical addition, and their sum are presented in Figure 4.4. Values increase with increasing carbon number, primarily because the vapor pressures decrease and so compounds partition more to the particle phase where they can be measured (Matsunaga and Ziemann, 2009). As we discuss briefly below and more thoroughly in a future publication, recent measurements indicate that semi-volatile compounds having a significant gas-phase component also partition to the chamber walls. This likely contributes to the decrease in yield below C_{14}, which is slightly more rapid than predicted by gas-particle partitioning theory (Pankow, 1994). The branching ratio for β-hydroxynitrate formation from the reaction of β-hydroxyperoxy radicals with NO also increases with carbon number, but this effect is minor for the C_9-C_{15} compounds studied here (Matsunaga and Ziemann, 2009). The total yields appear to reach a plateau at about

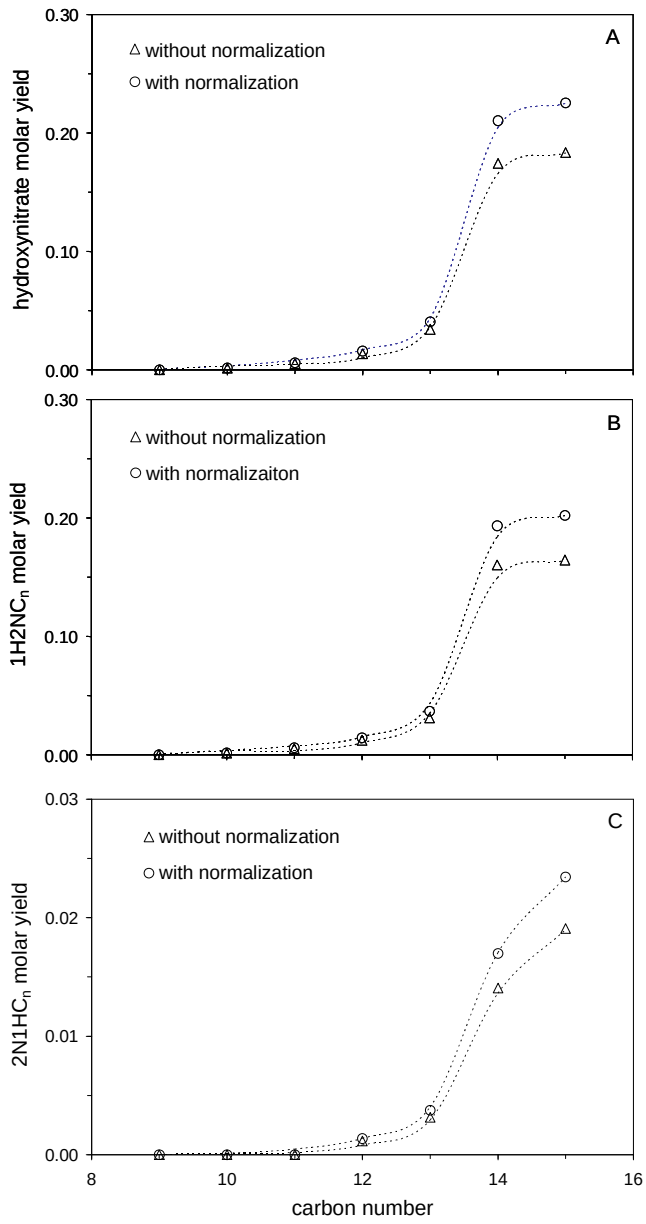

Figure 4.4 Molar yields of (A) total of both β-hydroxynitrate isomers, (B)1H2NC$_n$, and (C) 1N2HC$_n$ formed from the OH radical-initiated reaction of 2-methyl-1-alkenes in dry air in the presence of NO_x with normalization for the fraction of the OH radical reaction that occurred by addition to the double bond. The dashed curve through the yields was drawn to aid the eye.

C_{14} or C_{15}, where the small difference in yields is within measurement uncertainty. The C_{15} yields are 0.183 ± 0.005 and 0.225 ± 0.007 without and with normalization for OH radical addition, with reported uncertainties of one standard deviation. We believe that at this plateau these compounds are almost entirely in the particle phase, so the yields are essentially gas + particle values. In our previous measurements of the yields of β-hydroxynitrates formed from reactions of 1-alkenes (Matsunaga and Ziemann, 2009) a plateau was also reached at ~C_{14}, but there it was possible to observe that the plateau continued out to C_{17} because larger 1-alkenes were available for that study. To our knowledge, only Tuazon et al. (1998) have quantified the yield of β-hydroxynitrates for a similar reaction of 2-methyl-1-alkenes, obtaining a value of ~0.09 ± 0.03 (all products in the gas phase) for the reaction of 2-methyl-1-propene. This value is about half the plateau value measured here, as expected because of the much lower branching ratio at this small carbon number. The 1H2NC$_n$ isomer comprises ~90% of the total β-hydroxynitrates, so as expected the plot of the yields looks similar to that of the β-hydroxynitrates and appears to reach a plateau at C_{14} or C_{15}. The yields of the 1N2HC$_n$ isomer are more difficult to interpret; they may reach a plateau at C_{15}, but this could not be verified because larger 2-methyl-1-alkenes were not available (the vapor pressure of

commercially available 2-methyl-1-heptadecene is too low to carry out a gas-phase reaction). Nonetheless, on the basis of vapor pressures, the yield of the $1N2HC_{15}$ isomer should be close to a plateau. In our study of β-hydroxynitrates formed from reactions of 1-alkenes (Matsunaga et al., 2009), we estimated that the vapor pressures of $1N2HC_n$ isomers are ~3 times larger than those of $1H2NC_n$ isomers, equivalent to the effect of having one less CH_2 unit The partitioning of the $1N2HC_{15}$ isomer should therefore be similar to that of the $1H2NC_{14}$ isomer, which because it has essentially the same yield as the $1H2N2C_{15}$ isomer, appears to be almost entirely in the particle phase. The yields without and with normalization for OH radical addition are 0.164 ± 0.005 and 0.202 ± 0.007 for the $1H2NC_{15}$ isomer and 0.019 ± 0.001 and 0.023 ± 0.001 for the $1N2HC_{15}$ isomer, and the relative amounts of these two isomers are 0.90 and 0.10.

The plateau value of the OH addition-normalized yields of β-hydroxynitrates formed from 2-methyl-1-alkene reactions, 0.202, is slightly higher than the value of 0.162 measured for reactions of linear-1-alkenes but is much lower than the value of ~0.3 estimated from measurements of secondary alkyl nitrates formed from reactions of *n*-alkane (Arey et al., 2001). The lower yields of β-hydroxynitrates from the reactions of 1-alkenes is thought to be caused by weakening of the O-O bond in the β-hydroxyperoxy

radical-NO intermediate, RCO-O-NO, due to hydrogen bonding between the hydroxy and peroxy groups (O'Brien et al., 1998). The presence of a methyl group on the same carbon atom as the peroxy group (the structure for ~90% of the β-hydroxyperoxy radicals formed from reactions of 2-methyl-1-alkenes) appears to compensate somewhat for the effect of the hydroxy group, presumably by strengthening the O-O bond through electron donation.

Branching Ratios. As shown in Figure 4.1, the yield, Y, of a compound is equal to the product of the branching ratios along the pathway by which it is formed. For the β-hydroxynitrates 1H2NC$_n$ [P1] and 1H2NC$_n$ [P2], this means that $Y_{P1} = \alpha_1 \times \alpha_3$ and $Y_{P2} = \alpha_2 \times \alpha_4$, and therefore that $(\alpha_1/\alpha_{c=c}) = (Y_{P1}/\alpha_{c=c})/\alpha_3$ and $(\alpha_2/\alpha_{c=c}) = (Y_{P2}/\alpha_{c=c})/\alpha_4$. The values of $Y_{P1}/\alpha_{c=c}$ and $Y_{P2}/\alpha_{c=c}$ are the OH addition-normalized yields reported above. In our previous study of the reactions of linear 1-alkenes, we solved for these two equations simultaneously for values of the four branching ratios by assuming that α_3/α_4, which is ratio of the branching ratios for the formation of β-hydroxynitrates from reactions of NO with secondary and primary β-hydroxyperoxy radicals, is either 1 or 1.5 (Cassanelli et al., 2007). Here, we combine our measured yields from reactions of linear internal alkenes, linear 1-alkenes, and 2-methyl-1-alkenes to estimate (1) the branching ratios for the

formation of primary, secondary, and tertiary β-hydroxyperoxy radicals by OH radical addition to a C=C double bond, and (2) the branching ratios for the formation of β-hydroxynitrates from the reactions of these β-hydroxyperoxy radicals with NO. Starting with linear internal alkenes, for which two secondary β-hydroxyperoxy radicals are formed, $(\alpha_1/\alpha_{c=c}) = (\alpha_2/\alpha_{c=c}) = 0.5$ and $\alpha_3 = \alpha_4 = (Y_{P1}/\alpha_{c=c}) + (Y_{P2}/\alpha_{c=c}) = 0.15$. Using $\alpha_3 = 0.15$ for the secondary β-hydroxyperoxy radicals formed from 1-alkenes gives $(\alpha_1/\alpha_{c=c}) = (Y_{P1}/\alpha_{c=c})/\alpha_3 = 0.098/0.15 = 0.65$, so that for the primary β-hydroxyperoxy radicals formed from this reaction $(\alpha_2/\alpha_{c=c}) = 1 - (\alpha_1/\alpha_{c=c}) = 0.35$ and $\alpha_4 = (Y_{P2}/\alpha_{c=c})/(\alpha_2/\alpha_{c=c}) = 0.042/0.35 = 0.12$. Using these values for the primary β-hydroxyperoxy radicals formed from 2-methy-1-alkenes gives $(\alpha_2/\alpha_{c=c}) = (Y_{P2}/\alpha_{c=c})/\alpha_4 = 0.023/0.12 = 0.19$, so that for the tertiary β-hydroxyperoxy radicals formed in this reaction $(\alpha_1/\alpha_{c=c}) = 1 - (\alpha_2/\alpha_{c=c}) = 0.81$ and $\alpha_3 = (Y_{P1}/\alpha_{c=c})/(\alpha_1/\alpha_{c=c}) = 0.202/0.81 = 0.25$. The branching ratios of 0.35 and 0.65 for the formation of primary and secondary β-hydroxyperoxy radicals from reactions of linear 1-alkenes agree very well with the values of 0.65 and 0.35 measured by Cvetanovic (1976) for 1-propene. The branching ratios of 0.19 and 0.81 for the formation of primary and tertiary β-hydroxyperoxy radicals from reactions of 2-methyl-1-alkenes agree reasonably well with the values of 0.08 and 0.92 calculated using the structure-

activity method of Peeters et al. (2007). These branching ratios can be combined to give relative ratios for forming primary, secondary, and tertiary β-hydroxyalkyl radicals by OH radical addition to the double bond of 1.0:1.9:4.3. This result indicates that OH radical-addition to a C=C double bond preferentially forms the most stable β-hydroxyalkyl radicals, which follow the order: tertiary > secondary > primary.

The branching ratios of 0.12, 0.15, and 0.25 for β-hydroxynitrate formation from reactions of primary, secondary, and tertiary β-hydroxyperoxy radicals with NO correspond to secondary/primary and tertiary/primary ratios of 1.3 and 2.1. These values bracket well the values of 1.5 measured by Cassanelli et al. (2007) for the corresponding alkylperoxy radicals, although our results indicate an enhancement in the branching ratios for tertiary compared to secondary β-hydroxyperoxy radicals. From the results obtained here, the stability of the β-hydroxyperoxy radical-NO intermediate in the formation of β-hydroxynitrates follows the order: tertiary > secondary > primary.

Dihydroxynitrate and Trihydroxynitrate Yields. The total (sum of isomers) molar yields of dihydroxynitrates and trihydroxynitrates are presented in Appendix Table C.1. Total yields are presented because isomers could not be resolved, and for the trihydroxynitrates only the C_{14} and C_{15} compounds could be analyzed because for the

smaller ones the peak overlapped with the solvent peak. As shown in Figure 4.5, the yields of dihydroxynitrates increase with increasing carbon number to a plateau at C_{14} or C_{15}. The yields of C_{15} dihydroxynitrates without and with normailziation for OH radical-addition are 0.045 ± 0.005 and 0.055 ± 0.006. The yields decrease with decreasing carbon number less slowly than those of the β-hydroxynitrates because of lower vapor pressures and therefore enhanced partitioning to particles. The average yields of the C_{14} and C_{15} trihydroxynitrates, which are expected to be at a plateau since the more volatile dihydroxynitrates are at these carbon numbers, without and with normalization for OH-addition are 0.034 ± 0.005 and 0.042 ± 0.006.

Effects of Humidity and Ammonia on β-Hydoxynitrate, Dihydroxynitrate, and Trihydroxynitrate Yields. Experiments were also performed to investigate the possible effects of H_2O vapor and NH_3 on the yields of β-hydroxynitrates, dihydroxynitrates, and trihydroxynitrates Both are important atmospheric gases capable of forming complexes with peroxy radicals by hydrogen bonding (Clark et al., 2008; Bil and Latajka, 2005), and in previous studies of similar reactions of 1-tetradecene it was observed that yields of β-hydroxynitrates and dihydroxynitrates were reduced by ~75% in the presence in NH_3 but were not affected by H_2O vapor (Matsunaga and Ziemann, 2009).

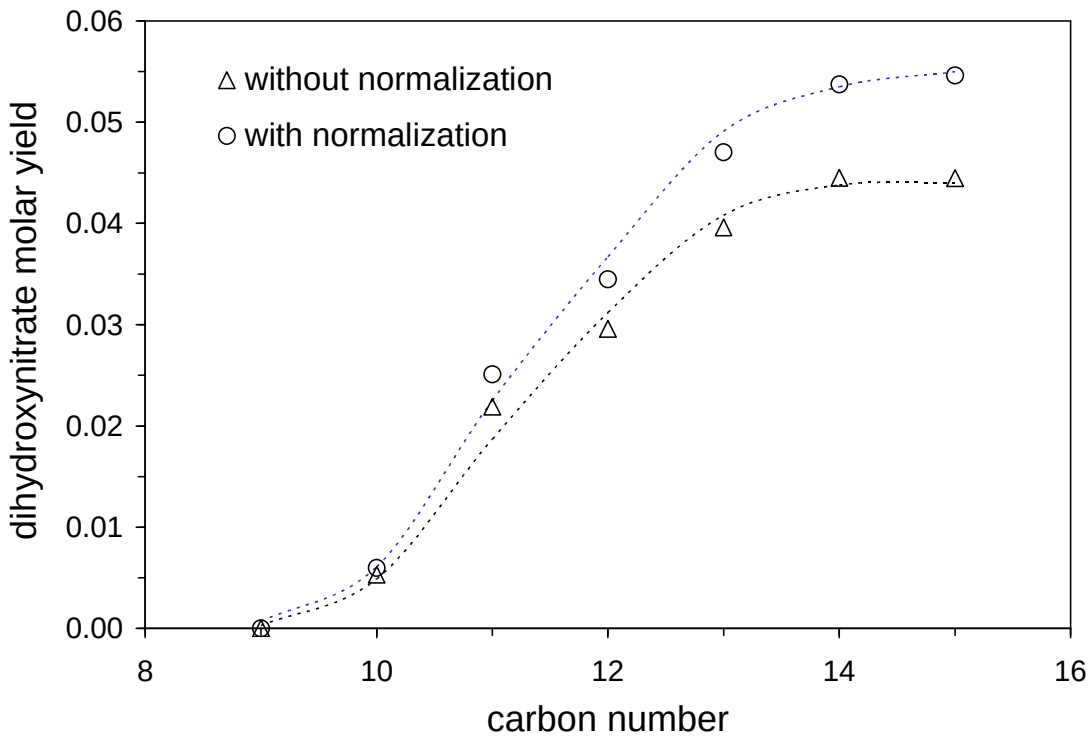

Figure 4.5 Molar yields of dihydroxynitrates formed from the OH radical-initiated reaction of 2-methyl-1-alkenes in dry air in the presence of NO_x with normalization for the fraction of the OH radical reaction that occurred by addition to the double bond. The dashed curve through the yields was drawn to aid the eye.

Yields measured for reactions of 2-methyl-1-tetradecene in dry air, dry air in the presence of 20 ppmv NH_3, and 50% RH, are shown in Table 4.1. The yields of dihydroxynitrates and trihydroxynitrates were the same under all conditions, whereas the yields of $1N2HC_{15}$ and $1H2NC_{15}$ appear to have been reduced by about 15% and 8% by NH_3 and the yield of $1H2NC_{15}$ increased by ~20% in the reaction at 50% RH (compared to dry air). The presence of a methyl group on the second carbon atom significantly reduces the effect of NH_3 on both β-hydroxynitrate and dihydroxynitrate yields (compared to the 75% decrease observed for the 1-tetradecen reaction), most likely by reducing the extent of hydrogen bonding between hydroxy and the peroxy groups. Whether this is due to electronic or steric effects is not clear. The observation that in reactions of linear 1-alkenes and 2-methyl-1-alkenes only the yield of the $1H2NC_{15}$ isomer was higher at 50% RH, and that the yields of all the other products were unaffected, indicates that the presence of a methyl group on the second carbon atom impacts the yield through electronic effects. Apparently, electron donation by the methyl group enhances clustering of H_2O to the β-hydroxyperoxy radical-NO intermediate, RCO-O-NO, and this strengthens the O-NO bond, possibly by reducing hydrogen bonding between the hydroxy and peroxy groups. We previously estimated that only ~1% of β-hydroxyperoxy

Table 4.1 Effects of Experimental Conditions on Molar Yields of β-Hydroxynitrates, Dihydroxynitrates, and Trihydroxynitrates Formed from OH Radical-Initiated Reactions of 2-Methyl-1-Tetradecene in the Presence of NO_x.

condition[a]	$1H2NC_{15}$	$1N2HC_{15}$	dihydroxynitrates[b]	trihydroxynitrates[c]
Dry	0.164	0.019	0.044	0.032
H_2O	0.198	0.019	0.040	0.032
NH_3	0.152	0.016	0.041	0.030

[a]Dry = <1% RH; H_2O = 50% RH; NH_3 = 20 ppmv NH_3.

[b]Dihydroxynitrate isomers are $1,2H4NC_{15}$ and $1,2H5NC_{15}$.

[c]Trihydroxynitrate isomers are $1,2,4H7NC_{15}$ and $1,2,5H8NC_{15}$.

radicals formed from reactions of linear 1-alkenes are complexed with H_2O at 50% RH (Matsunaga and Ziemann, 2009).

4.5 Conclusions.

In this study, β-hydroxynitrates, dihydroxynitrates, and trihydroxyntirates formed from OH radical-initiated reactions of C_9-C_{15} 2-methyl-1-alkenes in the presence of NO_x were identified and quantified and the results used to calculate yields without and with normalization for OH radical addition to the C=C double bond. Comparison with the results of our previous study of similar reactions of linear 1-alkenes (Matsunaga and Ziemann, 2009) shows that seemingly small changes in alkene structure can significantly impact product yields and the reaction mechanism. In this case, replacement of an H atom by a methyl group on the second carbon atom resulted in different relative yields for the two β-hydroxynitrate isomers, increased OH-addition normalized yields of β-hydroxynitrates, dihydroxynitrates, and trihydroxynitrates, with the latter not being observed previously, and also altered the effect of H_2O vapor and NH_3 on yields. Yields not normalized for OH-addition increased even more, because of enhanced OH radical addition relative to H-atom abstraction (Nishino et al., 2009). The effects are apparently

due to the electron donating properties of the methyl group, which helps to stabilize both the tertiary β-hydroxyalkoxy radical formed when an OH radical adds to the terminal carbon atom, leading to a strong preference for that addition pathway, and the β-hydroxyperoxy radical-NO intermediate, thereby enhancing β-hydroxynitrate formation. Electron donation by the methyl groups possibly increases yields of dihydroxynitrates by reducing hydrogen bonding between hydroxy and peroxy groups, which otherwise tends to reduce yields (O'Brien et al., 1998), and trihydroxynitrates appear in these reactions because the replacement of an H atom by a methyl group forces dihydroxyalkoxy radicals to isomerize by an alternate pathway.

Calculations carried out using β-hydroxynitrate yields (measured at the high carbon number plateau, where carbon number does not impact values) for reactions of 2-methyl-1-alkenes, linear 1-alkenes, and linear internal alkenes, reported here and previously (Matsunaga and Ziemann, 2009), indicate that the relative ratios for forming primary, secondary, and tertiary β-hydroxyalkyl radicals by OH radical addition to the C=C double bond are 1.0:1.9:4.3, and the branching ratios for forming β-hydroxynitrates from the reactions of primary, secondary, and tertiary β-hydroxyperoxy radicals with NO are 0.12, 0.15, and 0.25, corresponding to relative ratios of 1.0:1.3:2.1. These values

should be applicable to other systems; for example, the predicted yield of β-hydroxynitrates from the reaction of α-pinene, which forms a primary and a tertiary β-hydroxyalkyl radical and then the corresponding β-hydroxyperoxy radicals, is 0.23, in good agreement with a measured total organic nitrate yield of 0.18 (Nozière et al., 1999). Some of the overestimate may be due to the assumption that all reaction occurs by OH radical addition. As we have shown previously for the reactions of linear 1-alkenes (Matsuanga et al., 2009), measured yields of hydroxynitrates can be combined with yields of carbonyl decomposition products and results of structure-reactivity calculations to develop a complete reaction mechanism, which can then be used with gas-particle partitioning theory to model SOA formation. A quantitative reaction mechanism and SOA model developed for reactions of 2-methyl-1-alkenes will be the topic of a future publication.

4.6 Reference

Andreae, M. O. and Crutzen, P. J., 1997. Atmospheric Aerosols: Biogeochemical Sources and Role in Atmospheric Chemistry. *Science, 276,* 1052-1058.

Arey, J., Aschmann, S. M., Kwok, E. S. C., Atkinson, R., 2001. Alkyl Nitrate, Hydorxyalkyl Nitrate, and Hydroxycarbonyl Formation from the NO_x-Air Photooxidations of C_5-C_8 *n*-Alkanes. *J. Phys. Chem. A, 105,* 1020-1027.

Atkinson, R., 2007. Rate Constants for the Atmospheric Reactions of Alkoxy Radicals: An Updated Estimation Method. *Atmos. Environ.*, *41,* 8468-8485.

Atkinson R. and Arey J., 2003a. Atmospheric Degradation of Volatile Organic Compounds. *Chem. Rev.*, *103,* 4605-4638.

Atkinson, R. and Arey, J., 2003b. Gas-Phase Tropospheric Chemistry of Biogenic Volatile Organic Compounds: A Review. *Atmos. Environ.*, *37,* Suppl. 2, S197-S219.

Atkinson, R., Carter, W. P. L., Winer, A. M., Pitts, J. N., Jr., 1981. An Experimental Protocol for the Determination of OH Radical Rate Constants with Organics Using Methyl Nitrite Photolysis as an OH Radical Source. *Air Pollut. Control Assoc.*, *31,* 1090-1092.

Bil, A. and Latajka, Z., 2005. Hydroperoxy Radical as Hydrogen Bond Donor: NH_3-HOO Complex – Ab Initio and Topological Study. *Chem. Phys. Lett.*, *406,* 366-370.

Calvert, J. G., Atkinson, R., Kerr, J. A., Madronich, S., Moortgat, G. K., Wallington, T. J., Yarwood, G., 2000. The Mechanisms of Atmospheric Oxidation of the Alkenes. Oxford University Press, New York.

Cassanelli, P., Fox, D. J., Cox, R. A., 2007. Temperature Dependence of Pentyl Nitrate Formation from the Reaction of Pentyl Peroxy Radicals with NO. *Phys. Chem. Chem. Phys.*, *9,* 4332-4337.

Chattopadhyay, S. and Ziemann, P. J., 2005. Vapor Pressures of Substituted and Unsubstituted Monocarboxylic and Dicarboxylic Acids Measured Using an Improved Thermal Desorption Particle Beam Mass Spectrometry Method. *Aerosol Sci. Technol., 39*, 1085-1100.

Clark, J., English, A. M., Hansen, J. C., Francisco, J. S., 2008. Computational Study on the Existence of Organic Peroxy Radical-water Complexes ($RO_2 \cdot H_2O$). *J. Phys. Chem. A, 112*, 1587-1595.

Crable, G. F., and Coggeshall, N. D., 1958. Application of Total Ionization Principles to Mass Spectrometric Analysis. *Anal. Chem., 30*, 310-313.

Cvetanovic, R. J., 1976. unpublished report presented at the 12th International Symposium on Free Radicals, Laguna Beach, CA. Cited in: Calvert, J.G., Atkinson, R., Kerr, J.A., Madronich, S., Moortgat, G.K., Wallington, T.J., Yarwood, G., 2000. The Mechanisms of Atmospheric Oxidation of the Alkenes. Oxford University Press, New York.

De Gouw, J. and Jimenez, J. L., 2009. Organic Aerosols in the Earth's Atmosphere. *Environ. Sci. Technol.*, in press.

Docherty, K. S. and Ziemann, P. J., 2006. Reaction of Oleic Acid Particles with NO_3 Radicals: Products, Mechanism, and Implications for Radical-Initiated Organic Aerosol Oxidation. *J. Phys. Chem. A, 110*, 3567-3577.

Docherty, K. S., Wu, W.; Lim, Y. B., Ziemann, P. J., 2005. Contributions of Organic Peroxides to Secondary Aerosol Formed from Reactions of Monoterpenes with O_3. *Environ. Sci. Technol., 39*, 4049-4059.

Englert, N., 2004. Fine Particles and Human Health – a Review of Epidemiological Studies. *Toxicol. Lett., 149*, 235-242.

Finlayson-Pitts, B. J. and Pitts, J. N., Jr., 2000. Chemistry of the Upper and Lower Atmosphere. Academic Press, San Diego.

Gong, H., Matsunaga, A., Ziemann, P. J., 2005. Products and Mechanism of Secondary Organic Aerosol Formation from Reactions of Linear Alkenes with NO_3 Radicals. *J. Phys. Chem. A, 109,* 4312-4324.

Guenther, A., Hewitt, C. N., Erickson, D., Fall, R., Geron, C., Graedel, T., Harley, P., Klinger, L., Lerdau, M., McKay, W. A., Pierce, T., Scholes, B., Steinbrecher, R., Tallamraju, R., Taylor, J., Zimmermann, P., 1995. A Global Model of Natural Volatile Organic Compound Emissions. *J. Geophys. Res., 100,* 8873-8892.

Johnson, D., Jenkin, M. E., Wirtz, K., Martin-Reviejo, M., 2004. Simulating the Formation of Secondary Organic Aerosol from the Photooxidation of Toluene. *Environ. Chem., 4,* 150-165.

Kanakidou, M. et al. (21 co-authors), 2005. Organic Aerosol and Global Climate Modelling: A Review. *Atmos. Chem. Phys., 5,* 1053-1123.

Kroll, J. H., Seinfeld, J. H., 2008. Chemistry of Secondary Organic Aerosol: Formation and Evolution of Low-Volatility Organics in the Atmosphere. *Atmos. Environ., 42,* 3593-3624.

Kwok, E. S. C. and Atkinson. R., 1995. Estimation of Hydroxyl Radical Reaction Rate Constants for Gas-Phase Organic Compounds Using a Structure-Reactivity Relationship: An Update. *Atmos. Environ., 29,* 1685-1695.

Lim, Y. B. and Ziemann, P. J., 2009. Chemistry of Secondary Organic Aerosol Formation from OH Radical-Initiated Reactions of Linear, Branched, and Cyclic Alkanes in the Presence of NO_x. *Aerosol Sci. Technol., 43,* 604-619.

Liu, P., Ziemann, P. J., Kittelson, D. B., McMurry, P. H., 1995a. Generating Particle Beams of Controlled Dimensions and Divergence .1. Theory of Particle Motion in Aerodynamic Lenses and Nozzle Expansions. *Aerosol Sci. Technol., 22,* 293–313.

Liu, P., Ziemann, P. J., Kittelson, D. B., McMurry, P. H., 1995b. Generating Particle Beams of Controlled Dimensions and Divergence .2. Experimental Evaluation of Particle

Motion in Aerodynamic Lenses and Nozzle Expansions. *Aerosol Sci. Technol.*, *22,* 314–324.

Matsunaga, A. and Ziemann, P. J., 2009. Yields of β-hydroxynitrates and Dihydroxynitrates in Aerosol Formed from the OH Radical-Initiated Reactions of Linear Alkenes in the Presence of NO_x. *J. Phys. Chem. A, 113*, 599-606.

Matsunaga, A., Docherty, K. S., Lim, Y. B., Ziemann, P. J., 2009. Composition and Yields of Secondary Organic Aerosol Formed from OH Radical-Initiated Reactions of Linear Alkenes in the Presence of NO_x: Modeling and Measurements. *Atmos. Environ., 43*, 1349-1357.

McLafferty F. W. and Tureček, F., 1993. Interpretation of Mass Spectra. 4th Ed. University Science Books, Sausalito.

Nishino, N., Arey, J., Atkinson, R., 2009. Rate Constants for the Gas-Phase Reactions of OH Radicals with a Series of C_6-C_{14} Alkenes at 299 ± 2 K. *J. Phys. Chem. A, 113*, 852-857.

Nozière, B., Barnes, I., Becker, K.-H., 1999. Product Study and Mechanisms of the Reactions of α-Pinene and of Pinonaldehyde with OH Radicals. *J. Geophys. Res.*, *104*, 23645-23656.

O'Brien, J. M., Czuba, E., Hastie, D. R., Francisco, J. S., Shepson, P. B., 1998. Determination of the Hydroxy Nitrate Yields from the Reaction of C_2-C_6 Alkenes with OH in the Presence of NO. *J. Phys. Chem. A, 102*, 8903-8908.

Pankow, J. F., 1994. An Absorption Model of the Gas/Aerosol Partitioning Involved in the Formation of Secondary Organic Aerosol. *Atmos. Environ.*, *28*, 189-193.

Pavia, D. L., Lampman, G. M., Kriz, G. S., 2001. Introduction to Spectroscopy. 3rd ed., Brooks/Cole Thomson Learning, United States of America.

Peeters, J., Boullart, W., Pultau, V., Vandeberk, S., Vereecken, L., 2007. Structure-Activity Relationship for the Addition of OH to (Poly)alkenes: Site-Specific and Total Rate Constants. *J. Phys. Chem. A.*, *111*, 1618-1631.

Tobias, H. J. and Ziemann, P. J., 1999. Compound Identification in Organic Aerosols Using Temperature-Programmed Thermal Desorption Particle Beam Mass Spectrometry. *Anal. Chem.*, *71*, 3428–3435.

Tobias, H. J., Kooiman, P. M., Docherty, K. S., Ziemann, P. J., 2000. Real-Time Chemical Analysis of Organic Aerosols Using a Thermal Desorption Particle Beam Mass Spectrometer. *Aerosol Sci. Technol.*, *33*, 170-190.

Tuazon, E. C., Aschmann, S. M., Arey, J., Atkinson, R., 1998. Products of the Gas-Phase Reactions of a Series of Methyl-Substituted Ethenes with the OH Radical. *Environ. Sci. Technol.*, *32*, 2106-2112.

Wang, S. C. and Flagan, R. C., 1990. Scanning Electrical Mobility Spectrometer. *Aerosol Sci. Technol.*, *13*, 230-240.

Zhang, Q. et al. (35 co-authors), 2007. Ubiquity and Dominance of Oxygenated Species in Organic Aerosols in Anthrogenically-Influenced Northern Hemisphere Midlatitudes. *Geophys. Res. Lett.*, *34*, L13801, doi:10.1029/2007GL029979.

Chapter 5

Development of a Chemically-Speciated Model of Secondary Organic Aerosol Formation from OH Radical-Initiated Reactions of 2-Methyl-1-Alkenes in the Presence of NO_x

5.1 Abstract

The chemistry of secondary organic aerosol (SOA) formation from OH radical-initiated reactions of 2-methyl-1-alkenes in the presence of NO_x was investigated in an environmental chamber. SOA was composed primarily of β-hydroxynitrates, dihydroxynitrates, trihydroxynitrates, dihydroxycarbonyls, trihydroxycarbonyls, cyclic hemiacetals, and dihydrofurans formed by addition of OH radicals to the C=C double bond, with H-atom abstraction products being much less abundant. The simultaneous observation of dihydroxycarbonyls, trihydroxycarbonyls, cyclic hemiacetals, and dihydrofurans in SOA indicates that these compounds coexist in the particle phase, possibly in equilibrium. No dihydroxycarbonyl dimers were observed, unlike SOA formed from similar reactions of 1-alkenes. This can be explained by electron donation by the 2-methyl group, which stabilizes the zwitterionic resonance form of the carbonyl

group and thereby reduces the tendency of the β-hydroxycarbonyls to form hemiacetal dimers. A quantitative chemical reaction mechanism was developed using branching ratios calculated from measured product yields and kinetic data from the literature, and was combined with vapor pressures estimated from measurements of gas-particle particle partitioning and structure-activity relationships to create a model for calculating SOA composition and yield. Calculated SOA yields were significantly higher than measured values, indicating that the original mechanism was missing important alkoxy radical decomposition reactions that lead to the formation of volatile products that do not form SOA. It is therefore proposed that trihydroxy and tetrahydroxy α-hydroxyalkyl radical intermediates react to a large extent with O_2 and NO to form the corresponding alkoxy radicals, which then decompose, resulting in significantly less SOA than would otherwise be formed. These reactions need to be incorporated into the mechanism along with more detailed representations of H-atom abstraction and secondary reactions to create a more complete model for calculating SOA composition and yield.

5.2 Introduction

Modeling the composition and mass concentration of atmospheric secondary organic aerosol (SOA) is important for predicting the impacts of particles on human health (Englert, 2004), visibility (Finlayson-Pitts and Pitts, 2000), and global climate (Kanakidou et al., 2005). The major requirements for SOA modeling are data on emissions of volatile organic compounds (VOCs), primary organic aerosol particles, and NO_x, meteorology, and process models for describing transport and the atmospheric chemistry of VOCs and aerosols. Current models tend to underestimate atmospheric SOA mass concentrations by up to an order of magnitude or more (Johnson et al., 2006; Henze et al., 2008; de Gouw et al., 2005; Heald et al., 2006; Volkamer et al., 2006), for reasons that include inadequate information on the chemistry of VOCs and aerosols. To simplify SOA modeling, VOCs are generally lumped into a few classes based on compound reactivity and source, such as terpenes (Kanakidou et al., 2005), but this approach may lose important sources of SOA. For example, we recently reported large differences in SOA yields from reactions of linear, branched, and cyclic alkanes with the same carbon number (Lim and Ziemann 2009a), indicating that these compounds would best be treated separately in a model. Other sources of uncertainty are the vapor pressures used to

model partitioning of compounds between the gas and particle phases, particle-phase activity coefficients, and the possible role of particle-phase oligomer-forming reactions.

Recently, we developed a quantitative mechanism for OH radical-initiated reactions of 1-alkenes in the presence of NO_x and incorporated this into an SOA model (Matsunaga et al., 2009). The model predicted well the yields of SOA formed from reactions of large 1-alkenes, for which accurate gas-particle partitioning calculations were not important because the major products had sufficiently low vapor pressures to partition almost entirely to the particle phase. As the carbon number decreased and products became more volatile, however, uncertainties in gas-particle partitioning due to the effects of particle-phase reactions on product vapor pressures led to significant discrepancies between measured and predicted yields. In the study presented here, a quantitative mechanism was developed for similar reactions of C_9-C_{15} 2-methyl-1-alkenes to investigate the effects on SOA formation of adding a methyl group to the C=C double bond of the parent alkene. Such a structure is frequently observed in biogenic compounds, such as isoprene and α-pinene. Branching ratios for reaction pathways were calculated using the measured yields of β-hydroxynitrates, dihydroxynitrates, and trihydroxynitrates presented in Chapter 4 and also measured yields of 2-ketones, and

vapor pressures were estimated using measurements of gas-particle partitioning of hydroxynitrates and data from previous studies. The model results were compared with measured SOA yields, providing additional information about the reaction mechamism that can be used to improve the model.

5.3 Experimental Section

Chemicals. The following chemicals, with purities (when available) and suppliers, were used: 2-methyl-1-nonene (97%), 2-methyl-1-undecene (97%), 2-octanone (98%), 2-nonanone (99+%), and 1-pentadecene (98%) [Sigma-Aldrich], 2-methyl-1-octene (97%), 2-methyl-1-tridecene (99%), and 2-methyl-1-tetradecene (97%) [ChemSampCo], 2-methyl-1-decene (97%) and 2-methyl-1-dodecene (>97%) [Rieke Metals], dioctyl sebacate (≥97%) [Fluka], and NO [Matheson Tri Gas]. All chemicals were used without further purification. Methyl nitrite was synthesized (Taylor et al., 1980) and O_3 was generated using a Welsbach T-408 O_3 generator.

Environmental Chamber Method. The OH radical-initiated reactions of C_9-C_{15} 2-methyl-1-alkenes in the presence of NO_x were conducted in a 5900 L PTFE environmental chamber that is equipped with blacklights covering two walls. The

chamber was filled with clean, dry air (<5 ppbv hydrocarbons, <1% RH, <50 ppbv NO_x, <10 ppbv O_3) from an Aadco clean air system and experiments were performed at room temperature (~25 °C) and atmospheric pressure. 2-methyl-1-alkenes, methyl nitrite, and NO were added to the chamber by flushing measured amounts from a glass bulb using clean air or N_2, and dioctyl sebacate (DOS) seed particles were generated by evaporation-condensation and flushed into the chamber using N_2. The NO was added to suppress the formation of O_3 and NO_3 radicals. A Teflon-coated fan was run for ~1 min to mix the chamber contents. Initial concentrations of 2-methyl-1-alkenes, methyl nitrite, NO, and DOS seed particles were approximately 1, 5, and 5 ppmv and 200 μg m^{-3}. Reactions of 2-methyl-1-tetradecene were also performed in the presence of 20 ppmv of NH_3 added in the same way as the other gases.

The reaction was initiated by turning on the blacklights to generate OH radicals by methyl nitrite photolysis (Atkinson et al., 1981). After 6 min the blacklights were turned off, immediately terminating OH radical formation. In a typical experiment, SOA formation was observed within 1 min of turning on the blacklights, 40-50 % of the alkene reacted, and the average OH radical concentration was ~3 x 10^7 cm^{-3}, estimated from the amount of alkene reacted and OH radical rate constant (Nishino et al., 2009).

Concentrations of O_3, NO, and NO_x were measured using a Dasibi model 1003-AH O_3 monitor and a Thermo Environmental Instruments Inc. 42C NO-NO_2-NO_x analyzer.

Particle Mass Spectrometric Analysis. A thermal desorption particle beam mass spectrometer (TDPBMS) was used to analyze particle composition in real-time (Tobias et al., 2000) and by temperature-programmed thermal desorption (TPTD) (Tobias and Ziemann, 1999). Particles are sampled from the chamber into the TDPBMS using an aerodynamic lens (Liu et al., 1995a; Liu et al., 1995b) and the resulting particle beam impacts in a V-shaped notch at the tip of a copper vaporizer rod coated with nonstick polymer (Chattopadhyay and Ziemann, 2005). For real-time analysis the vaporizer temperature was 160°C, hot enough for near-instantaneous particle evaporation. For TPTD analysis the vaporizer was cooled to -40°C, particles were collected for 30 min, and the vaporizer was allowed to warm to 5°C before being heated to 200°C with a computer controlled linear temperature ramp of 2°C min^{-1}. In this case components were separated according to volatility. Evaporated compounds diffuse into an ABB Extrel MEXM 500 quadrupole mass spectrometer where they are ionized by 70 eV electrons and the ions are mass analyzed. The mass spectrometer was scanned from *m/z* 40-500 (*m/z* 10-500 for the NH_3 experiment) in 30 sec.

SOA Yield Measurements. SOA yields [SOA formed (μg m^{-3})/alkene reacted (μg m^{-3})] were calculated using aerosol volume concentrations measured with a scanning mobility particle sizer (SMPS), measured SOA density, and the mass of reacted alkene measured by gas chromatography with flame ionization detection (GC-FID). Particle size distributions were measured every 2 min during a reaction using an SMPS (Wang and Flagan, 1990) that consists of a ^{210}Po bipolar charger, a long differential mobility analyzer similar design to the TSI model 3934, a TSI Model 3010 Condensation Particle Counter, and a scanning/inversion program developed by the McMurry group at the University of Minnesota for use with Labview software. Particles were assumed to have a density of 1.1 g cm^{-3}, the density of a dried filter extract of SOA formed from the reaction of 2-methyl-1-tridecene in the absence of seed aerosol. The density was measured using a microliter syringe and a balance. Alkene concentrations were measured before and after reaction by collecting 100 cm^{-3} air samples on TenaxTA solid adsorbent, desorbing at 250°C in the GC inlet, and analyzing by GC-FID (Docherty et al., 2005). The GC-FID signals of the 2-methyl-1-alkenes prior to reaction were all within ± 5% of those expected for initial chamber concentrations of 1 ppmv, as determined from calibration curves created by analyzing solutions of the authentic compounds. This result and the

observation that GC-FID signals were within ± 5% for replicate samples taken at 30 min intervals both before and after reaction indicated that no wall loss corrections were necessary.

Ketone Yield Measurements. Concentrations of 2-octanone and 2-nonanone formed from the reactions of 2-methyl-1-octene and 2-methyl-1-nonene were measured by collecting 500 cm^{-3} air samples on TenaxTA solid adsorbent and analyzing by GC-FID. Ketones were identified by retention times and concentrations were calculated using GC-FID calibration curves created by analyzing solutions of the authentic compounds. These values were then used to calculate molar yields (moles ketone formed/moles alkene reacted).

5.4 Development of a Chemical Mechanism and Model of SOA Formation

Reaction Mechanism. Figure 5.1 shows the mechanism of OH radical-initiated reactions of 2-methyl-1-alkenes in the presence of NO_x, where R represents an alkyl group. The mechanism was developed based on previous gas (Atkinson and Arey, 2003a) and SOA (Matsunaga et al., 2009) studies. The reaction is initiated either by addition of an OH radical to the C=C double bond or by abstraction of an H atom from the carbon

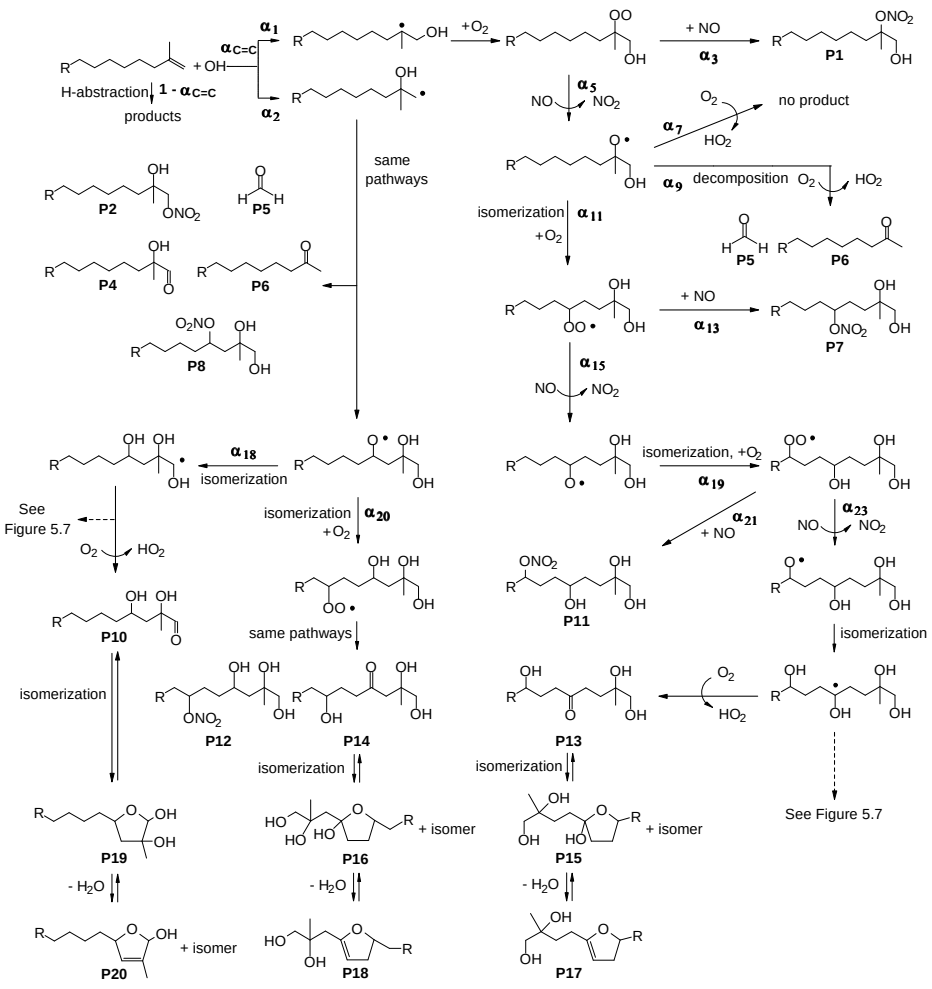

Figure 5.1 Mechanism of the OH radical-initiated reaction of 2-methyl-1-alkenes in the presence of NO_x.

chain, forming a β-hydroxyalkyl radical or alkyl radical, respectively. For the most part, the subsequent reactions of these two radicals are similar, with products formed from β-hydroxyalkyl radicals having an additional hydroxy group. Both pathways can contribute to SOA formation. In this section we discuss in detail the OH radical addition pathways and products. The reader is referred to studies of OH radical-initiated reactions of alkanes (Atkinson and Arey, 2003b; Lim and Ziemann, 2009b) for details on H-atom abstraction reactions, since alkanes react exclusively by that pathway. The major H-atom abstraction products thought to contribute to SOA formation from reactions of 2-methyl-1-alkenes are discussed in a section below.

Addition of an OH radical to the C=C double bond occurs at either carbon atom, forming a pair of β-hydroxyalkyl radical isomers that then react with O_2 to form β-hydroxyperoxy radicals. β-hydroxyperoxy radicals react with NO to form β-hydroxynitrates [P1, P2] or β-hydroxyalkoxy radicals. β-hydroxyalkoxy radicals react with O_2 to form α-hydroxcarbonyls [P4], decompose and react with O_2 to form formaldehyde [P5] and a ketone [P6], or isomerize and react with O_2 to form dihydroxyperoxy radicals. In reactions of 2-methyl-1-alkenes, no α-hydroxyketone [P3] is formed because of the absence of an H atom on the α-carbon of a tertiary β-

hydroxyalkoxy radical. Dihydroxyperoxy radicals react with NO to form dihydroxynitrates or dihydroxyalkoxy radicals, with the latter then reacting by one of two possible 1, 5 H-atom shift isomerization pathways. The predominant pathway is H-atom abstraction from the carbon atom on which the OH group is located (Atkinson, 2007), but when no such H atom is present one is instead abstracted from a CH_2 group further along the carbon chain. The resulting products (following reaction with O_2) are dihydroxyaldehydes [P10] and trihydroxyperoxy radicals, with no P9 isomer formed corresponding to P10. The trihydroxyperoxy radicals react with NO to form trihydroxynitrates [P11, P12] or trihydroxyalkoxy radicals, and the latter then isomerize and react with O_2 to form trihydroxyketones [P13, P14]. Dihydroxyaldehydes [P10] and trihydroxyketones [P13, P14] present in particles or on chamber walls can isomerize to cyclic hemiacetals [P19, P15, P16, and isomers], which can then dehydrate to form dihydrofurans [P20, P17, P18, and isomers] (Atkinson et al., 2008; Lim and Ziemann, 2009b). The pathways indicated by dashed arrows in Figure 5.1 are discussed later; they are less well established but their occurrence is indicated by discrepancies between SOA yield calculations and measurements.

Branching Ratios and Product Yields. In Figure 5.1, α_i is the branching ratio for the reaction of a specie by pathway *i*, defined as $\alpha_i = r_i/\Sigma r_i$, where r_i is the reaction rate for pathway *i* and the sum is over all pathways for the specie and equal to 1. The branching ratios for pathways originating from 1-hydroxyalkyl and 2-hydroxyalkyl radicals are labeled by odd and even numbers, respectively. The values used in the model are presented in Table 5.1, and the calculation method is explained in Appendix D. The branching ratios are consistent with the measured yields of β-hydroxynitrates, dihydroxynitrates, and trihydroxynitrates reported in Chapter 4, ketone yields of 0.453 ± 0.024 measured here for 2-octanone and 2-nonanone formed from the reactions of 2-methyl-1-octene and 2-methyl-1-nonene, the rate constants for OH radical-initiated reactions of 2-methyl-1-alkenes (Kwok and Atkinson, 1995; Nishino et al., 2009), and the rate constants for β-hydroxyalkoxy radical reactions (Atkinson, 2007).

Molar yields of the products normalized for OH radical addition to the C=C double bond [(moles of product formed/moles of alkene reacted)/$\alpha_{C=C}$] and for H-atom abstraction [(moles of product formed/moles of alkene reacted)/(1 – $\alpha_{C=C}$)] are given in Table 5.2. These molar yields are equal to the product of the branching ratios along the pathway by which each compound is formed.

Table 5.1 Branching Ratios used to Model SOA Formation from OH Radical-Initiated Reactions of 2-Methyl-1-Alkenes in the Presence of NO_x.

branching ratio	
$\alpha_{C=C}$[a]	$\alpha_{C=C}$[a]
α_1	0.81 x $\alpha_{C=C}$[a]
α_2	0.19 x $\alpha_{C=C}$[a]
α_3	0.25
α_4	0.12
α_5	0.75
α_6	0.88
α_7, α_8	0.00
α_9	0.62
α_{10}	0.46
α_{11}	0.38
α_{12}	0.54
α_{13}, α_{14}	0.17
α_{15}, α_{16}	0.83
α_{17}	0.00
α_{18}	0.76
α_{19}	1.00
α_{20}	0.24
α_{21}, α_{22}	0.20
α_{23}, α_{24}	0.80

[a]Values of $\alpha_{C=C}$ were calculated as described in Appendix D.

Table 5.2 Normalized Molar Yields of Products used to Model SOA Formation from OH Radical Addition and H-atom Abstraction Reactions of 2-Methyl-1-Alkenes in the Presence of NO_x.

product	normalized molar yield[a]	product	normalized molar yield[a]
OH radical addition			
β-hydroxynitrates		dihydroxycarbonyls	
P1	0.203 [0.202][b]	P9	0.000
P2	0.023 [0.023][b]	P10	0.057
P1 + P2	0.226 [0.225][b]	P9 + P10	0.057
β-hydroxycarbonyls		trihydroxynitrates	
P3	0.000	P11	0.038
P4	0.000	P12	0.004
carbonyls		P11+P12	0.042 [0.042][b]
P5	0.454	trihydroxycarbonyls	
P6	0.454 [0.453][c]	P13	0.153
dihydroxynitrates		P14	0.014
P7	0.039	P13+P14	0.167
P8	0.015		
P7 + P8	0.054 [0.055][b]		
H-atom abstraction			
1,4-hydroxynitrates	0.1		

[a]Normalized molar yields were calculated as (moles of product/moles of alkene reacted)/$\alpha_{C=C}$ for OH radical addition and as (moles of product/moles of alkene reacted)/(1 – $\alpha_{C=C}$) for H-atom abstraction. Values of $\alpha_{C=C}$ were calculated as described in Appendix D.

[b]From Chapter 4.

[c]From this study.

H-atom Abstraction and Secondary Reactions. First-generation products formed through H-atom abstraction pathways and second-generation products formed by reactions of OH radicals with all first-generation products are also potential sources of SOA. Because, however, only ~10-20% of the reactions of 2-methyl-1-alkenes with OH radicals occurs by H-atom abstraction and the reaction mechanisms are complex (Lim and Ziemann, 2009b), these products were not included explicitly in the mechanism shown in Figure 5.1 or in the SOA model. Instead, they were incorporated using a simplified approach that attempts to estimate upper limits to the possible contributions of these products to SOA mass (Matsunaga et al., 2009). The major first-generation products of H-atom abstraction reactions are expected to be the same as those formed from OH radical-initiated reactions of *n*-alkanes: alkyl nitrates, 1,4-hydroxycarbonyls, and 1,4-hydroxynitrates, but with a C=C double bond. Alkyl nitrates and 1,4-hydroxycarbonyls are more volatile than 1,4-hydroxynitrates, so in TPTD analysis they will desorb at lower temperatures than 1,4-hydroxynitrates. In thermal desorption profiles shown in Chapter 4, there is no evidence of alkyl nitrates or 1,4-hydroxycarbonyls in particles, probably because alkyl nitrates are too volatile and 1,4-hydroxycarbonyls isomerize to cyclic hemiacetals that can dehydrate to form dihydrofurans that then evaporate (Matsunaga et

al., 2009; Lim and Ziemann, 2009b). These cyclization-dehydration reactions can lead to sharply increasing and then decreasing signals in time profiles of ions that are characteristic of cyclic hemiacetals (Lim and Ziemann, 2009b). This was not observed here, indicating that cyclic hemiacetals formed through H-atom abstraction pathways do not contribute significantly to SOA formation. Nonetheless, in the future we intend to incorporate these heterogenous reactions into the mechanism explicitly by using an approach developed recently for reactions of alkanes (Lim and Ziemann, 2009c). Here, it was assumed that 1,4-hydroxynitrates were the only first-generation H-atom abstraction product that contributed to SOA formation and that their H-atom abstraction-normalized yield was 0.1 (Lim and Ziemann, 2005; Reisen et al., 2005). The contribution of secondary reactions to SOA formation was estimated using a kinetic model written in FACSIMILE (Matsunaga et al., 2009). The rate constants for OH radical addition and H-atom abstraction for alkenes and first-generation products were calculated using equations from Nishino et al. (2009) and Kwok and Atkinson (1995). The yields of products formed by OH radical addition followed by H-atom abstraction were calculated by assuming that all first-generation OH radical addition products (saturated β-hydroxynitrates, dihydroxynitrates, trihydroxynitrates, dihydroxycarbonyls, and

trihydroxycarbonyls) other than carbonyls were in gas-particle partitioning equilibrium. For simplicity, it was assumed that these compounds have the same vapor pressures as β-hydroxynitrates. Since β-hydroxynitrates have the highest vapor pressures among the products listed above, values calculated using this assumption should overestimate the contributions from this pathway to SOA formation. The carbonyls [P5, P6] were excluded because they generally react with OH radicals to form even smaller carbonyls (Atkinson and Arey, 2003a). The yields of products from H-atom abstraction followed by OH radical addition were calculated by assuming that all first-generation H-atom abstraction products (unsaturated alkyl nitrates, 1,4-hydroxycarbonyls, and 1,4-hydroxynitrates) were in the gas phase and so available for OH radical addition reactions. Since 1,4-hydroxynitrates undergo gas-particle partitioning, these calculations should overestimate the contributions of these pathways to SOA formation.

Gas-Particle Partitioning and SOA Yield Calculations. Gas-particle partitioning of each product was calculated using the theory introduced by Pankow (1994). The theory assumes that particulate organic matter is a single, liquid organic phase, and should be a valid here because dried SOA filter extracts were clear liquids. An equilibrium partitioning coefficient was calculated for each compound from the mean

molecular weight of particulate organic matter, the activity coefficient of the compound in the organic phase, and the liquid-phase vapor pressure of the compound. The mean molecular weight of particulate organic material was assumed to be that of β-hydroxynitrates, activity coefficients were assumed to be unity (Seinfeld et al., 2001), and vapor pressures were estimated using the equations shown in Table 5.3, which were obtained using the approaches described below.

To estimate vapor pressures of β-hydroxynitrates, dihydroxynitrates, and trihydroxynitrates, the fractions of each compound in the particle phase [moles in particle phase/(moles in particle phase + gas phase)] were calculated as a function of carbon number as the ratio of the measured yield to the yield in the plateau region, where the compounds are expected to be entirely in the particle phase. The results are presented in Figure 5.2. The measured yields used in the calculations were presented in Chapter 4, with the exception of the C_9 trihydroxynitrate yield. This value could not be measured because the HPLC peak overlapped with the solvent peak, and so was estimated here from the aerosol yield for the reaction assuming that products other than trihydroxynitrates were formed in negligible amounts or were too volatile to partition into

Table 5.3 Parameters used to Calculate Compound Vapor Pressures from the Equation $\log P\ (Pa) = A - (0.4537 \times C_n)$.

Compounds	A
1-hydroxy-2-nitrooxyalkanes	3.979
1-nitrooxy-2-hydroxyalkanes	4.511
dihydroxynitrates	2.979
trihydroxynitrates	1.979
dihydroxycarbonyls	4.034
trihydroxycarbonyls	3.034
1,4-hydroxynitrates	4.698

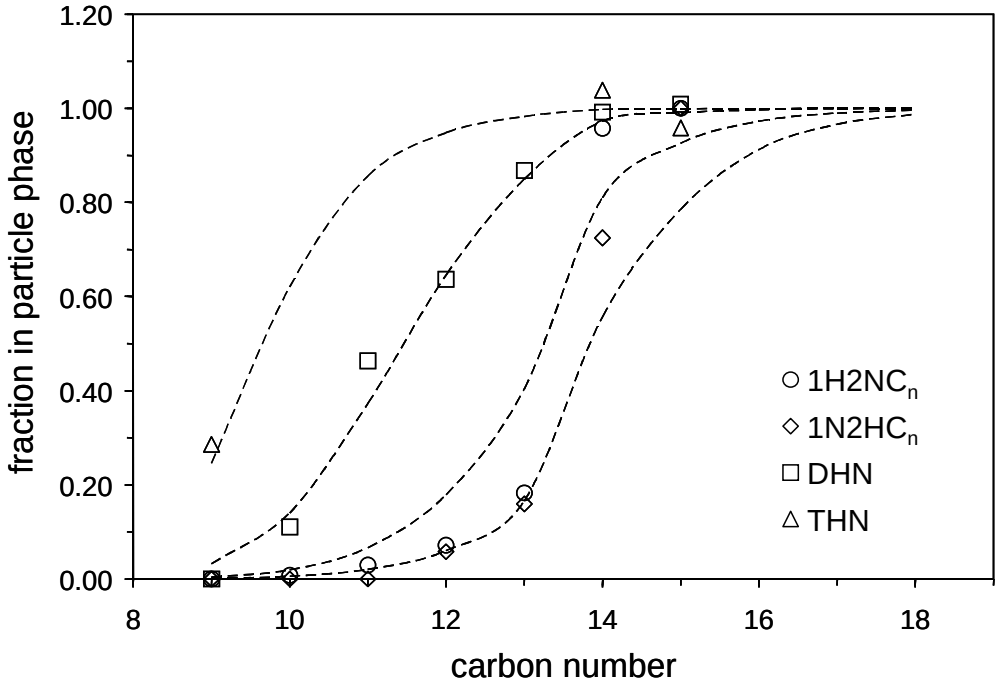

Figure 5.2 Fractions of β-hydroxynitrates [1-hydroxy-2-nitrooxyalkanes ($1H2NC_n$) and 2-nitrooxy-1-hydroxyalkanes ($1N2HC_n$)], dihydroxynitrates (DHN), and trihydroxynitrates (THN) formed from the OH radical-initiated reactions of 2-methyl-1-alkenes in the presence of NO_x, measured in the particle phase. The dashed curves were calculated using gas-particle partitioning theory with compound vapor pressures adjusted to achieve good visual fits to the data.

the particles. The dashed curves in Figure 5.2 are fits of the data to gas-particle partitioning theory (Pankow, 1994). For these calculations, the mean molecular weights of particulate organic compounds were assumed to be the same as those of β-hydroxynitrates, activity coefficients were assumed to be unity (Seinfeld et al., 2001), organic aerosol mass concentrations were measured, and vapor pressures were adjusted to achieve visually good fits to the data. The vapor pressures were assumed to obey an equation of the form $\log P\ (Pa) = A - (0.4537 \times C_n)$, where the value of 0.4537 (equivalent to a decrease in vapor pressure of a factor of 2.85 per carbon number) was calculated using a linear least-squares fit to vapor pressures measured for 1,2-dialkyl nitrates using gas chromatography (Fisher and Ballschmiter, 1998). Fitting data for a class of hydroxynitrates therefore involved adjusting the value of A. Vapor pressures for non-nitrates, for which yields were not measured, were estimated by group contribution methods. The vapor pressure equations are given in Table 5.3. They are similar to those presented previously for the products formed from reactions of 1-alkenes (Matsunaga et al., 2009). The vapor pressures of the two β-hydroxynitrate isomers differ by about a factor of 3, and the vapor pressures of dihydroxynitrates and trihydroxynitrates are about 10 and 100 times lower than those of the less volatile β-hydroxynitrate isomers (1-

hydroxy-2-nitrooxyalkanes) due to the addition of one and two hydroxy groups, respectively. The vapor pressures of 1,4-hydroxynitrates formed through H-atom abstraction pathways were assumed to be the same as those of the more volatile β-hydroxynitrate isomers (1-nitrooxy-2-hydroxyalkanes), because vapor pressures are higher when functional groups are located away from the ends of a molecule. Vapor pressures of dihydroxycarbonyls and trihydroxycarbonyls were calculated by assuming that the vapor pressures of β-diols are the same as those of the more volatile β-hydroxynitrate isomers and then reducing the vapor pressure by a factor of 3 due to the addition of a carbonyl group, and an additional factor of 10 due to the addition of a hydroxy group. The estimated vapor pressures are somewhat higher than those estimated using group contribution methods (Pankow and Asher, 2008). The estimated vapor pressures are, for the most part, also consistent with the observed trends in desorption temperatures discussed below: dihydroxycarbonyls < β-hydroxynitrates ~ 1,4-hydroxynitrates < trihydroxycarbonyls ~ dihydroxynitrates < trihydroxynitrates. The major discrepancy is dihydroxycarbonyls, which are expected to desorb at about the same temperature as β-hydroxynitrates. One should remember that interactions among

molecules in particles can affect vapor pressures in ways that are difficult to predict and are not accounted for in these calculations.

To calculate SOA yields, the total (gas + particle) mass concentration of each product was calculated by multiplying the normalized molar yield by either $\alpha_{C=C}$ or $1 - \alpha_{C=C}$ (for OH radical addition and H-atom abstraction products, respectively), and then multiplying this value by moles of alkene reacted x molecular weight of product. The fraction of each product in the particle phase was calculated by multiplying the equilibrium partitioning coefficient by the concentration of organic particulate matter, equal here to the sum of the mass concentrations of DOS seed particles and SOA. These fractions were then multiplied by the total mass concentration of each product to obtain the mass concentration of each product in the particle phase, which were then summed and divided by the mass of reacted alkene to obtain the SOA yield. The calculations were carried out iteratively using the procedure of Colville and Griffin (2004).

5.5 Results and Discussion

SOA Product Identification. The real-time mass spectrum of SOA formed from the reaction of 2-methyl-1-tetradecene is shown in Figure 5.3A, and thermal desorption

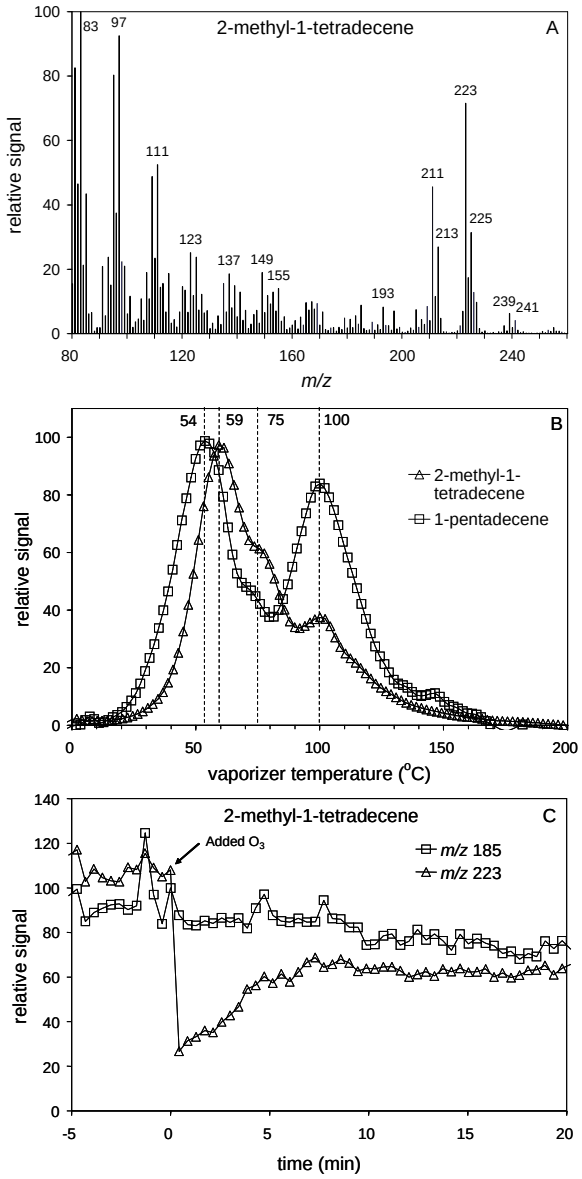

Figure 5.3 Mass spectral analyses of SOA formed from the OH radical-initiated reactions of 2-methyl-1-tetradecene or 1-pentadecene in the presence of NO_x. (A) Real-time TDPBMS mass spectra, (B) total ion (*m/z* 50-500) thermal desorption profiles, and (C) real-time TDPBMS signals of characteristic ion of dihydrofurans (*m/z* 223) after adding O_3 to the chamber containing SOA. Thermal desorption profiles were smoothed and normalized to peak values, and signals in (C) were normalized to values at 0 min.

profiles of total ion signal of SOA formed from reactions of 2-methyl-1-tetradecene and 1-pentadecene are shown in Figure 5.3B. The total ion signal is proportional to organic mass (Crable and Coggeshall, 1958), and since compounds with lower vapor pressures desorb at higher temperatures, the profiles in Figure 5.3B represent distributions of SOA mass with respect to volatility. Three peaks or shoulders are present in both profiles at approximately 50-60°C, 75°C, and 100°C, with the first two corresponding to β-hydroxynitrates and dihydroxynitrates. In Figure 5.3A, the peak at *m/z* 213, and those at *m/z* 211 and 193, are characteristic of these two compounds. The β-hydroxynitrates, dihydroxynitrates, and trihydroxynitrates formed from the reaction of 2-methyl-1-tetradecene have been identified from mass spectra after HPLC separation, desorption profiles of characteristic ions, fragmentation pathways, and ^{1}H NMR analyses as described in Chapter 4. The profile shown for the reaction of 1-pentadecene is the same that discussed previously for the reaction of 1-tetradecene (Matsunaga et al., 2009; Matsunaga and Ziemann, 2009), except that the desorption temperatures of the products are shifted to the right due to lower volatility of the products. The first two peaks are from β-hydroxynitrates and dihydroxynitrates with structures similar to P1, P2 and P7, P8, respectively.

The peaks at 100°C in Figure 5.3B are from products less volatile than dihydroxynitrates. For the 1-pentadecene reaction, this peak is assigned to cyclic hemiacetals (similar structure to P19) and dihydrofurans (similar structure to P20) formed primarily from dihydroxyketones, and dimers formed primarily from dihydroxyaldehydes (similar structure to P10), as discussed previously (Matsunaga et al., 2009). For the 2-methyl-1-tetradecene reaction, the peak at 100^{o}C also has contributions from cyclic hemiacetals and dihydrofurans. Ions present at *m/z* 241 and 223 in Figure 5.3A are characteristic of a cyclic hemiacetal [P19] and dihydrofurans [P20 and isomer] formed from the dihydroxyaldehyde [P10], and *m/z* 225 and 239 are characteristic of cyclic hemiacetals [P15, P16, and isomers] and dihydrofurans [P17, P18, and isomers] formed from trihydroxyketones [P13, P14]. The *m/z* 241, 223, and 239 ions are formed by loss of OH from the molecular ion (Matsunaga et al., 2009; Gong et al., 2005; Lim and Ziemann, 2005), whereas the *m/z* 225 ion is formed by scission of the C-C bond between the two functional groups (Matsunaga et al., 2009). The assignment of dihydrofurans to *m/z* 223 is supported by the results shown in Figure 5.3C. In this experiment, 20 ppmv of O_3 was added to the chamber 4 h after the lights were turned off. The intensity of the *m/z* 223 peak dropped immediately after O_3 addition due to reaction of O_3 with the dihydrofuran

C=C double bond. The increase in signal after the sharp drop is due to SOA formation from the reaction of 2-methyl-1-tetradecene with NO_3 radicals (Gong et al., 2005) formed from reaction of O_3 with NO_2. The intensity of the *m/z* 239 peak also decreased after O_3 was added, but it was not as obvious because of the low initial intensity and the large signal from SOA products formed from the reaction of 2-methyl-1-tetradecene with NO_3. The assignments for *m/z* 223 and 225 are also consistent with the single ion desorption profiles shown in Figure 5.4A, which both exhibit peaks at ~100°C. In reactions of 1-alkenes, it appears that cyclic hemiacetals and dihydrofurans are formed primarily from dihydroxyketones, and dimers are formed primarily from dihydroxyaldehydes (Matsunaga et al., 2009; Holt et al., 2005; Kern and Spiteller, 1996). Although dihydroxyalkehydes [P10] are formed from the reaction of 2-methyl-1-tetradecene, there is no indication of dimer formation. This could be due to a low yield of dihydroxyaldehyde, predicted to be 0.044 (Table 5.2) compared to 0.157 for those formed from reactions of 1-alkenes (Matsunaga et al., 2009). It could also be due to a smaller driving force for the formation of dimers, which are hemiacetals that may or may not undergo further cyclization reactions. The reactivity of the carbonyl group involved in hemiacetal formation can be altered by α- and β-substituents through their effect on the

the zwitterionic resonance structure of the carbonyl group (Bruckner, 2002). Electron-donating substitutents such as alkyl groups stabilize the structure, reducing reactivity, while electron-withdrawing substitutents such as hydroxy groups have the opposite effect. As a result, aldehydes are more reactive than ketones and β-hydroxyaldehydes are more reactive than aldehydes. The dihydroxyaldehydes formed from reactions of 1-alkenes and 2-methyl-1-alkenes are both β-hydroxyaldehydes, but the latter have a methyl group instead of an H atom at the β position and so are expected to have less tendency to form hemiacetals.

The desorption profiles of *m/z* 223 and *m/z* 225 exhibit multiple peaks, indicating the presence of more than one compound. In addition to coming from dihydrofurans, *m/z* 223 ions are also expected from 1,4-hydroxynitrates, formed by loss of H_2O and NO_2 from the molecular ion (Lim and Ziemann, 2009b). The peak at 57°C is most likely from 1,4-hydroxynitrates, since β-hydroxyntirates also desorb at 57°C, as described in Chapter 4, and the vapor pressures of the two compounds are expected to be similar. In addition to coming from cyclic hemiacetals, *m/z* 225 ions are also expected from the dihydroxycarbonyl [P10] and trihydroxycarbonyls [P13, P14]. The *m/z* 225 ion is formed from the dihydroxycarbonyl by losing CH_3 and H_2O from the molecular ion

(McLafferty and Tureček, 1993), and from trihydroxycarbonyls by scission of the C-C bond between the two functional groups (Matsunaga et al., 2009). Based on relative vapor pressures, the peaks at 33°C and 63-78°C are expected to be from the dihydroxycarbonyl and trihydroxycarbonyls. The dihydroxycarbonyl assignment is supported by the results shown in Figure 5.4B for the reaction of 2-methyl-1-tetradecene in the presence of 20 ppmv of NH_3. Since the formation of 1,4-hydroxynitrates is not affected by NH_3 (Lim and Ziemann, 2009b), the intensity of the 1,4-hydroxynitrate *m/z* 223 peak at 53°C in Figure 5.4B was scaled to match the intensity of the peak at 57°C in Figure 5.4A, and then all other signals in Figure 5.4B were multiplied by the same scaling factor. This allowed comparison of relative intensities in the two profiles. The intensity of the peak at 31°C in the *m/z* 225 profile in Figure 5.4B is much higher than the corresponding peak at 33^{o}C in Figure 5.4B, which is expected for the dihydroxycarbonyl since NH_3 neutralizes HNO_3 (formed from by OH + NO_2 reaction) that catalyzes its particle-phase isomerization to a cyclic hemiacetal (Lim and Ziemann, 2009b). The lower intensities of the peaks at 98-113 °C in the *m/z* 223 and 225 profiles in Figure 5.4B, compared to the corresponding peaks at 104-112°C in Figure 5.4A, is also consistent with the assignment of these peaks to cyclic hemiacetals and dihydrofurans, since the

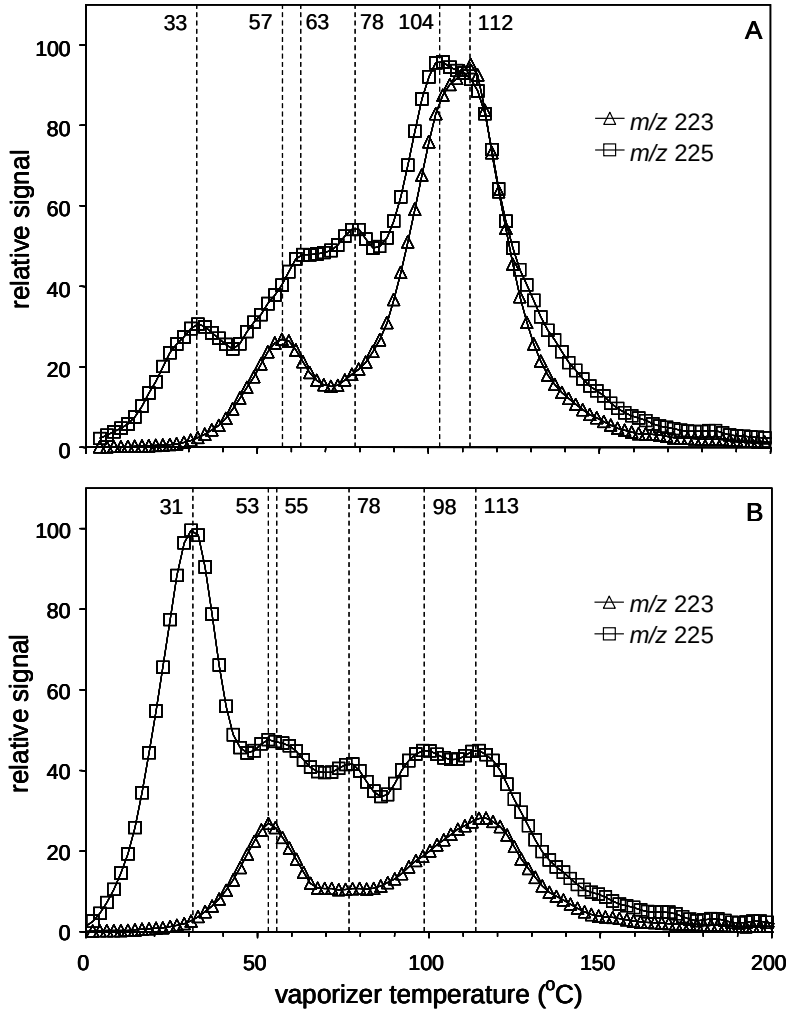

Figure 5.4 Thermal desorption profiles of ions characteristic of dihydrofurans and 1,4-hydroxynitrates (*m/z* 223) and dihydroxycarbonyl, trihydroxycarbonyls, and cyclic hemiacetals (*m/z* 225) formed from the OH radical-initiated reaction of 2-methyl-1-tetradecene in the presence of NO_x (A) without and (B) with NH_3 in the chamber. In (A), thermal desorption profiles were smoothed and normalized to the peak value. In (B), profiles were scaled by a single factor so that *m/z* 223 signal for 1,4-hydroxynitrates at 53°C peak in (B) and 57°C peak in (A) were equal.

formation of these compounds should be much slower (possibly negligible) in the presence of NH_3. Based on these results, it appears that the dihydroxycarbonyl, trihydroxycarbonyls, cyclic hemiacetals, and dihydrofurans co-exist in equilibrium in SOA formed from the 2-methyl-1-tetradecene reaction, consistent with the conclusion that the formation of cyclic hemiacetals and dihydrofurans from dihydroxycarbonyl is reversible (Matsunaga et al., 2009).

The thermal desorption profiles also provide information that can be used to better constrain the reaction mechanism and SOA model. Although the dihydroxycarbonyl is apparently responsible for the peak in the *m/z* 225 profile at 33^{o}C in Figure 5.4A, the absence of a peak or shoulder at 33^{o}C in the total ion profile in Figure 5.3B indicates that this compound contributes very little SOA mass. One possibility is that the dihydroxycarbonyls exist primarily in the form of cyclic hemiacetals and dihydrofurans, which contribute to the total ion peak at 100^{o}C. From the area under the curve, this peak is responsible for ~25% of the SOA yield of 0.465, equal to 0.116. Subtracting the contribution of 0.049 from trihydroxynitrates, which have been quantified and desorb at the same location, the contribution of cyclic hemiacetals and dihydrofurans to the SOA yield is estimated to be 0.067. This is close to the dihydroxycarbonyl yield of

0.057 predicted by the model. This result indicates that dihydroxycarbonyls exist in SOA primarily in the form of cyclic hemiacetals and dihydrofurans, which are essentially non-volatile, whereas trihydroxycarbonyls are primarily in their linear form and can partition between the gas and particle phases. This information is used in some of the model calculations presented below.

SOA Composition and Yields: Model Results and Measurements. The product SOA yields (molar yield x product molecular weight/alkene molecular weight) calculated without contributions from secondary reactions are shown in Figure 5.5 and Appendix Tables D.1 and D.2. The yields shown in Figure 5.5A were calculated assuming that all products were in gas-particle partitioning equilibrium (gpp model), and those shown in Figure 5.5B were calculated in the same way except that dihydroxycarbonyls were assumed to be in the form of non-volatile cyclic hemiacetals and dihydrofurans present entirely in the particle phase (nv model). As shown in Figure 5.5, the model results are similar at high carbon numbers; this is because dihydroxycarbonyls were entirely in the particle phase regardless of their chemical form. For the C_{15} reaction, the yields calculated with the nv model (values are essentially the same for the two models) are: β-hydroxynitrates (0.235), dihydroxynitrates (0.064),

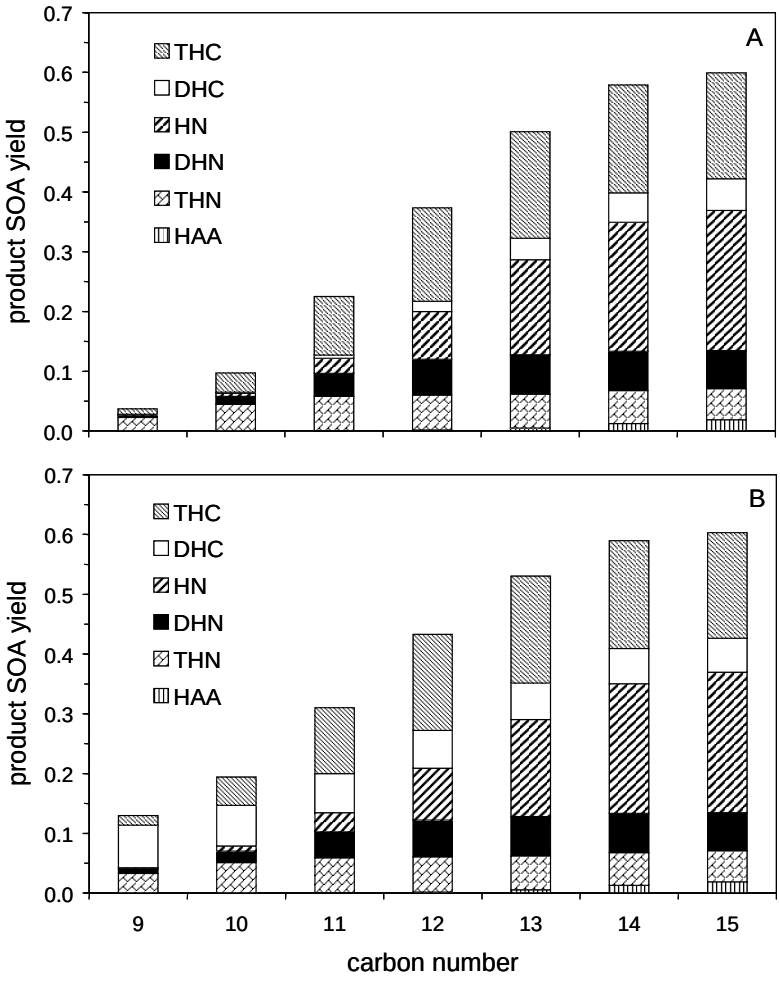

Figure 5.5 Calculated product SOA yields (mass of product in SOA/mass of alkene reacted) formed from the OH radical-initiated reactions of 2-methyl-1-alkenes in the presence of NO_x. Products are trihydroxycarbonyls (THC), dihydroxycarbonyls (DHC), β-hydroxynitrates (HN), dihydroxynitrates (DHN), and trihydroxynitrates (THN) formed by OH radical addition pathways, and 1,4-hydroxynitrates formed by the H-atom abstraction (HAA) pathway. Models assumptions: (A) all products were in gas-particle partitioning equilibrium and no secondary reaction products were formed; (B) same as (A) but dihydroxycarbonyls were in the form of non-volatile cyclic hemiacetals and dihydrofurans and so present entirely in the particle phase.

trihydroxynitrates (0.052), dihydroxycarbonyls (0.057), trihydroxycarbonyls (0.177), 1,4-hydroxynitrates (0.019), and SOA (0.604). The measured yields of C_{15} β-hydroxynitrates, dihydroxynitrates, and trihydroxynitrates, compounds that were all in the particle phase,are 0.251, 0.064, and 0.049, in good agreement with the model values (as they should be since these yields were used to develop the models). The model predictions diverge as the carbon number decreases, such that at C_9 the gpp and nv models predict SOA yields of 0.037 and 0.130.

The SOA yields calculated as described above are compared with measured values in Figures 5.6A and 5.6B. The gpp and nv models both over-predict SOA yields, although at low carbon numbers the gpp model results agree reasonably well with measured values. At C_{15}, where differences in model results due to different treatments of dihydroxycarbonyl gas-particle partitioning are negligible, the SOA yields calculated with the gpp and nv models are 0.597 and 0.604, ~30% higher than the measured SOA yield of 0.465. This discrepancy must be due to the model treatment of reaction products other than β-hydroxynitrates, dihydroxynitrates, trihydroxynitrates, and 2-ketones, since the model predictions for these compounds agree with measured yields. Furthermore, since the model over-predicts SOA yields, the mechanism must under-predict the

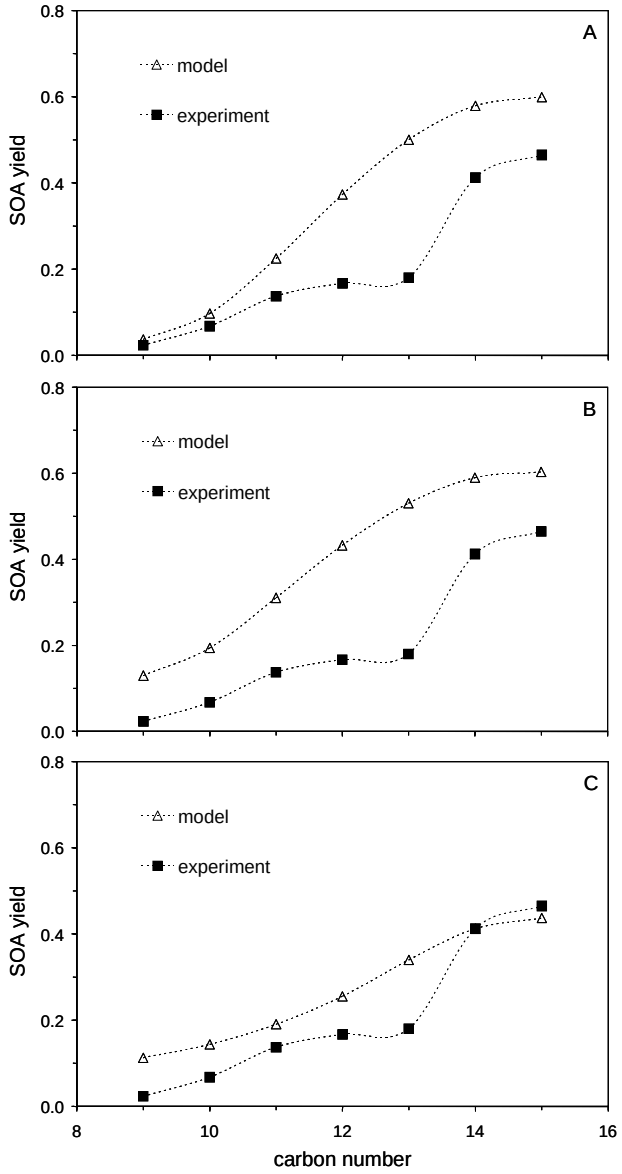

Figure 5.6 Calculated and measured yields of SOA formed from the OH radical-initiated reactions of 2-methyl-1-alkenes in the presence of NO_x. Models assumptions: (A) all products were in gas-particle partitioning equilibrium and no secondary reaction products were formed; (B) same as (A) but dihydroxycarbonyls were in the form of non-volatile cyclic hemiacetals and dihydrofurans and so present entirely in the particle phase; (C) same as (B) but the yield of trihydroxycarbonyls was reduced from 0.191 to 0.038 to achieve agreement between calculated and measured C_{15} yields.

formation of volatile decomposition products that do not form SOA. In the current mechanism the only decomposition products are 2-ketones, and their yields are well constrained by measurements with an uncertainty of ± 0.024. The discrepancy therefore appears to lie in over-predictions of the yields of dihydroxycarbonyls and trihydroxycarbonyls (the only other products), because of missing decomposition pathways. The yields of C_{15} 1,4-hydroxynitrates, dihydroxycarbonyls, and trihydroxycarbonyls predicted by the models are 0.019, 0.057 and 0.177, for a total of 0.253 out of a predicted SOA yield 0.604. This is more than twice the value of 0.101 expected from the difference in the measured SOA yield of 0.465 and the sum of the measured yields of β-hydroxynitrates, dihydroxynitrates, and trihydroxynitrates of 0.364. In order to account for the discrepancy, it is therefore necessary to add a new alkoxy radical decomposition pathway to the mechanism that reduces the total yield of 1,4-hydroxynitrates, dihydroxycarbonyls, and trihydroxycarbonyls. All the alkoxy radicals shown in Figure 5.1 (including one not shown that occurs in the formation of 1,4-hydroxynitrates) are expected to isomerize rather than decompose (Atkinson, 2007), except for the β-hydroxyalkoxy radicals, for which decomposition to carbonyls [P5, P6] is already included. We therefore propose that the α-hydroxyalkyl radicals shown

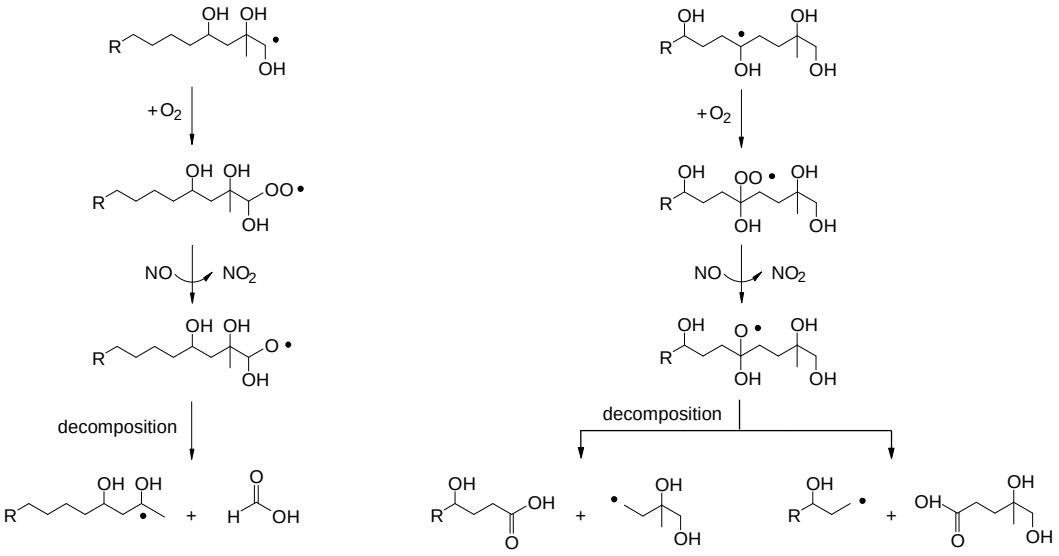

Figure 5.7 Mechanism of the reaction of α-hydroxyperoxy radicals formed in OH radical-initiated reaction of 2-methyl-1-alkenes in the presence of NO_x.

reacting with O_2 to form HO_2 and a dihydroxycarbonyl [P10] and trihydroxycarbonyls [P13, P14], also react as shown in Figure 5.7 to form α-hydroxyperoxy radicals that are sufficiently stable to react with NO. The products of the NO reaction will be hydroxynitrates and α-hydroxalkoxy radicals, with the latter (at least in part) decomposing to form volatile products that do not form SOA. This alternative pathway for the O_2 reaction has been shown to occur for α-hydroxyalkyl radicals having only one hydroxy group (Orlando et al., 2000; Atkinson et al., 1995). It is possible that hydrogen bonding between the peroxy group and the two or three additional hydroxy groups present on the α-hydroxyperoxy radicals formed here lead to additional stabilization, thereby enhancing the reaction with NO to form α-hydroxyalkoxy radicals that then decompose. Agreement between predicted and measured C_{15} SOA yields would be achieved if the yield of volatile products formed from these pathways was 0.152, reducing the sum of the yields of SOA-forming 1,4-hydroxynitrates, dihydroxycarbonyls, and trihydroxycarbonyls from 0.253 to 0.101. Since mass spectra and thermal desorption profiles indicate that dihydroxycarbonyls are formed with yields similar to those predicted by the model, the simplest assumption is that all decomposition occurs via the pathway leading to trihydroxycarbonyls. This implies that ~90% of the α-hydroxyalkyl

radicals that would otherwise react to form trihydroxycarbonyls instead react to form volatile decompositon products. Figure 5.6C and Appendix Table D.3 shows SOA yields calculated as in Figure 5.6B, but with the assumption that the yield of trihydroxycarbonyls (gas + particle) is reduced by 0.152 from 0.177 to 0.025. These yields are of course in much better agreement with measurements at high carbon numbers compared to those calculated using the other models, but at low carbon numbers the gpp model (Figure 5.6A) gives the best agreement.

Figures 5.8A and 5.8B show SOA yields calculated using the same models as in Figures 5.6A and 5.6B, but with contributions from secondary reaction products that are given in Appendix Table D.4. As expected, SOA yields are higher when secondary reaction products are included, and the agreement with measured values is worse over the entire range of carbon numbers. The average yields of C_{15} 1,4-hydroxynitrates, dihydroxycarbonyls, and trihydroxycarbonyls for the models are still 0.019, 0.057, and 0.177. But when the yield of 0.090 for secondary reaction products is added the total is 0.343 for products other than the quantified β-hydroxynitrates, dihydroxynitrates, and trihydroxynitrates, out of a predicted SOA yield 0.694. This is more than three times the value of 0.101 expected from the difference in the measured SOA yield of 0.465 and the

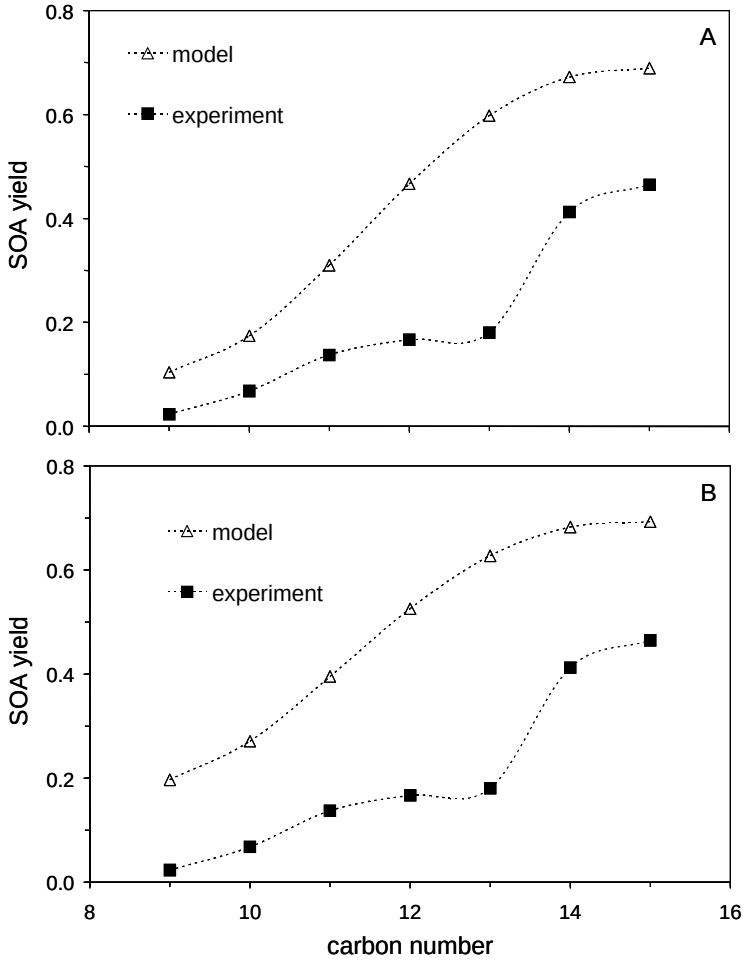

Figure 5.8 Calculated and measured yields of SOA formed from the OH radical-initiated reaction of 2-methyl-1-alkenes in the presence of NO_x. Models assumptions: (A) all products were in gas-particle partitioning equilibrium and secondary reaction products were formed; (B) same as (A) but dihydroxycarbonyls were in the form of non-volatile cyclic hemiacetals and dihydrofurans and so present entirely in the particle phase.

sum of the measured yields of β-hydroxynitrates, dihydroxynitrates, and trihydroxynitrates of 0.364. Eliminating the discrepancy between predicted and measured SOA yields would require yields of volatile decomposition products of 0.229, reducing the yields of SOA-forming dihydroxycarbonyls and trihydroxycarbonyls from 0.234 to ~ 0. It is clear that this conclusion is not correct, since measurements show that dihydroxycarbonyls and trihydroxycarbonyls are present in the aerosol. Nonetheless, the yields of these compounds must be significantly lower than those predicted by the original models, indicating that additional alkoxy radical formation/decomposition pathways such as those proposed here need to be included in the reaction mechanism. Adding a more detailed mechanism for SOA formation from H-atom abstraction and secondary reactions will also be important.

5.6 Conclusions

The composition of secondary organic aerosol (SOA) formed from OH radical-initiated reactions of 2-methyl-1-alkenes in the presence of NO_x differs in interesting ways from that formed from similar reactions of 1-alkenes, demonstrating the significant effects that simply adding a methyl group to the C=C double bond can have on chemistry.

As was shown in Chapter 4, this change in structure results in different branching ratios for the addition of OH radicals and the reactions of β-hydroxyperoxy radicals with NO, and leads to the formation of trihydroxynitrates. Here, some additional differences were identified. No dihydroxycarbonyl dimers were observed in SOA, apparently because electron donation by the methyl group reduces the tendency of the β-hydroxycarbonyls to form hemiacetal dimers. And from the significant discrepancies observed between calculated and measured SOA yields it is concluded that a large fraction of α-hydroxyalkyl radical intermediates react with O_2 and then NO to form the corresponding alkoxy radicals, which then decompose, resulting in significantly less SOA than would otherwise be formed. This pathway, although recognized in previous studies, is usually thought to be minor. So, even though our expectations were that modeling SOA formation from reactions of 2-methyl-1-alkenes would be easier than it was for 1-alkenes (where low volatility dimers and cyclic compounds formed by complex particle-phase reactions are major SOA components), these reactions offer their own challenges. Nonetheless, since most of the branching ratios for reaction pathways have been quantified, and good vapor pressure data based primarily on measurements rather than structure-activity calculations are available for estimating gas-particle partitioning, it is

expected that once additional α-hydroxyalkyl radical reactions are incorporated into the mechanism along with more detailed representations of H-atom abstraction and secondary reactions it will be possible to achieve to a more complete model for calculating SOA composition and yield. This model may be useful not only for understanding SOA formation from reactions of these particular alkenes, but also from more complex and atmospherically abundant compounds such as terpenes.

5.7 Reference

Atkinson, R., 2007. Rate Constants for the Atmospheric Reactions of Alkoxy Radicals: An Updated Estimation Method. *Atmos. Environ.*, *41*, 8468-8485.

Atkinson, R. and Arey, J., 2003a. Gas-Phase Tropospheric Chemistry of Biogenic Volatile Organic Compounds: A Review. *Atmos. Environ.*, *37*, Suppl. 2, S197-S219.

Atkinson R. and Arey J., 2003b. Atmospheric Degradation of Volatile Organic Compounds. *Chem. Rev.*, *103*, 4605-4638.

Atkinson, R., Carter, W. P. L., Winer, A. M., Pitts, J. N., Jr., 1981. An Experimental Protocol for the Determination of OH Radical Rate Constants with Organics Using Methyl Nitrite Photolysis as an OH Radical Source. *Air Pollut. Control Assoc.*, *31*, 1090-1092.

Atkinson, R., Tuazon, E. C., Aschmann, S. M., 1995. Products of the Gas-Phase Reactions of a Series of 1-Alkenes and 1-Methylcyclohexene with the OH Radical in the Presence of NO. *Environ. Sci. Technol.*, *29*, 1674-1680.

Atkinson, R., Arey, J., Aschmann, S. M., 2008. Atmospheric Chemistry of Alkanes: Review and Recent Developments. *Atmos. Environ.*, *42*, 5859-5871.

Bruckner, R., 2002. Advanced Organic Chemistry. Academic Press, San Diego.

Chattopadhyay, S. and Ziemann, P. J., 2005. Vapor Pressures of Substituted and Unsubstituted Monocarboxylic and Dicarboxylic Acids Measured Using an Improved Thermal Desorption Particle Beam Mass Spectrometry Method. *Aerosol Sci. Technol.*, *39*, 1085-1100.

Colville, C. J., Griffin, R. J., 2004. The Roles of Individual Oxidants in Secondary Organic Aerosol Formation from Δ^3-Carene: 2. Soa Formation and Oxidant Contribution. *Atmos. Environ.*, *38*, 4013-4023.

Crable, G. F., and Coggeshall, N. D., 1958. Application of Total Ionization Principles to Mass Spectrometric Analysis. *Anal. Chem., 30,* 310-313.

de Gouw, J. A., Middlebrook, A. M., Warneke, C., Goldan, P. D., Kuster, W. C., Roberts, J. M., Fehsenfeld, F. C., Worsnop, D. R., Canagaratna, M. R., Pszenny, A. A. P., Keene, W. C., Marchewka, M., Bertman, S. B., Bates, T. S., 2005. Budget of Organic Carbon in a Polluted Atmosphere: Results from the New England Air Quality Study in 2002. *J. Geophys. Res., 110,* doi:10.1029/2004JD005623.

Docherty, K. S., Wu, W.; Lim, Y. B., Ziemann, P. J., 2005. Contributions of Organic Peroxides to Secondary Aerosol Formed from Reactions of Monoterpenes with O_3. *Environ. Sci. Technol., 39,* 4049-4059.

Englert, N., 2004. Fine Particles and Human Health – a Review of Epidemiological Studies. *Toxicol. Lett., 149,* 235-242.

Finlayson-Pitts, B. J. and Pitts, J. N., Jr., 2000. Chemistry of the Upper and Lower Atmosphere. Academic Press, San Diego.

Fischer, R. G. and Ballschmiter, K., 1998. Prediction of the Environmental Distribution of Alkyl Dinitrates – Chromatographic Determination Of Vapor Pressure p^o, Water Solubility S_{H2O}, Gas Water Partition Coefficient K_{GW} (Henry's law constant) and Octanol-Water Partition Coefficient K_{OW}. *Fresenius J. Anal. Chem., 360,* 769-776.

Gong, H., Matsunaga, A., Ziemann, P. J., 2005. Products and Mechanism of Secondary Organic Aerosol Formation from Reactions of Linear Alkenes with NO_3 Radicals. *J. Phys. Chem. A, 109,* 4312-4324.

Heald, C. L., Jacob, D. J., Turquenty, S., Hudman R. C., Weber, R. J., Sullivan, A. P., Peltier, R. E., Atlas, E. L., de Gorw, J. A., Warneke, C., Holloway, J. S., Neuman, J. A., Flocke, F. M., Seinfeld, J. H., 2006. Concentrations and Sources of Organic Carbon Aerosols in the Free Troposphere over North America. *J. Geophys. Res., 111,* doi:10.1029/2006JD007705.

Henze, D. K., Seinfeld, J. H., Ng, N. L., Kroll, J. H., Fu, T. –M., Jacob, D. J., Heald, C. L., 2008. Global Modeling of Secondary Organic Aerosol Formation from Aromatic Hydrocarbons: High- vs. Low-Yield Pathways. *Atmos. Chem. Phys., 8*, 2405-2421.

Holt, T., Atkinson, R., Arey, J., 2005. Effect of Water Vapor Concentration on the Conversion of a Series of 1,4-Hydroxycabonyls to Dihydrofurans. *J. Photochem. Photobiol. A: Chem., 176*, 231-237.

Johnson, D., Utembe, S. R., Jenkin, M. E., 2006. Simulating the Detailed Chemical Composition of Secondary Organic Aerosol Formed on a Regional Scale During the TORCH 2003 Campaign in the Southern UK. *Atmos. Chem. Phys., 6*, 419-431.

Kanakidou, M. et al. (21 co-authors), 2005. Organic Aerosol and Global Climate Modelling: A Review. *Atmos. Chem. Phys., 5*, 1053-1123.

Kern, W., Spiteller, G., 1996. Synthesis and Properties of Naturally Occurring α-Hydroxyaldehydes. *Tetrahedron, 12*, 4347-4362.

Kwok, E. S. C. and Atkinson. R., 1995. Estimation of Hydroxyl Radical Reaction Rate Constants for Gas-Phase Organic Compounds Using a Structure-Reactivity Relationship: An Update. *Atmos. Environ., 29*, 1685-1695.

Lim, Y. B. and Ziemann, P. J., 2005. Products and Mechanism of Secondary Organic Aerosol Formation from Reactions of *n*-Alkanes with OH Radicals in the Presence of NO_x. *Environ. Sci. Technol., 39*, 9229-9236.

Lim, Y. B. and Ziemann, P. J., 2009a. Effects of Molecular Structure on Aerosol Yields from OH Radical-Initiated Reactions of Linear, Branched, and Cyclic Alkanes in the Presence of NO_x. *Environ. Sci. Technol., 43*, 2328-2334.

Lim, Y. B. and Ziemann, P. J., 2009b. Chemistry of Secondary Organic Aerosol Formation from OH Radical-Initiated Reactions of Linear, Branched, and Cyclic Alkanes in the Presence of NO_x. *Aerosol Sci. Technol., 43*, 604-619.

Lim, Y. B. and Ziemann, P. J., 2009c. Kinetics of the Heterogeneous Conversion of 1,4-Hydroxycarbonyls to Cyclic Hemiacetals and Dihydrofurans on Organic Aerosol Particles. *Phys. Chem. Chem. Phys.*, doi: 10.1039/b904333k.

Liu, P., Ziemann, P. J., Kittelson, D. B., McMurry, P. H., 1995a. Generating Particle Beams of Controlled Dimensions and Divergence .1. Theory of Particle Motion in Aerodynamic Lenses and Nozzle Expansions. *Aerosol Sci. Technol.*, *22*, 293–313.

Liu, P., Ziemann, P. J., Kittelson, D. B., McMurry, P. H., 1995b. Generating Particle Beams of Controlled Dimensions and Divergence .2. Experimental Evaluation of Particle Motion in Aerodynamic Lenses and Nozzle Expansions. *Aerosol Sci. Technol.*, *22*, 314–324.

Matsunaga, A. and Ziemann, P. J., 2009. Yields of *β*-hydroxynitrates and Dihydroxynitrates in Aerosol Formed from the OH Radical-Initiated Reactions of Linear Alkenes in the Presence of NO_x. *J. Phys. Chem. A*, *113*, 599-606.

Matsunaga, A., Docherty, K. S., Lim, Y. B., Ziemann, P. J., 2009. Composition and Yields of Secondary Organic Aerosol Formed from OH Radical-Initiated Reactions of Linear Alkenes in the Presence of NO_x: Modeling and Measurements. *Atmos. Environ.*, *43*, 1349-1357.

McLafferty F. W. and Tureček, F., 1993. Interpretation of Mass Spectra. 4th Ed. University Science Books, Sausalito.

Nishino, N., Arey, J., Atkinson, R., 2009. Rate Constants for the Gas-Phase Reactions of OH Radicals with a Series of C_6-C_{14} Alkenes at 299 ± 2 K. *J. Phys. Chem. A, 113*, 852-857.

Orlando, J. J., Nozière, B., Tyndall, G. S., Orzechowska, G. E., Paulson, S. E., Rudich, Y., 2000. Product Studies of the OH- and Ozone-Initiated Oxidation of Some Monoterpenes. *J. Geophys. Res.*, *105*, 11561-11572.

Pankow, J. F., 1994. An Absorption Model of the Gas/Aerosol Partitioning Involved in the Formation of Secondary Organic Aerosol. *Atmos. Environ.*, *28*, 189-193.

Pankow, J. F. and Asher, W. E., 2008. SIMPOL.1: A Simple Group Contribution Method for Predicting Vapor Pressures and Enthalpies of Vaporization of Multifunctional Organic Compounds. *Atmos. Chem. Phys.*, *8*, 2773-2796.

Reisen, F., Ashmann, S. M., Atkinson, R., Arey. J., 2005. 1,4-Hydroxycarbonyl Products of the OH Radical Initiated Reactions of C5-C8 Alkanes in the Presence of NO. *Environ. Sci. Technol.*, *39*, 4447-4453.

Seinfeld, J. H., Erdakos, G. B., Asher, W. E., Pankow, J. F., 2001. Modeling the Formation of Secondary Organic Aerosol (SOA). 2. The Predicted Effects of Relative Humidity on Aerosol Formation in the α-Pinene-, β-Pinene-, Sabinene-, Δ^3-Carene-, and Cyclohexene-Ozone Systems. *Environ. Sci. Technol.*, *35*, 1806-1817.

Taylor, W. D., Allston, T. D., Moscato, M. J., Fazekas, G. B., Kozlowski, R., Takacs, G. A., 1980. Atmospheric Photodissociation Lifetimes for Nitromethane, Methyl Nitrite, and Methyl Nitrate. *Int. J. Chem. Kinet.*, *12*, 231-240.

Tobias, H. J. and Ziemann, P. J., 1999. Compound Identification in Organic Aerosols Using Temperature-Programmed Thermal Desorption Particle Beam Mass Spectrometry. *Anal. Chem.*, *71*, 3428–3435.

Tobias, H. J., Kooiman, P. M., Docherty, K. S., Ziemann, P. J., 2000. Real-Time Chemical Analysis of Organic Aerosols Using a Thermal Desorption Particle Beam Mass Spectrometer. *Aerosol Sci. Technol.*, *33*, 170-190.

Volkamer, R., Jimenez, J. L., San Martini, F., Dzepina, K., Zhang, Q., Salacedo, D., Molina, L. T., Worsnop, D. R., Molina, M. J., 2006. Secondary Organic Aerosol Formation from Anthropogenic Air Pollution: Rapid and Higher than Expected. *Geophys. Res. Lett.*, *33*, doi:10.1029/2006GL026899.

Wang, S. C. and Flagan, R. C., 1990. Scanning Electrical Mobility Spectrometer. *Aerosol Sci. Technol., 13,* 230-240.

Chapter 6

Products and Mechanism of Secondary Organic Aerosol Formation from Reactions of Linear Alkenes with NO_3 Radicals

6.1 Abstract

Secondary organic aerosol (SOA) formation from reactions of linear alkenes with NO_3 radicals was investigated in an environmental chamber using a thermal desorption particle beam mass spectrometer for particle analysis. A general chemical mechanism was developed to explain the formation of the observed SOA products. The major first-generation SOA products were hydroxynitrates, carbonylnitrates, nitrooxy peroxynitrates,dihydroxynitrates, and dihydroxy peroxynitrates. The major second-generation SOA products were hydroxy and oxo dinitrooxytetrahydrofurans, which have not been observed previously. The latter compounds were formed by a series of reactions in which δ-hydroxycarbonyls isomerize to cyclic hemiacetals, which then dehydrate to form substituted dihydrofurans (unsaturated compounds) that rapidly react with NO_3 radicals to form very low volatility products. For the ~1 ppmv alkene concentrations used here, aerosol formed only for alkenes $\geq C_7$. SOA formed from C_7-C_9 alkenes consisted only of second-generation products, while for larger alkenes first-generation products

were also present and contributions increased with increasing carbon number apparently due to the formation of lower volatility products. The estimated mass fractions of first- and second-generation products were approximately 50:50, 30:70, 10:90, and 0:100, for 1-tetradecene, 1-dodecene, 1-decene, and 1-octene SOA, respectively. This study shows that δ-hydroxycarbonyls play a key role in the formation of SOA in alkene-NO_3 reactions, and are likely to be important in other systems since δ-hydroxycarbonyls can also be formed from reactions of OH radicals and O_3 with hydrocarbons.

6.2 Introdution

Organic particles are emitted directly into the atmosphere as products of incomplete combustion and are also formed by gas-to-particle conversion of volatile organic compounds (VOCs) emitted from anthropogenic and biogenic sources (Seinfeld and Pandis, 1998). In the latter process, VOCs are oxidized to less volatile compounds that condense to form secondary organic aerosol (SOA). The major atmospheric reactions of VOCs are those involving OH and NO_3 radicals and O_3 (Atkinson, 2000). Reactions with OH radicals occur almost exclusively during the day, reactions with NO_3 radicals occur primarily at night, and reactions with O_3 occur during the day and at night. Most studies of SOA chemistry have focused on reactions of OH radicals with aromatics (Jang and Kamens, 2001) and alkenes (Larsen et al., 2001) and on reactions of O_3 with alkenes (Yu et al, 1999; Tobias and Ziemann, 2000). Little is known about the chemistry of SOA formation from NO_3 radical reactions.

Nitrate radicals are formed in the atmosphere by the reaction of NO_2 with O_3. Concentrations are maintained at very low levels during the day by photolysis (Orlando et al., 1993) and by reaction with NO, but increase near sunset and at night such that reactions with NO_3 radicals can become an important sink for organic compounds

including unsaturated hydrocarbons, phenols, aldehydes, and dimethyl sulfide (Atkinson, 1991; wayner et al., 1991). For example, recent field studies in two major urban areas have demonstrated that NO_3 radicals can contribute significantly to the oxidation of some VOCs (Geyer et al., 2001; Geyer et al., 2003). It has also been suggested that reactions of VOCs with NO_3 radicals may be important in indoor air chemistry (Nazaroff and Weschler, 2004). Although the kinetics, mechanisms, and gas-phase products of alkene-NO_3 reactions have been the subject of a relatively large number of laboratory studies (for reviews see Atkinson, 1997; Calvert et al., 2000), investigations of SOA formation are limited to a few measurements of aerosol yields (Hallquist et al., 1999; Griffin et al., 1999; Noda and Ljungström, 2002; Moldanova and Ljungström, 2000). Nonetheless, these studies show that the reactions can be efficient aerosol sources, as indicated by SOA yields approaching unity for some monoterpenes (Griffin et al., 1999).

In this study, the chemistry of SOA formation from reactions of NO_3 radicals with a suite of linear alkenes was investigated using a thermal desorption particle beam mass spectrometer (TDPBMS) for on-line aerosol analysis (Tobias et al., 2000; Tobias and Ziemann, 1999). This instrument makes it possible to identify low-volatility multifunctional organic nitrates that have not been observed previously because of the

inability of off-line methods (e.g., gas chromatography) to analyze these labile compounds. The compounds investigated included simple linear alkenes with double bonds in either terminal or internal locations. In the atmosphere, those with internal double bonds have lifetimes (calculated using rate constants from Calvert et al., 2000 and background oxidant concentrations from Atkinson and Arey, 2003) with respect to reaction with NO_3 radicals of ~3 hr, which is comparable to reactions with O_3 and OH radicals. Terminal alkenes react with NO_3 radicals (and O_3) much more slowly, so their atmospheric lifetime is determined by reaction with OH radicals. Although the emissions of linear alkenes large enough to form condensable products are probably too small to contribute significantly to atmospheric SOA formation, these compounds provide very useful models for the more abundant and complex monoterpenes. Because the present study represents the beginning of a larger investigation into the chemistry of SOA formation from alkene-NO_3 reactions, linear alkenes were selected in order to simplify the chemistry while still providing insight into the effects of molecular structure on the pathways that lead to aerosol products.

6.3 Experimental Section

Materials. The alkenes 1-hexene (99%), 1-heptene (99%), 1-octene (98%), 1-decene (94%), 1-dodecene (95%), and 1-tetradecene (92%) were obtained from Sigma-Aldrich, and 3,5,5-trimethyl-1-hexene (99%), 2-methyl-1-octene, and 7-tetradecene were obtained from ChemSampCo. All chemicals were used without further purification.

Environmental Chamber Technique. Reactions of alkenes with NO_3 radicals were performed in the dark in a ~7000 L PTFE environmental chamber at room temperature (~23^{o}C) and pressure (~96 kPa). The chamber was flushed overnight and filled with clean, dry air (< 5 ppbv hydrocarbons, < 0.1% RH) from an Aadco pure air generator. A measured amount of alkene was evaporated from a glass bulb using gentle heating and flushed into the chamber in a clean air stream. Nitrate radicals were added in the form of N_2O_5, which thermally dissociates into NO_3 and NO_2. N_2O_5 was synthesized according to the procedure of Atkinson et al. (1984) and kept frozen in liquid N_2 on a glass vacuum rack until needed. When used, N_2O_5 was warmed and evaporated into an evacuated, calibrated 2.0 L bulb until an appropriate pressure was reached. The bulb was then flushed into the chamber using clean air. During these additions, a fan in the chamber was run to mix the reactants. Particles formed by homogeneous nucleation,

typically within a minute of adding N_2O_5 and increased from background concentrations of ~10 cm^{-3} to a peak of ~10^4-10^6 cm^{-3} a few minutes later. Average particle diameters were ~0.2-0.4 μm.

The initial concentration of alkene in the chamber was 1 ppmv. The amount of N_2O_5 added to the bulb (~0.34 kPa) was intended to also achieve this concentration. Some N_2O_5, however, was lost to the walls of the vacuum rack, glass bulb, and chamber. From the amount of reacted alkene measured in a few experiments, N_2O_5 losses were apparently < 20%. At an initial N_2O_5 concentration of 1 ppmv, the equilibrium concentrations of NO_3 and NO_2 are 37 ppbv (calculated using an equilibrium constant of 2.9×10^{-11} cm^3 $molecule^{-1}$ (Finlayson-Pitts and Pitts, 2000)). As the alkene-NO_3 reaction proceeds, [NO_3] decreases due to reaction and to the shift in equilibrium as [N_2O_5] decreases and [NO_2] increases. The amount of alkene reacted at any time depends on the rate constant, which in turn depends on the structure of the molecule. For the compounds investigated here, the rate constants (Calvert et al., 2000) are approximately 1×10^{-14} (terminal alkenes) and 3.6×10^{-13} (2-methyl-1-octene, 7-tetradecene) cm^3 $molecule^{-1}$ s^{-1}. Using the appropriate second order kinetics expression and assuming no wall losses of

N_2O_5, the amounts of alkene reacted in one hour are calculated to be ~70% and ~98% for these two classes of compounds, respectively.

Particle Mass Spectrometric Analysis. The TDPBMS was used to analyze particle composition in real-time (Tobias et al., 2000) and by temperature-programmed thermal desorption (Tobias and Ziemann, 1999). Aerosol is sampled from the chamber through stainless steel tubing and enters the TDPBMS through a 0.1 mm critical orifice that reduces the pressure from atmosphere to ~300 Pa. Particles are focused in an aerodynamic lens (Liu et al., 1995a; Liu et al., 1995b) and the resulting beam passes through a nozzle and two flat-plate skimmers before entering the detection chamber. In the detection chamber (~10^{-5} Pa), particles impact in a V-shaped notch in the tip of a copper vaporizer rod that for real-time analysis is resistively heated to ~165^{o}C. Particles are completely vaporized upon impact and vapor diffuses into an ABB Extrel MEXM 500 quadrupole mass spectrometer where molecules are ionized by electrons, mass-filtered, and detected using a conversion dynode/pulse counting detector. For TPTD analysis, the vaporizer rod was cooled to -30^{o}C and particles were collected for ~15 min. The rod was allowed to warm to -5^{o}C and was then heated to ~90-120^{o}C using a computer controlled linear temperature ramp of 2^{o}C min^{-1}. Compounds desorb from the vaporizer according to

their vapor pressures, allowing separation of components for mass spectral analysis. The mass spectrometer was typically scanned from *m/z* 10-400 in ~30 s. Although slightly better resolution might be obtained with a slower ramp, radiative heating by the ionizer sets a minimum heating rate of ~1-2^{o}C min^{-1}. This effect could be reduced with active cooling during ramping, but it would then be much more difficult to produce the exceptionally linear ramp we currently achieve and also lengthen the analysis time.

Aerosol Yield Measurements. In a few experiments, the aerosol yield [aerosol mass formed (µg m^{-3})/VOC mass reacted (µg m^{-3})] (Odum et al., 1996) was determined from measurements of aerosol mass and reacted alkene concentrations.

The amount of alkene consumed was determined from the alkene concentrations measured before and after reaction using gas chromatography. For these measurements, 100 cm^3 of air was sampled onto solid Tenax TA adsorbent and analyzed immediately using a Hewlett Packard (HP) 6890 GC system equipped with an HP-1701 fused-silica capillary column (30 m x 0.53 mm with a 1.0 µm film thickness) and a flame ionization detector (FID). The Tenax TA samples were placed in a split/splitless inlet that was run in the splitless mode. The inlet was initially at room temperature, and then ramped to 250 ^{o}C at a rate of ~23 ^{o}C min^{-1} after inserting the tube. The FID transfer line was maintained at

280 ^{o}C. The FID response was compared with standard calibrations to determine alkene concentrations.

The aerosol mass formed in a reaction was measured using a scanning mobility particle sizer (SMPS) (Wang and Flagan, 1990). The SMPS consisted of a ^{210}Po bipolar charger, a long differential mobility analyzer similar in design to the TSI model 3934, a TSI Model 3010 Condensation Particle Counter, and a scanning/inversion program developed by the McMurry group at the University of Minnesota for use with Labview software (Tobias et al., 2001). The SMPS was operated at aerosol and sheath air flows of approximately 0.5 and 2.5 L min^{-1}, respectively, which provide a resolution of ~20% in particle size measurements. The software output includes the particle size distribution, number concentration, and volume concentration, the latter of which can be converted to a particle mass concentration by multiplying by the particle density. The density was assumed to be 1 g cm^{-3}.

6.4 Results and Discussion

Reaction Mechanism. *First-Generation Products.* On the basis of previous studies of the gas-phase products of the reactions of alkenes with NO_3 radicals (Jay and

Stiglitz, 1989; Barnes et al., 1990; Skov et al., 1992; Wänberg, 1993; Kwork et al., 1996; Turazon et al., 1999), the reaction of NO_3 radicals with a linear alkene [designated here as $R_X(CH_2)_3CH=CHR_Y$, where R_X and R_Y are alkyl groups] can potentially form first-generation products **1**-**16** by the mechanism shown in Figure 6.1. The reaction is initiated by the addition of NO_3 to the carbon-carbon double bond, with H-atom abstraction being negligible. Addition occurs predominantly at the less-substituted carbon atom due to the enhanced stability imparted to the radical site by the electron-donating alkyl group. For terminal alkenes, this means NO_3 adds primarily at the end of the molecule. The resulting nitrooxyalkyl radical reacts solely with O_2 to form a nitrooxyalkylperoxy radical. This radical can react with NO_2 to form a nitrooxyalkyl peroxynitrate [**1**], which is thermally unstable and therefore acts as a temporary reservoir for the nitrooxyalkylperoxy radical. The nitrooxyalkylperoxy radical can also react with HO_2 to form a hydroperoxynitrate [**2**] or with other organic peroxy radicals (RO_2•) to form a hydroxynitrate [**3**], carbonylnitrate [**4**], or nitrooxyalkoxy radical. The nitrooxyalkoxy radical can decompose to aldehydes [**5**, **6**], isomerize through a 1,5 H-atom shift to a nitrooxyhydroxyalkyl radical, react with O_2 to form compound **4**, or react with NO_2 to

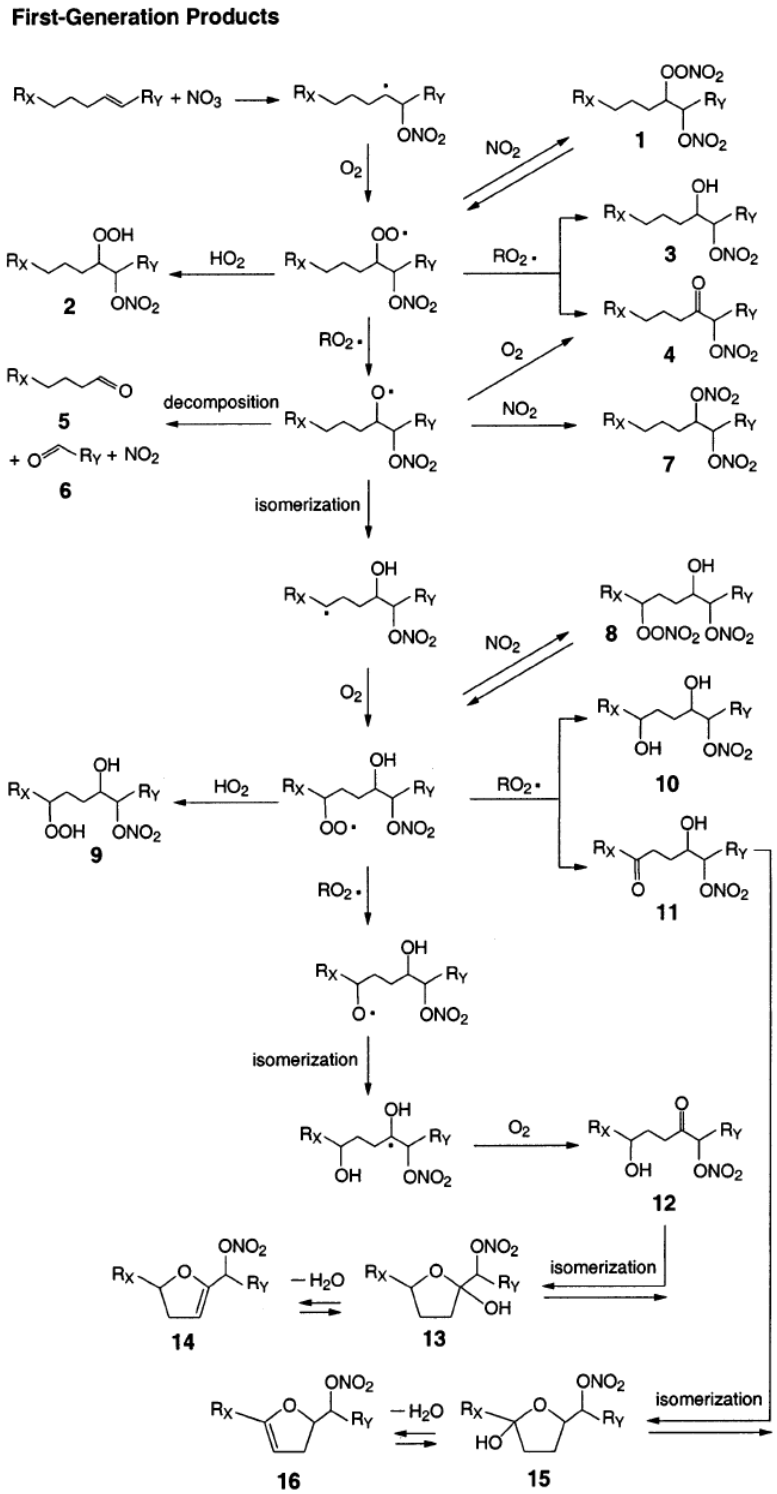

Figure 6.1 Proposed mechanism for forming first-generation products in reactions of linear alkenes with NO_3 radicals.

form an alkyl dinitrate [**7**]. The nitrooxyhydroxyalkyl radical can subsequently undergo reactions similar to the nitrooxyalkyl radical to form products **8-12**.

Isomerization of δ-Hydroxycarbonyls: a Gateway to Second-Generation Reaction Products. The first-generation reaction products **1-12** are saturated compounds that react too slowly with NO_3 radicals for further reactions to occur. Recently, however, it has been shown that δ-hydroxycarbonyls (i.e., compounds in which CHOH and C=O groups are separated by two carbon atoms) similar to compounds **11** and **12** exist in the gas phase in equilibrium with a cyclic hemiacetal isomer, which in turn is in equilibrium with a substituted dihydrofuran formed by dehydration (Cavalli et al., 2000; Martion et al., 2002). The equilibria shift in the direction of the substituted dihydrofuran with decreasing relative humidity (RH). For 5-hydroxy-2-pentanone (the only commercially available δ-hydroxycarbonyl), the lifetime for conversion to 4,5-dihydro-2-methylfuran is ~1.1 hr at RH <<1% (Martin et al., 2002). More recent studies on δ-hydroxycarbonyls created in chamber reactions have shown that as the carbon number of the δ-hydroxycarbonyl increases the equilibria shift toward the substituted dihydrofuran, with dehydration occurring as quickly as a few minutes or less (Reisen et al., 2005; Baker et al., 2005; Holt et al., 2005).

For compounds **11** and **12**, isomerization leads to cyclic hemiacetals **13** and **15**, which then lose water to form substituted dihydrofurans **14** and **16**, respectively. As shown below, formation of substituted dihydrofurans and their subsequent reactions with NO_3 radicals provides an important pathway to second-generation products of lower volatility and greater aerosol forming potential.

Second-Generation Products. It has been shown that the reaction of NO_3 radicals with 4,5-dihydro-2-methylfuran is orders of magnitude faster than with alkenes (Martin et al., 2002). The substituted dihydrofuran compounds **14** and **16** therefore react rapidly with NO_3 radicals to form second-generation products. The proposed mechanism is shown in Figure 6.2 and is essentially the same as that shown in Figure 6.1 for alkenes (no reactions of nitrooxyalkoxy radicals with NO_2 are shown for reasons explained below, and an additional decomposition reaction leads to nitrooxycarbonyl esters [**21, 29**]). The potential second-generation products of the reactions of compounds **14** and **16** are substituted tetrahydrofurans including nitroperoxy [**17, 18, 25, 26**], hydroperoxy [**19**, **20**, **27**, **28**], hydroxy [**22**, **23**, **30**, **31**], and oxo [**24**, **32**] dinitrooxytetrahydrofurans.

Mass Spectral Analysis of Aerosol Products. The major challenge in using TDPBMS mass spectra to identify reaction products is that mass spectral standards are

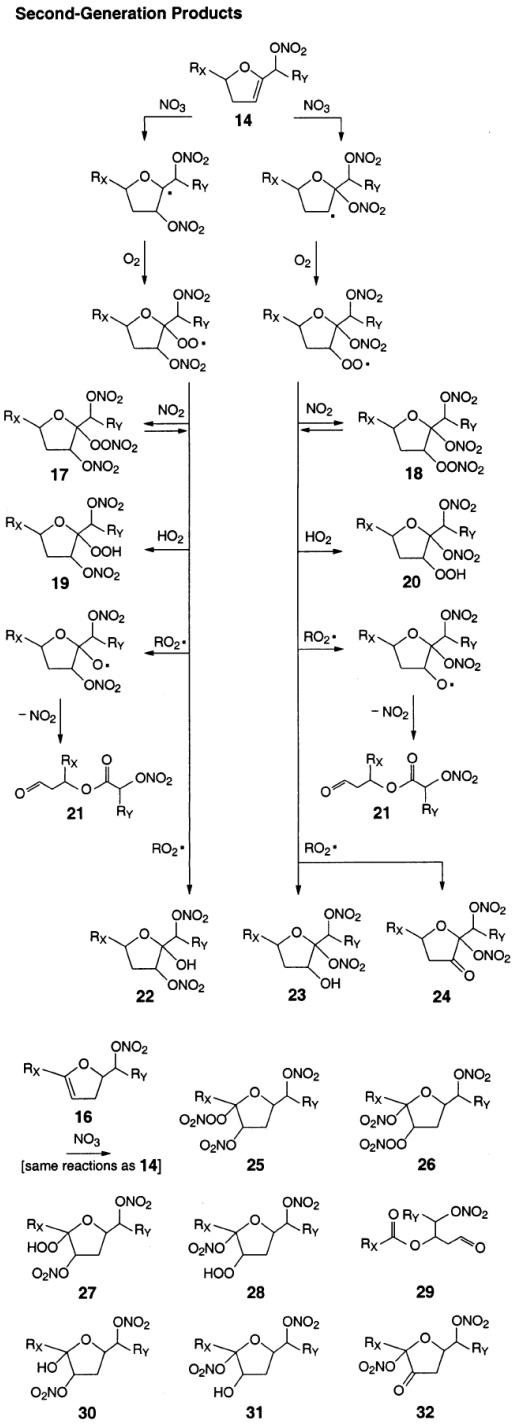

Figure 6.2 Proposed mechanism for forming second-generation products in reactions of linear alkenes with NO_3 radicals.

only available for the aldehyde products (**5** and **6**) formed by the mechanisms shown in Figures 1 and 2. The mass spectra of other potential products are not present in libraries nor are the compounds commercially available. The approach taken here was to use mass spectra of compounds with related structures, well-known electron ionization (EI) fragmentation pathways (McLafferty and Turecek, 1993), and TPTD profiles to determine which products of the proposed mechanisms appear to be present.

1-Tetradecene. The real-time mass spectrum obtained for the reaction of 1-tetradecene [$CH_3(CH_2)_{11}CH{=}CH_2$] with NO_3 radicals is shown in Figure 6.3. Significant high-mass peaks are present at *m/z* 333, 288, 286, 272, 258, 227, 211, 199, and 197. The TPTD desorption profiles for these and other selected *m/z* values are shown in Figure 6.4. For any single compound, the profiles of all *m/z* values that are present in its mass spectrum will exhibit maxima at the same temperature. A maximum in a desorption profile is therefore indicative of a single compound or a group of compounds having very similar vapor pressures. Although the TPTD technique was not able to completely separate the components of this mixture in order to obtain mass spectra of single compounds, by comparing profiles of different *m/z* values it was possible to identify 6

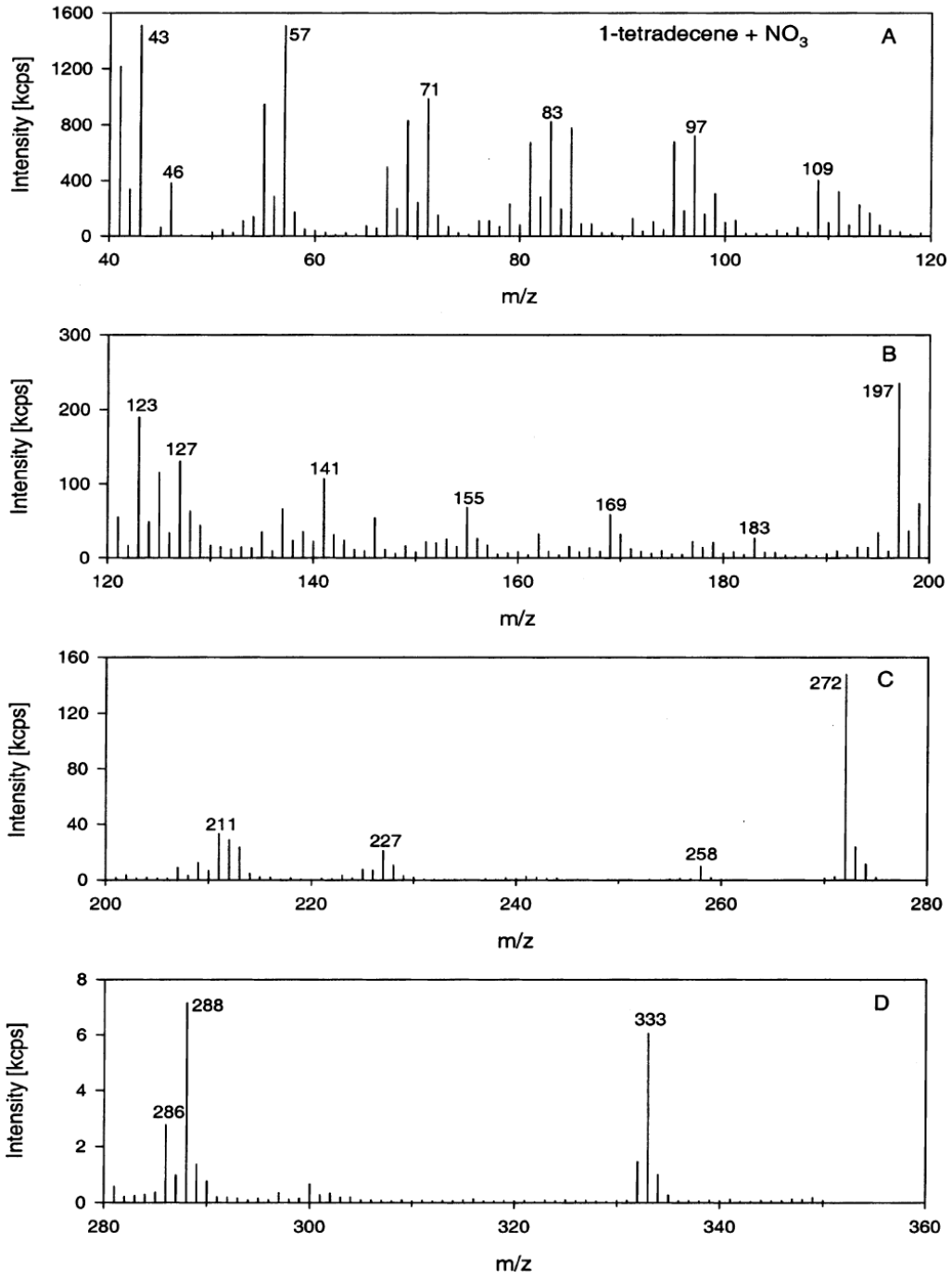

Figure 6.3 Real-time mass spectrum of aerosol formed in the reaction of 1-teradecene with NO_3 radicals.

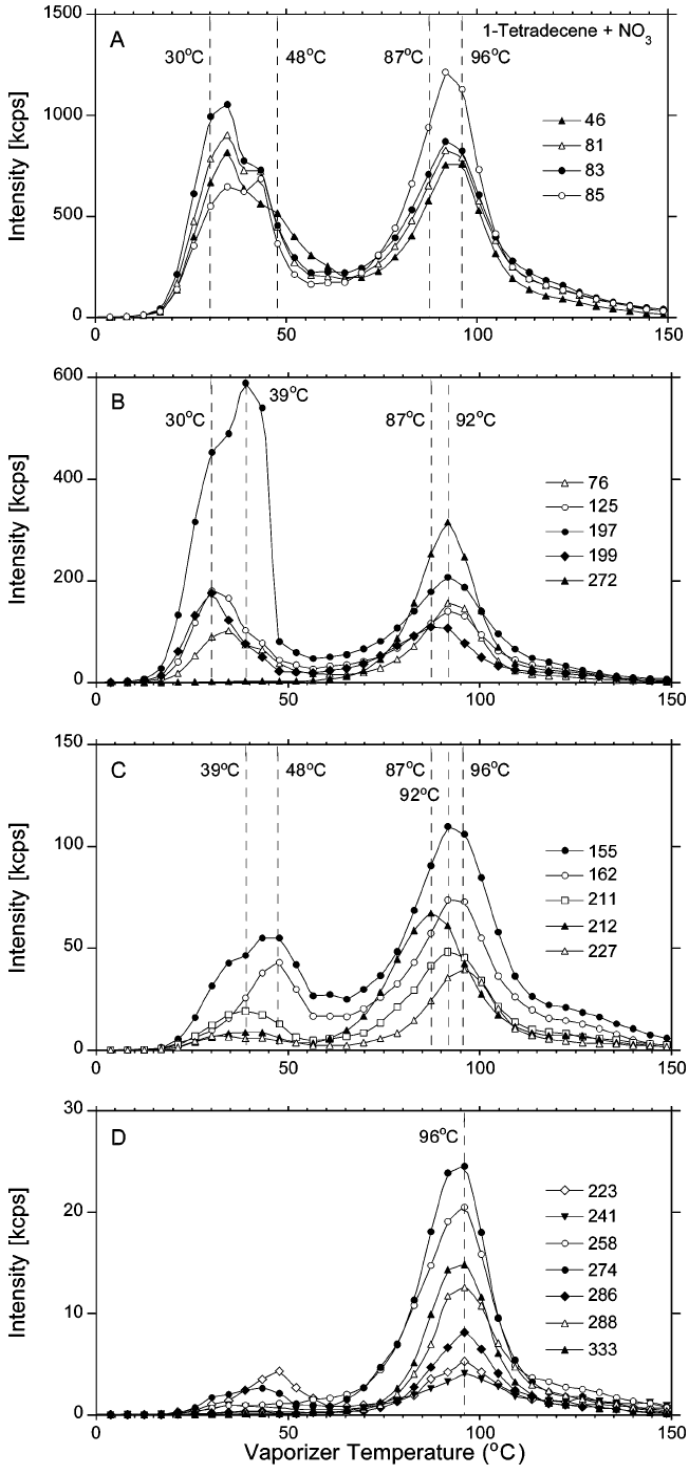

Figure 6.4 Thermal desorption profiles for selected *m/z* values for aerosol formed in the reaction of 1-tetradecene with NO_3 radicals.

compounds (or groups of compounds), corresponding to maxima at 30, 39, 48, 87, 92, and 96 ^{o}C.

The compound(s) responsible for each maximum was assigned by comparing potential reaction products, measured volatilities (as indicated by desorption temperatures), and major mass spectral peaks. For 1-tetradecene, $R_X = CH_3(CH_2)_8$ and $R_Y = H$ in the reaction schemes shown in Figures 6.1 and 6.2. The proposed aerosol products are shown in Figure 6.5 along with proposed pathways for creating the characteristic ions used for compound identification. The pathways are consistent with well-established electron ionization (EI) fragmentation mechanisms (McLafferty and Turecek, 1993). All the major mass spectral peaks associated with TPTD maxima can be assigned to stable ions generated from the proposed reaction products by loss of the molecular species H_2O, NO_2, HNO_2, NO_3, HNO_3, HCHO, $CH_2=CH_2$, and CO, and OH and alkyl radicals. The systematic procedure used to assign the products is described in detail below.

As a starting point, we note that compounds equivalent to **1**-**7** have been observed among the major gas-phase products of alkene-NO_3 reactions (Atkinson, 1997; Calvert et al., 2000; Atkinson and Arey, 2003). Whether or not these compounds are found in the

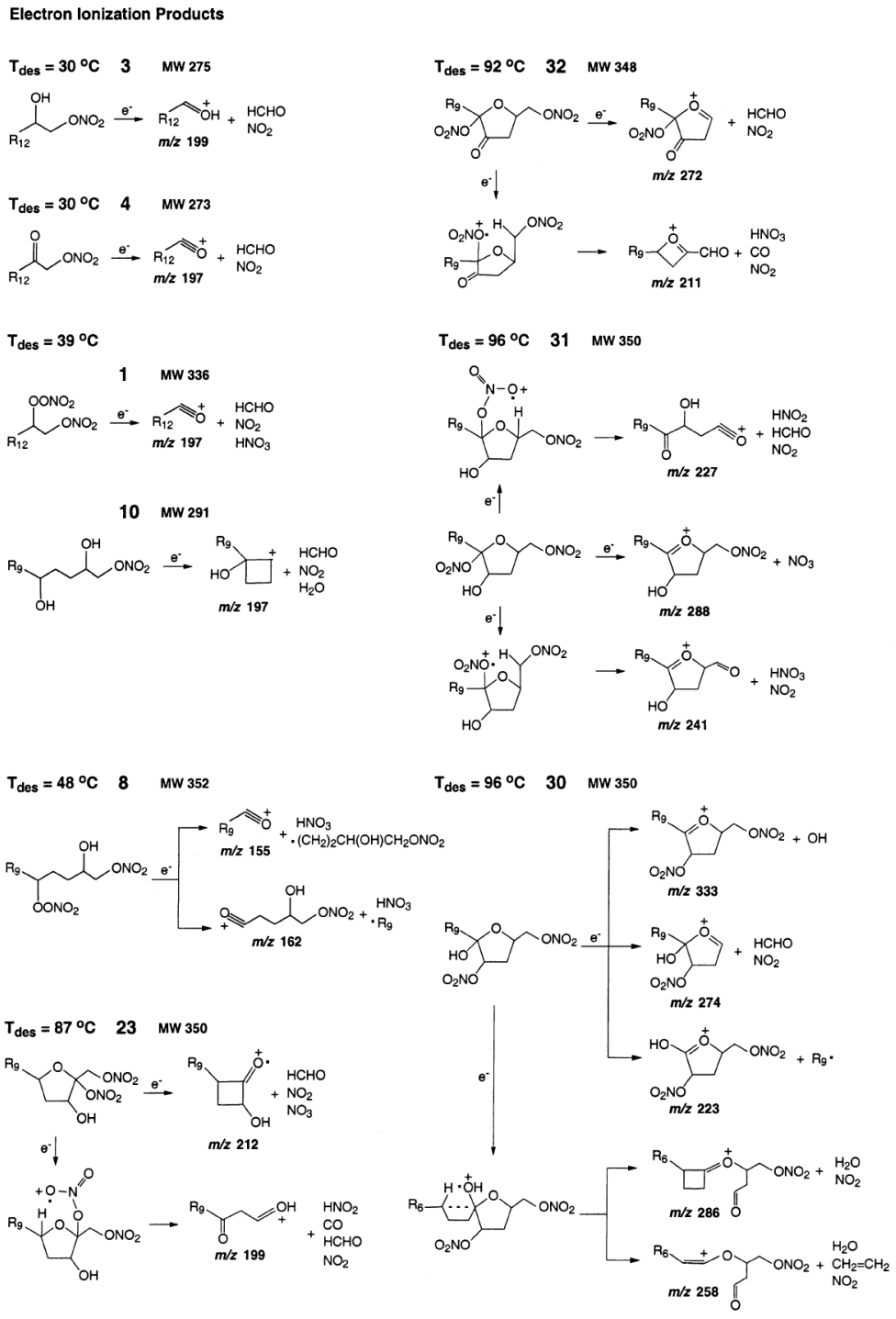

Figure 6.5 Proposed aerosol products for the reaction of 1-tetradecene with NO_3 radicals and electron ionization fragmentation pathways. In this figure, $R_{12} = CH_3(CH_2)_{11}$, $R_9 = CH_3(CH_2)_8$, and $R_6 = CH_3(CH_2)_5$.

aerosol analyzed here depends on the reaction conditions and the alkene carbon number, since products must have sufficiently low vapor pressures to partition into particles.

As shown in Figures 6.1 and 6.2, because the reaction of unsaturated compounds with NO_3 radicals is initiated by addition of NO_3 to the double bond, most of the products are expected to be nitrates with the exception of a few decomposition products. In EI mass spectra of organic nitrates, such as those shown in Figure E.1 (Appendix) for alkyl nitrate standards, *m/z* 46 is a characteristic mass fragment due to NO_2^+. The TPTD profile of *m/z* 46 for aerosol formed from the 1-tetradecene reaction is shown in Figure 6.4A along with those for *m/z* 81, 83, and 85. The latter three ions are associated with many different products, and their profiles span the entire range of temperatures over which aerosol products desorb. The overlap of the desorption profiles of these peaks (as well as all others) with *m/z* 46 suggests that all the aerosol compounds are nitrates. Nonetheless, as we begin our analysis we will not assume this is the case. It is also important to note that many of the small mass fragments (e.g., *m/z* 46, 76, 81, 83, 85) have desorption profiles with maxima at temperatures other than those labeled in Figure 6.4. The reason for this is that these ions are associated with multiple compounds that are not completely separated by TPTD analysis. The low-mass *m/z* profiles therefore represent contributions

from multiple products. In most cases, they exhibit maxima approximately midway between those of the labeled compound(s). High-mass fragments are more often characteristic of a single compound or isomers, and are therefore more useful for identification.

We begin by determining whether or not any of the compounds **1**-**7** are present among the most volatile aerosol products, since their counterparts have been identified as gas-phase products in other alkene-NO_3 reactions. Beginning with the compound(s) that desorbs at 30 ^oC, we note that the highest *m/z* value that exhibits a maximum at this temperature is 199 (Figure 6.4B). This cannot be compound **5** (tridecanal) or **6** (formaldehyde), since our previous studies of 1-tetradecene ozonolysis (Tobias and Ziemann, 2000) have shown that tridecanal (the least volatile of these) is too volatile to form particles under these conditions. Furthermore, the molecular weight of tridecanal is only198. Compound **7** is eliminated from consideration because dinitrate formation through reactions of alkoxy radicals with NO_2 should be negligible under the conditions of these experiments. For example, using a rate constant ratio of 4×10^3 for the reaction of alkoxy radicals with NO_2 relative to O_2 (Atkinson, 1997) and the maximum value of $[NO_2]/[O_2] = 5 \times 10^{-6}$ in our experiments indicates that less than 2% of the

nitrooxyalkoxy radicals react with NO_2. Isomerization and decomposition reactions will reduce this percentage further. Compound **2** is ruled out because in previous studies we observed that the mass spectra of hydroperoxides always contain a large peak at *m/z* M-33 (M is the molecular ion mass) due to the loss of HO_2 (Tobias and Ziemann, 2000; Ziemann, 2003). This should result in a maximum in the *m/z* 258 profile at 30 ^{o}C, which is absent (Figure 6.4D).

Among the gas-phase products that have been observed in previous studies, compounds **1**, **3**, and **4** remain as possibilities and our results suggest that the maxima at 30 and 39 ^{o}C are due to a combination of these three compounds. The assignment of compound **3**, a hydroxynitrate, as a contributor to the 30 ^{o}C compound(s) is consistent with the maximum in the *m/z* 199 profile shown in Figure 6.4B. Although mass spectra are not available for any of the proposed products, EI mass spectra are available for related compounds. For example, the mass spectrum of a 1,2-dihydroxytetradecane [$CH_3(CH_2)_{11}CH(OH)CH_2OH$] standard, which has a similar structure to compound **3**, is shown in Figure E.1 (Appendix). The highest mass peak is a large one at *m/z* 199 corresponding to the $CH_3(CH_2)_{11}CHOH^+$ ion formed by loss of $\bullet CH_2OH$. Formation of this ion should be even more favored for compound **3** because of the greater stability of

the HCHO and NO_2 molecules lost during decomposition (Figure 6.5) as compared to a $\bullet CH_2OH$ radical. As expected, *m/z* 125 and some of the other ions in the $C_nH_{2n-1}^+$ series that is prominent in the 1,2-dihydroxytetradecane mass spectrum also exhibit maxima at 30 ^oC.

It appears that a second compound also desorbs at 30 ^oC. In the *m/z* 197 profile, (Figure 6.4B) there is a shoulder at 30 ^oC and a peak at 39 ^oC. It is unlikely that the mass spectrum of compound **3** would have such an intense peak (~2-3 times larger than *m/z* 199) at this mass. We therefore assign this fragment to another compound with essentially the same volatility. The best candidate is compound **4**, a carbonylnitrate. It is reasonable that the volatility of this compound would be similar to compound **3**, since they only differ by carbonyl and hydroxyl groups. The large peak at *m/z* 197 is expected for compound **4**, due to the stable acylium ion, $CH_3(CH_2)_{11}CO^+$, formed by loss of HCHO and NO_2 (Figure 6.5). For comparison, the mass spectrum of a 2-oxoadipic acid [$HO(O)C(CH_2)_3C(O)C(O)OH$] standard shown in Figure E.1 (Appendix) has an intense high-mass peak at *m/z* 115 from the acylium ion $HO(O)C(CH_2)_3CO^+$ formed by loss of the $\bullet C(O)OH$ radical.

This assignment of compounds **3** and **4** is also consistent with the mass spectra of the alkyl nitrate standards (M = 147) shown in Figure E.1 (Appendix). The 1-nitrooxyhexane [$CH_3(CH_2)_4CH_2ONO_2$] standard has a terminal nitrooxy group, as do compounds **3** and **4**. Bond scission at the nitrooxy carbon, which is the pathway proposed for compounds **3** and **4**, leads to *m/z* 71 [$CH_3(CH_2)_4^+$] or 76 [$CH_2ONO_2^+$] for 1-nitrooxyhexane and *m/z* 57 [$CH_3(CH_2)_3^+$] or 90 [$CH_3CHONO_2^+$] for 2-nitrooxyhexane [$CH_3(CH_2)_3CH(ONO_2)CH_3$], depending on which fragment retains the charge. The *m/z* 85 ion observed for both standards is due to loss of NO_3. This is not a major fragmentation pathway for compounds **3** and **4**, but is important for some second-generation products discussed below.

The maximum at 39 ^oC is most likely due to compound(s) **1** and/or **10**. Compound **1** is a nitrooxy peroxynitrate and compound **10** is a dihydroxy nitrate. Both should be less volatile than **3** and **4**, and can easily produce *m/z* 197 ions (Figure 5). It is worth noting that the similar R-CH_2ONO_2 structures of compounds **1**, **3**, **4**, and **10** should lead to $CH_2ONO_2^+$ ions in the mass spectra of all four compounds. The *m/z* 76 desorption profile shown in Figure 6.4B exhibits a maximum between 30 and 39 ^oC, indicating that all these compounds fragment by this pathway.

The compound that desorbs at 48 ^{o}C is assigned as compound **8**, a nitrooxyhydroxyalkyl peroxynitrate. If this compound fragments by pathways similar to compound **1**, the major ions contributing to the mass spectrum should be acylium ions corresponding to *m/z* 155 and 162 (Figure 6.5). The desorption profiles of both these ions exhibit maxima at 48 ^{o}C.

The next maximum observed in any desorption profile is at 87 ^{o}C, followed by maxima at 92 and 96 ^{o}C. The large temperature gap between these three maxima and those at 30, 39, and 48 ^{o}C is indicative of a significant reduction in compound vapor pressures. The much higher masses of many of the fragment ions in the mass spectra associated with the lower volatility compounds indicate they have significantly different molecular structures. In the process of analyzing these data, it became obvious that the mass spectra could not be explained on the basis of first-generation products similar to those observed in previous gas-phase studies. For example, only two first-generation products, compounds **1** (M = 336) and **8** (M = 352), have M $\geq$ 333 as is necessary to produce a mass spectral peak at *m/z* 333. Neither of these compounds can be responsible for this peak, however, since no plausible fragmentation pathways can lead to a loss of 3 or 19 mass units. The low volatilities and high molecular weights of the products

indicated that reactions were occurring that allowed a second nitrate group to be added to the molecule, since a large number of carbonyl and/or hydroxyl groups would be needed to achieve a similar effect. It appeared, therefore, that new double bonds were being formed during the reaction that allowed further addition of NO_3 radicals. This led us to the work of Martin et al. (2002), who showed that δ-hydroxycarbonyls undergo isomerization-dehydration reactions that lead to unsaturated dihydrofuran products. The rapid reaction of the dihydrofurans with NO_3 radicals would quickly form much lower volatility compounds. We therefore propose that the compounds that desorb at 87, 92, and 96 ^{o}C correspond to second-generation products consisting of hydroxy [**22**, **23**, **30**, **31**] and oxo [**24**, **32**] dinitrooxytetrahydrofurans formed by the mechanism shown in Figure 6.2.

All the major high-mass peaks in the mass spectrum, as well as some less prominent peaks, can be explained as stable ions formed from hydroxy and oxo dinitrooxytetrahydrofurans by loss of the molecular species H_2O, NO_2, HNO_2, NO_3, HNO_3, HCHO, $CH_2=CH_2$, and CO, and OH and alkyl radicals, as shown in Figure 6.5. For these compounds, major fragmentation pathways leading to high-mass ions are those involving the loss of substituents from the 2 and 5 positions on the ring (i.e., the two

carbon atoms adjacent to the O-atom). This is demonstrated in the mass spectrum of 2-hydroxytetrahydrofuran shown in Figure E.2 (Appendix), where loss of OH leads to the large peak at *m/z* 71. The *m/z* 333, 288, 274, 272, and 223 peaks from the 1-tetradecene reaction can all be explained by this mechanism. Functional groups in the 3 or 4 positions on the ring are apparently not lost directly, as indicated by the absence of a *m/z* 71 peak in the mass spectrum of 3-hydroxytetrahydrofuran shown in Figure E.2 (Appendix). This indicates that the peaks at *m/z* 333 and 288, for example, are derived from different isomers having similar volatilities (Figure 6.5). The other major fragmentation pathways are initiated by H-atom abstraction enhanced by the formation of a 6-member ring (7-member in the case of *m/z* 227) transition state, which is a well-established mechanism (McLafferty and Turecek, 1993). This leads to the loss of H_2O (*m/z* 286 and 258), HNO_3 (*m/z* 241 and 211), and HNO_2 (*m/z* 227 and 199) followed by other stable molecules such as $CH_2{=}CH_2$, CO, HCHO, and NO_2. As shown below, the absence of a peak corresponding to *m/z* 286 for the reaction products of $C_n \leq 8$ alkenes is consistent with this pathway. It is important to note that although mass spectra of the hydroperoxy dinitrooxytetrahydofurans **19**, **20**, **27**, and **28** (M = 366) would also probably have significant peaks at *m/z* 333 due to loss of HO_2, the other observed ions are not consistent

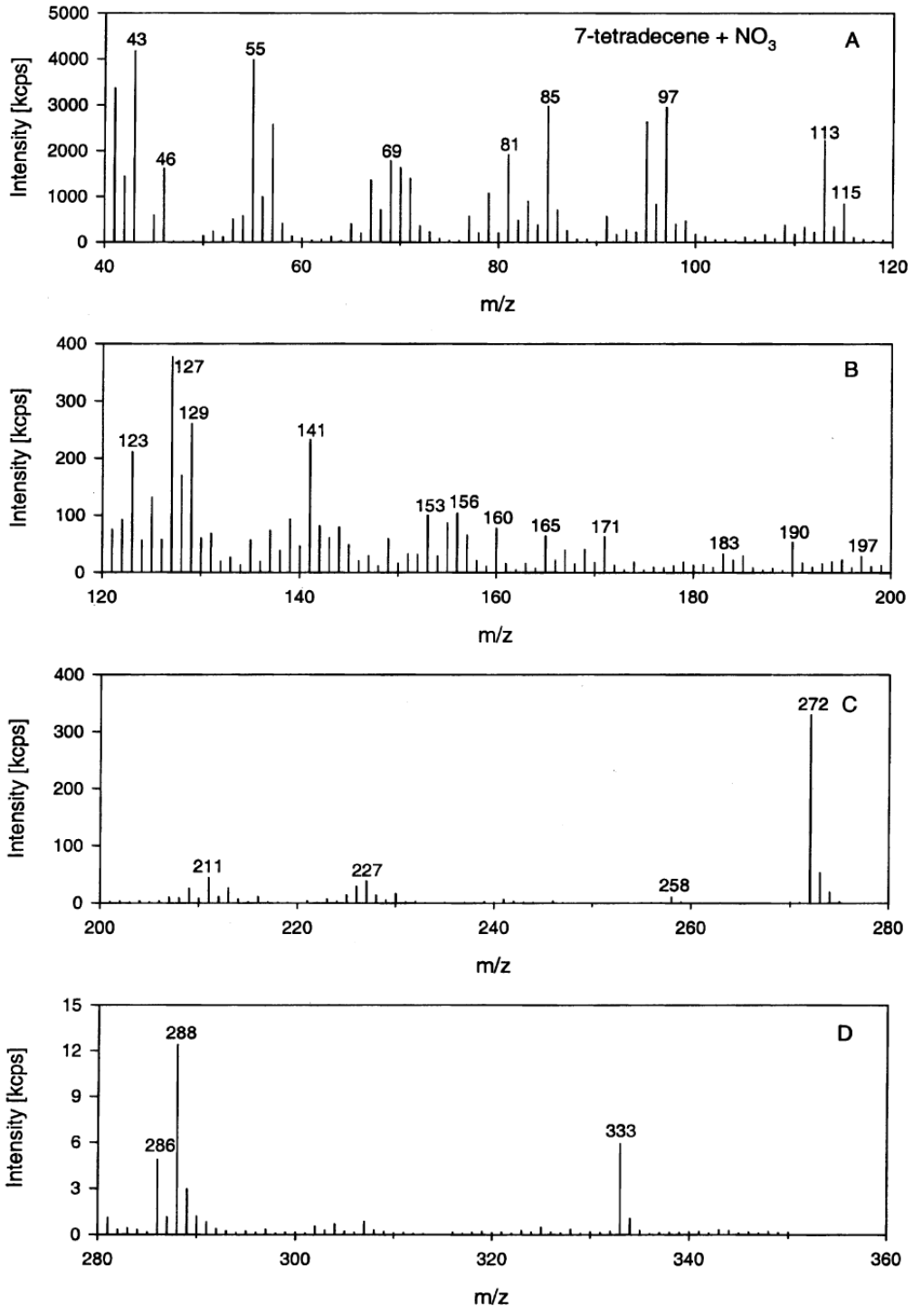

Figure 6.6 Real-time mass spectrum of aerosol formed in the reaction of 7-tetradecene with NO_3 radicals.

with fragmentation of these compounds. The second-generation products identified here have not been observed previously.

7-Tetradecene. The linear alkene 7-tetradecene [$CH_3(CH_2)_5CH=CH(CH_2)_5CH_3$] is an isomer of 1-tetradecene with the double bond in the middle of the molecule. In this case, $R_X = CH_3(CH_2)_2$ and $R_Y = CH_3(CH_2)_5$ in Figures 6.1 and 6.2. As shown in Figure 6.6, this change in structure has only a minor effect on the real-time mass spectrum of the aerosol products. The same high-mass peaks are present at *m/z* 333, 288, 286, 274, 272, 258, 227, and 211. The peaks at *m/z* 199 and 197 are much reduced because of the change in length of the carbon chain adjacent to the double bond, and a few important new peaks appear, at *m/z* 160 and 190. The desorption profiles for selected *m/z* values are shown in Figure 6.7, and again indicate the presence of two groups of compounds: a more volatile group (first-generation products) with maxima between 14 and 42 ^oC, and a less volatile group (second-generation products) with maxima between 79 and 84 ^oC. The fragmentation pathways proposed to be responsible for the major mass spectral peaks are shown in Figure 8, and are similar to those proposed for the 1-tetradecene reaction products.

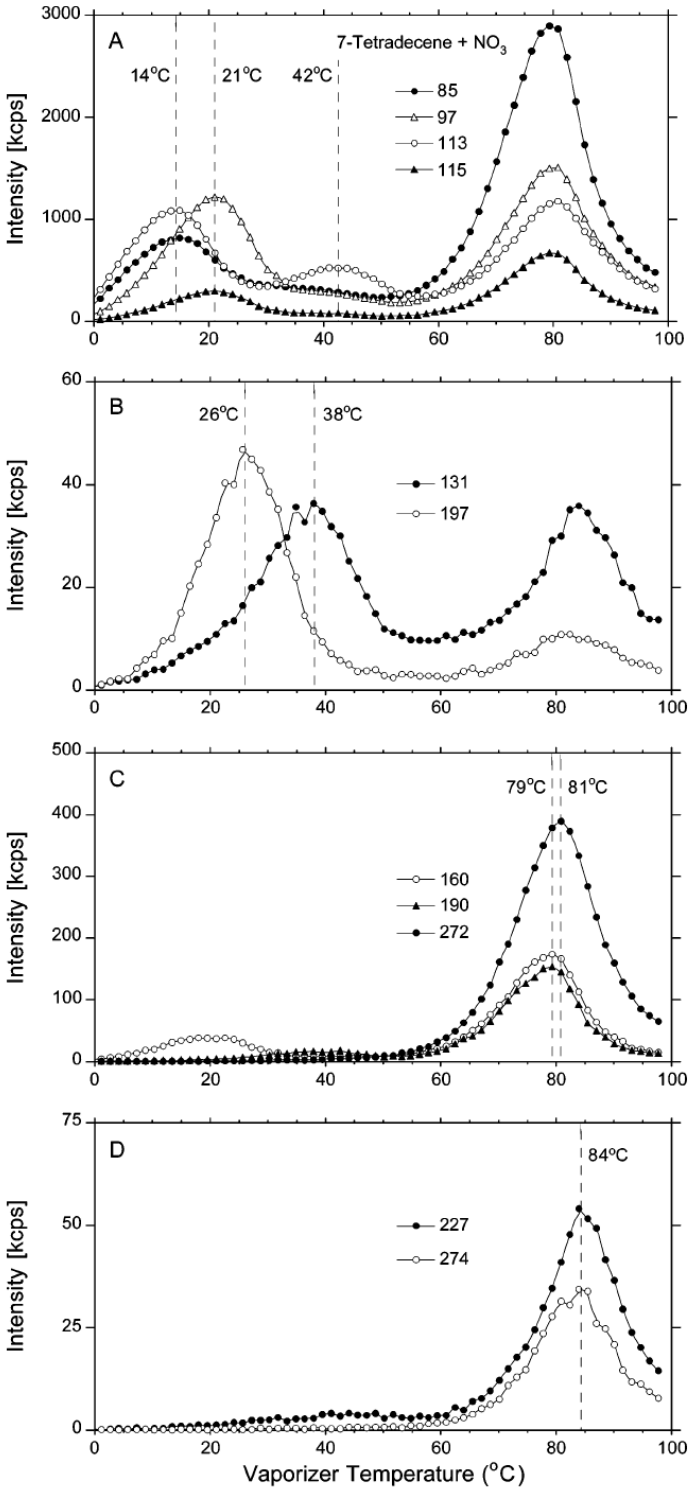

Figure 6.7 Thermal desorption profiles for selected *m/z* values for aerosol formed in the reaction of 7-tetradecene with NO_3 radicals.

The two most volatile aerosol products desorb at 14 and 21 ^{o}C. As with 1-tetradecene, they are assigned to compounds **3** and **4**. These compounds are more volatile than the corresponding 1-tetradecene products, and also differ slightly in volatility with respect to each other. These differences are because of the shift of the functional groups from the end of the molecule to the center. The desorption profiles of *m/z* 85 and 113, which are indicative of a carbonylnitrate, both have maxima at 14 ^{o}C, whereas the profiles of *m/z* 97 and 115, which are indicative of a hydroxynitrate, both have maxima at 21 ^{o}C. The desorption profile of *m/z* 160 has a broad maximum spanning the region from 14 to 21 ^{o}C indicating that this fragment comes from both compounds. The *m/z* 113, 115, and 160 peaks are analogous to the *m/z* 197, 199, and 76 peaks, respectively, observed in the 1-tetradecene reaction mass spectrum. Further fragmentation of the *m/z* 113 and 115 ions yield large peaks at *m/z* 85 and *m/z* 97 by loss of CO and H_2O, respectively. These pathways were not observed for the *m/z* 197 and 199 ions from the 1-tetradecene reaction products because of the greater stability of larger $RCHOH^+$ and RCO^+ ions. This size effect is demonstrated in the mass spectra of 5-hydroxytetradecane [$CH_3(CH_2)_3CH(OH)(CH_2)_8CH_3$] and 7-hydroxytetradecane [$CH_3(CH_2)_5CH(OH)(CH_2)_6CH_3$] shown in Figure E.3 (Appendix). The

$CH_3(CH_2)_8CHOH^+$ *m/z* 157 ion from 5-hydroxytetradecane does not lose H_2O to give a peak at *m/z* 139, whereas for 7-hydroxytetradecane the loss of H_2O from the smaller $CH_3(CH_2)_5CHOH^+$ and $CH_3(CH_2)_6CHOH^+$ ions is indicated by the peaks at *m/z* 115 and 97 and at *m/z* 129 and 111, respectively.

There are also maxima at 26, 38, and 42 ^oC in the desorption profiles of *m/z* 197, 131, and 113, respectively. On the basis of volatility and probable fragmentation pathways (Figure 6.8), the maxima at 38 and 42 ^oC are assigned to compounds **10** and **1**, respectively, but no plausible assignment could be made to the 26 ^oC maximum.

The compounds that exhibit desorption maxima between 79 and 84 ^oC are assigned to second-generation products, similar to the products of the 1-tetradecene reaction. Some of the desorption profiles are broader and less well resolved, but the oxo [**32** and/or **24**] and hydroxy [**30**, **31** and/or **22, 23**] dinitrooxytetrahydrofurans still desorb at slightly different temperatures. This is demonstrated in Figures 6.7C,D for some of the most intense high-mass fragments. It is worth noting that in order to form the *m/z* 272 and 274 ions by loss of HCHO and NO_2, an H-atom and alkyl group must exchange positions on the ring. This was unnecessary for the 1-tetradecene reaction products, and suggests a strong propensity for the formation of these ions. One other difference is that for the 7-

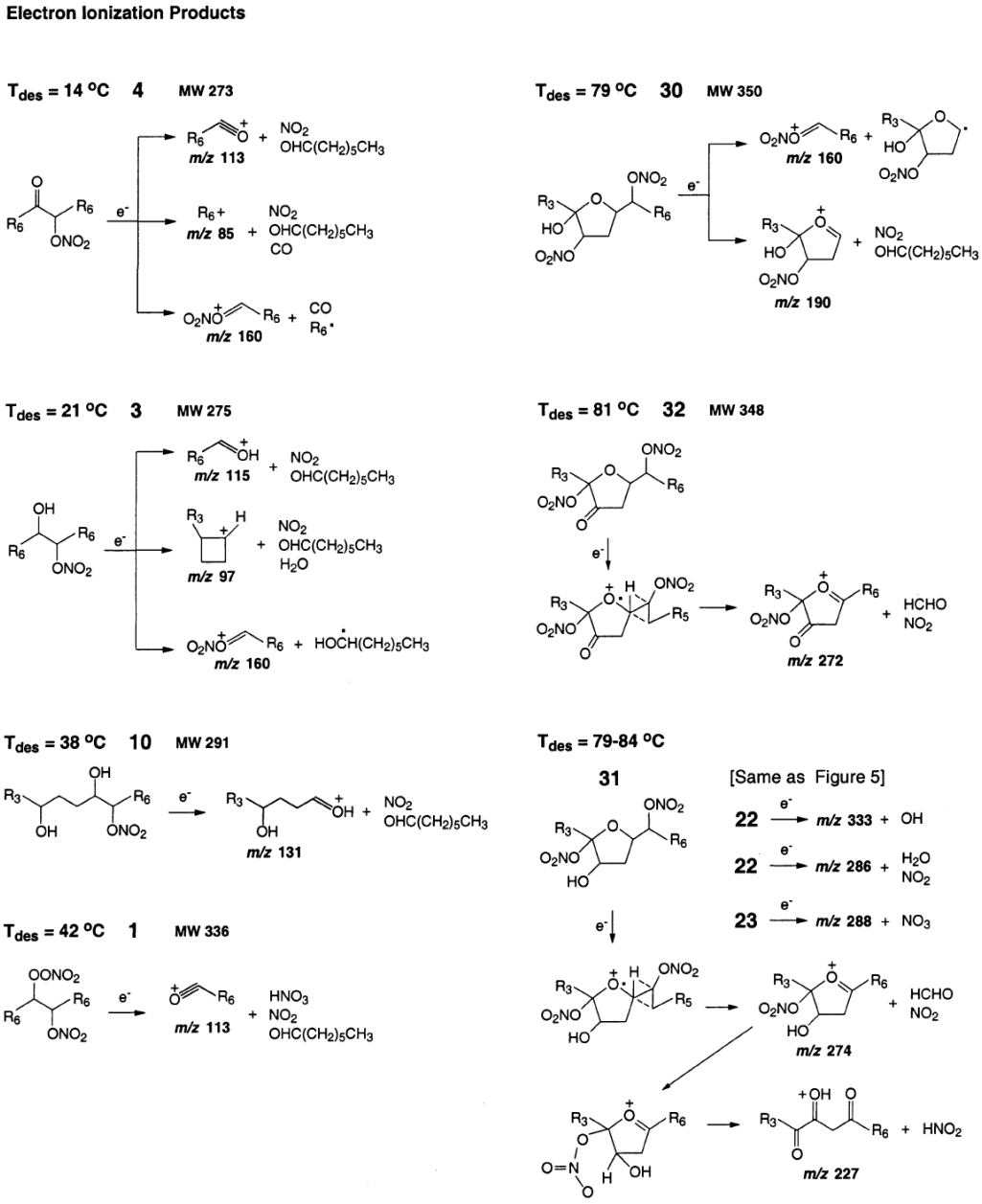

Figure 6.8 Proposed aerosol products for the reaction of 7-tetradecene with NO_3 radicals and electron ionization fragmentation pathways. In this figure, $R_6 = CH_3(CH_2)_5$, $R_5 = CH_3(CH_2)_4$, and $R_3 = CH_3(CH_2)_2$.

tetradecene reaction the *m/z* 286 ion is apparently formed from compound **22** rather than **30**, since the alkyl group must be sufficiently large for isomerization. Lastly, one very important observation that provides strong support for the identification of hydroxyl dinitrooxytetrahydrofurans is that the *m/z* 160 and 190 desorption profiles both have maxima at 79 ^{o}C. These are new fragments that appear because of the different position of the double bond in 7-tetradecene. They are formed when compound **30** (and/or **31**), which has a molecular weight of 350, splits into fragments with mass 160 and 190.

The proposed first- and second-generation SOA products from the reactions of 1-tetradecene and 7-tetradecene are summarized in Table E.1 (Appendix) along with desorption temperatures (T_{des}) and vapor pressures at 25^{o}C (P_{25}). The P_{25} values were estimated from T_{des} values using an empirical correlation [$\log P_{25}(Pa) = -0.0854 \times T_{des}(^{o}C) - 1.792$] obtained from vapor pressures of a series of C_{13}-C_{22} monocarboxylic acids (chattopadhyay and Ziemann, 2005) measured using the TPTD technique (Chattopadhyay et al., 2001). These values are probably accurate to within about one order of magnitude.

Homologous Linear Alkenes. The mass spectral patterns observed for the aerosol products from reactions of other linear alkenes are consistent with those from 1-tetradecene and 7-tetradecene. The real-time mass spectrum of aerosol from the reaction

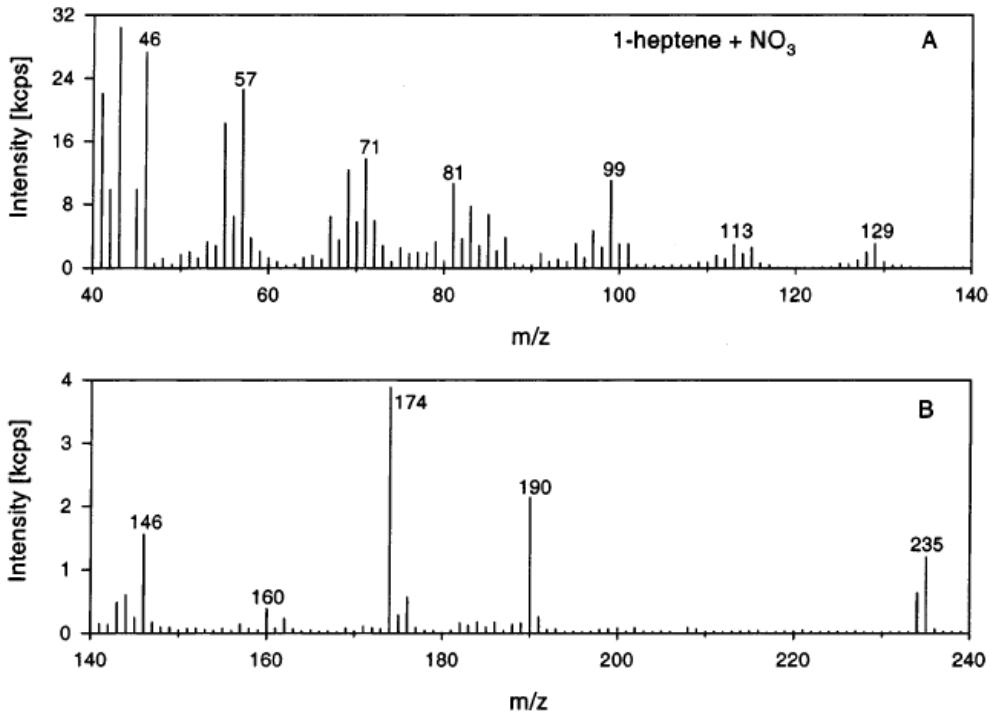

Figure 6.9 Real-time mass spectrum of aerosol formed in the reaction of 1-heptene with NO_3 radicals.

of 1-heptene [$CH_3(CH_2)_4CH=CH_2$], which was the smallest alkene to form aerosol, is shown in Figure 6.9. For this alkene, $R_X = CH_3CH_2$ and $R_Y = H$ in Figures 6.1 and 6.2. The molecular weight of 1-heptene is 98 compared to 196 for 1-tetradecene, so corresponding peaks in the mass spectra differ by 98 mass units. As expected, major high-mass peaks in the 1-heptene reaction mass spectrum are present at *m/z* 235, 190, and 174, corresponding to *m/z* 333, 288, and 272 for the 1-tetradecene reaction. No peak is present at *m/z* 188, which corresponds to *m/z* 286. This is apparently because the pathway for forming the *m/z* 286 ion, as proposed in Figure 6.5, is not accessible to the 1-heptene reaction product. This pathway involves a 6-member ring transition state, and so requires a terminal alkene having at least 8 carbons. We observed peaks indicative of this pathway in the mass spectra from reactions of 1-tetradecene, 1-dodecene and 1-decene, but not 1-octene and 1-heptene. The absence of a peak for 1-octene, even though it has 8 carbons, is probably because abstraction would occur at a primary hydrogen. This requires more energy than for the secondary hydrogens available in terminal alkenes having 9 or more carbons.

Contributions of First- and Second-Generation Reaction Products to SOA Formation. Thermal desorption profiles of single *m/z* values are valuable for identifying

products, but do not provide quantitative information. Profiles of the total ion signal, however, can be used for this purpose. Because the total ion signal is approximately proportional to the organic mass (Crable and Coggeshall, 1958), the mass fraction of a component can be estimated from the normalized area under its desorption peak. This is equivalent to using a total ion chromatogram to estimate compound concentrations in GC-MS analysis. The approach is demonstrated in Figure 6.10 for aerosol formed from reactions of the homologous series of terminal alkenes: 1-tetradecene, 1-dodecene, 1-decene, and 1-octene.

In most cases, single compounds cannot be resolved in the plots of total ion signal, and peaks instead represent a group of compounds with similar volatilities. For example, peaks are observed at 34, 46, and 92 ^{o}C in the profile for 1-tetradecene (Figure 6.10A). Comparing with profiles for single *m/z* values (Figure 6.4) indicates the peak at 34 ^{o}C is from compounds that desorb at 30 and 39 ^{o}C, while the peak at 46 ^{o}C is from the compounds that desorb at 39 ^{o}C and 48 ^{o}C. The peak at 92 ^{o}C is from second-generation products that desorb between 87 and 96 ^{o}C. The interpretation of the profiles for other compounds is similar. As expected, product volatility increases as the molecular weight of the parent alkene decreases. For 1-tetradecene, 1-dodecene, 1-decene, and 1-octene,

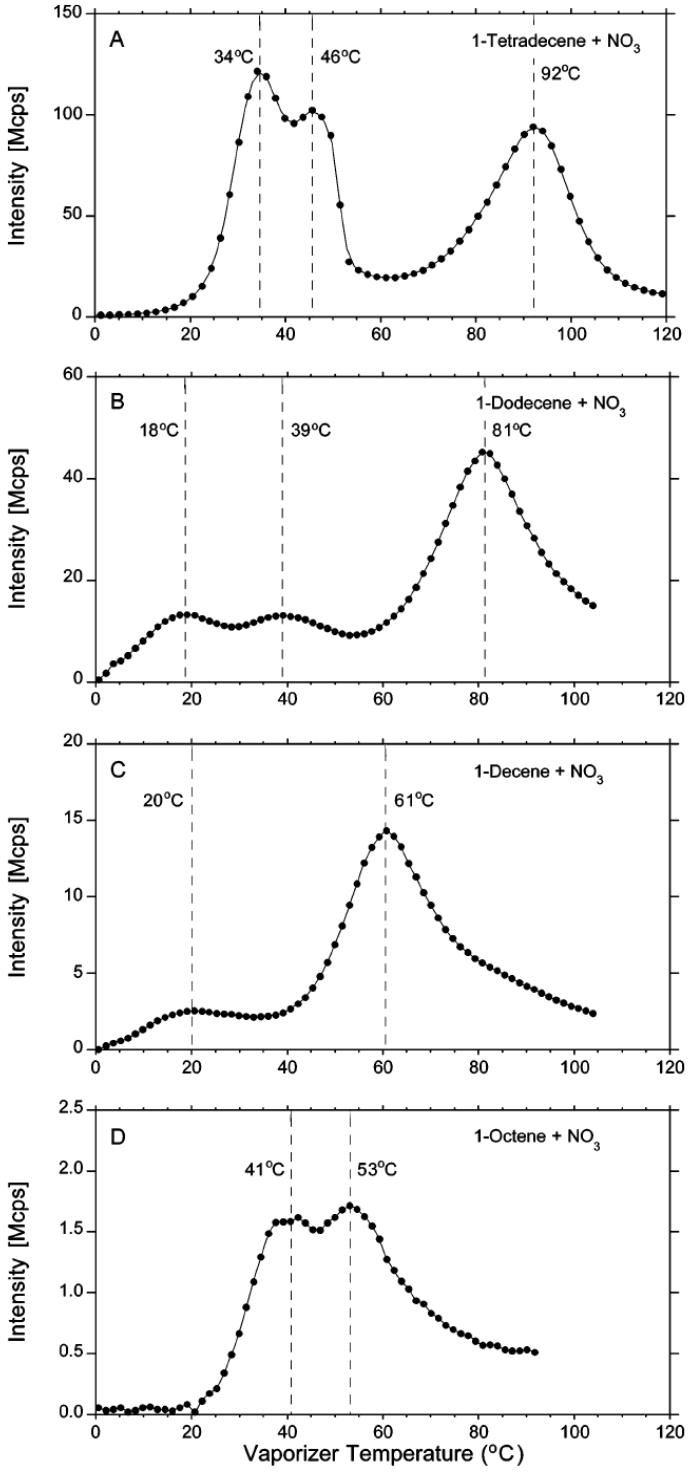

Figure 6.10 Total ion desorption profiles from TPTD analysis of aerosol formed in the reactions of (A) 1-tetradecene, (B) 1-dodecene, (C) 1-decene, and (D) 1-octene with NO_3 radicals.

the mean desorption temperatures are 92, 81, 61, and 47 ^{o}C for second-generation products and 40, 29, and 20 for first-generation products (no 1-octene peak).

Although the resolution is not sufficient to quantify single compounds, it is possible to use these results to estimate the relative contributions of first- and second-generation products to the aerosol yield. Based on the discussion above, we can assume that the dividing line between first- and second-generation products in 1-tetradecene aerosol is the minimum in the curve at ~63 ^{o}C (Figure 6.10A). We then use the normalized signal below and above this temperature to calculate the fraction of aerosol mass from the two components. We do the same for the other profiles using temperatures of 55 and 35 ^{o}C for 1-dodecene and 1-decene, respectively, while 1-octene has only second-generation products. The results of this analysis indicate that the mass fractions of first- and second-generation products are approximately 50:50, 30:70, 10:90, and 0:100, for 1-tetradecene, 1-dodecene, 1-decene, and 1-octene aerosol, respectively.

An Additional Test of the Proposed Reaction Mechanism. As shown in Figure 6.2, the proposed mechanism for forming second-generation reaction products requires the presence of δ-hydroxycarbonyls, which isomerize and dehydrate to form unsaturated compounds that then react with NO_3 radicals. A key step in the formation of

δ-hydroxycarbonyls is a 1,5 H-atom shift within the alkoxy radical intermediate. For all the terminal alkenes discussed above, this isomerization pathway is available to the β-alkoxy radicals formed subsequent to addition of NO_3 at the terminal carbon and leads to δ-hydroxycarbonyl nitrate products **11** and **12**. Terminal alkenes without H-atoms on the 5-carbon cannot form δ-hydroxycarbonyls or second-generation reaction products.

One terminal alkene that has no H-atoms on the 5-carbon is 3,5,5-trimethyl-1-hexene [$CH_3C(CH_3)_2CH_2CH(CH_3)CH=CH_2$], which is commercially available. As a test of the proposed mechanism, this compound was reacted with N_2O_5. A reaction was also performed using 2-methyl-1-octene [$CH_3(CH_2)_5C(CH_3)=CH_2$], which is an isomer of 3,5,5-trimethyl-1-hexene that can form second-generation products. From the discussion above regarding the desorption profiles in Figure 6.10, aerosol formed from C_9 alkenes is composed almost entirely of second-generation products. One would therefore expect that if the mechanism proposed here is correct, the aerosol yield from the reaction of 3,5,5-trimethyl-1-hexene should be very small and much less than that from 2-methyl-1-octene. Reactions were carried out with 1 ppmv 3,5,5-trimethyl-1-hexene and 10 ppmv N_2O_5, and 1 ppmv 2-methyl-1-octene and 2 ppmv N_2O_5. Under these conditions, reactions of both alkenes are calculated to be >90% complete within 30 min, as was

verified by GC analysis of the amount of reacted alkene. The results of the experiments were consistent with the predictions of the reaction mechanism: the aerosol yield from 2-methyl-1-octene was 10%, while no aerosol was formed from 3,5,5-trimethyl-1-hexene.

6.5 Conclusions

The results of this study show that SOA formation from reactions of NO_3 radicals with linear alkenes involves both first- and second-generation products. The most important first-generation aerosol products are hydroxynitrates, carbonylnitrates, nitrooxyperoxy nitrates, and dihydroxynitrates. Although δ-hydroxycarbonyls are too volatile to form SOA directly, they are key intermediates in the formation of lower volatility second-generation products. Because of the 1,4 configuration of the hydroxyl and carbonyl groups in δ-hydroxycarbonyls, these compounds can readily isomerize to cyclic hemiacetals and then dehydrate to form substituted dihydrofurans. The double bonds in dihydrofurans are extremely reactive towards NO_3 radicals, so these compounds are rapidly converted to lower volatility hydroxy and oxo dinitrooxytetrahydrofurans. It is not known if the isomerization of δ-hydroxycarbonyls to cyclic hemiacetals occurs in

the gas phase or requires a surface (particles or walls), but our previous studies indicated that hydroperoxycarbonyls can isomerize in the gas phase (Ziemann, 2003).

For the C_6-C_{14} alkenes studied here at concentrations of 1 ppmv, SOA formed only for alkenes $\geq C_7$. The SOA formed from reactions of C_7-C_9 alkenes consisted solely of second-generation products. First-generation products first appeared in SOA from C_{10} alkenes, and their contribution to the aerosol mass increased with increasing carbon number. In the case of 1-tetradecene, the largest alkene studied, the mass fractions of first- and second-generation products in the aerosol were ~50:50. These results are indicative of enhanced gas-to-particle partitioning for the lower volatility products formed from larger alkenes.

The important role observed here for *d*-hydroxycarbonyls (through conversion to dihydrofurans) in SOA formation is likely to be of general applicability since *d*-hydroxycarbonyls are also formed from reactions of hydrocarbons with OH radicals and O_3. In the atmosphere, dihydrofurans should react primarily with O_3 and NO_3 radicals (Martin et al., 2002), which indicates that the importance of these oxidants in SOA formation is not limited to reactions of unsaturated hydrocarbons. These reactions open efficient pathways for forming low volatility products, which are not currently included

in models of SOA chemistry. Elsewhere we will demonstrate the importance of *d*-hydroxycarbonyls in SOA formation from reactions of alkanes with OH radicals in the presence of NO_x (Lim and Ziemann, 2005).

6.6 References

Atkinson, R., 1991. Kinetics and Mechanisms of the Gas-Phase Reactions of the NO_3 Radical with Organic Compounds. *J. Phys. Chem. Ref. Data*, *20*, 459–507.

Atkinson, R., 1997. Gas-Phase Tropospheric Chemistry of Volatile Organic Compounds: 1. Alkane and Alkenes. *J. Phys. Chem. Ref. Data*, *26*, 215-290.

Atkinson R., 2000. Atmospheric Chemistry of VOCs and NO_x. *Atmos. Environ.*, *34*, 2063–2101.

Atkinson R. and Arey J., 2003.Atmospheric Degradation of Volatile Organic Compounds. *Chem. Rev.*, *103*, 4605-4638.

Atkinson, R., Plum, C. N., Carter, W. P. L., Winer, A. M., Pitts, J. N., Jr., 1984. Rate Constants for the Gas-Phase Reactions of Nitrate Radicals with a Series of Organics in Air at 298 ± 1K. *J. Phys. Chem.*, *88*, 1210-1215.

Baker, J., Arey, J., Atkinson, R., 2005. Rate Constants for the Reactions of OH Radicals with a Series of 1,4-Hydroxyketones. *Atmos. Environ.*, *176*, 143-148.

Barnes, I., Bastian, V., Becker, K. H., Tong, Z., 1990. Kinetics and Products of the Reactions of NO_3 with Monoalkenes, Dialkenes, and Monoterpenes. *J. Phys. Chem.*, *94*, 2413–2419.

Calvert, J. G., Atkinson, R., Kerr, J. A., Madronich, S., Moortgat, G. K., Wallington, T. J., Yarwood, G., 2000. The Mechanisms of Atmospheric Oxidation of the Alkenes. Oxford University Press, New York.

Cavalli, F., Barnes, I., Becker, K. H., 2000. FT-IR Kinetic and Product Study f the OH Radical-Initiated Oxidation of 1-pentanol. *Environ. Sci. Technol.*, *34*, 4111–4116.

Chattopadhyay, S. and Ziemann, P. J., 2005. Vapor Pressures of Substituted and Unsubstituted Monocarboxylic and Dicarboxylic Acids Measured Using an Improved

Thermal Desorption Particle Beam Mass Spectrometry Method. *Aerosol Sci. Technol., 39*, 1085-1100.

Chattopadhyay, S., Tobias, H. J., Ziemann, P. J., 2001. A Method for Measuring Vapor Pressures of Low-Volatility Organic Aerosol Compounds Using a Thermal Desorption Particle Beam Mass Spectrometer. *Anal. Chem., 73*, 3797-3803.

Crable, G. F. and Coggeshall, N. D., 1958. Application of Total Ionization Principles to Mass Spectrometric Analysis. *Anal. Chem., 30*, 310-313.

Finlayson-Pitts, B. J. and Pitts, J. N., Jr., 2000. Chemistry of the Upper and Lower Atmosphere. Academic Press, San Diego.

Geyer, A., Alicke, B., Konrad, S., Schimitz, T., Stutz, J., Platt, U., 2001. chemistry and Oxidation Capacity of the Nitrate Radical in the Continental Boundary Layer Near Berlin. *J. Geophys. Res., 106*, 8013–8025.

Geyer, A., Alicke, B., Ackermann, R., Martinez, M., Harder, H., Brune, W., di Carlo, P., Williams, E., Jobson, T., Hall, S., Shetter, R., Stutz, J., 2003. Direct Observations of Daytime NO_3: Implications for Urban Boundary Layer Chemistry. *J. Geophys. Res., 108*, 4368–4378.

Griffin, R. J., Cocker, D. R., III, Flagan, R. C., Seinfeld, J. H., 1999. Organic Aerosol Formation from the Oxidation of Biogenic Hydrocarbons. *J. Geophys. Res., 104*, 3555–3567.

Hallquist, M., Wängberg, I., Ljungström, E., Barnes, I., Becker, K. H., 1999. Aerosol and Product Yields from NO_3 Radical-Initiated Oxidation of Selected Monoterpenes. *Environ. Sci. Technol., 33*, 553–559.

Holt, T., Atkinson, R., Arey, J., 2005. Effect of Water Vapor Concentration on the Conversion of a Series of 1,4-Hydroxycabonyls to Dihydrofurans. *J. Photochem. Photobiol. A: Chem., 176*, 231-237.

Jang, M. and Kamens, R. M., 2001. characterization of Secondary Aerosol from the Photooxidation of Toluene in the Presence of NO_x and 1-Propene. *Environ. Sci. Technol.*, *35*, 3626–3639.

Jay, K. and Stieglitz, L., 1989. The Gas Phase Addition of NO_x to Olefins. *Chemosphere*, *19*,1939–1950.

Kwok, E. S. C., Aschmann, S. M., Arey, J., Atkinson, R., 1996. Product Formation from the Reaction of the NO_3 Radical with Isoprene and Rate Constants for the Reactions of Methacrolein and Methyl Vinyl Ketone with the NO_3 Radical. *Int. J. Chem. Kinet.*, *28*, 925–934.

Larsen, B.R., Di Bella, D., Glasius, M., Winterhalter, R., Jensen, N.R., Hjorth, J., 2001. Gas-Phase OH Oxidation of Monoterpenes: Gaseous and Particulate Products. *J. Atmos. Chem.*, *38*, 231–276.

Lim, Y. B. and Ziemann, P. J., 2005. Products and Mechanism of Secondary Organic Aerosol Formation from Reactions of *n*-Alkanes with OH Radicals in the Presence of NO_x. *Environ. Sci. Technol.*, *39*, 9229-9236.

Liu, P., Ziemann, P. J., Kittelson, D. B., McMurry, P. H., 1995a. Generating Particle Beams of Controlled Dimensions and Divergence .1. Theory of Particle Motion in Aerodynamic Lenses and Nozzle Expansions. *Aerosol Sci. Technol.*, *22*, 293–313.

Liu, P., Ziemann, P. J., Kittelson, D. B., McMurry, P. H., 1995b. Generating Particle Beams of Controlled Dimensions and Divergence .2. Experimental Evaluation of Particle Motion in Aerodynamic Lenses and Nozzle Expansions. *Aerosol Sci. Technol.*, *22*, 314–324.

Martin, P., Tuazon, E. C., Aschmann, S. M., Arey, J., Atkinson, R., 2002. Formation and Atmospheric Reactions of 4,5-Dihydro-2-Methylfuran. *J. Phys. Chem. A*, *106*, 11492–11501.

McLafferty F. W. and Turecek, F., 1993. Interpretation of Mass Spectra. 4th Ed. University Science Books, Sausalito.

Moldanova, J. and Ljungström, E., 2000. Modelling of Particle Formation from NO_3 Oxidation of Selected Monoterpenes. *J. Aerosol. Sci., 31*, 1317–1333.

Nazaroff, W. W. and Weschler, C. J., 2004. Cleaning Products and Air Fresheners: Exposure to Primary and Secondary Air Pollutants. *Atmos. Environ., 38*, 2841-2865.

Noda, J. and Ljungström, E., 2002. Aerosol Formation in Connection with NO_3 Oxidation of Unsaturated Alcohols. *Atmos. Environ., 36*, 521–525.

Odum, J. R., Hoffmann, T., Bowman, F., Collins, D., Flagan, R. C., Seinfeld, J. H., 1996. Gas/Particle Partitioning and Secondary Organic Aerosol Yields. *Environ. Sci. Technol., 30*, 2580-2585.

Orlando, J. J., Tyndall, G. S., Moortgat, G. K., Calvert, J. G., 1993. quantum Yields for NO_3 Photolysis Between 570 and 635 nm. *J. Phys. Chem., 97*, 10996–11000.

Reisen, F., Ashmann, S. M., Atkinson, R., Arey. J., 2005. 1,4-Hydroxycarbonyl Products of the OH Radical Initiated Reactions of C5-C8 Alkanes in the Presence of NO. *Environ. Sci. Technol., 39*, 4447-4453.

Seinfeld, J. H., Pandis, S. N., 1998. Atmospheric Chemistry and Physics. John Wiley & Sons, New York.

Skov, H., Hjorth, J., Lohse, C., Jensen, N. R., Restelli, G., 1992. Products and Mechanism of the Reactions of the Nitrate Radical (NO_3) with Isoprene, 1,3-Butadiene and 2,3-Dimethyl-1,3-Butadiene in Air. *Atmos. Environ., 26A*, 2771–2783.

Tobias, H. J. and Ziemann, P. J., 1999. Compound Identification in Organic Aerosols Using Temperature-Programmed Thermal Desorption Particle Beam Mass Spectrometry. *Anal. Chem., 71*, 3428–3435.

Tobias, H. J. and Ziemann, P. J., 2000. Thermal Desorption Mass Spectrometric Analysis of Organic Aerosol Formed from Reactions of 1-Tetradecene and O_3 in the Presence of Alcohols and Carboxylic Acids. *Environ. Sci. Technol., 34*, 2105-2115.

Tobias, H. J., Kooiman, P. M., Docherty, K. S., Ziemann, P. J., 2000. Real-Time Chemical Analysis of Organic Aerosols Using a Thermal Desorption Particle Beam Mass Spectrometer. *Aerosol Sci. Technol., 33,* 170-190.

Tobias, H. J., Beving, D. E., Ziemann, P. J., Sakurai, H., Zuk, M., McMurry, P. H., Zarling, D., Waytulonis, R., Kittelson, D. B., 2001. Chemical Analysis of Diesel Engine Nanoparticles Using a Nano-DMA/Thermal Desorption Particle Beam Mass Spectrometer. *Environ. Sci. Technol., 35,* 2233-2243.

Tuazon, E. C., Alvarado, A., Aschmann, S. M., Atkinson, R., Arey, J., 1999. Products of the Gas-Phase Reactions of 1,3-Butadiene with OH and NO_3 Radicals. *Environ. Sci. Technol., 33,* 3586–3595.

Wang, S. C. and Flagan, R. C., 1990. Scanning Electrical Mobility Spectrometer. *Aerosol Sci. Technol., 13,* 230-240.

Wängberg, I., 1993. Mechanism and Products of the Reactions of NO_3 with Cycloalkenes. *J. Atmos. Chem., 17*, 229–247.

Wayne, R. P., Barnes, I., Biggs, P., Burrows, J. P., Canosa-Mas, C. E., Hjorth, J., Le Bras, G., Moortgat, G. K., Perner, D., Poulet, G., Restelli, G., Sidebottom, H., 1991. The Nitrate Radical – Physics, Chemistry, and the Atmosphere. *Atmos. Environ., 25A*, 1–203.

Yu, J., Cocker, D. R., Griffin, R. J., Flagan, R. C., Seinfeld, J. H., 1999. Gas-Phase Ozone Oxidation of Monoterpenes: Gaseous and Particulate Products. *J. Atmos. Chem., 34*, 207-258.

Ziemann, P. J., 2003. Formation of Alkoxyhydroperoxy Aldehydes and Cyclic Peroxyhemiacetals from Reactions of Cyclic Alkenes with O_3 in the Presence of Alcohols. *J. Phys. Chem. A, 107*, 2048-2060.

Chapter 7

General Conclusion

This thesis is focused on the mechanism of secondary organic aerosol (SOA) formation from the OH and NO_3 radical-initiated reactions of the alkenes in an environmental chamber. For selected systems, the mechanisms are modeled based on yield measurements, branching ratios, and vapor pressures. The chemical compositions of aerosol products were analyzed with a thermal desorption particle beam mass spectrometer (TDPBMS), and nitrate products were quantified with a high-performance liquid chromatograph (HPLC) with a UV-vis detector. The nitrate products were identified by coupling a TDPBMS to a HPLC as well as ^{1}H NMR spectroscopy analysis.

Yield measurements of β-hydroxynitrates and dihydroxynitrates in the SOA formed from linear alkene reactions with OH-radicals in the presence of NO_x are discussed in Chapter 2. The normalized β-hydroxynitrate yields in SOA for OH radical addition to a C=C double bond, which increased as the carbon number increases in C_8-C_{17} 1-alkenes and reached the plateau at C_{14}, was 0.140 ± 0.009 for an average of C_{14}-C_{17}. The yields of dihydroxynitrates were constant over the range of C_{10}-C_{17} with an average yield f 0.039 ± 0.006. Based on measured yields of the β-hydroxynitrates, the branching

ratios for the formation of the β-hydroxynitrates from reactions of β-hydroxyperoxy radicals with NO were estimated as 0.13-0.15. The lower yields of β-hydroxynitrates compared to alkyl nitrates is due to hydrogen bonding between hydroxy and peroxy groups of β-hydroxyperoxy radical-NO intermediates. This effect was enhanced by the presence of NH_3, suggesting hydrogen bonding between the intermediate and NH_3.

In Chapter 3, a model is developed to calculate the composition and yields of SOA formed from OH radical-initiated reactions of linear alkenes in the presence of NO_x. The model includes a quantitative chemical mechanism developed using the measured yields of products, calculated branching ratios, and estimated vapor pressures. The major SOA products are β-hydroxynitates, dihydroxynitrates, cyclic hemiacetals, dihydrofurans, and dimers formed from dihydroxycarbonyls. Cyclic hemiacetals, dihydrofurans, and dimers in the SOA are all formed from dihydroxycarbonyls, and the yields of those dihydroxycarbonyl products in the SOA were estimated using the branching ratios and compound vapor pressures. Gas-particle partitioning of the dihydroxycarbonyl products was calculated for two different cases. In one case, all the products were assumed to be entirely in non-volatile form such as cyclic hemiacetals, and in the other case the products were assumed to undergo gas-particle partitioning with the vapor pressures of

linear dihydroxycarbonyls. The SOA yields calculated with both models agree very well with the measured SOA yields in the high carbon number region where the models predict similar gas-particle partitioning. In the region where differences in gas-particle partitioning are significant, below C_{13} in this study, the SOA yields predicted by the non-volatile model are too high and those predicted by the gas-particle partitioning model are too low. This indicates that the formation of products from dihydroxycarbonyls occurs through reversible reactions, which will be difficult to incorporate into the model without more information.

In Chapter 4, results of measurements of the yields of organic nitrate products formed from OH radical-initiated reactions of 2-methyl-1-alkenes in the presence of NO_x are disussed. The OH addition-normalized yields of large β-hydroxynitrates, dihydroxynitrates, and trihydroxynitrates, whose formation is not affected by carbon number, were 0.225 ± 0.007, 0.055 ± 0.006, and 0.042 ± 0.006, respectively. The β-hydroxynitrate yield was not affected by the addition of NH_3, but increased by ~20% (compared to dry air) at 50% RH. Combining the β--hydroxynitrate yields measured in Chapters 2 and 4, the relative ratios for forming primary, secondary, and tertiary β-hydroxyalkyl radicals by OH radical addition to the double bond are 1.0:1.9:4.3, and the

branching ratios for forming β-hydroxynitrates from reactions of primary, secondary, and tertiary β-hydroxyperoxy radicals with NO are 0.12, 0.15, and 0.25.

A quantitative chemical model of OH radical-initiated reactions of 2-methyl-1-alkenes in the presence of NO_x is developed in Chapter 5. For 2-methyl-1-alkenes, the major products were β-hydroxynitrates, dihydroxynitrates, trihydroxynitrates, dihydroxycarbonyls, trihydroxycarbonyls, cyclic hemiacetals, and dihydrofurans. No dimer formation was observed for this system, unlike the reactions of 1-alkenes, apparently because of low yields of dihydroxycarbonyls and/or reduced reactivity of dihydroxyaldehydes due to electron donation by the added methyl group. Desorption profiles of characteristic peaks of trihydroxycarbonyls and dihydroxycarbonyls are indicative of equilibrium between dihydroxycarbonyls or trihydroxycarbonyls, cyclic hemiacetals, and dihydrofurans. The models initially over-predicted the SOA yields for high carbon numbers. This led to a re-evaluation of the reaction mechanism and consideration of the possibility that decomposition pathways involving α-hydroxyalkoxy radicals should be added. In order to achieve agreement between the model and measurememts, ~90% of α-hydroxyalkyl radicals, which initially were all expected to react to form SOA products, would need to react to form volatile decomposition products.

With this adjustment, the model worked fairly well for the range of carbon numbers studied here, indicating that the estimated product vapor pressures were reasonably accurate.

NO_3 radical-initiated reactions of C_6-C_{14} alkenes are investigated and discussed in Chapter 6. First-generation products and second-generation products were observed in this study. The major first-generation SOA products include hydroxynitrates, carbonylnitrates, nitrooxyperoxynitrates, and dihydroxynitrates. δ-Hydroxycarbonyls, which are first-generation products, are generally too volatile to be observed in SOA, but they partition into particles by isomerizing to form cyclic hemiacetals. Cyclic hemiacetals dehydrate to form dihydrofurans, and dihydrofurans react with NO_3 radicals to generate second-generation products. The isomerization pathway was confirmed by the results of reactions of 3,5,5-trimethyl-1-hexene and 2-methyl-1-octene with NO_3 radicals. The major second-generation SOA products were hydroxy- and oxo-dinitrooxytetrahydrofurans. For reactions of C_7-C_9 alkenes, the SOA is comprised entirely of second-generation products, but for larger alkenes first-generation products also contribute.

The studies presented in this dissertation add substantial new insights into the mechanisms and chemistry of SOA formation from radical-initiated reactions of alkenes. The organic nitrate measurements are the first to date of the yields of β-hydroxynitrates, dihydroxynitrates, and trihydroxynitrates in SOA formed from OH radical-initiated reactions of linear alkenes and 2-methyl-1-alkenes in the presence of NO_x. The technique used for identification, which consists of the TDPBMS coupled to a HPLC via an atomizer, can also be used to identify and quantify other compounds. The quantified relative ratios for forming primary, secondary, and tertiary β-hydroxyalkyl radicals by OH radical addition to the double bond and the branching ratios for forming β-hydroxynitrates from reactions of primary, secondary, and tertiary β-hydroxyperoxy radicals comprise complete sets of values that can be incorporated into other models. The comparisons made between measured SOA yields and values calculate using the models developed here indicate that the chemical composition and yields of SOA can be accurately modeled when sufficiently detailed mechanisms and vapor pressures are available, but that it will be necessary in the future to better understand the particle-phase chemistry that can form SOA products. Such information should help to improve the agreement between the SOA model results and ambient measurements from field studies.

Appendix A

Supporting Informaiton for Chapter 2

Table A.1

Molar Yields of β-Hydroxynitrates and Dihydroxynitrates Formed from Reactions of 1-Alkenes and Internal Alkenes with OH Radicals under Dry Conditions.

		β-hydroxynitrates						dihydroxynitrates	
		$1H2NC_n$		$1N2HC_n$		$1H2NC_n + 1N2HC_n$			
carbon number	$a_{C=C}$[a]	yield	yield / $a_{C=C}$	yield	yield / $a_{C=C}$	yield	yield / $a_{C=C}$	yield	yield / $a_{C=C}$
1-C_8	0.842	0	0.000	0	0	0	0	NA[b]	
1-C_9	0.816	0.005	0.006	0	0	0.005	0.006	NA[b]	
1-C_{10}	0.793	0.006	0.008	0	0	0.006	0.008	0.024	0.030
1-C_{11}	0.770	0.014	0.018	0	0	0.014	0.018	0.031	0.040
1-C_{12}	0.749	0.031	0.041	0	0	0.031	0.041	0.034	0.045
1-C_{13}	0.729	0.046	0.063	0.007	0.010	0.053	0.073	0.030	0.041
1-C_{14}	0.710	0.078	0.110	0.018	0.025	0.096	0.135	0.033	0.046
1-C_{15}	0.691	0.070	0.101	0.022	0.032	0.092	0.133	0.031	0.045
1-C_{16}	0.674	0059	0.088	0.029	0.043	0.088	0.131	0.023	0.034
1-C_{17}	0.657	0.062	0.094	0.026	0.040	0.088	0.134	0.022	0.033
7-C_{14}	0.822					0.011	0.013	0.003	0.004
7-C_{15}	0.808					0.065	0.080	0.006	0.007
8-C_{17}	0.780					0.116	0.149	0.005	0.006

[a]The fraction of the OH radical reaction that occurred by addition to the double bond, $a_{C=C} = k_{add}/(k_{add} + k_{abs})$, where k_{add} and k_{abs} are the rate constants for OH radical addition and H-atom abstraction, respectively, were calculated using equations for k_{abs} (Kwok and Atkinson, 1995) and k_{add} (Nishino et al., 2009) developed by Atkinson and co-workers from measured rate constant data. For 1-alkenes, $k_{abs} = 2.47 + 1.4 \times (CN-5)$ and $k_{add} = 28 + 9 \times [1-\exp(-0.35 \times (CN-3))]$, where CN is the carbon number and k values are in units of 10^{-12} cm^3 $molecule^{-1}$ s^{-1}. For cis and trans internal alkenes, $k_{abs} = 4.93 + 1.4 \times (CN-8)$, $k_{add}(cis) = 56.4$, and $k_{add}(trans) = 64$. These equations were used to calculate $a_{C=C}$ values for 7-tetradecene, 7-pentadecene, and 8-heptadecene using their measured *cis* and *trans* isomer fractions of 0.30:70, 0.25:0.75, and 0.25:0.75.

[b]The C_8 and C_9 dihydroxynitrates could not be analyzed because of peak overlap with the solvent.

References

Kwok, E. S. C. and Atkinson. R., 1995. Estimation of Hydroxyl Radical Reaction Rate Constants for Gas-Phase Organic Compounds Using a Structure-Reactivity Relationship: An Update. *Atmos. Environ., 29*, 1685-1695.

Nishino, N., Arey, J., Atkinson, R., 2009. Rate Constants for the Gas-Phase Reactions of OH Radicals with a Series of C_6-C_{14} Alkenes at 299 ± 2 K. *J. Phys. Chem. A, 113*, 852-857.

Table A.2

^{1}H NMR Spectral Data for β-Hydroxynitrates and Dihydroxynitrates.

compound	chemical shift (ppm)		assignment
	C_{14} [this study]	C_4 [Muthuramu et al., 1993]	
1H2NC$_n$	0.889 (t, 3H)	1.010 (t, 3H)	C<u>H</u>$_3$
	1.337 (m)		(C<u>H</u>$_2$)$_{10}$
	1.698 (m, 3H)	1.747 (m, 2H)	C<u>H</u>$_2$CH-ONO$_2$
		2.200 (br, 1H)	CH$_2$-O<u>H</u>
	3.745 (dd, 1H)	3.741 (dd, 1H)	C<u>H</u>$_2$-OH
	3.849 (dd, 1H)	3.839 (dd, 1H)	C<u>H</u>$_2$-OH
	5.126 (m, 1H)	5.064 (m, 1H)	C<u>H</u>-ONO$_2$
1N2HC$_n$	0.889 (t, 3H)	1.018 (t, 3H)	C<u>H</u>$_3$
	1.270 (m)		(C<u>H</u>$_2$)$_{10}$
	1.535 (m, 3H)	1.581 (m, 2H)	C<u>H</u>$_2$CH-OH
		2.330 (br, 1H)	CH-O<u>H</u>
	3.955 (m, 1H)	3.875 (m, 1H)	C<u>H</u>-OH
	4.362 (dd, 1H)	4.365 (dd, 1H)	C<u>H</u>$_2$-ONO$_2$
	4.497 (dd, 1H)	4.502 (dd, 1H)	C<u>H</u>$_2$-ONO$_2$
4N1,2HC$_{14}$ + 5N1,2HC$_{14}$	0.889 (t, 3H)		C<u>H</u>$_3$
	1.270-1.872		(C<u>H</u>$_2$)$_x$
	3.467 (dd, 1H)		C<u>H</u>-OH
	3.704 (m, 2H)		C<u>H</u>$_2$-OH
	5.069 (m, 1H)		C<u>H</u>-ONO$_2$

Abbreviations used: doublet of doublet (dd), multiplet (m), triplet (t), broad (br)

The NMR peak assignments for C_{14} β–hydroxynitrates and dihydroxynitrates formed in the chamber reaction of 1-tetradecene are shown in Table A.2. For comparison, assignments from Muthuramu et al. (1993) for C_4 β–hydroxynitrates are also shown. The chemical shifts were similar for C_{14} and C_4 β–hydroxynitrates, with two exceptions: large peaks corresponding to $(CH_2)_{10}$ protons were observed for C_{14} but not C_4, as expected, and CH-OH hydroxy protons observed at 2.200 and 2.330 ppm for the two C_4 isomers were not clearly observed for the C_{14} isomers. This is not surprising, since the position of hydroxy proton peaks can vary with analysis conditions. The hydroxy proton peaks in the C_{14} isomers probably overlapped with CH_2 proton peaks at 1.535 ppm from CH_2-CHOH in the $1N2HC_{14}$ isomer and at 1.698 ppm from CH_2-$CHONO_2$ in the $1H2NC_{14}$ isomer. This conclusion is supported by the observation that the integrated proton signals for the CH_2 groups at 1.535 and 1.698 ppm corresponded to 3 rather than 2 protons. Dihydroxynitrate peaks were assigned based on β–hydroxynitrate peak assignments. The chemical shifts of the CH_3 and CH-ONO_2 protons matched those in the $1H2NC_{14}$ isomer. Alkyl protons in CH-OH and CH_2-OH groups appeared in the same region as the corresponding protons in the β–hydroxynitrates. The peaks were differentiated based on

the number of protons. A large peak from $(CH_2)_x$ groups was present at 1.270 ppm, as in the $1N2HC_{14}$ isomer, and additional smaller peaks were also observed downfield as far as 1.872 ppm.

Reference

Muthuramu, K., Shepson, P. B., O'Brien, J. M., 1993. Preparation, Analysis, and Atmospheric Production of Multifunctional Organic Nitrates. *Environ. Sci. Technol.*, *27*, 1117-1124.

Appendix B

Supporting Information for Chapter 3

Branching Ratio Calculations

Branching ratios for OH radical addition to the double bond, $\alpha_{C=C} = k_{add}/(k_{add} + k_{abs})$, and for H-atom abstraction, $1-\alpha_{C=C}$, where k_{add} and k_{abs} are rate constants for addition and abstraction and their sum is equal to the total rate constant, were calculated using equations for k_{abs} (Kwok and Atkinson, 1995) and k_{add} (Nishino et al., 2008) developed by Atkinson and co-workers from measured rate constants. For 1-alkenes, $k_{abs} = 2.47 + 1.4 \times (CN-5)$ and $k_{add} = 28 + 9 \times [1-\exp(-0.35 \times (CN-3))]$, where CN is the carbon number and k values are in units of 10^{-12} cm^3 $molecule^{-1}$ s^{-1}. For *cis* and *trans* internal alkenes, $k_{abs} = 4.93 + 1.4 \times (CN-8)$, $k_{add}(cis) = 56.4$, and $k_{add}(trans) = 64$, and were used with the measured fractions of *cis* and *trans* isomers to calculate weighted values of $\alpha_{C=C}$ (Matsunaga and Ziemann, 2008).

Values for α_1-α_6 were taken from (Matsunaga and Ziemann, 2008). They were determined from measured yields of β-hydroxynitrates [**P1**, **P2**]. For 1-alkenes, α_1 and α_2 are different, whereas for internal alkenes, it was assumed the size of alkyl groups R_1 and

R_2 do not affect branching ratios so $\alpha_1 = \alpha_2$. Values of α_3-α_6 differed between the two classes of alkenes, but within a class it was assumed that branching ratios for formation of β-hydroxynitrates from reactions of NO with β-hydroxyperoxy radicals are the same, so $\alpha_3 = \alpha_4$ and $\alpha_5 = \alpha_6$. As discussed previously (Matsunaga and Ziemann, 2008), one can instead assume that α_3 = 1.5 x α_4 for β-hydroxyperoxy radicals formed from reactions of 1-alkenes, as is the case for alkylperoxy radicals (Cassanelli et al., 2007). A slightly different set of branching ratios are obtained, but when these were used instead the results were essentially the same, and so are not presented.

Values for α_7-α_{16} were estimated using alkoxy radical rate constants calculated using the structure-reactivity method of Atkinson (2007), measured aldehyde yields [**P5**, **P6**] (Aschmann and Atkinson, in preparation), and measured β-hydroxynitrate [**P1**, **P2**] and dihydroxynitrate [**P7**, **P8**] yields (Matsunaga and Ziemann, 2008). Rate constants calculated for alkoxy radicals formed from alkenes studied here predict O_2 reactions are too slow to compete with decomposition or isomerization, so $\alpha_7 = \alpha_8 = 0$. The branching ratios α_9-α_{16} were determined with the aid of Fig. 1, which shows that the molar yield (moles of product formed/moles of alkene reacted) of a compound is equal to the product of branching ratios along the pathway leading to its formation.

For 1-alkenes, the molar yield of **P6** per OH addition, $Y_{P6}/\alpha_{C=C}$, which has contributions from both OH radical addition pathways, is equal to ($[\alpha_1/\alpha_{C=C}]$ x α_5 x α_9) + ($[\alpha_2/\alpha_{C=C}]$ x α_6 x α_{10}). Substituting α_1, α_2, α_5, and α_6 from Table 1, $\alpha_{C=C}$ = 0.84 and Y_{P6} = 0.33 for the sum of heptanal (0.28) and 4-hydroxyheptanal (0.05) (4-hydroxyheptanal is not shown in Figure 1, but is also formed by the alkoxy radical decomposition pathway) from reaction of 1-octene (Aschmann and Atkinson, in preparation), gives $0.60\alpha_9$ + $0.26\alpha_{10}$ = 0.39. This equation was combined with the ratio α_9/α_{10} = 1.5 calculated using the structure-reactivity method of Atkinson (2007) to give α_9 = 0.51 and α_{10} = 0.34, and then α_{11} = 0.49 and α_{12} = 0.66. Similarly, $(Y_{P7} + Y_{P8})/\alpha_{C=C}$, which is 0.040 for 1-alkenes (Matsunaga and Ziemann, 2008) and has contributions from both OH radical addition pathways, is equal to ($[\alpha_1/\alpha_{C=C}]$ x α_5 x α_{11} x α_{13}) + ($[\alpha_2/\alpha_{C=C}]$ x α_6 x α_{12} x α_{14}). Substituting $\alpha_1/\alpha_{C=C}$, $\alpha_2/\alpha_{C=C}$, α_5, α_6, α_{11} and α_{12} from Table 1 and assuming branching ratios for dihydroxynitrate formation from dihydroxyalkoxy radicals are equal, gives α_{13} = α_{14} = 0.08 and then α_{15} = α_{16} = 0.92.

For internal alkenes, it was assumed that the size of alkyl groups R_1 and R_2 do not affect branching ratios so α_9 = α_{10}, α_{11} = α_{12}, α_{13} = α_{14}, and α_{15} = α_{16}. The molar yield of **P6** per OH addition, $Y_{P6}/\alpha_{C=C}$, which has equal contributions from both OH radical

addition pathways, is equal to $[2\alpha_1/\alpha_{C=C}]$ x α_5 x α_9. Substituting values for α_1 and α_5 from Table 1, $\alpha_{C=C} = 0.82$, and $Y_{P6} = 0.47$ for the reaction of *trans*-7-tetradecene (Aschmann and Atkinson, in preparation) (note the measured sum of the yields of heptanal (0.86) and 4-hydroxyheptanal (0.07) was 0.93, but for this symmetric alkene alkoxy radical decomposition leads to two heptanal molecules, only one of which corresponds to **P6**) gives $\alpha_9 = \alpha_{10} = 0.67$ and therefore $\alpha_{11} = \alpha_{12} = 0.33$. Similarly, $(Y_{P7} + Y_{P8})/\alpha_{C=C}$, which is equal to 0.006 for internal alkenes (Matsunaga and Ziemann, 2008) and has equal contributions from both OH radical addition pathways, is equal to $[2\alpha_1/\alpha_{C=C}]$ x α_5 x α_{11} x α_{13}. Substituting values for $\alpha_1/\alpha_{C=C}$, α_5, and α_{11} from Table 1 gives $\alpha_{13} = \alpha_{14} = 0.02$ and therefore $\alpha_{15} = \alpha_{16} = 0.98$. The lower branching ratios for formation of organic nitrates from reactions of NO with dihydroxyalkoxy radicals, α_{13} and α_{14}, compared to β-hydroxyalkoxy radicals, α_3 and α_4, suggests a significant influence of hydrogen bonding, which is reasonable (O'Brien et al., 1998).

References

Aschmann, S. M. and Atkinson, R., 2008. Rate Constants for the Gas-Phase Reactions of OH Radicals with E-7-Tetradecene, 2-Methyl-1-Tridecene, and the C_7-C_{14} 1-alkenes at 295 ± 1 K. *Phys. Chem. Chem. Phys.*, *10*, 4159-4164.

Aschmann, S. M.and Atkinson, R. Products and Mechanism of the OH Radical-Initiated Reactions of 1-octene and 7-tetradecene in the Presence of NO. *Environ. Sci. Technol.*, in preparation.

Atkinson, R., 2007. Rate Constants for the Atmospheric Reactions of Alkoxy Radicals: An Updated Estimation Method. *Atmos. Environ.*, *41*, 8468-8485.

Cassanelli, P., Fox, D. J., Cox, R. A., 2007. Temperature Dependence of Pentyl Nitrate Formation from the Reaction of Pentyl Peroxy Radicals with NO. *Phys. Chem. Chem. Phys.*, *9*, 4332-4337.

Kwok E. S. C. and Atkinson, R. J., 1995. Estimation of Hydroxyl Radical Reaction Rate Constants for Gas-Phase Organic Compounds Using a Structure-Reactivity Relationship: An Update. *Atmos. Environ.*, *29*, 1685-1695.

Matsunaga, A. and Ziemann, P. J., 2009. Yields of β-hydroxynitrates and Dihydroxynitrates in Aerosol Formed from the OH Radical-Initiated Reactions of Linear Alkenes in the Presence of NO_x. *J. Phys. Chem. A, 113*, 599-606.

Nishino, N., Arey, J., Atkinson, R., 2009. Rate Constants for the Gas-Phase Reactions of OH Radicals with a Series of C_6-C_{14} Alkenes at 299 ± 2 K. *J. Phys. Chem. A, 113*, 852-857.

O'Brien, J. M., Czuba, E., Hastie, D. R., Francisco, J. S., Shepson, P. S., 1998. Determination of the Hydroxy Nitrate Yields from the Reaction of C2-C6 Alkenes with OH in the Presence of NO. *J. Phys. Chem. A, 102*, 8903-8908.

Figure B.1

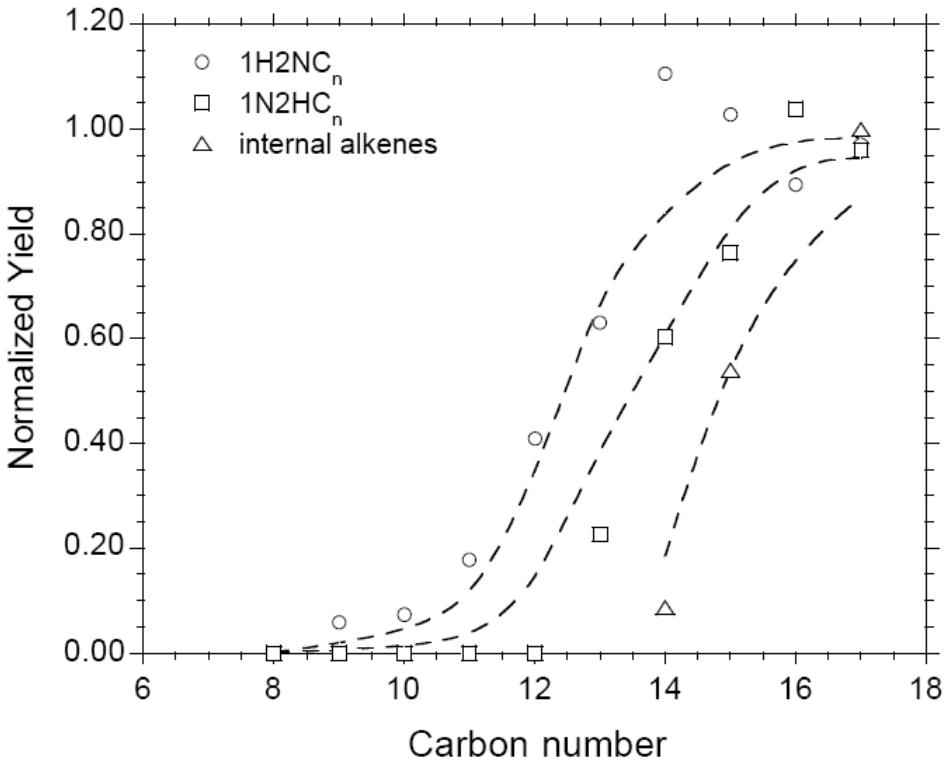

The fraction of β-hydroxynitrate in the particle phase calculated as the ratio of the measured yield to the yield in the plateau region, where the compound is essentially entirely in the particle phase. The curves were calculated using gas-particle partitioning theory (Pankow, 1994), estimated mean molecular weights of particulate organic compounds assumed to be the same as the hydroxynitrates formed in the alkene reaction (equal to the molecular weight of the alkene + 79), assumed activity coefficients of unity, measured organic aerosol mass concentrations, and vapor pressures chosen to achieve good fits to the data. The vapor pressure equations are given in Table B.1.

Reference

Pankow, J. F., 1994. An Absorption Model of the Gas/Aerosol Partitioning Involved in the Formation of Secondary Organic Aerosol. *Atmos. Environ.*, *28*, 189-193.

Table B.1

Vapor pressure equations used to calculate the curves shown in Fig. S1 and gas-particle partitioning in SOA yield calculations.

	logP(Pa) = A-(0.4537 x carbon number) A
1-alkenes	
$1H2NC_n$	3.900
$1N2HC_n$	4.432
dihydroxynitrates	2.424
dihydroxycarbonyls	3.955
1,4-hydroxynitrates	4.698
internal alkenes	
β-hydroxynitrates	4.698
dihydroxynitrates	3.221
dihydroxycarbonyls	4.221
1,4-hydroxynitrates	4.698

Vapor pressures of $1H2NC_n$ isomers were calculated using a linear least-squares fit to vapor pressures measured for 1,2-dialkyl nitrates using gas chromatography (Fischer and Ballschmiter, 1998), multiplied by a factor of 2, which provides a good fit to the data in Fig. S1. Vapor pressures of $1N2HC_n$ isomers and β-hydroxynitrates formed from internal alkenes were calculated by multiplying the values for $1H2NC_n$ isomers by 3.4 and 6.3. The good agreement with 1,2-dialkyl nitrate vapor pressures for the $1H2NC_n$ isomers is reasonable, since 8-nitrooxyhexadecane and 8-hydroxyhexadecane present in a mixture desorbed at similar temperatures during TPTD analysis (unpublished results), indicating that nitrate and hydroxyl groups have similar effects on vapor pressure. Furthermore, vapor pressures are sensitive to the positions of functional groups on the carbon chain [values for 1- and 2-alkyl nitrates differ by a factor of ~2 (Luxenhofer and Ballschmiter, 1996)] so differences in the vapor pressures of isomers is not surprising. Dihydroxynitrate vapor pressures were calculated by dividing the values for $1H2NC_n$ isomers and β-hydroxynitrate isomers formed from internal alkenes by 30, the difference in vapor pressures of 1-alkyl nitrates and 1,2-dialkyl nitrates. Dihydroxycarbonyl vapor pressures were calculated by dividing the values for $1N2HC_n$ isomers and β-hydroxynitrates formed from internal alkenes by 3, which our thermal desorption studies

of multifunctional long-chain compounds indicate gives a reasonable estimate for the effect of a carbonyl group. For 1,4-hydroxynitrate products of H-atom abstraction, vapor pressures were assumed to be the same as those of β-hydroxynitrate isomers formed from internal alkenes.

References

Fischer, R. G. and Ballschmiter, K., 1998. Prediction of the Environmental Distribution of Alkyl Dinitrates – Chromatographic Determination of Vapor Pressure P^o, Water Solubility S_{H2O}, Gas Water Partition Coefficient K_{GW} (Henry's Law Constant) and Octanol-Water Partition Coefficient K_{OW}. *Fresenius J. Anal. Chem.*, *360*, 769-776.

Luxenhofer, O. and Ballschmiter, K., 1996. Semivolatile Long Chain C6-C17 Alkyl Nitrates as Trace Compounds in Air. *Chemosphere*, *33*, 393-404.

Table B.2

Estimated contributions of secondary reaction products to yields of SOA formed from OH radical-initiated reactions of 1-alkenes and internal alkenes in dry air in the presence of NO_x.

alkenes	yield		
1-alkenes	addition then abstraction	abstraction then addition	total
C_8	0.028	0.039	0.067
C_9	0.031	0.044	0.075
C_{10}	0.034	0.048	0.082
C_{11}	0.035	0.053	0.088
C_{12}	0.036	0.057	0.093
C_{13}	0.031	0.060	0.091
C_{14}	0.021	0.063	0.084
C_{15}	0.012	0.067	0.079
C_{16}	0.007	0.070	0.077
C_{17}	0.007	0.073	0.080
internal alkenes			
C_{14}	0.005	0.062	0.067
C_{15}	0.005	0.067	0.072
C_{17}	0.003	0.075	0.078

[a]The yield is (mass of product in SOA)/(mass of alkene reacted).

Table B.3

Modeled Yields of SOA Products Formed from OH Radical-Initiated Reactions of Linear Alkenes in the Presence of NO_x, Assuming Dihydroxycarbonyls were in Gas-Particle Partitioning Equilibrium.

alkenes	yield[a]								
	HN		DHN		DHC		HAA	Total	Measured
1-alkenes	P1	P2	P7	P8	P9	P10			
C_8	0.000	0.000	0.001	0.001	0.000	0.000	0.000	0.002	0.048
C_9	0.002	0.000	0.011	0.006	0.004	0.002	0.000	0.025	0.154
C_{10}	0.002	0.000	0.009	0.005	0.004	0.002	0.000	0.022	0.317
C_{11}	0.003	0.000	0.013	0.008	0.006	0.004	0.000	0.034	0.344
C_{12}	0.018	0.003	0.024	0.014	0.039	0.022	0.001	0.121	0.468
C_{13}	0.067	0.016	0.026	0.015	0.156	0.090	0.009	0.379	0.459
C_{14}	0.082	0.025	0.025	0.014	0.196	0.113	0.018	0.473	0.501
C_{15}	0.087	0.033	0.024	0.014	0.214	0.124	0.030	0.526	0.530
C_{16}	0.087	0.035	0.023	0.013	0.216	0.125	0.038	0.537	0.538
C_{17}	0.085	0.035	0.022	0.013	0.210	0.122	0.041	0.528	0.487
internal alkenes									
C_{14}	0.026	0.026	0.003	0.003	0.079	0.079	0.007	0.223	0.105
C_{15}	0.055	0.055	0.003	0.003	0.117	0.117	0.017	0.367	0.188
C_{17}	0.068	0.068	0.003	0.003	0.123	0.123	0.025	0.413	0.405

[a]The yield is (mass of product in SOA)/(mass of alkene reacted). Products are hydroxynitrates (HN), dihydroxynitrates (DHN), dihydroxycarbonyls (DHC), and products formed by the H-atom abstraction pathway (HAA). Refer to Figure 1 for structures of products P1, P2, …

Table B.4

Modeled Yields of SOA Products Formed from OH Radical-Initiated Reactions of Linear Alkenes in the Presence of NO_x, Assuming Dihydroxycarbonyls were Entirely in the Particle Phase as Non-Volatile Cyclic Hemiacetals, Dihydrofurans, or Dimers.

alkenes	yield[a]								
	HN		DHN		DHC		HAA	Total	Measured
1-alkenes	P1	P2	P7	P8	P9	P10			
C_8	0.001	0.000	0.007	0.004	0.326	0.188	0.000	0.526	0.048
C_9	0.004	0.001	0.017	0.010	0.306	0.177	0.000	0.515	0.154
C_{10}	0.007	0.001	0.020	0.012	0.289	0.167	0.000	0.496	0.317
C_{11}	0.017	0.002	0.024	0.014	0.274	0.158	0.001	0.490	0.344
C_{12}	0.038	0.006	0.026	0.015	0.261	0.151	0.003	0.500	0.468
C_{13}	0.072	0.018	0.026	0.015	0.250	0.144	0.011	0.536	0.459
C_{14}	0.083	0.026	0.025	0.014	0.240	0.138	0.019	0.545	0.501
C_{15}	0.087	0.033	0.024	0.014	0.230	0.133	0.030	0.551	0.530
C_{16}	0.087	0.035	0.023	0.013	0.222	0.128	0.039	0.547	0.538
C_{17}	0.085	0.035	0.022	0.013	0.214	0.124	0.041	0.534	0.487
internal alkenes									
C_{14}	0.035	0.035	0.004	0.004	0.141	0.141	0.010	0.370	0.105
C_{15}	0.057	0.057	0.003	0.003	0.136	0.136	0.018	0.410	0.188
C_{17}	0.068	0.068	0.003	0.003	0.129	0.129	0.025	0.425	0.405

[a]The yield is (mass of product in SOA)/(mass of alkene reacted). Products are hydroxynitrates (HN), dihydroxynitrates (DHN), dihydroxycarbonyls (DHC), and products formed by the H-atom abstraction pathway (HAA). Refer to Figure 1 for structures of products P1, P2, …

Appendix C

Supporting Information for Chapter 4

Table C.1

Molar Yields of β-Hydroxynitrates, Dihydroxynitrates, and Trihydroxynitates Formed from OH Radical-Initiated Reactions of 2-Methyl-1-Alkenes in the Presence of NO_x under Dry Conditions.

		β-hydroxynitrates						dihydroxynitrates		trihydroxynitrates	
carbon number	$\alpha_{C=C}$[a]	1H2NC$_n$		1N2HC$_n$		1H2NC$_n$ + 1N2HC$_n$					
		yield	yield / $\alpha_{C=C}$	yield	yield / $\alpha_{C=C}$	yield	yield / $\alpha_{C=C}$	yield	yield / $\alpha_{C=C}$	yield	yield / $\alpha_{C=C}$
C_9	0.904	0	0	0	0	0	0	NA[b]	NA[b]	NA[b]	NA[b]
C_{10}	0.888	0.001	0.002	0	0	0.001	0.002	0.005	0.006	NA[b]	NA[b]
C_{11}	0.872	0.005	0.006	0	0	0.005	0.006	0.022	0.025	NA[b]	NA[b]
C_{12}	0.857	0.012	0.015	0.001	0.001	0.013	0.016	0.030	0.035	NA[b]	NA[b]
C_{13}	0.842	0.031	0.037	0.003	0.004	0.034	0.041	0.040	0.047	NA[b]	NA[b]
C_{14}	0.828	0.160	0.193	0.014	0.017	0.174	0.210	0.045	0.054	0.036	0.043
C_{15}	0.814	0.164	0.202	0.019	0.023	0.183	0.225	0.044	0.055	0.032	0.040

[a]The fraction of the OH radical reaction that occurred by addition to the double bond, $\alpha_{C=C} = k_{add}/(k_{add} + k_{abs})$, where k_{add} and k_{abs} are the rate constants for OH radical addition and H-atom abstraction, respectively, were calculated using equations for k_{abs} (Kwok and Atkinson, 1995) and k_{add} (Nishino et al., 2009) developed by Atkinson and co-workers from measured rate constant data. For 2-methyl-1-alkenes, $k_{abs} = 2.6 + 1.4 \times (C_n-6)$ and $k_{add} = 51 + 16 \times [1-\exp(-0.35 \times (C_n-3))]$, where C_n is the carbon number and k values are in units of 10^{-12} cm^3 molecule^{-1} s^{-1}.

[b]The C_9 dihydroxynitrates and $C_9 - C_{13}$ trihydroxynitrates could not be analyzed because of peak overlap with the solvent.

References

Kwok, E. S. C. and Atkinson. R., 1995. Estimation of Hydroxyl Radical Reaction Rate Constants for Gas-Phase Organic Compounds Using a Structure-Reactivity Relationship: An Update. *Atmos. Environ., 29*, 1685-1695.

Nishino, N., Arey, J., Atkinson, R., 2009. Rate Constants for the Gas-Phase Reactions of OH Radicals with a Series of C_6-C_{14} Alkenes at 299 ± 2 K. *J. Phys. Chem. A, 113*, 852-857.

Table C.2

^{1}H NMR Spectral Data for β-Hydroxynitrates, Dihydroxynitrates, and Trihydroxynitrates Formed from OH Radical-Initiated Reactions of 2-Methyl-1-Tridecene and 1-Tetradecene in the Presence of NO_x.

compound	chemical shift (ppm)		assignment
	2-methyl-1-tridecene [this study]	1-tetradecene [Matsunaga and Ziemann, 2009]	
1H2NC$_{14}$	0.888 (t, 3H)	0.889 (t, 3H)	C<u>H</u>$_3$
	1.265		C<u>H</u>$_3$-C
		1.337 (m)	(C<u>H</u>$_2$)$_x$
	1.265-1.738	1.698 (m, 3H)	CH$_2$-O<u>H</u> C<u>H</u>$_2$CH-ONO$_2$ or C<u>H</u>$_2$C-ONO$_2$
	3.772 (d, 1H)	3.745 (dd, 1H)	C<u>H</u>$_2$-OH
	3.832 (d, 1H)	3.849 (dd, 1H)	C<u>H</u>$_2$-OH
		5.126 (m, 1H)	C<u>H</u>-ONO$_2$
1,2H4NC$_{14}$ + 1,2H5NC$_{14}$	0.888 (t, 3H)	0.889 (t, 3H)	C<u>H</u>$_3$
	1.182 (d, 3H)		C<u>H</u>$_3$-C
	1.267-1.857	1.270-1.872	(C<u>H</u>$_2$)$_x$ hydroxyl protons
		3.467 (dd, 1H)	C<u>H</u>-OH
	3.464 (m, 2H)	3.704 (m, 2H)	C<u>H</u>$_2$-OH
	5.045 (m, 1H)	5.069 (m, 1H)	C<u>H</u>-ONO$_2$
1,2,4H7NC$_{14}$ + 1,2,5H8NC$_{14}$	0.897 (t, 3H)		C<u>H</u>$_3$
	1.202 (s, 3H)		C<u>H</u>$_3$-C
	1.293-2.137		(C<u>H</u>$_2$)$_x$ hydroxyl protons
	3.493 (br, 2H)		C<u>H</u>$_2$-OH
	3.643 (br, 1H)		C<u>H</u>-OH
	5.062 (m, 1H)		C<u>H</u>-ONO$_2$

Abbreviations used: doublet of doublet (dd), multiplet (m), triplet (t), broad (br)

The NMR peak assignments for β–hydroxynitrates, dihydroxynitrates, and trihydroxynitrates formed in the chamber reaction of 2-methyl-1-tridecene are shown in Table S2. For comparison, assignments from Matsunaga and Ziemann (2009) for linear β–hydroxynitrates and dihydroxynitrates formed from the reaction of 1-tetradecene are also shown. For 2-methyl-β–hydroxynitrates, $1N2HC_{14}$ data were not available because of the low yield of this compound. As expected, a peak from CH_3-C protons is observed only in 2-methyl-β–hydroxynitrates, and no peak is observed for a CH-ONO_2 proton. Chemical shifts were similar for all β–hydroxynitrates, except that peaks appeared at 1.265-1.738 ppm for 2-methyl-β–hydroxynitrates. A peak from CH_3-C is present at 1.265 ppm, and additional peaks, which are not resolved, are also observed downfield as far as 1.738 ppm. Those small peaks are expected to be from $(CH_2)_x$ protons, a hydroxyl proton, and CH_2 protons of CH_2-ONO_2. Chemical shifts are also similar for all dihydroxynitrates, except for the CH_2 protons from CH_2-OH. The peak from 2-methyl-dihydroxynitrate appears at 3.464 ppm, 0.24 ppm lower than the peak from the linear dihydroxynitrate. This suggests that the chemical shifts of CH_2 protons from CH_2-OH are affected by functional groups at the β position: a methyl group for 2-methyl-dihydroxynitrates, and a H atom for lineardihydroxynitrates. The CH_2 protons from CH_2-OH of 2-methyl-

dihydroxynitrates are probably shielded by a methyl group, which is electron-donating, and appears slightly upfield from the CH_2 protons from CH_2-OH in linear dihydroxynitrates. A peak from CH_3-C protons is observed only in 2-methyl-dihydroxynitrates and no peak is observed for the CH proton from CH-OH of 2-methyl-dihydroxynitrates, as expected. The peaks from $(CH_2)_x$ and hydroxyl protons overlap in the regions from 1.267-1.857 ppm and 1.270-1.872 ppm for 2-methyl-dihydroxynitrates and linear dihydroxynitrates, respectively. Trihydroxynitrate peaks are assigned based on dihydroxynitrate peak assignments. The chemical shifts of corresponding trihydroxynitrate and dihydroxynitrate peaks are similar, and the peak from the CH proton in CH-OH in the trihydroxynitrate appears at a similar chemical shift to the peak from the CH_2 protons in CH_2-OH in the dihydroxynitrates.

Reference

Matsunaga, A. and Ziemann, P. J., 2009. Yields of β-hydroxynitrates and Dihydroxynitrates in Aerosol Formed from the OH Radical-Initiated Reactions of Linear Alkenes in the Presence of NO_x. *J. Phys. Chem. A*, *113*, 599-606.

Appendix D

Supporting Information for Chapter 5

Branching Ratio Calculations

The fraction of OH radical reactions that occurred by addition to the double bond, $a_{C=C} = k_{add}/(k_{add} + k_{abs})$, where k_{add} and k_{abs} are the rate constants for OH radical addition and H-atom abstraction, respectively, was calculated using equations for k_{abs} (Kwok and Atkinson, 1995) and k_{add} (Nishino et al., 2009) developed by Atkinson and co-workers from measured rate constant data. For 2-methyl-1-alkenes, $k_{abs} = 2.6 + 1.4 \times (C_n-6)$ and $k_{add} = 51 + 16 \times [1-\exp(-0.35 \times (C_n-3))]$, where C_n is the carbon number and k values are in units of 10^{-12} cm^3 $molecule^{-1}$ s^{-1}.

Values for α_1-α_6 were taken from Chapter 4, and values for α_7-α_{12} and α_{17}-α_{20} were estimated using alkoxy radical rate constants calculated using the structure-reactivity method of Atkinson (2007) and OH addition-normalized ketone yields [**P6**] measured in this study. Rates of reactions of O_2 with β-hydroxyalkoxy radicals formed from 2-methyl-1-alkenes studied here are predicted to be too slow to compete with

decomposition or isomerization, so $\alpha_7 = \alpha_8 = 0$. The branching ratios $\alpha_{17} = 0$, because there is no H atom available for abstraction in dihydroxyalkoxy radicals with the alkoxy group in the 5-position of the carbon chain. This indicates that all these dihydroxyalkoxy radical isomers isomerize instead by abstraction from a CH_2 group, so $\alpha_{19} = 1.0$. The branching ratios α_{18} and α_{20} were calculated using the structure-reactivity method of Atkinson (2007). The branching ratios α_9-α_{16} and α_{21}-α_{24} were determined with the aid of Figure 5.1, which shows that the molar yield (moles of product formed/moles of alkene reacted) of a compound is equal to the product of branching ratios along the pathway leading to its formation. The molar yield of **P6** per OH addition, $Y_{P6}/\alpha_{C=C}$, which has contributions from both OH radical addition pathways, is equal to ($[\alpha_1/\alpha_{C=C}]$ x α_5 x α_9) + ($[\alpha_2/\alpha_{C=C}]$ x α_6 x α_{10}). Substituting α_1, α_2, α_5, and α_6 from Table 5.1 and $Y_{P6}/\alpha_{C=C} = 0.453$ gives $0.61\alpha_9 + 0.17\alpha_{10} = 0.453$. This equation was combined with the ratio $\alpha_9/\alpha_{10} = 1.35$ calculated using the structure-reactivity method of Atkinson (2007) to give $\alpha_9 = 0.62$ and $\alpha_{10} = 0.46$, and then $\alpha_{11} = 0.38$ and $\alpha_{12} = 0.54$.

For α_{13}-α_{16}, $(Y_{P7} + Y_{P8})/\alpha_{C=C}$, which is 0.055 for 2-methyl-1-alkenes as shown in Chapter 4 and has contributions from both OH radical addition pathways, is equal to ($[\alpha_1/\alpha_{C=C}]$ x α_5 x α_{11} x α_{13}) + ($[\alpha_2/\alpha_{C=C}]$ x α_6 x α_{12} x α_{14}). Substituting $\alpha_1/\alpha_{C=C}$, $\alpha_2/\alpha_{C=C}$,

α_5, α_6, α_{11} and α_{12} from Table 5.1 and assuming branching ratios for dihydroxynitrate formation from reactions of dihydroxyperoxy radicals with NO are equal, gives $\alpha_{13} = \alpha_{14} = 0.17$ and then $\alpha_{15} = \alpha_{16} = 0.83$.

Similarly, $(Y_{P11} + Y_{P12})/\alpha_{C=C}$, which is 0.042 for 2-methyl-1-alkenes as shown in Chapter 4 and has contributions from both OH radical addition pathways, is equal to $([\alpha_1/\alpha_{C=C}] \text{ x } \alpha_5 \text{ x } \alpha_{11} \text{ x } \alpha_{15} \text{ x } \alpha_{19} \text{ x } \alpha_{21}) + ([\alpha_2/\alpha_{C=C}] \text{ x } \alpha_6 \text{ x } \alpha_{12} \text{ x } \alpha_{16} \text{ x } \alpha_{20} \text{ x } \alpha_{22})$. Substituting $\alpha_1/\alpha_{C=C}$, $\alpha_2/\alpha_{C=C}$, α_5, α_6, α_{11}, α_{12}, α_{19}, and α_{20} from Table 5.1 and assuming branching ratios for trihydroxynitrate formation from reactions of trihydroxyperoxy radicals with NO are equal, gives $\alpha_{21} = \alpha_{22} = 0.20$ and then $\alpha_{23} = \alpha_{24} = 0.80$.

References

Atkinson, R., 2007. Rate Constants for the Atmospheric Reactions of Alkoxy Radicals: An Updated Estimation Method. *Atmos. Environ.*, *41*, 8468-8485.

Kwok, E. S. C. and Atkinson. R., 1995. Estimation of Hydroxyl Radical Reaction Rate Constants for Gas-Phase Organic Compounds Using a Structure-Reactivity Relationship: An Update. *Atmos. Environ.*, *29*, 1685-1695.

Nishino, N., Arey, J., Atkinson, R., 2009. Rate Constants for the Gas-Phase Reactions of OH Radicals with a Series of C_6-C_{14} Alkenes at 299 ± 2 K. *J. Phys. Chem. A, 113*, 852-857.

Table D.1

Calculated SOA Yields of Products Formed from OH Radical-Initiated Reactions of 2-Methyl-1-Alkenes in the Presence of NO_x, Assuming Dihydroxycarbonyls and Trihydroxycarbonyls were in Gas-Particle Partitioning Equilibrium.

product		SOA yield						
		C_9	C_{10}	C_{11}	C_{12}	C_{13}	C_{14}	C_{15}
HN	P1	0.001	0.005	0.025	0.076	0.150	0.200	0.213
	P2	0.000	0.000	0.001	0.003	0.009	0.016	0.021
DHN	P7	0.003	0.010	0.028	0.043	0.047	0.047	0.046
	P8	0.001	0.004	0.011	0.017	0.019	0.019	0.018
THN	P11	0.021	0.040	0.053	0.054	0.052	0.050	0.046
	P12	0.002	0.004	0.005	0.005	0.005	0.005	0.004
DHC	P9	0.000	0.000	0.000	0.000	0.000	0.000	0.000
	P10	0.000	0.001	0.005	0.017	0.036	0.049	0.053
THC	P13	0.008	0.029	0.089	0.143	0.163	0.165	0.162
	P14	0.001	0.003	0.008	0.013	0.015	0.016	0.015
HAA		0.000	0.000	0.000	0.002	0.005	0.012	0.019
Total		0.037	0.096	0.225	0.373	0.501	0.579	0.597
Measured		0.023	0.068	0.137	0.167	0.180	0.412	0.465

[a]The product SOA yield is the mass of product in SOA/mass of alkene reacted. Products are hydroxynitrates (HN), dihydroxynitrates (DHN), trihydroxynitrates (THN), dihydroxycarbonyls (DHC), trihydroxycarbonyls (THC), and products formed by the H-atom abstraction pathway (HAA). Refer to Figure 5.1 for structures of products P1, P2,...

Table D.2

Calculated SOA Yields of Products Formed from OH Radical-Initiated Reactions of 2-Methyl-1-Alkenes in the Presence of NO_x, Assuming Dihydroxycarbonyls were Entirely in the Particle Phase as Non-Volatile Cyclic Hemiacetals and Dihydrofurans.

product		SOA yield						
		C_9	C_{10}	C_{11}	C_{12}	C_{13}	C_{14}	C_{15}
HN	P1	0.003	0.009	0.031	0.083	0.153	0.200	0.214
	P2	0.000	0.000	0.001	0.004	0.009	0.016	0.021
DHN	P7	0.005	0.014	0.031	0.044	0.047	0.047	0.046
	P8	0.002	0.005	0.012	0.017	0.019	0.019	0.018
THN	P11	0.030	0.046	0.054	0.054	0.052	0.050	0.048
	P12	0.003	0.005	0.005	0.005	0.005	0.005	0.004
DHC	P9	0.000	0.000	0.000	0.000	0.000	0.000	0.000
	P10	0.071	0.068	0.065	0.063	0.061	0.059	0.057
THC	P13	0.015	0.043	0.101	0.147	0.164	0.165	0.162
	P14	0.001	0.004	0.010	0.014	0.015	0.016	0.015
HAA		0.000	0.000	0.000	0.002	0.005	0.012	0.019
Total		0.130	0.194	0.310	0.433	0.530	0.589	0.604
Measured		0.023	0.068	0.137	0.167	0.180	0.412	0.465

[a]The product SOA yield is the mass of product in SOA/mass of alkene reacted. Products are hydroxynitrates (HN), dihydroxynitrates (DHN), trihydroxynitrates (THN), dihydroxycarbonyls (DHC), trihydroxycarbonyls (THC), and products formed by the H-atom abstraction pathway (HAA). Refer to Figure 5.1 for structures of products P1, P2,...

Table D.3

Calculated Yields of SOA Products Formed from OH Radical-Initiated Reactions of 2-Methyl-1-Alkenes in the Presence of NO_x, Assuming Dihydroxycarbonyls were Entirely in the Particle Phase as Non-Volatile Cyclic Hemiacetals and Dihydrofurans and the Yield of Trihydroxycarbonyls (Gas + Particle) is Reduced from 0.177 to 0.025.

product		SOA yield						
		C_9	C_{10}	C_{11}	C_{12}	C_{13}	C_{14}	C_{15}
HN	P1	0.002	0.007	0.022	0.060	0.130	0.190	0.209
	P2	0.000	0.000	0.001	0.002	0.007	0.014	0.020
DHN	P7	0.005	0.012	0.026	0.040	0.046	0.047	0.046
	P8	0.002	0.005	0.010	0.016	0.018	0.019	0.018
THN	P11	0.029	0.044	0.052	0.053	0.052	0.050	0.048
	P12	0.003	0.004	0.004	0.005	0.005	0.005	0.004
DHC	P9	0.000	0.000	0.000	0.000	0.000	0.000	0.000
	P10	0.071	0.068	0.065	0.063	0.061	0.059	0.057
THC	P13	0.001	0.004	0.008	0.013	0.015	0.017	0.016
	P14	0.000	0.000	0.001	0.001	0.002	0.002	0.002
HAA		0.000	0.000	0.000	0.001	0.004	0.011	0.017
Total		0.113	0.144	0.189	0.254	0.340	0.414	0.437
Measured		0.023	0.068	0.137	0.167	0.180	0.412	0.465

[a]The product SOA yield is the mass of product in SOA/mass of alkene reacted. Products are hydroxynitrates (HN), dihydroxynitrates (DHN), trihydroxynitrates (THN), dihydroxycarbonyls (DHC), trihydroxycarbonyls (THC), and products formed by the H-atom abstraction pathway (HAA). Refer to Figure 5.1 for structures of products P1, P2,…

Table D.4

Estimated SOA Yields of Secondary Reaction Products Formed from OH Radical-Initiated Reactions of 2-Methyl-1-Alkenes in the Presence of NO_x.

alkenes	SOA yield[a]		
	OH radical addition + H-atom abstraction	H-atom abstraction + OH radical addition	total
C_9	0.028	0.039	0.067
C_{10}	0.032	0.045	0.077
C_{11}	0.035	0.050	0.085
C_{12}	0.038	0.055	0.093
C_{13}	0.037	0.060	0.097
C_{14}	0.029	0.064	0.093
C_{15}	0.022	0.069	0.090

[a]The product SOA yield is the mass of product in SOA/mass of alkene reacted.

Appendix E

Supporting Information for Chapter 6

Figure E.1

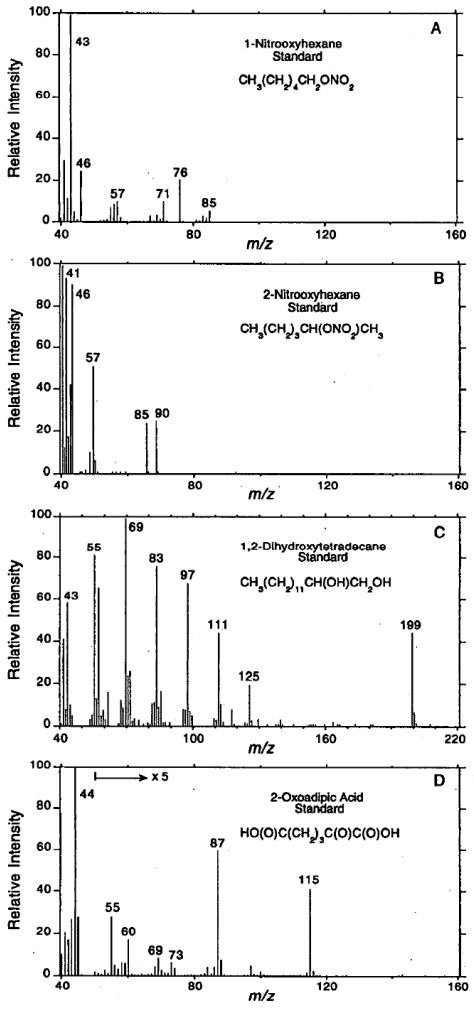

Electron ionization mass spectra of (A) 1-nitrooxyhexane, (B) 2-nitrooxyhexane, (C) 1,2-dihydroxytetradecane, and (D) 2-oxoadipic acid standards. Mass spectra A-C are from the Wiley Mass Spectral Database and D was measured by real-time TDPBMS.

Figure E.2

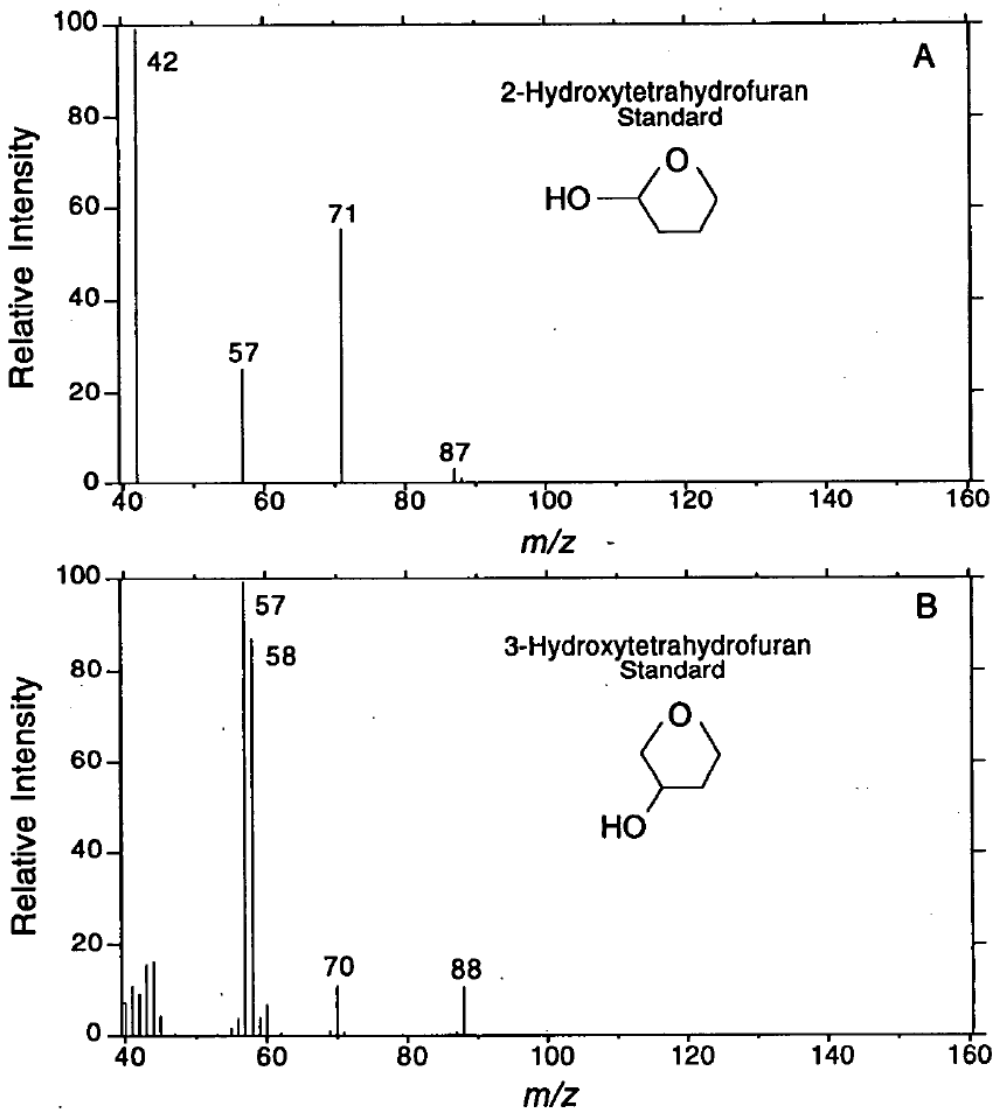

Electron ionization mass spectra of (A) 2-hydroxytetrahydrofuran and (B) 3-hydroxytetrahydrofuran standards from the Wiley Mass Spectral Database.

Figure E.3

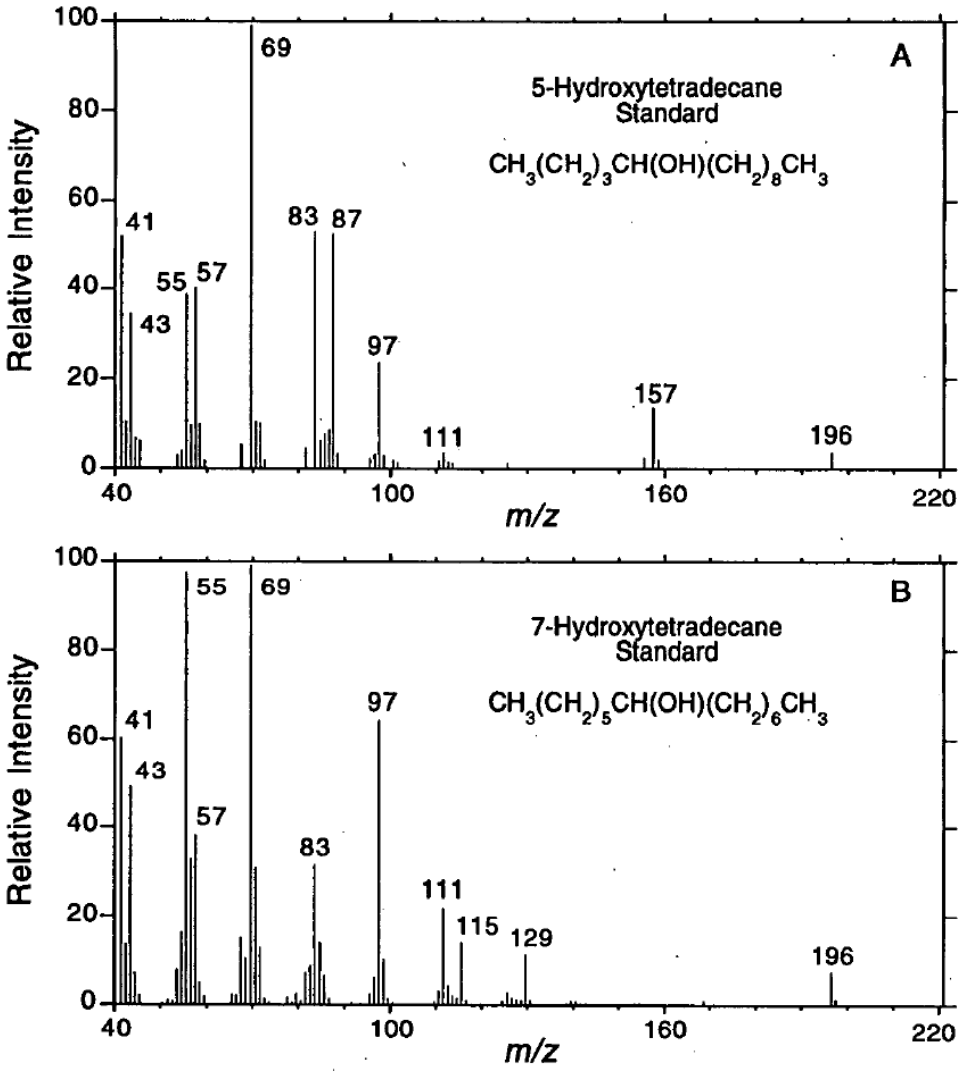

Electron ionization mass spectra of (A) 5-hydroxytetradecane and (B) 7-hydroxytetradecane standards from the Wiley Mass Spectral Database.